Flux measurements at the land-atmosphere interface

Extending the theory and implementation of the true eddy accumulation and eddy covariance measurement techniques

Dissertation
to attain the doctoral degree (Dr. rer. nat.)
of the Faculty of Forest Sciences and Forest Ecology
Georg-August-Universität Göttingen

Submitted by

Anas Emad

born in Swaida, Syria

Göttingen, February 2023

1. Referee: Prof. Dr. Alexander Knohl
2. Referee: Prof. Dr. Janne Rinne
3. Referee: Prof. Dr. Christoph Thomas
4. Examiner: Dr. Lukas Siebicke
5. Examiner: Prof. Dr. Edzo Veldkamp

Date of oral examination: 26.05.2023

Abstract

Interactions between the biosphere and the atmosphere have profound effects on the global climate and the future trajectory of the Earth system. Understanding the dynamics and controls of these interactions requires continuous monitoring of the surface-atmosphere exchange of energy and matter (the flux). Eddy covariance (EC) has become the state-of-the-art method to directly observe the fluxes of energy, momentum and several important atmospheric constituents such as CO_2 and H_2O. However, the EC method is limited to a few atmospheric constituents for which fast-response gas analyzers are available.

True eddy accumulation (TEA) provides an alternative method to measuring fluxes with slow-response gas analyzers. TEA uses conditional sampling of air to overcome the need for fast measurements of scalar concentration. The TEA method has many promising applications for direct micrometeorological measurements. Nevertheless, several challenges in theory and implementation have prevented the wide adoption of the TEA method.

This thesis aims to improve the theory and implementation of the TEA method to make it a reliable tool to study the land-atmosphere exchange. First, a new proof-of-concept implementation of a TEA system is presented. The new system is based on a new dynamic mass flow controller that can resolve turbulence at a frequency of 10 Hz and higher. Flux measurements of CO_2 using the new system showed a good match against a reference conventional EC system (R^2 of 0.86, slope of 0.98). The new system solved multiple implementation challenges including automatic gas handling and the real-time processing of wind statistics. The work presented in this thesis contributed to the field verification of the new mass flow controller, the characterization of density effects on air sampling and the processing of measured fluxes.

Secondly, we investigate the problem of TEA under non-ideal conditions where the mean vertical wind velocity is nonzero. We propose a new TEA formulation that effectively isolates and minimizes the systematic error in the flux under non-ideal conditions. We analyze the magnitude of the systematic error and propose two methods to estimate and correct the error. We then show how the conventional formulations for the TEA method are related to the new formula and evaluate them with the newly proposed correction methods.

Thirdly, we explore the limitations of the fixed accumulation time in the conventional TEA formulation. We propose a new variation of the eddy accumulation method that overcomes this limitation. The new method, termed short-time eddy accumulation (STEA), enables more robust and flexible treatments of sample accumulation and allows for realizing a continuous flow-through accumulation system. A flow-through TEA system has been developed earlier to limit the complexity and nonstationarities associated with bag-based accumulation systems. The STEA formulation extends the flow-through TEA system to allow a rigorous treatment of continuous sample accumulation. An STEA system was implemented and evaluated against a reference EC system over an agricultural field. The measured fluxes matched very well between the two systems yielding an R^2 of 0.86 and a slope of 1.04. The use of buffer volumes with the STEA method was analyzed and an empirical correction was proposed.

Finally, we analyze the problem of spectral attenuation in measured atmospheric signals with the

aim to develop a direct spectral correction method that can be used with TEA measurements. The analysis showed that the conventional spectral correction methods introduce systematic errors and increased uncertainty to the corrected fluxes due to the assumptions of spectral similarity, the use of inappropriate transfer functions, and due to ignoring the non-linear phase contributions. We propose a novel direct correction scheme based on Wiener deconvolution. The new approach brings multiple advantages and does not require the assumption of an ideal spectrum for each averaging interval. Therefore, it can be used to restore attenuated atmospheric signals measured with the TEA method where an assumption about the ideal spectra is hard to justify.
In conclusion, the developments presented in this thesis provide the next level of an improved implementation and theory of the TEA method. This work demonstrated in practice the actual fitness and the potential for wider applications of the TEA method as a reliable direct method to measure atmospheric fluxes.

Key words Micrometeorology, flux measurements, true eddy accumulation, eddy covariance, spectral corrections.

Zusammenfassung

Wechselwirkungen zwischen der Biosphäre und der Atmosphäre haben weitreichende Auswirkungen auf das globale Klima und die zukünftige Entwicklung der Erde. Um die Dynamik und die Einflussgrößen dieser Wechselwirkungen zu verstehen, ist es notwendig, den Energie- und Materieaustausch (oder -fluss) zwischen der Erdoberfläche und der Atmosphäre kontinuierlich zu erfassen. Die Eddy-Kovarianz (EK) Methode ist die State-of-the-Art Methode zur direkten Messung des Energie- und Impulsaustauschs, sowie des Austauschs verschiedener wichtiger atmosphärischer Komponenten wie zum Beispiel CO_2 und H_2O. Die EK Methode kann jedoch nur für einige wenige Komponenten der Atmosphäre verwendet werden, für die Gasanalysatoren mit ausreichend hoher Messfrequenz vorhanden sind. Eine alternative Methode zur Messung von Flussgrößen bietet die auf langsamen Gasanalysatoren basierende sogenannte echte Eddy Akkumulation (oder: true eddy accumulation, TEA). Diese Methode nutzt die konditionale Entnahme einer Luftprobe, um die Notwendigkeit einer hohen Messfrequenz der skalaren Konzentration zu überwinden. Diese Methode hat etliche vielversprechende Anwendungen für mikrometeorologische Messungen. Allerdings haben verschiedene Herausforderungen, sowohl im Bereich der Theorie als auch in der Umsetzung eine weitreichende Einführung der TEA Methode verhindert. Diese Doktorarbeit zielt darauf ab, sowohl die Theorie als auch die Implementierung der TEA Methode zu verbessern, um diese zu einem verlässlichen Werkzeug zur Analyse von Austauschprozessen zwischen Erdoberfläche und Atmosphäre zu machen. Zuerst wird als Machbarkeitsnachweis eine neue Implementierung eines TEA Systems vorgestellt. Das neue System basiert auf neuen dynamischen Massenflussreglern, mit denen die turbulenten Prozesse mit Messfrequenzen von 10 Hz oder mehr aufgelöst werden können. Flussmessungen des Spurengases Kohlenstoffdioxid mit dem neuen System zeigten eine gute Übereinstimmung mit einem konventionellen EK-Referenzsystem. (R^2 = 0.86, Steigung 0.98). Das neue System stellte sich mehrerer Herausforderungen bei der Umsetzung der TEA Methode, wie zum Beispiel die Automatisierung des Gastransports und die Echtzeitberechnung der Windstatistik.

Die Arbeit, die hier präsentiert wird, hat zur Verifikation des neuen Massenflussreglers im Feld, zur Charakterisierung von Dichteeffekten bei der Entnahme einer Luftprobe und zur Berechnung der gemessenen Flüsse beigetragen.

Zweitens untersuchen wir die Problematik der TEA Methode unter nicht idealen Bedingungen, in denen die mittlere vertikale Windgeschwindigkeit nicht Null beträgt. Wir schlagen eine neue Formulierung der TEA vor, in welcher die systematischen Fehler des berechneten Flusses unter nicht-idealen Bedingungen isoliert und minimiert werden. Wir analysieren die Größe dieser systematischen Fehler und stellen zwei Methoden zur Fehlerabschätzung und Fehlerkorrektur vor. Anschließend zeigen wir, wie die unterschiedlichen Formulierungen der TEA Methode mit den neuen Formeln zur Fehlerabschätzung zusammenhängen und evaluieren sie mit den hier vorgestellten Korrekturmethoden.

Drittens untersuchen wir die Beschränkungen, die sich durch die feste Akkumulationszeit in der konventionellen Formulierung der TEA ergeben. Wir stellen eine neue Variation der Eddy-Akkumulation vor, die diese Beschränkungen überwindet. Diese neue Methode, im Folgenden bezeichnet als Kurzzeit-Eddy-Akkumulations (oder: short-time eddy accumulation – STEA), ermöglicht robustere und flexiblere

Verfahren der Probennahme und erlaubt die Realisierung eines Akkumulationssystems mit kontinuierlichem Durchfluss. Ein TEA System mit kontinuierlichem Durchfluss (oder: flow-through TEA) wurde bereits früher entwickelt, um die Komplexität und die Nichtstationarität zu begrenzen, die mit einem auf variablen Probevolumen basierenden Akkumulationssystem (Luftakkumulation in Probenahmetüten) zusammenhängen. Die STEA Formulierung erweitert das flow-through TEA System und ermöglicht eine gründliche Behandlung kontinuierlicher Probenakkumulation. Ein STEA System wurde über einer Agrarfläche implementiert und mit einem EC-Referenzsystem evaluiert. Die mit den beiden verschiedenen Systemen gemessenen Flüsse stimmten sehr gut überein und ergaben ein R^2 von 0.87 bei einer Steigung von 1.04. Die Verwendung von Puffervolumen mit der STEA Methode wurde analysiert und hierfür wurde eine empirische Korrektur aufgestellt. Zum Schluss analysieren wir das Problem der spektralen Dämpfung in gemessenen Atmosphärensignalen, um eine direkte Methode zur spektralen Korrektur zu entwickeln, die für TEA Messungen verwendet werden kann. Diese Analyse zeigt, dass durch die konventionellen Methoden zur spektralen Korrektur systematische Fehler und Unsicherheiten in den korrigierten Flüssen entstehen, die sich auf die Annahmen spektraler Ähnlichkeiten, die Nutzung ungeeigneter Transferfunktionen und auf die Vernachlässigung nichtlinearer Phasenbeiträge zurückführen lassen. Wir stellen eine neue, direkte, auf Wiener-Dekonvolution basierende Korrekturmethode vor. Diese neue Methode hat viele Vorteile und ist frei von der Annahme eines idealen Spektrums für jedes Mittelungsintervall. Aus diesem Grund kann sie verwendet werden, um die mit dem TEA System gemessenen Atmosphärensignale zu korrigieren, während hier die Annahme eines idealen Spektrums schwer zu rechtfertigen ist. Die Entwicklungen, die in dieser Arbeit vorgestellt werden, heben die TEA Methode durch Verbesserungen in Umsetzung und Theorie schlussendlich auf die nächste Ebene. Diese Arbeit zeigte im Praxistest die tatsächliche Eignung der TEA Methode als eine zuverlässige direkte Methode zur Messung von Austauschprozessen in der Atmosphäre mit Potenzial für breitere Anwendungsgebiete.

Declaration

I hereby declare that I wrote this PhD thesis under the supervision of Dr. Lukas Siebicke and Prof. Alexander Knohl. Any sources of information and used literature have been acknowledged.

Göttingen, January 2023 Anas Emad

Contents

1 Introduction

1.1 Background

1.1.1 Biosphere-atmosphere interactions

The biosphere-atmosphere interactions are fundamental to the study of the Earth system. Biological, physical, and chemical processes in the biosphere have a large influence on regional and global environmental conditions. The release and uptake of trace gases such as CO_2 and CH_4 change the physical and chemical properties of the atmosphere. Similarly, processes in the biosphere affect the earth's energy budget by modifying the energy flow and radiative forcings in the climate system. In turn, the composition of the atmosphere and the state of the climate have direct influences on the functioning and health of individual organisms and ecosystems (Fowler et al., 2009; Scholes et al., 2003). The mutual interactions create strong positive and negative feedbacks that determine how the Earth system develops in time (Fig. 1.1).

The Earth system is best studied as a dynamic system evolving in time. Therefore, monitoring the development of the system state through time is a critical step toward understanding and potentially controlling the trajectories of the system. Characterizing the system state is only possible if the exchange rates of energy and matter between the different components of the earth system (the fluxes) are measured. The study of fluxes across space and time helps to understand the functioning of the different components of the earth system and predict their response to change (Baldocchi, 2020). For example, carbon and water fluxes improve the understanding of the role of the terrestrial biosphere in the global carbon cycle. Furthermore, modeling these fluxes allows for making predictions about the future state of the earth system. Understanding the controls of the fluxes is critical as it enables predicting the response of the system to disturbances and the development of potential management strategies, such as land use and forest management (Monson and Baldocchi, 2014). In addition to carbon and water, the fluxes of gaseous pollutants (O_3, NO_2, NO, SO_2), aerosols, and microplastic are important to the study of atmospheric chemistry and pollutant transport (Scholes et al., 2003). The concept of flux is not limited to gaseous atmospheric constituents but is also useful for studying biological particles in the atmosphere such as bacteria and DNA (Burrows et al., 2009).

The first few kilometers of the atmosphere closest to the earth's surface play a major role in the exchange processes. This layer is directly influenced by the earth's surface and is known as the atmospheric boundary layer (ABL). ABL acts as an active link between the atmosphere and the surface. The earth's surface affects the ABL through forcings such as friction, evaporation and transpiration, heat and matter

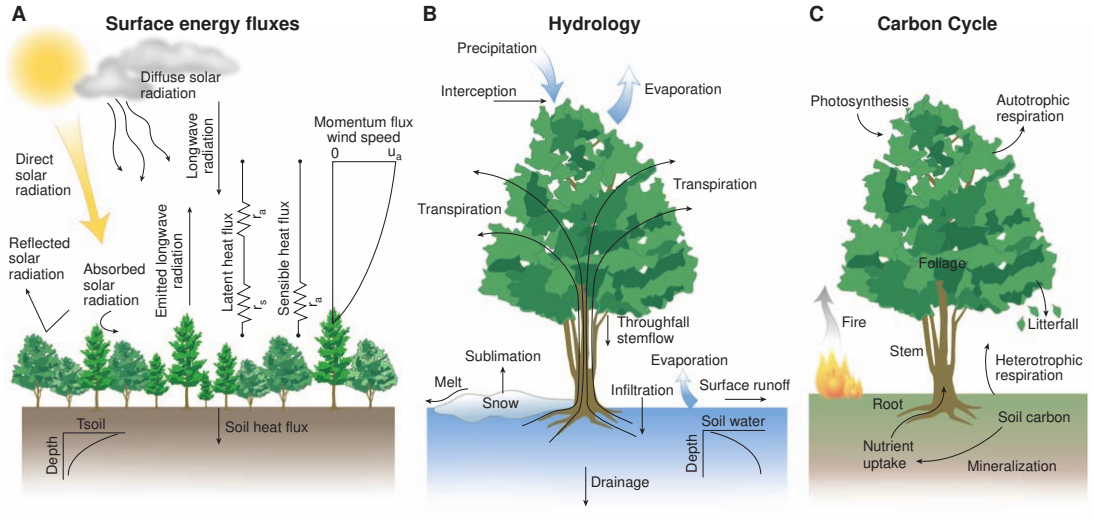

Figure 1.1: Examples of biosphere-atmosphere interactions. Fluxes play a central role in the exchange of energy, momentum and atmospheric constituents between the terrestrial vegetation and the atmosphere. Fluxes profoundly shape the energy balance, the hydrological cycle, and the carbon cycle by transporting the trace gases and energy produced and modulated by plants and the soil. Adapted from (Bonan, 2008).

transfer, and flow modifications (Stull, 1988). The transport in the boundary layer is mainly driven by the mixing of air by atmospheric turbulence. Turbulent flows are generated by solar heating and the frictional drag of air flowing over the surface. Turbulent flows are characterized by a superposition of chaotic swirls of motion called eddies. Eddies have different scales ranging from the depth of the boundary layer to the scale of diffusion by molecular viscosity. Eddies can be best seen as superimposed waves of different sizes. Therefore, the frequency representation as waves (spectra and cospectra) is very useful for studying turbulent flows. Spectral representation of measured atmospheric signals allows associating the contribution of each frequency scale to the total variance or covariance (Kaimal and Finnigan, 1994).

Fluxes in the atmosphere span several orders of magnitude of time and space. On the scale of plant canopies, micrometeorological methods provide an integrated measurement of atmospheric fluxes suitable for ecosystem research. The most common micrometeorological method is the eddy covariance method.

1.1.2 Eddy covariance method

The eddy covariance (EC) method is the most common method to measure the atmospheric fluxes on the scale of plant canopies. The EC method is considered a direct method as it does not require modeled parameters or empirical estimates to calculate the flux (Baldocchi, 2003; Hicks and Baldocchi, 2020).

EC provides continuous and non-invasive observations of atmospheric fluxes. Currently, EC measurements are regularly collected around the world across different environments and ecosystem types. The majority of sites are organized in regional and global networks with more than 900 sites registered in FLUXNET (Baldocchi et al., 2001).

Theoretically, the turbulent flux in the EC method is found from the principles of energy and mass conservation. The turbulent flux is expressed as the covariance between the vertical wind velocity w and the concentration of the atmospheric constituent of interest (such as CO_2).

$$\mathrm{F}_{ec} = \overline{\rho}\,\overline{w'c'} \tag{1.1}$$

Here, w is the vertical wind velocity, c is the concentration of the atmospheric constituent (amount fraction), $\overline{\rho}$ is the averaged air density, overbars represent averaging that obeys Reynolds rules and the primes are deviations from the mean. The previous formulation is reached under the simplifying assumption of horizontal homogeneity and stationarity. Horizontal homogeneity implies that the mean fluxes in the streamwise and lateral coordinates are zero. Stationarity assumes that the measured time series statistics are stable with respect to time. If these assumptions are met, the total ecosystem flux at the measurement height h is assumed to be equal to the measured eddy flux (Foken and Nappo, 2008).

A typical EC setup consists of an ultrasonic anemometer and a gas analyzer. High measurement frequencies (> 10Hz) are required to resolve the turbulent frequencies relevant to scalar transport. Measured quantities required for calculating EC fluxes are prone to systematic errors and require multiple corrections to reach the final flux. Despite the efforts to standardize the processing of EC fluxes, there is no consensus on the optimal calculation scheme and flux corrections. Several challenges related to the representativeness and correctness of the flux remain open (Hicks and Baldocchi, 2020).

The availability of fast-response sensors remains a major obstacle limiting the EC method to a handful of atmospheric constituents. The true eddy accumulation method (TEA) aims to solve this challenge.

1.1.3 True eddy accumulation method

For many atmospheric constituents, available gas analyzers are not fast enough or not suitable for field and continuous operation. Therefore, the fluxes of these constituents can not be measured directly with the EC method. To overcome this limitation, several methods that work with slow-response gas analyzers have been developed (Rinne et al., 2021). Among these methods, the true eddy accumulation method (TEA) is the most direct and mathematically equivalent to eddy covariance (Desjardins, 1972; Hicks and McMillen, 1984).

The TEA method depends on the conditional sampling and accumulation of air for later measurements. In its essence, the product of the scalar concentration and the vertical wind velocity, wc is realized physically by accumulating a sample of air that has a mass proportional to the magnitude of vertical wind velocity (Fig 1.2). Therefore, for the flux integration periods, the air is collected at a mass flow rate proportional to the magnitude of vertical wind velocity. The collected samples are stored in updraft or downdraft reservoirs depending on the direction of the vertical wind velocity. The flux is then calculated for the averaging interval as the difference between the accumulated mass in updraft and downdraft reservoirs.

$$\mathrm{F}_{\mathrm{tea}} = \bar{\rho}\left(\overline{c^{\uparrow}|w^{\uparrow}|} - \overline{c^{\downarrow}|w^{\downarrow}|}\right) \tag{1.2}$$

where the arrows indicate the direction of the vertical wind velocity (updraft or downdraft).

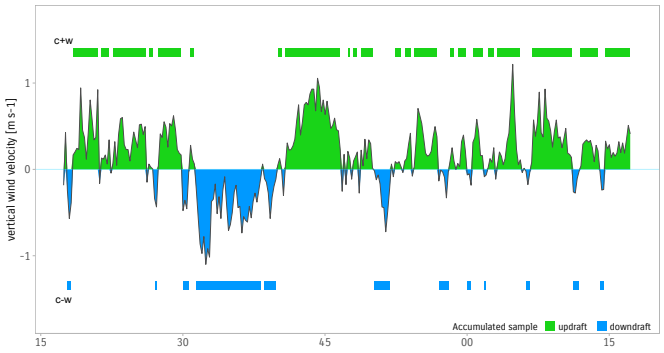

Figure 1.2: Conceptual figure of the true eddy accumulation method principle. Samples of air are collected with a flow rate proportional to the magnitude of vertical wind velocity and partitioned following its sign into updraft and downdraft reservoirs. The flux is directly related to the difference in accumulated mass between updraft and downdraft.

1.2 Challenges to the true eddy accumulation and eddy covariance methods

Despite the promising potential of the TEA method to replace indirect micrometeorological methods as a direct and accurate flux measurement method, it has faced several challenges in theory and implementation that prevented its widespread adoption (Businger and Oncley, 1990). Besides the common challenges shared with the EC method such as the representation of the fluxes and the spectral attenuation, TEA has unique additional constraints due to the lack of high-frequency scalar concentration information. A graphical summary of the challenges addressed in this thesis is provided in Fig 1.3.

The challenges addressed in this thesis are:

- **Unavailable field-ready TEA implementation.** A field-ready TEA implementation of sufficient performance is not available. Two components to implement a TEA system are needed: a fast air sampler, and the required processing pipeline to handle real-time wind statistics.

- **TEA under non-ideal conditions.** The TEA method is formulated under the assumption of ideal conditions where the mean vertical wind velocity is zero. This assumption is rarely met and can not be imposed in post-processing which leads to a systematically biased flux.

- **Accumulation time limitations.** Conventional TEA formulation is restricted in binding the sample accumulation time to the flux averaging time, a more flexible approach is needed.

- **Frequency losses**. Similar to EC measurements, fluxes measured with the TEA method suffer from unavoidable frequency losses due to instrumental and practical limitations. A direct spectral correction method suitable for EC and TEA is desired to avoid the dependence on the assumptions of ideal spectra and spectral similarity.

Figure 1.3: Conceptual figure showing the main true eddy accumulation challenges addressed in this thesis categorized by four distinct categories. The challenges are numbered by the order they appear in the thesis. A comparison with the eddy covariance method for each category is provided as a reference.

1.3 Objectives

The overarching goal of this thesis is to develop the TEA method as a reliable tool to observe ecosystem fluxes by addressing its most critical limitations. This goal is demonstrated in the following specific objectives

- To evaluate the initial proof-of-concept TEA system by improving the implementation and verification of field performance of the TEA sampler and developing the flux processing pipeline.
- To extend the theory of the TEA method to non-ideal conditions under which the assumption of zero mean vertical wind velocity is violated.
- To develop the theory and improve the implementation of a robust and more flexible continuous flow-through eddy accumulation system. In particular, developing a rigorous theoretical framework for the sample accumulation in flow-through mode and modeling the effect of buffer volumes used in the flow-through TEA.
- To develop a direct spectral correction scheme for attenuated measured atmospheric signals that does not assume spectral similarity such that it can be used for EC and TEA.

1.4 Structure of the thesis

The four scientific contributions of this thesis are presented in the following chapters

- **Chapter 2: True eddy accumulation trace gas flux measurements: proof of concept**
  Paper published in *Atmospheric measurement techniques* (Siebicke and Emad, 2019). Siebicke, L. and Emad, A.: True Eddy Accumulation Trace Gas Flux Measurements: Proof of Concept, Atmospheric Measurement Techniques, 12, 4393–4420, doi:10.5194/amt-12-4393-2019, 2019.

  This study presents an implementation and evaluation of a TEA system. A proof-of-concept TEA sampler with a novel dynamic flow rate controller is presented and evaluated against a reference conventional EC system. My contribution to this paper was evaluating the field performance of the new mass flow controllers, developing calibration routines, characterizing the effect of air density on sample accumulation and scalar concentration, developing the flux processing software for TEA flux calculation, and processing the raw data to produce the final fluxes.

- **Chapter 3: True eddy accumulation Part 1: Solutions to the problem of non-vanishing mean vertical wind velocity**
  Paper published in *Atmospheric measurement techniques* and selected as highlight paper (Emad and Siebicke, 2023a).
  Emad, A. and Siebicke, L.: True eddy accumulation – Part 1: Solutions to the problem of non-vanishing mean vertical wind velocity, Atmos. Meas. Tech., 16, 29–40,
  doi:10.5194/amt-16-29-2023, 2023.

  This study investigates the TEA method under non-ideal conditions and proposes solutions to constrain and correct the systematic error due to nonzero mean vertical wind velocity.

- **Chapter 4 True eddy accumulation – Part 2: Theory and experiment of the short-time eddy accumulation method**
  Paper published in *Atmospheric measurement techniques* (Emad and Siebicke, 2023b).
  Emad, A. and Siebicke, L.: True eddy accumulation – Part 2: Theory and experiment of the short-time eddy accumulation method, Atmos. Meas. Tech., 16, 41–55,
  doi:10.5194/amt-16-41-2023, 2023.

  This paper focuses on the limitation of the fixed accumulation time in the TEA method and proposes a new variant eddy accumulation method called short-time eddy accumulation (STEA) which brings multiple advantages to flux measurements. The work presented in this paper extends the flow-through TEA system by developing theoretical frameworks for continuous sample accumulation and the effect of buffer volumes. An experimental implementation of STEA is evaluated and discussed.

- **Chapter 5 Optimal frequency-response corrections for eddy covariance flux measurements using the Wiener deconvolution method**
  Paper published in *Boundary layer meteorology* (Emad, 2023).
  Emad, Anas: Optimal Frequency-Response Corrections for Eddy Covariance Flux Measurements Using the Wiener Deconvolution Method, Boundary-Layer Meteorology, 188, 29–53, doi:10.1007/s10546-023-00799-w, 2023.

  This paper presents an analysis of the problem of spectral attenuation of measured atmospheric signals and puts forward a direct correction scheme based on Wiener deconvolution. The problems of conventional methods are identified and explored in a numerical simulation including the effects of using inappropriate transfer functions, the contributions of the nonlinear phase, and the consequences of spectral similarity assumptions.

- **Chapter 6 Technical note: An integrated platform for near real-time flux data management and analysis**
  This chapter presents the development of a data management and processing platform for flux data. The principles of data traceability, interoperability, quality control, and accessibility are discussed in the context of flux measurements. The system architecture and technical implementation are detailed.

Bibliography

Baldocchi, D., Falge, E., Gu, L., Olson, R., Hollinger, D., Running, S., Anthoni, P., Bernhofer, C., Davis, K., Evans, R., Fuentes, J., Goldstein, A., Katul, G., Law, B., Lee, X., Malhi, Y., Meyers, T., Munger, W., Oechel, W., Paw, K. T., Pilegaard, K., Schmid, H. P., Valentini, R., Verma, S., Vesala, T., Wilson, K., Wofsy, S., Baldocchi, D., Falge, E., Gu, L., Olson, R., Hollinger, D., Running, S., Anthoni, P., Bernhofer, C., Davis, K., Evans, R., Fuentes, J., Goldstein, A., Katul, G., Law, B., Lee, X., Malhi, Y., Meyers, T., Munger, W., Oechel, W., Paw, K. T., Pilegaard, K., Schmid, H. P., Valentini, R., Verma, S., Vesala, T., Wilson, K., and Wofsy, S.: FLUXNET: A New Tool to Study the Temporal and Spatial Variability of Ecosystem–Scale Carbon Dioxide, Water Vapor, and Energy Flux Densities, Bulletin of the American Meteorological Society, 82, 2415–2434, doi:10.1175/1520-0477(2001)082<2415:FANTTS>2.3.CO;2, 2001.

Baldocchi, D. D.: Assessing the Eddy Covariance Technique for Evaluating Carbon Dioxide Exchange Rates of Ecosystems: Past, Present and Future, Global Change Biology, 9, 479–492, doi:10.1046/j.1365-2486.2003.00629.x, 2003.

Baldocchi, D. D.: How Eddy Covariance Flux Measurements Have Contributed to Our Understanding of Global Change Biology, Global Change Biology, 26, 242–260, doi:10.1111/gcb.14807, 2020.

Bonan, G. B.: Forests and Climate Change: Forcings, Feedbacks, and the Climate Benefits of Forests, Science, 320, 1444–1449, doi:10.1126/science.1155121, 2008.

Burrows, S. M., Elbert, W., Lawrence, M. G., and Pöschl, U.: Bacteria in the Global Atmosphere – Part 1: Review and Synthesis of Literature Data for Different Ecosystems, Atmospheric Chemistry and Physics, 9, 9263–9280, doi:10.5194/acp-9-9263-2009, 2009.

Businger, J. A. and Oncley, S. P.: Flux Measurement with Conditional Sampling, Journal of Atmospheric and Oceanic Technology, 7, 349–352, doi:10.1175/1520-0426(1990)007<0349:FMWCS>2.0.CO;2, 1990.

Desjardins, R. L.: A Study of Carbon Dioxide and Sensible Heat Fluxes Using the Eddy Correlation Technique, Cornell University, 1972.

Emad, A.: Optimal Frequency-Response Corrections for Eddy Covariance Flux Measurements Using the Wiener Deconvolution Method, Boundary-Layer Meteorology, 188, 29–53, doi:10.1007/s10546-023-00799-w, 2023.

Emad, A. and Siebicke, L.: True Eddy Accumulation – Part 1: Solutions to the Problem of Non-Vanishing Mean Vertical Wind Velocity, Atmospheric Measurement Techniques, 16, 29–40, doi:10.5194/amt-16-29-2023, 2023a.

Emad, A. and Siebicke, L.: True Eddy Accumulation – Part 2: Theory and Experiment of the Short-Time Eddy Accumulation Method, Atmospheric Measurement Techniques, 16, 41–55, doi:10.5194/amt-16-41-2023, 2023b.

Foken, Th. and Nappo, C. J.: Micrometeorology, Springer, 2008.

Fowler, D., Pilegaard, K., Sutton, M. A., Ambus, P., Raivonen, M., Duyzer, J., Simpson, D., Fagerli, H., Fuzzi, S., Schjoerring, J. K., Granier, C., Neftel, A., Isaksen, I. S. A., Laj, P., Maione, M., Monks, P. S., Burkhardt, J., Daemmgen, U., Neirynck, J., Personne, E., Wichink-Kruit, R., Butterbach-Bahl, K., Flechard, C., Tuovinen, J. P., Coyle, M., Gerosa, G., Loubet, B., Altimir, N., Gruenhage, L., Ammann, C., Cieslik, S., Paoletti, E., Mikkelsen, T. N., Ro-Poulsen, H., Cellier, P., Cape, J. N., Horváth, L., Loreto, F., Niinemets, Ü., Palmer, P. I., Rinne, J., Misztal, P., Nemitz, E., Nilsson, D., Pryor, S., Gallagher, M. W., Vesala, T., Skiba, U., Brüggemann, N., Zechmeister-Boltenstern, S., Williams, J., O'Dowd, C., Facchini, M. C., de Leeuw, G., Flossman, A., Chaumerliac, N., and Erisman, J. W.: Atmospheric Composition Change: Ecosystems–Atmosphere Interactions, Atmospheric Environment, 43, 5193–5267, doi:10.1016/j.atmosenv.2009.07.068, 2009.

Hicks, B. B. and Baldocchi, D. D.: Measurement of Fluxes Over Land: Capabilities, Origins, and Remaining Challenges, Boundary-Layer Meteorology, 177, 365–394, doi:10.1007/s10546-020-00531-y, 2020.

Hicks, B. B. and McMillen, R. T.: A Simulation of the Eddy Accumulation Method for Measuring Pollutant Fluxes, Journal of Climate and Applied Meteorology, 23, 637–643, doi:10.1175/1520-0450(1984)023<0637:ASOTEA>2.0.CO;2, 1984.

Kaimal, J. C. and Finnigan, J. J.: Atmospheric Boundary Layer Flows: Their Structure and Measurement, Oxford University Press, 1994.

Monson, R. and Baldocchi, D.: Terrestrial Biosphere-Atmosphere Fluxes, Cambridge University Press, Cambridge, doi:10.1017/CBO9781139629218, 2014.

Rinne, J., Ammann, C., Pattey, E., Paw U, K. T., and Desjardins, R. L.: Alternative Turbulent Trace Gas Flux Measurement Methods, in: Springer Handbook of Atmospheric Measurements, edited by Foken, T., Springer Handbooks, pp. 1505–1530, Springer International Publishing, Cham, doi:10.1007/978-3-030-52171-4_56, 2021.

Scholes, M., Matrai, P., Andreae, M., Smith, K., Manning, M., Artaxo, P., Barrie, L., Bates, T., Butler, J., Ciccioli, P., Cieslik, S., Delmas, R., Dentener, F., Duce, R., Iii, D. E., Galbally, I., Guenther, A., Jaenicke, R., Jähne, B., Kettle, A., Kiene, R., Lacaux, J.-P., Liss, P., Malin, G., Matson, P., Mosier, A., Neue, H.-U., Paerl, H., Platt, U., Quinn, P., Seiler, W., and Weiss, R.: Biosphere-Atmosphere Interactions, in: Atmospheric Chemistry in a Changing World. An Integration and Synthesis of a Decade of Tropospheric Chemistry Research, Series Global Change, the IGBP Series, pp. 19–71, doi:10.1007/978-3-642-18984-5_2, 2003.

Siebicke, L. and Emad, A.: True Eddy Accumulation Trace Gas Flux Measurements: Proof of Concept, Atmospheric Measurement Techniques, 12, 4393–4420, doi:10.5194/amt-12-4393-2019, 2019.

Stull, R. B.: An Introduction to Boundary Layer Meteorology, Atmospheric and Oceanographic Sciences Library, Springer Netherlands, doi:10.1007/978-94-009-3027-8, 1988.

2 True eddy accumulation trace gas flux measurements: proof of concept

Paper published in *Atmospheric measurement techniques* (Siebicke and Emad, 2019).

Siebicke, L. and Emad, A.: True Eddy Accumulation Trace Gas Flux Measurements: Proof of Concept, *Atmospheric Measurement Techniques*, 12, 4393–4420, doi:10.5194/amt-12-4393-2019, 2019.

Abstract

Micrometeorological methods to quantify fluxes of atmospheric constituents are key to understanding and managing the impact of land surface sources and sinks on air quality and atmospheric composition.

Important greenhouse gases are water vapor, carbon dioxide, methane, and nitrous oxide. Further important atmospheric constituents are aerosols, which impact air quality and cloud formation, and volatile organic compounds. Many atmospheric constituents therefore critically affect the health of ecosystems and humans, as well as climate.

The micrometeorological eddy covariance (EC) method has evolved as the method of choice for CO_2 and water vapor flux measurements using fast-response gas analyzers. While the EC method has also been used to measure other atmospheric constituents including methane, nitrous oxide, and ozone, the often relatively small fluxes of these constituents over ecosystems are much more challenging to measure using eddy covariance than CO_2 and water vapor fluxes. For many further atmospheric constituents, eddy covariance is not an option due to the lack of sufficiently accurate and fast-response gas analyzers.

Therefore, alternative flux measurement methods are required for the observation of atmospheric constituent fluxes for which no fast-response gas analyzers exist or which require more accurate measurements. True eddy accumulation (TEA) is a direct flux measurement technique capable of using slow-response gas analyzers. Unlike its more frequently used derivative, known as the relaxed eddy accumulation (REA) method, TEA does not require the use of proxies and is therefore superior to the indirect REA method.

The true eddy accumulation method is by design ideally suited for measuring a wide range of trace gases and other conserved constituents transported with the air. This is because TEA obtains whole air samples and is, in combination with constituent-specific fast or slow analyzers, a universal method for conserved scalars.

Despite the recognized value of the method, true eddy accumulation flux measurements remain very challenging to perform as they require fast and dynamic modulation of the air sampling mass flow rate proportional to the magnitude of the instantaneous vertical wind velocity. Appropriate techniques for dynamic mass flow control have long been unavailable, preventing the unlocking of the TEA method's potential for more than 40 years.

Recently, a new dynamic and accurate mass flow controller which can resolve turbulence at a frequency of 10 Hz and higher has been developed by the first author. This study presents the proof of concept that practical true eddy accumulation trace gas flux measurements are possible today using dynamic mass flow control, advanced real-time processing of wind measurements, and fully automatic gas handling.

We describe setup and methods of the TEA and EC reference flux measurements. The experiment was conducted over grassland and comprised 7 d of continuous flux measurements at 30 min flux integration intervals. The results show that fluxes obtained by TEA compared favorably to EC reference flux measurements, with coefficients of determination of up to 86 % and a slope of 0.98.

We present a quantitative analysis of uncertainties of the mass flow control system, the gas analyzer, and gas handling system and their impact on trace gas flux uncertainty, the impact of different approaches to coordinate rotation, and uncertainties of vertical wind velocity measurements.

Challenges of TEA are highlighted and solutions presented. The current results are put into the context of previous works. Finally, based on the current successful proof of concept, we suggest specific improvements towards long-term and reliable true eddy accumulation flux measurements.

2.1 Introduction

The ability to observe the exchange of trace gases between the earth's surface and the atmosphere is key to understanding the functioning of ecosystems. Trace gas flux measurements allow quantification of how natural and anthropogenic systems affect atmospheric composition.

Many studies over the past decades have observed carbon dioxide (CO_2) and water vapor fluxes at ecosystem scale using micrometeorological methods (Baldocchi et al., 1988). Eddy covariance (EC) (Baldocchi, 2003, 2014) has become the most widely used method for measuring turbulent fluxes. Today the EC method is routinely being applied the world over including the major flux networks FLUXNET, ICOS, and NEON.

The EC method requires fast-response gas analyzers which only exist for a few trace gas species, above all CO_2 and water vapor but more recently also other trace gases, including methane (CH_4) and nitrous oxide (N_2O). However, for a large number of trace gases and atmospheric constituents, the applicability of the EC method is limited by a lack of fast-response gas analyzers, by the high power demand necessary for sustaining high sample flow rates in some closed-path gas analyzer systems, and by a possibly small signal-to-noise ratio of high-frequency measurements.

A number of alternative turbulent flux measurement methods exist which can use slow-response gas analyzers and might provide more accurate results than eddy covariance with fast-response analyzers. These methods are applicable to a wide range of conserved trace gases, isotopes, aerosols, volatile organic compounds, and other atmospheric constituents. An overview on selected micrometeorological methods applicable to slow-response gas analyzers follows, presenting the air sampling principles and timings and stating advantages and disadvantages of each method.

True eddy accumulation (TEA) is an alternative to the EC method. Unique properties of the TEA method are highlighted which make TEA stand out from other methods. This study is a contribution towards a practical implementation of the TEA method.

2.1.1 Micrometeorological methods suitable for slow-response gas analyzers

True eddy accumulation (TEA)

True eddy accumulation (Desjardins, 1977; Hicks and McMillen, 1984) refers to the sampling of air, separating updrafts and downdrafts on the condition of the sign of the vertical wind velocity. The mass flow rate of physical air samples needs to be proportional to the magnitude of the vertical wind velocity and controlled at 10 Hz or above to resolve flux-relevant turbulence scales. For conserved scalars, the net flux can then be determined from the difference in scalar concentration between the accumulated updraft and downdraft samples, respectively, over a certain flux integration interval, e.g., 30 min.

The idea of eddy accumulation (EA) goes back to early considerations by Desjardins (1972) who proposed the method for physically sampling trace gas fluxes. He reported a first experiment of conditionally sampling temperature and deriving sensible heat flux through mathematical accumulation (Desjardins, 1977). We use the term "true eddy accumulation" rather than just "eddy accumulation" to

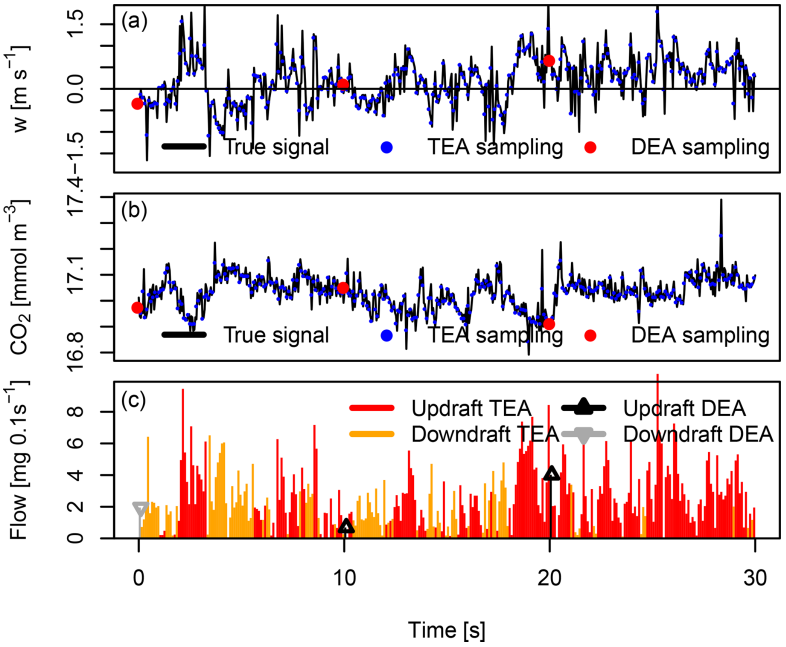

Figure 2.1: True eddy accumulation (TEA; see Sect. 2.1.1) and disjunct eddy accumulation (DEA; see Sect. 2.1.1) sampling scheme. Vertical wind, w, **(a)**, scalar density, CO_2, **(b)** and vertical wind proportional mass flow rate **(c)**. Black solid lines indicate the continuous true atmospheric signal. Sampling resolution of TEA and DEA are 10 Hz and 10 s, respectively. Note that active sampling time for DEA is only 1 % of the sampling time for TEA.

refer to the original formulation of eddy accumulation (Desjardins, 1977; Hicks and McMillen, 1984), specifically with vertical wind proportional air sampling, as opposed to later derivatives of eddy accumulation such as “relaxed eddy accumulation”, which is subject to constant mass flow and further limitations (see Sect. 2.1.1).

Literature on true eddy accumulation is sparse, with just over a dozen published studies. Very few studies performed actual flux measurements. Desjardins (1977), Speer et al. (1985), Neumann et al. (1989), Beier (1991), and Komori et al. (2004) presented early prototypes of true eddy accumulators and disjunct true eddy accumulators (Rinne et al., 2000). Others conducted simulations (Hicks and McMillen, 1984; Businger and Oncley, 1990) and contributed technology (Buckley et al., 1988) and reviews (Businger, 1986; Speer et al., 1986; Hicks et al., 1986). However, its practical implementation has long been difficult, particularly the accurate and dynamic control of mass flow rates. None of the experiments above produced significant long-term data sets. Correlation of TEA fluxes with EC fluxes was generally relatively low with coefficients of determination of, e.g., $R^2 = 0.07$ (Speer et al., 1985), $R^2 = 0.41$ (Neumann et al., 1989), and $R^2 = 0.64$ (Komori et al., 2004). Until today there has been no TEA instrument commercially available.

Recently we have successfully performed a series of TEA flux experiments using a new and fully digital approach to dynamic and fast mass flow control and real-time processing of wind data. We are further working to advance TEA flux corrections and TEA simulations. Those experiments (unpublished) yielded a tight correlation between TEA and EC flux measurements, with coefficients of determination of up to $R^2 = 0.96$, exceeding R^2 values from any of the above cited literature. The current work presents the first of the TEA and EC intercomparison experiments performed over short vegetation during spring 2015 in detail.

The concept of the TEA sampling scheme is illustrated in Fig. 2.1. The true vertical wind velocity (Fig. 1a, black line) is sampled at a frequency of, e.g., 10 Hz (Fig. 1a, blue dots), using an ultrasonic anemometer. Likewise, the air sampling device samples the true atmospheric time series of the scalar, e.g., CO_2 (Fig. 1b, black line), at the same time resolution of 10 Hz (Fig. 1b, blue dots). The time variable flow rates at which samples are being accumulated are shown in Fig. 1c. Separate accumulation of updrafts (red lines) and downdrafts (orange lines) is distinguished.

Following whole air sampling, the atmospheric constituent of interest can be trapped in a number of ways. Constituents can be accumulated as whole air samples in bags, absorbed in gas washing reservoirs, adsorbed on to chemicals using cartridges, continuously sampled with denuders, trapped as reaction products with chemicals, or retained using mechanical filters.

The true eddy accumulation principle is not limited to passive trace gases. Here, we suggest that the TEA method has the potential to measure fluxes of dust, pollen, bacteria, fungi, and other biological material carrying physical, chemical, and genetic information. The latter materials can be accumulated on appropriate filter media.

True eddy accumulation has a number of advantages over other methods. Sample accumulation over the duration of typical flux averaging intervals of 30 to 60 min allows for the use of slow-response gas analyzers. The key advantage of TEA over EC is the applicability to a much wider range of atmospheric constituents, assuming that slow-response analyzers are more readily available than fast-response analyzers, and better accuracy can be obtained through signal averaging.

The key advantage of TEA over other variants of eddy accumulation, i.e., relaxed eddy accumulation or hyperbolic relaxed eddy accumulation, is that true eddy accumulation is the only direct method in the family of accumulation methods. As a direct method it does not require the use of proxies (other scalars) and coefficients like the β coefficient in relaxed eddy accumulation and therefore does not depend on scalar similarity (Ruppert et al., 2006). This property of a direct measurement method is essential for quantifying fluxes of constituents which cannot be measured by other means (e.g., the EC method). Scalar similarity of the fluxes of the constituent of interest and the proxy cannot be assessed without first quantifying both fluxes themselves. The direct TEA method is independent of prior knowledge.

Another advantage over other types of eddy accumulation (relaxed eddy accumulation or hyperbolic relaxed eddy accumulation) or any type of disjunct eddy sampling (e.g., the disjunct eddy covariance method or the disjunct eddy accumulation method) is the continuous sampling of the air by the TEA method such that the signal is recovered in its entirety. Continuous sampling avoids noise associated with disjunct sampling (Lenschow et al., 1994). Likewise, omitting samples at times of small vertical wind velocities, which is common practice in relaxed eddy accumulation, would effectively be disjunct sampling, trading in noise for the sake of higher concentration differences between accumulated updrafts and downdrafts.

The long averaging intervals further allow for repeated measurements of the same sample, improving precision. The trace gas concentration of the accumulated samples, which is by design constant, at the time of analysis and the typically long analysis integration times are best matched with low sample flow rates through the gas analyzer. Low flow rates result in low power consumption and a low pressure drop over system components. A low pressure drop is beneficial for the stability and accuracy of the gas analyzer's reading.

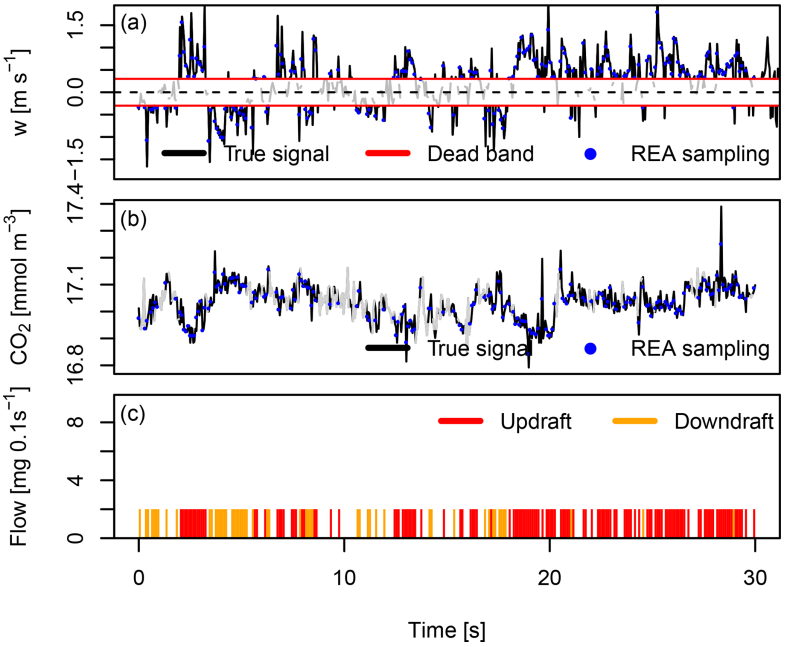

Figure 2.2: Relaxed eddy accumulation sampling scheme. Vertical wind, w **(a)**, scalar density, CO_2 **(b)**, and mass flow rate **(c)**. Black solid lines indicate the continuous true atmospheric signal. Sampling resolution of REA is 10 Hz. A fraction of the CO_2 time series (gray lines, **b**) is not sampled by REA due to use of a vertical wind velocity dead band for small velocities (thresholds indicated by red lines, **a**). This dead band causes gaps in the otherwise constant mass flow rate **(c)**.

Relaxed eddy accumulation (REA)

Given the challenges associated with the original formulation of true eddy accumulation, Businger and Oncley (1990) proposed a modified version of eddy accumulation, today known as relaxed eddy accumulation (REA). REA is based on the concept of flux–variance similarity. In order to relate the scalar flux to the variance of the vertical wind velocity, a proportionality factor, β, was introduced, so REA became an indirect method.

The advantage of the relaxed eddy accumulation method is that air is sampled at a constant flow rate (Fig. 2.2c). This meant that the dynamic high-frequency modulation of flow rates as a function of the magnitude of the vertical wind velocity as in the TEA method was no longer required. REA still accumulates updrafts and downdraft separately controlled by the sign of the vertical wind velocity.

A second modification was introduced in REA: at times of small positive or negative vertical wind velocities, no air samples are taken. This “dead band” is illustrated in Fig. 2.2a. Figure 2b shows the air sampling scheme: the true scalar time series, e.g., CO_2 density (black line), is sampled at a regular frequency of, e.g., 10 Hz (blue dots), if the vertical wind velocity (Fig. 2.2a, black line), sampled at the same 10 Hz frequency (Fig. 2.2a, blue dots), is larger than the thresholds defining the dead band. A certain fraction of the scalar time series is thus omitted from sampling (Fig. 2.2b, gray line).

The use of a dead band has two advantages: the concentration difference between the updraft and downdraft accumulated samples increases (Pattey et al., 1993; Katul et al., 1996), improving the ratio of the flux signal to the noise of the gas analyzer. Secondly, use of a dead band leads to less frequent switching between updraft and downdraft samples, which relaxes the need for fast-response valves

to some degree and would reduce material wear. However, a lack of scalar similarity can lead to flux underestimation as simulated by Ruppert et al. (2002), who also found that flux errors increased with dead-band size. Another disadvantage is the impact of the dead band on the flux itself of unknown magnitude, depending on the co-spectrum of scalar and vertical wind velocity.

The simplifications of the REA method relative to the TEA method, particularly the constant mass flow rate, have facilitated wide adoption of the REA method. More than 200 studies on REA flux measurements and simulations have been published since its description less than 30 years ago (Businger and Oncley, 1990). The significant number of REA studies suggests that there is a need for alternatives to the eddy covariance method for certain applications.

Despite being simpler to implement than TEA, REA has distinct disadvantages. Being an indirect method, the accuracy of REA remains critically dependent on the correct determination of an a priori unknown β factor. β varies with scalar and with atmospheric conditions. Typical β values obtained from measurements and simulations (Wyngaard and Moeng, 1992; Businger and Oncley, 1990; Oncley et al., 1993; Pattey et al., 1993; Baker et al., 1992; Gao, 1995; Milne et al., 1999; Katul et al., 1996; Baker, 2000; Ammann and Meixner, 2002; Held et al., 2008) are around 0.55 but range from ca. 0.4 to ca. 0.7, introducing significant uncertainty of up to several tens of percent of the measured flux.

Scalar similarity between a constituent of interest and a suitable proxy for determination of the β factor is often lacking (Ruppert et al., 2006; Cancelli et al., 2015). The alternative use of a constant β factor leads to lower accuracy of the estimated flux (Foken and Napo, 2008; Ruppert et al., 2002).

A variant of REA is hyperbolic relaxed eddy accumulation (HREA) (Shaw, 1985; Bowling et al., 1999). HREA maximizes concentration differences between accumulation reservoirs through the use of hyperbolic dead bands. Thus, HREA can resolve small fluxes such as stable isotope fluxes of ^{13}C and ^{18}O (Bowling et al., 1999; Wichura et al., 2000). However, HREA requires proxies similar to REA and omits about two-thirds of total sampling time through the use of dead bands. Dead bands can increase flux uncertainty by omitting parts of the signal due to incomplete sampling of the time series.

Disjunct eddy accumulation (DEA) and disjunct eddy covariance (DEC)

Disjunct eddy sampling (Rinne et al., 2000; Turnipseed et al., 2009) is based on considerations by Lenschow et al. (1994) for representing turbulent time series by temporal subsamples. Disjunct eddy covariance (DEC) takes very short grab samples (ca. 0.1 s), followed by a pause (e.g., 5 to 60 s) for gas analysis with relatively slow instruments. Similarly, disjunct eddy accumulation can be used to obtain short grab samples at a mass flow rate proportional to the magnitude of vertical wind velocity when continuous dynamic mass flow control can not be performed.

The disjunct sampling principle is illustrated in Fig. 2.1 for the DEA method and in Fig. 2.3 for the DEC method. Comparing the few disjunct samplings at a resolution of 10 s of the DEA method (flow rate indicated by black vertical lines in Fig. 2.1c at times of 0, 10, and 20 s) relative to the continuous flow rate of the TEA method (red and orange vertical lines in Fig. 2.1c) illustrates the small fraction of the total time series being actually sampled by DEA.

Disjunct sampling allows more time for the analysis of the chemical species than continuous sampling. However, the uncertainty of disjunctly sampled scalar and wind time series, and as a result the flux uncertainty, is larger compared to continuous sampling. Turnipseed et al. (2009) found an additional uncertainty of ±30 % of the flux due to disjunct sampling and estimated the overall uncertainty of their

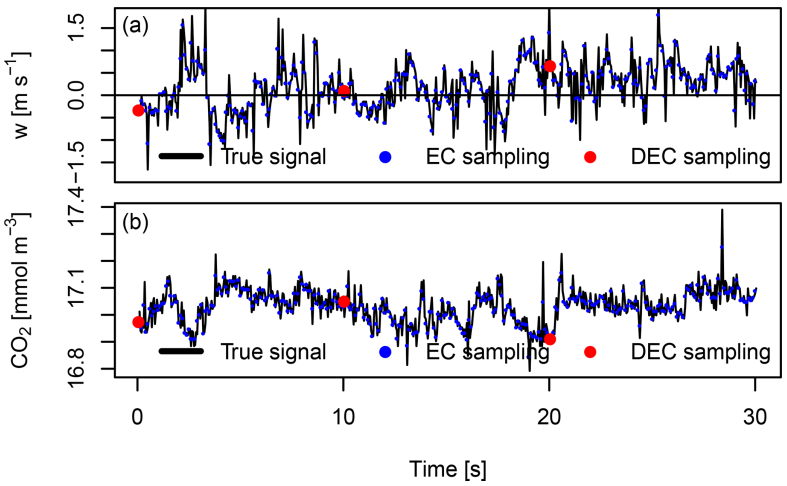

Figure 2.3: Eddy covariance and disjunct eddy covariance sampling scheme. Vertical wind, w **(a)**, scalar density, CO_2 **(b)**. Black solid lines indicate the continuous true atmospheric signal. Sampling resolution of EC and DEC are 10 Hz and 10 s, respectively. Note that active sampling time for DEC is only 1 % of the sampling time for EC.

DEA flux measurements as ±40 %.

Challenges of eddy accumulation

There are a number of challenges associated with eddy accumulation flux measurements (see also Hicks and McMillen, 1984). The first two listed below are specific to the TEA and DEA methods. The others are common to all eddy accumulation methods.

1. *Mass flow control.* The air sampling, i.e., the separation of updrafts and downdrafts as well as the response of the vertical wind velocity proportional mass flow control, needs to be sufficiently fast (10 to 20 Hz) and dynamic to resolve the relevant turbulent fluctuations. Further, the mass flow control needs to be accurate, even under dynamically changing flow rate conditions despite the compressibility of air. Finally, the dynamic range of the mass flow control, i.e., the ratio of the largest to the smallest accurately controllable mass flow, needs to be on the order of 100 or higher to limit flux errors (Hicks and McMillen, 1984). No commercially or otherwise readily available technology for fast, dynamic, and accurate control of mass flow rates exists or has been demonstrated to perform well in TEA.

2. *Density fluctuation effects.* Density fluctuations due to heat and water vapor transfer affect the flux of the scalar of interest. Corresponding corrections specific to the TEA method have been unavailable.

3. *Spectra and co-spectra.* No turbulence spectrum of the scalar nor the co-spectrum of the scalar and the vertical wind velocity can be obtained from the accumulated samples as they are mixed, and time-resolved analysis is therefore not possible. Spectral information on the wind is of course available as in any other method using a fast-response ultrasonic anemometer.

4. *Coordinate rotation* (see further details in Sect. 2.2.7). Sampling decisions need to be performed in real time, and they are definitive; i.e., they cannot be modified in post-processing. This is an

important difference to the EC method. The separation of updrafts and downdrafts depends on the definition of vertical wind velocity, w. The mean w over the averaging period needs to be zero (see Sect. 5.3, Eq. 2.6). One way to minimize mean w is to align the coordinate system of the wind measurements to the mean streamlines through coordinate rotation (Wilczak et al., 2001).

In eddy accumulation, the coordinate rotation needs to be performed in preprocessing to be available in real time. Coordinate rotation and any other operation attempting to nullify mean w over the flux averaging interval would require knowledge of w over the entire interval, including future observations. However, only past and present data are available in real time to approximate coordinate rotation and perform sampling decisions based on the sign and magnitude of w. Remaining nonzero mean w causes flux bias.

5. *Decorrelation through sensor separation.* Spatial separation of the gas sampling inlets and the wind sensing volume causes a time lag between the wind measurement and the time for obtaining the corresponding air sample. Not accounting for time lags leads to decorrelation of wind and scalar and therefore flux loss. Contrary to the EC method, where time lags can be detected through covariance maximization and corrected for, in eddy accumulation such post-processing is not possible because high-frequency scalar time series are not obtained. Therefore the wind measurement and the air inlet need to be co-located as close as possible.

6. *Analyzer sensitivity*. Trace gas concentration differences between reservoirs might be too small to be resolved by given gas analyzers.

7. *Reliability*. Eddy accumulation systems are mechanically and electronically complex machines. Particularly moving parts pose the risk of failure. Careful design is required for robust implementations and unattended long-term deployments.

We address the above challenges in the following ways:

1. A new type of digital and highly dynamic mass flow controller was deployed. The technology previously developed by the first author has a fast and dynamic response sufficient to resolve relevant turbulent scales at 10 Hz and above. The design accounts for the compressibility of air in dynamic sampling. See Sect. 2.3.2 for further details.

2. TEA-specific adaptation of flux corrections accounting for density fluctuations as proposed for the EC method by Webb et al. (1980) is subject to ongoing research by the authors.

3. Here we propose that, in absence of co-spectral information which is required to correct for flux attenuation due to sonic anemometer path length averaging and due to the separation of the air inlet and the sonic sensing volume, further research should investigate whether a proxy scalar such as air temperature or sonic temperature might be used to estimate the attenuation. While this would imply scalar similarity of the proxy and the scalar of interest, the impact of potential non-similarity would be limited to the spectral attenuation flux correction term, which is typically small relative to the flux itself, and the uncertainty from the scalar similarity constraint would be even smaller.

4. Nonzero mean vertical wind velocities were minimized through real-time coordinate rotation with continuous near-real-time updates of the rotation coefficients as well as a procedure to minimize remaining bias in the mean vertical wind velocity (see Sect. 5.3). Further, a correction accounting for volume mismatch between updraft and downdraft reservoirs due to nonzero mean vertical wind velocities (Turnipseed et al., 2009) has been applied (see Sect. 5.3).

5. Spatial separation of the wind sensing volume and the point of air sampling can be minimized through integration of the air inlet inside the wind sensing volume of the sonic anemometer. A certain degree of time lag between the wind signal and the scalar sampling will ultimately remain as long as the wind is sensed over a measurement volume rather than at a point and with discrete finite time resolution rather than truly instantly.

6. Performance analysis of a typical infrared gas analyzer model for the measurement of CO_2 gave satisfactory results in terms of the resolution but revealed limited stability. Subsequent work by the authors with current laser spectrometers gave superior results due to their improved stability. Details on the latter work will be reported separately.

7. Suggestions towards a robust design of an eddy accumulator are given in the conclusions of the current study.

2.1.2 Objectives

Out of all the methods discussed above, the true eddy accumulation method is the only alternative to the eddy covariance method for directly measuring the physical flux. Every effort should be made towards mastering the dynamic mass flow control necessary for direct TEA as well as addressing the other challenges listed above.

It is the objective of this work to deliver the proof of concept of true eddy accumulation trace gas flux measurements based on dynamic and accurate mass flow control proportional to vertical wind velocity and based on fully digital and real-time signal processing.

2.2 Materials and methods

2.2.1 Experimental design

The experimental design comprises three elements: novel true eddy accumulation flux measurements of CO_2 and water vapor, conventional eddy covariance flux measurements of CO_2 and water vapor, and meteorological measurements. All measurements were performed side by side. This allowed for the performance of the new TEA system to be evaluated on its ability to measure turbulent fluxes of CO_2 by relating the observed fluxes to meteorological drivers and by comparing the TEA CO_2 flux measurements to conventional EC CO_2 flux measurements. This section provides details on the measurement site, the meteorological measurements, the TEA method, technical implementation, and flux computation as well as information on the reference flux measurements by EC.

2.2.2 Experimental site

Flux measurements were performed at a grassland experimental field site of the University of Göttingen, Germany, located at 51°33′3″ N, 9°57′2″ E. The flux tower was installed at an altitude of 230 m above sea level on a flat area of about 50 m by 50 m situated on a south–southeast-facing hill, with a slope angle of 5° and length of 800 m. Vegetation height of the grass was 0.2 m during the experiment. Vegetation further comprised patches of bushes and trees with a minimum distance from the flux tower of 50 m (west of the tower).

Table 2.1: Instrumentation used for turbulent flux and meteorological measurements. Manufacturer key: Gill Instruments (Lymington, UK), Li-COR Environmental Inc. (Lincoln, Nebraska, USA), Kipp & Zonen B.V. (Delft, The Netherlands), Bosch Sensortec (Stuttgart, Germany), Adolf Thies GmbH & Co. KG (Göttingen, Germany), Imko Mikromodultechnik GmbH (Ettlingen, Germany), Hukseflux Thermal Sensors B.V. (Delft, the Netherlands).

Variable	Sensor	Manuf.	Method	Freq.
Wind u, v, w	R3	Gill	TEA, EC	10 Hz
Sonic temp. T_s	R3	Gill	TEA, EC	10 Hz
CO_2 density	LI-7500	Li-COR	EC	10 Hz
H_2O density	LI-7500	Li-COR	EC	10 Hz
CO_2 density	LI-6262	Li-COR	TEA	1 Hz
H_2O density	LI-6262	Li-COR	TEA	1 Hz
Air pressure	BME280	Bosch	TEA	1 Hz
Air temperature	BME280	Bosch	TEA	1 Hz
Global radiation	CMP3	Kipp	Meteo	10 min
Photon flux density	PAR sensor	Thies	Meteo	10 min
Net radiation	NR Lite	Kipp	Meteo	10 min
Air pressure	DL16 internal	Thies	Meteo	10 min
Air temperature	Galtec	Thies	Meteo	10 min
Precipitation	Tipping bucket	Thies	Meteo	10 min
Wind velocity	Cup anemometer	Thies	Meteo	10 min
Wind direction	Wind vane	Thies	Meteo	10 min
Soil temperature	Trime Pico 32	Imko	Meteo	10 min
Soil moisture	Trime Pico 32	Imko	Meteo	10 min
Soil heat flux	HFP01	Huksef.	Meteo	10 min

2.2.3 Experimental period

The TEA flux measurements presented in this study were conducted from 4 to 10 April 2015. After a cold and wet month of March, this period was characterized by increasing physiological activity of the grasses due to increasing light availability, increasing temperatures during the day, less frequent frost events, and increasing CO_2 fluxes.

Prior to the flux experiment, the TEA instrument and method were further developed and tested in the field, with continuous operation starting on 5 March 2015. The TEA deployment continued after 10 April until 17 June 2015. However, the frequent charging and discharging of the air sampling bags led to material fatigue and progressive leakage. Therefore, no meaningful flux measurements are available after 10 April 2015. The period from 10 April to 17 June 2015 was used for testing different kinds of air bags and for further developing the TEA method. Altogether, the TEA air sampling system in its current form was in continuous operation from 5 March to 17 June 2015, corresponding to more than 5000 30 min TEA flux sampling intervals.

2.2.4 Instrumentation

The instrumentation used for meteorological measurements, TEA flux measurements, and EC flux measurements and the respective variables measured are listed in Table 2.1.

Meteorological variables (Table 2.1) were logged using a DL16 data logger (Adolf Thies GmbH & Co. KG Göttingen, Germany). All raw data needed for TEA and EC flux measurements, including the sonic anemometer data and data from the two infrared gas analyzers LI-6262 and LI-7500, were synchronized and logged on the central TEA controller. Using a mobile network link, raw data were continuously mirrored to a central server for archival and flux processing.

2.2.5 Meteorological measurements

The following set of meteorological variables was measured on site to support the computation and interpretation of turbulent fluxes: global radiation, photosynthetically active radiation (PAR), net radiation, air temperature at 2 m a.g.l., air pressure, relative humidity at 2 m a.g.l., precipitation, wind velocity at 2 m a.g.l., wind direction at 2 m a.g.l., soil temperature at 0.3 m b.g.l. (three probes), soil moisture at 0.3 m b.g.l.(three probes), and soil heat flux.

2.2.6 Experimental data

The above-described meteorological measurements, as well as the turbulent flux measurements obtained by the true eddy accumulation and the two eddy covariance instrumental setups, have been published via open access (Siebicke and Emad, 2019) to foster open science in general and the scientific advancement of true eddy accumulation in particular.

2.2.7 Coordinate systems and net ecosystem exchange

If the trace gas source and sink strength of the ecosystem is of interest, as is typically the case when investigating biological, physiological, or biogeochemical processes or deriving trace gas budgets, then the total flux in and out of the ecosystem needs to be determined. For the exchange of the ecosystem with the atmosphere, the concept of a virtual control volume is often used. Net ecosystem exchange (NEE), i.e., the net flux across the surfaces of this control volume, can be written as (e.g., Aubinet et al., 2003; Siebicke et al., 2012)

$$\begin{aligned} \mathrm{NEE} = & \frac{1}{V_\mathrm{m}} \underbrace{\int_0^h \left(\frac{\partial \overline{c}}{\partial t} \right) \mathrm{d}z}_{\mathrm{I}} + \frac{1}{V_\mathrm{m}} \underbrace{\left(\overline{w'c'} \right)_h}_{\mathrm{II}} \\ & + \frac{1}{V_\mathrm{m}} \int_0^h \left(\underbrace{\overline{w}(z) \frac{\partial \overline{c}}{\partial z}}_{\mathrm{IIIa}} + \underbrace{\overline{c}(z) \frac{\partial \overline{w}}{\partial z}}_{\mathrm{IIIb}} \right) \mathrm{d}z \\ & + \frac{1}{V_\mathrm{m}} \int_0^h \underbrace{\left(\overline{u}(z) \frac{\partial \overline{c}}{\partial x} + \overline{v}(z) \frac{\partial \overline{c}}{\partial y} \right)}_{\mathrm{IV}} \mathrm{d}z \\ & + \frac{1}{V_\mathrm{m}} \int_0^h \underbrace{\left(\frac{\partial \left(\overline{u'c'} \right)}{\partial x} + \frac{\partial \left(\overline{v'c'} \right)}{\partial y} \right)}_{\mathrm{V}} \mathrm{d}z, \end{aligned} \tag{2.1}$$

with the molar volume of dry air V_m, CO_2 concentration c, time t, horizontal distances x and y, vertical distance above ground z, height of the control volume h, horizontal wind velocity u along the x direction, horizontal wind velocity v along the y direction, and vertical wind velocity w along the z direction. Overbars denote temporal means, and primes denote the temporal fluctuations relative to the temporal mean.

The terms on the right hand side of Eq. (2.1) are the change of storage (I), the vertical turbulent flux (II), vertical advection (IIIa), vertical mass flow from the surface, e.g., due to evaporation (IIIb) according to Webb et al. (1980), horizontal advection (IV), and flux divergence (V). The form of NEE presented in Eq. (2.1) excludes the horizontal variation of the vertical turbulent flux and the horizontal variation of

vertical advection. Most flux measurements typically only determine the vertical turbulent flux density (term II) and sometimes the storage flux density (term I), neglecting the remaining terms due to a lack of spatially distributed information.

The choice of the reference coordinate system (Finnigan, 2004) is important for the attribution of the total flux to its components (Eq. 2.1) and therefore for the interpretation of turbulent flux density measurements relative in their ability to approximate the net ecosystem exchange. If NEE is to be assessed, and available flux observations are restricted to the turbulent vertical flux density at a single location above the ecosystem, a reference coordinate system is needed which minimizes the remaining flux terms. Sun et al. (2007, Table 1) summarize coordinate systems. In streamline coordinates (Finnigan, 2004; Sun et al., 2007), the long-term flow is tangential to long-term streamlines. This means that, in streamline coordinates, the velocity normal to the streamlines becomes zero, implying that the long-term vertical advection vanishes. There are various methods for coordinate rotation (Finnigan et al., 2003), i.e., the transformation of the wind measurements from the coordinate reference frame of the sonic anemometer to the coordinate system of the flux measurements, also known as tilt correction (Tanner and Thurtell, 1969; Hyson et al., 1977; Kaimal and Finnigan, 1994; McMillen, 1988; Paw U et al., 2000; Wilczak et al., 2001).

Over flat terrain or planar terrain with a uniform slope, the mean streamlines close to the surface approximately follow the terrain surface. The planar fit method (Paw U et al., 2000; Wilczak et al., 2001) is often used to obtain long-term streamline coordinates. In contrast to the double rotation method (Kaimal and Finnigan, 1994), which nullifies the mean vertical wind velocity $\overline{w}$ of the flux integration interval, planar fit rotated $\overline{w}$, using the original formulation of Wilczak et al. (2001), is typically small but not zero. Even the long-term $\overline{w}$ only becomes zero if mean streamlines are planar, and there is no instrumental bias in measurements of w. Nonzero $\overline{w}$ would imply existence of a vertical advection term proportional to $\overline{w}$ in the presence of vertical trace gas concentration gradients, which for CO_2 typically exist close to the surface.

A variant to the planar fit method proposed by Van Dijk et al. (2004) removes velocity bias relative to the flux integration interval, addressing instrument offsets. This procedure can lead to local misalignment of streamlines for nonplanar mean flow fields. Nullifying $\overline{w}$ over the flux integration period would formally remove vertical advection terms from the flux budget equation (Eq. 2.1). However, this procedure would also still ignore the effect of misalignment of the reference coordinate system and the streamlines over the flux integration interval on the vertical turbulent flux. The mismatched length and timing of the planar fit period relative to the shorter individual flux integration intervals acts as a high pass filter and results in loss of low-frequency flux contributions and in unresolved distortion of co-spectra of the shorter flux intervals (Finnigan et al., 2003).

On a related matter, Siebicke et al. (2012) performed an explicit treatment of the length and timing of the reference period for planar fit rotation. They demonstrated changes of up to 50 % of advective CO_2 fluxes over forest depending on the window size of a new serial planar fit approach.

Over complex nonplanar terrain, the mean streamlines are not tangential to a plane. Even over planar surfaces, streamlines further away from the surface may not be tangential to the terrain surface due to vertical velocity divergence (Sun et al., 2007). For curved streamlines, other terms of the mass flow equation (Finnigan, 2004), in addition to vertical turbulent flux and vertical advection, become important. For curved streamlines, horizontal trace gas advection is not proportional to the gradient of trace gas concentrations along the streamlines.

Several authors have suggested variants to the planar fit method to account for steep slopes, where

buoyancy forces are no longer normal to the terrain surface (Oldroyd et al., 2016), for obstructed flow (Griessbaum and Schmidt, 2009), and for complex topography, where $\overline{w}$ becomes a function of wind azimuth angle. Consequently, several studies apply the planar fit rotation separately for different wind direction sectors (Foken and Napo, 2008; Yuan et al., 2011, and others). However, this introduces discontinuities in $\overline{w}$ at wind direction sector limits and in the definition of the reference coordinate system.

Here we propose that a more general approach avoiding directional discontinuities would be to fit a surface rather than a plane, where the curvature of the surface adapts to long-term streamlines as a function of one or more parameters, i.e., wind direction and optionally other variables, such as horizontal wind velocity. A related approach has recently been proposed by Ross and Grant (2015), who also suggest tilt correction as a continuous function of wind direction instead of the relatively common discrete sectoral approach used currently. Siebicke et al. (2012) showed that the effect of atmospheric stratification, friction velocity, stationarity, and integral turbulence characteristics (Foken et al., 2004) on sectoral planar fit rotation was small relative to the wind direction effect over a forest.

In the presence of flow distortion due to obstacles, terrain features, towers and sensor mounts, or non-omnidirectional sonic anemometer designs (Li et al., 2013), distorted sectors need to be excluded from the definition of the coordinate system and subsequent flux derivations, unless distortions are characterized and corrected for (Van Dijk et al., 2004; Griessbaum and Schmidt, 2009; see also Sect. 2.2.8, current study).

All the above considerations on coordinate rotation apply to both the EC and EA methods, respectively, including their derivatives. However, there is one conceptual difference: in EC, high-frequency observations of both the scalar and the wind are measured and stored for post-processing. Therefore it is feasible to fit the coordinate rotation plane to all observations from one or several 30 min flux integration intervals, including observations which were obtained before and after any wind measurement which is to be rotated. This includes the possibility to center the planar fit period around the time of interest.

Conversely, in EA, in absence of high-frequency scalar observations, any decision on the reference coordinate system becomes final on obtaining and mixing individual high-frequency air samples, precluding post-processing and any reconsideration of the coordinate system. In EA, the reference period defining the coordinate system necessarily cannot coincide and never fully overlap with the flux integration interval for any sample but the last one in the flux integration interval, if any. Due to this conceptual difference, the contribution of other flux terms, in particular vertical advection, may not be identical for EC and EA if not using the same reference period to align the coordinate system to the mean streamlines.

Nonvanishing mean vertical wind velocities $\overline{w}$ over the flux integration interval can nominally be removed in EC through subtraction of $\overline{w}$ from instant vertical velocities (Van Dijk et al., 2004) and in EA through application of the volume mismatch correction (Turnipseed et al., 2009); see Eq. (2.11) above. However, distortion of co-spectra (Finnigan et al., 2003) remains uncorrected.

We distinguish in evaluating the implications of discussed deviations of the real flow from any chosen ideal reference conditions: (i) the case of deploying turbulent vertical flux measurements to estimate net ecosystem exchange and (ii) the case of comparing the EA method and instruments side by side to the chosen reference method EC for assessing whether the EA method's physical air sampling principle produces comparable results to the mathematical computation of covariances for the EC method. This study is concerned with the latter case only. Most of the above issues of coordinate frames and the

spatiotemporal variability of the flow field afflict both methods alike. Only the unavoidable differences in the application of the coordinate rotations between the two methods, i.e., the nonmatching rotation periods, need to be of concern when evaluating the relative performance of the two turbulent flux observation methods. To eliminate this remaining difference, identical rotation procedures and planar fit reference periods need to be applied to both EA and EC, accepting the EA version as the reference.

2.2.8 Flow distortion and angle of attack correction

The physical structure of sonic anemometer probes distorts the air flow they intend to measure (Wyngaard, 1981), introducing systematic errors in flux measurements. Measurement errors, due to probe-induced flow distortion and self-sheltering of ultrasonic transducers (Gash and Dolman, 2003), depend on the "angle of attack" (Kaimal and Finnigan, 1994), i.e., the angle between horizontal and the instantaneous wind vector. A wind tunnel calibration for anemometer models R2 and R3 (Gill Instruments Ltd., UK) was provided by van der Molen et al. (2004) and updated by Nakai et al. (2006). The representativity of the wind tunnel calibrations for turbulent conditions in the field has been questioned (Högström and Smedman, 2004) and is still under debate (Huq et al., 2017). Nakai and Shimoyama (2012) proposed an improved correction based on field measurements under turbulent conditions for the R3 and Windmaster models (Gill Instruments Ltd., UK). There is still no consensus on whether this correction should be applied, and care must be taken as the correction applies to certain instrument models (Gill Windmaster) and serial numbers only.

In the current study, which uses two R3-type anemometers (Gill Instruments Ltd., UK), we do not apply any angle-of-attack correction because (i) the applicability of the wind tunnel calibration (Nakai et al., 2006) may or may not be applicable; (ii) there is contrasting information on the applicability of the calibration under turbulent conditions (Nakai and Shimoyama, 2012), specifically to the R3 model (recommended for R3 by original authors but not according to later information from Gill Instruments, UK, and LI-COR Env., USA); (iii) no angle-of-attack correction was available in the current TEA system software at the time of the field experiment nor can the TEA flux measurements be post-processed to include the correction. For the above reasons, no angle-of-attack correction was applied to the presented results of the current study, neither to TEA nor to EC fluxes. However, we did assess the impact of the angle-of-attack correction on EC CO_2 fluxes for the two sonic anemometers.

2.2.9 True eddy accumulation (TEA) flux measurements

TEA method

The true eddy accumulation method determines the flux, $\overline{wc}$, of a scalar (such as a trace gas) as the sum of the covariance, $\overline{w'c'}$ of the scalar, c, and the vertical wind velocity, w, and the product of the time averages of scalar and vertical wind velocity, $\overline{w}\,\overline{c}$, as

$$\overline{wc} = \overline{w'c'} + \overline{w}\,\overline{c}, \tag{2.2}$$

where overbars denote time averages over the averaging period, T_{avg}, and primes denote fluctuations from the mean. Eq. (2.2) is analog to the eddy covariance (EC) method.

However, in contrast to EC, which requires high-frequency observations of the scalar and the vertical wind velocity and mathematical derivation of the covariance through post-processing, in the case of TEA, the separate sampling of the wind and scalar time series is replaced by physically collecting

separate air samples of updrafts and downdrafts proportionally to the magnitude of the vertical wind velocity. The TEA flux over a given averaging period, T_{avg}, can thus be obtained as (Desjardins, 1977; Hicks and McMillen, 1984)

$$\overline{wc} = \frac{1}{T_{\text{avg}}} \int_0^{T_{\text{avg}}} (\delta^+ cw + \delta^- cw) \mathrm{d}t, \tag{2.3}$$

where $\delta^+ = 1$ when $w > \overline{w}$ and 0 when $w < \overline{w}$, and $\delta^- = 1$ when $w < \overline{w}$ and 0 when $w > \overline{w}$. The amount of air, cw, sampled per unit time, $\mathrm{d}t$, contains the molar fraction of the scalar of interest, c.

Assuming ideal conditions such that the mean vertical wind velocity over the integration period, $\overline{w}$, was zero, the mean term, $\overline{w}\,\overline{c}$, becomes zero and the scalar flux, F_c, becomes

$$F_c = \overline{w'c'} \tag{2.4}$$

in kinematic units of meters per second ($\mathrm{m\,s^{-1}}$). Multiplying by moist air density ρ, we obtain the constituent mass flux, F_c, per unit area and unit time in units of kilograms per square meter per second ($\mathrm{kg\,m^{-2}\,s^{-1}}$) as

$$F_c = \overline{w'c'}\overline{\rho}. \tag{2.5}$$

Given $\overline{w} = 0$, the volume of the air samples accumulated in the updraft reservoir is identical to the volume of the downdraft reservoir given

$$w^+ + w^- = \overline{w} = 0, \tag{2.6}$$

where w^+ is vertical wind larger than $\overline{w}$, and w^- is vertical wind smaller than $\overline{w}$.

A practical implementation of TEA then determines the scalar flux, F_c, as half of the difference between the mole fraction of the scalar in the updraft reservoir, $\overline{c^+}$, and the mole fraction of the scalar in the downdraft reservoir, $\overline{c^-}$, multiplied by the mean of the absolute value of vertical wind velocity, assuming $\overline{w} = 0$.

$$F_c = \frac{\overline{|w|}}{2}(\overline{c^+} - \overline{c^-})\overline{\rho} \tag{2.7}$$

in units of kilograms per square meter per second ($\mathrm{kg\,m^{-2}\,s^{-1}}$) or

$$F_c = \frac{\overline{|w|}}{2}(\overline{c^+} - \overline{c^-})\frac{1}{V_m} \tag{2.8}$$

in units of moles per square meter per second ($\mathrm{mol\,m^{-2}\,s^{-1}}$), with the molar volume of air, V_m ($\mathrm{m^3\,mol^{-1}}$), according to the ideal gas law,

$$V_m = \frac{RT}{P}, \tag{2.9}$$

with temperature, T, pressure, P, and the ideal gas constant, R. Note that Eqs. (2.7) and (2.8) write $\overline{|w|}$, not $|\overline{w}|$; i.e., the order of math operations is important.

For comparison of TEA and REA methods, we include here the formulation of the flux using the REA method (Businger and Oncley, 1990), expressed as mole fraction measurements of the constituent, c,

$$F_c = \beta\sigma_w \left(\overline{c^+} - \overline{c^-}\right)\overline{\rho}, \tag{2.10}$$

with the standard deviation of vertical wind velocity, σ_w, and the REA flux-variance similarity factor, β.

In any practical flux measurement application the observed mean vertical wind velocity over the integration period is likely unequal to zero, i.e., $\overline{w} \neq 0$. In eddy covariance the assumption of $\overline{w} = 0$ is satisfied in post-processing once all observations of the entire integration period are available. This is commonly achieved by rotating the coordinate frame of the wind measurements to minimize or even nullify $\overline{w}$ followed by subtraction of $\overline{w}$ from individual vertical wind velocity measurements, w, so $\overline{w}$ becomes zero.

Conversely, for TEA, knowledge of the mean vertical wind velocity over the flux averaging period, $\overline{w}$, is required at any time throughout the averaging period, in order to be able to classify vertical winds as updrafts or downdrafts and accumulate air samples in the corresponding reservoirs. At any time during the averaging interval only the past and present vertical wind measurements are known. Therefore, any attempt to obtain $\overline{w} = 0$ needs to rely in part on an estimate of the mean vertical wind velocity of the entire averaging period without knowledge of future observations from the present through to the end of the averaging period. In practice, this situation can lead to $\overline{w} \neq 0$, resulting in unequal sample volumes accumulated over the averaging period in the updraft and downdraft reservoirs.

Following Turnipseed et al. (2009) the flux needs to be corrected by a term accounting for the mismatch between the volume of accumulated updrafts, V^+, and downdrafts, V^-, respectively, for $V^+ \neq V^-$. The flux due to a mismatch of volumes V^+ and V^- is

$$F_{c,\text{volume\_mismatch}} = \overline{w}\left(\frac{(\overline{c^+} + \overline{c^-})}{2} - \overline{{}^{v}c}\right)\frac{1}{V_m}, \tag{2.11}$$

where $\overline{w}$ is the mean vertical velocity for the averaging period. The volume mismatch correction term is the difference between the unweighted mean density of the reservoirs, $(\overline{c^+} + \overline{c^-})/2$, and the volume weighted mean density,

$$\overline{{}^{v}c} = \frac{(\overline{c^+}\,V^+ + \overline{c^-}\,V^-)/2}{(V^+ + V^-)/2}, \tag{2.12}$$

weighted by the updraft and downdraft volumes, V^+ and V^-, respectively.

Inserting Eq. (2.11) in Eq. (2.8) yields the volume-mismatch-corrected TEA flux,

$$F_c = \left(\frac{\overline{|w|}}{2}(\overline{c^+} - \overline{c^-}) + \overline{w}\left(\frac{(\overline{c^+} + \overline{c^-})}{2} - \overline{{}^{v}c}\right)\right)\frac{1}{V_m}. \tag{2.13}$$

In practical applications, the instant sampling volume per unit time, V_i, is related to instant vertical wind velocity, w_i, through a proportionality factor, k, as

$$V_i = k|w_i|. \tag{2.14}$$

Correction of trace gas mole fractions for the effects of water vapor

When measuring trace gases such as CO_2 in moist air with infrared gas analyzers, two corrections are required to remove the effect of water vapor on the measurement of the mole fraction of the trace gas. The first correction accounts for pressure broadening due to the presence of water vapor. This is known as the "pressure broadening correction" (Licor, 1996, Li-COR LI-6262 manual, Sect. 3.5, 25 pp., Eq. 3–30).

The second correction accounts for the dilution of the trace gas by water vapor in the sample. This

correction is known as "dilution correction" and is required to convert the wet mole fraction, c_{wet}, to the dry mole fraction, c_{dry}. The dry mole fraction is needed for calculating the trace gas flux, F_c, based on Eq. (2.5). The dry mole fraction is obtained from the wet mole fraction following the instructions for the infrared gas analyzer (Licor, 1996):

$$c_{\mathrm{s}}^{\mathrm{wr}} = c_{\mathrm{s}}^{\mathrm{ws}} \left(\frac{1 - X_{\mathrm{w,ref}}/1000}{1 - X_{\mathrm{w}}/1000} \right), \tag{2.15}$$

where X_{w} is the mole fraction of water vapor in the sample cell, $X_{\mathrm{w,ref}}$ is the water vapor mole fraction in the reference cell, $c_{\mathrm{s}}^{\mathrm{ws}}$ is the actual mole fraction of the trace gas in the sample cell diluted by X_{w}, and $c_{\mathrm{s}}^{\mathrm{wr}}$ is the equivalent sample cell CO_2 mole fraction if it were diluted by $X_{\mathrm{w,ref}}$.

TEA instrumentation and technical implementation

The TEA instrumentation used in this study was developed with particular attention to accurate and dynamic sampling of air and to real-time processing of wind data. The system was further designed to minimize time lags and jitter in wind data processing and in air sampling and to minimize dead volumes in the gas sampling system.

Vertical and horizontal wind velocities and the sonic temperature were measured using an ultrasonic anemometer R3 (Gill Instruments Ltd.), the same type which was also used for the side-by-side eddy covariance reference flux measurements. Wind velocity data were logged at a 10 Hz frequency.

Instant observations of vertical wind velocity were subject to real-time coordinate rotation to align the coordinate system of the sonic anemometer with the mean streamlines prior to controlling the sampling of air into updraft or downdraft reservoirs using the planar fit method (Wilczak et al., 2001). To the best of our knowledge, this study is the first eddy accumulation study to deploy a real-time coordinate rotation based on the planar fit rotation (Wilczak et al., 2001). A moving window of 1 d was used to estimate planar fit rotation coefficients, with an update frequency of the rotation coefficients of 30 min. The coefficients were then applied to rotate the instant raw wind measurements, w_i, 10 times per second.

To minimize $\overline{w}$ over the flux averaging period the following procedure was applied: the mean vertical wind velocity of the current accumulation interval was approximated by the mean rotated vertical wind velocity over the most recent samples over a period with length equal to the length of the accumulation period, in this case 30 min. This estimate of mean vertical wind velocity was updated every 2 min and subtracted from every instantaneous vertical wind velocity measurement after coordinate rotation, i.e., 10 times per second.

The decision on updrafts and downdrafts was based on the sign of rotated w_i. Sample volumes were computed following Eq. (2.14). k was determined such that instant flow rates would not exceed the maximum possible flow rate of 3 L min^{-1}, with a probability of 99 % based on absolute wind data in the period from 30 min ago to present. The proportionality factor, k, which was based on the 99 % quantile multiplied by a factor of 2, was updated every 30 min.

Air inlets were co-located with the wind measurement and positioned 18 cm below and 2 cm beside the center of the sonic anemometer. Two separate air sampling lines were used, one for obtaining the updraft samples and one for the downdraft samples, respectively. In contrast to many previous eddy accumulation studies, which used a single air inlet and a 3/2-way valve to direct the samples towards the appropriate updraft or downdraft reservoir, the current design with two separate sampling

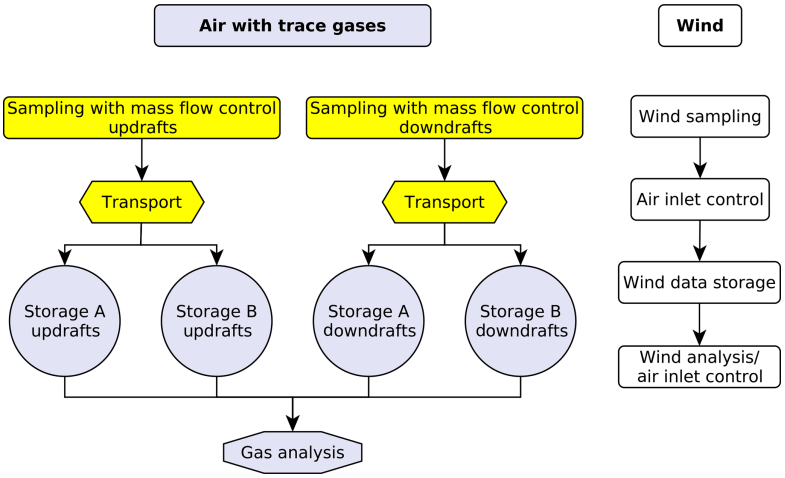

Figure 2.4: Schematic functional flowchart of true eddy accumulation system. Sampling of air with atmospheric constituents (scalars) shown on the left, sampling of wind vector shown on the right. Updrafts and downdrafts were sampled and stored via separate lines. One single analyzer was used with the sample supply alternating between the updraft and downdraft reservoirs every 150 s (see Fig. 2.6). During a particular 30 min period, bag set A was being filled with updraft and downdraft samples in the updraft and downdraft bags, respectively. At the same time bag set B was being analyzed and discharged, with the analysis alternating between updrafts and downdrafts. Every 30 min, the operation of bag sets A and B, either filling or discharging, was swapped. The vertical wind velocity data (right) control the air sampling via instantaneous wind measurements and wind statistics.

lines avoids any undesired mixing of updrafts with downdrafts in the system. A detailed technical description and layout of the true eddy accumulation system with the two separate sample lines is presented in Fig. 2.5, including piping layout and system components, operating pressure conditions, pressure drops, dead volumes, and transit times of air samples through the system.

The intake of air was controlled by fast-response mass flow controllers with a dynamic response resolving turbulent eddies at 10 Hz. The mass flow controllers used for this study were calibrated using conventional thermal mass flow controllers (Vögtlin red-y smart series). The accuracy of the new dynamic mass flow controllers was equal to or better than 0.3 %, which corresponds to the accuracy of the conventional mass flow controller model used for calibration.

The new type of mass flow controller was tested for potential leaks, both relative to the ambient air and also for potential flow during times when the respective sampling line was inactive. The tests showed that the mass flow controller (MFC) was virtually leak-free. The combined leak rate of the MFCs, the pumps, the filters, tubing, and fittings was 0.0086 ± 0.0003, expressed as the leak rate relative to the average inlet flow rate. In terms of flux uncertainty this would mean that a theoretical maximum of 0.86 ± 0.03 % and, considering the other system components, likely far less of the flux uncertainty would be related to potential leakage or undesired nonzero flow of the mass flow controllers.

Air sampling lines were made of Teflon with a 6 mm outer and 4 mm inner diameter and a length of 5 m between intake and accumulation reservoirs. The air was filtered before entering the pumps and the bag reservoirs using PTFE membrane Gelman Acro Disc filters with a 50 mm diameter and a 2 µm pore size. Another filter was placed directly upstream of the gas analyzer.

At any time, one of the air sampling lines was active, with the selection of the line depending on the sign of the vertical wind velocity. The wind was measured at a frequency of 10 Hz using the sonic

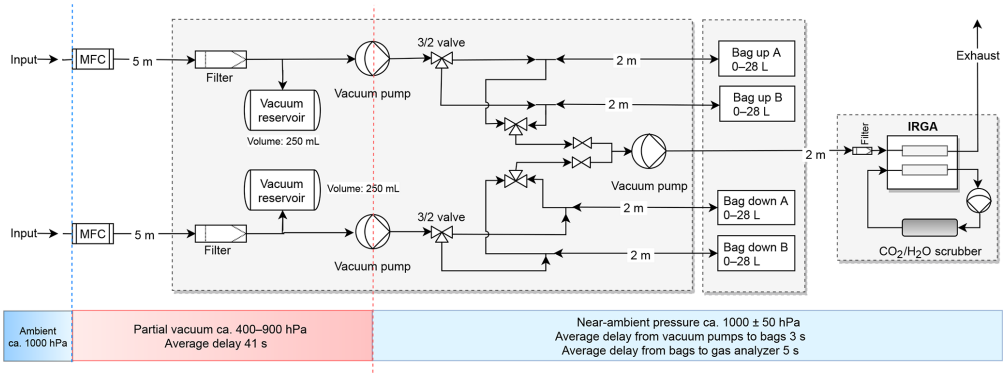

Figure 2.5: Hydraulic and functional schematic of the true eddy accumulation system with components layout, properties, and operating conditions. System components shown are the piping layout, mass flow controllers (MFCs), pumps, valves, filters, reservoirs, and the gas analyzer. Piping lengths and volume of air reservoirs are shown alongside the components. The operating pressure is shown for three distinct regions of the system below the system layout (colored bars) together with the average transit times of air through specific sections of the system. The air sampling bags are marked with "up" for collecting updrafts and "down" for collecting downdrafts. Bag sets A and B alternate their function (charge, discharge) every 30 min.

anemometer. With every new reading of vertical wind velocity, i.e., every 100 ms, the selection of the active inlet (updraft or downdraft) was updated depending on the sign of the vertical wind velocity and an air sample obtained with mass proportional to vertical wind velocity.

In contrast to common practice in many relaxed eddy accumulation studies, which typically define a minimum vertical wind velocity for air sampling, in the current design, air samples were obtained for all magnitudes of vertical wind velocity (except for the 0.5 % most positive and most negative values of w, respectively, as per the definition of k above).

Air samples were collected using two variable speed separate brushless DC membrane pumps (KNF Neuberger GmbH, Germany) with a maximum flow rate of 3 L min^{-1}, each, feeding air into the bag reservoirs at flow rates between 0 and 3 L min^{-1}.

Air was collected in lab grade, chemically inert Alumini® air sample bags (Westphalen AG, Germany) with a volume of 28 L. The composite wall of the bags was made of (from outside to inside) polyethylene terephthalate (PET), polyethylene (PE), aluminum (ALU), oriented polyamide (OPA), and polyethylene (PE).

The layout of the TEA system is shown in Fig. 2.4. The system was designed for continuous operation, with continuous sampling of air and continuous on-site gas analysis. Air was collected in bags over periods of 30 min. Subsequently the air was analyzed over the following 30 min periods. A total of four bags was used at any time. A set of two bags (marked with "A" in Fig. 2.4) was charged with samples over 30 min, with one bag accumulating samples corresponding to updrafts (marked "updraft") and one bag accumulating samples corresponding to downdrafts (marked "downdraft"). A second set of two bags (marked with "B" in Fig. 2.4), which contained air samples from the previous 30 min interval, was discharged and analyzed in parallel to the filling of the first set of bags. Every 30 min the two bag sets A and B would swap their function from being charged to being discharged. Note that data analysis revealed a leak in one of the bag sets, so that the data of every other half hour had to be discarded.

The accumulated air was analyzed for molar density of CO_2 (µmol mol−1) and of water vapor (mmol mol−1) using a dual cell infrared gas analyzer, model LI-6262 (Li-COR Env. Inc, USA). Air samples were dis-

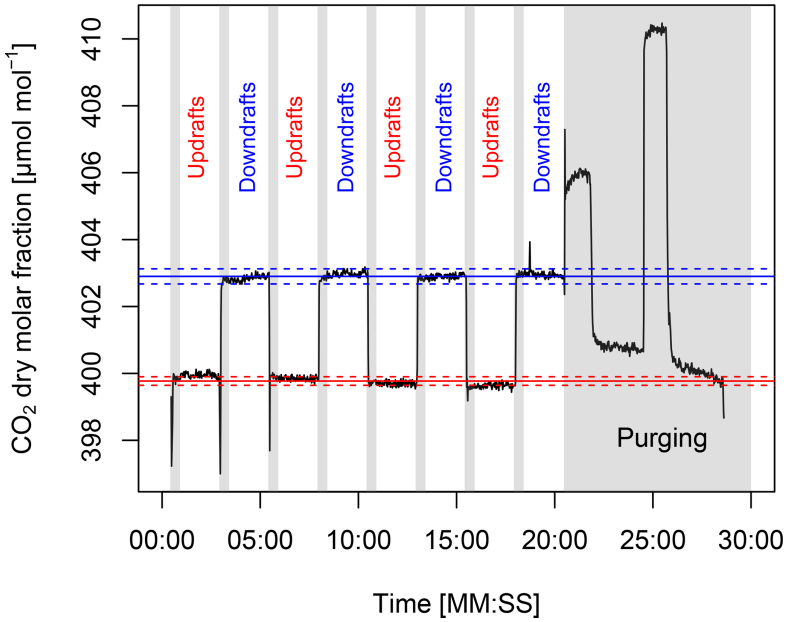

Figure 2.6: CO_2 dry molar fraction measured as a sequence alternating between updraft and downdraft reservoirs. First the updraft reservoir was measured for 150 s, then the downdraft reservoir for 150 s, discarding the initial 30 s of measurements from each block. This sequence was repeated four times. During the remaining 10 min of the 30 min period any remaining air in the reservoirs was purged and not used for analysis (gray shaded area). The means of the despiked updraft and downdraft dry molar fractions are indicated by a red and blue solid line, respectively. The dashed lines indicate the mean ±1 standard deviation. The start date of the time series is 10 April 2015 13:00:00 UTC.

charged by a membrane pump (KNF Neuberger, Germany) from the sample bags through the sample cell of the gas analyzer at a flow rate of 0.6 L min^{-1}. The sampling frequency of the gas analyzer was 1 Hz. The reference cell was purged by dry and CO_2-free zero gas obtained by circulating air through a scrubber filled with soda lime and Drierite desiccant. 3/2-way solenoid valves were used to select the appropriate gas bag for gas analysis.

During any 30 min period, the gas analysis alternated between sampling the updraft and downdraft reservoir, respectively (Fig. 2.6). Each bag was sampled for 150 s at a time. The first eight measurements periods of 150 s each were used for further analysis, resulting in four replicate measurements of the gas densities of the updraft reservoir and likewise four replicates of the downdraft reservoirs. Gas density measurements were tagged by the TEA controller with the respective active channel, either updraft or downdraft reservoir, for flux processing. The alternating sampling sequence lasted 1200 s. Over the remaining 600 s of the 30 min period, the remaining air was discharged from the bags to the atmosphere at a flow rate of 1.5 L min^{-1} until depletion.

The fully automatic TEA system was controlled by an ARM-based single-board Linux computer of the type “Raspberry Pi” (Raspberry Pi Foundation, UK), the “TEA controller”. All sensor measurement data, including the wind and gas density measurements, were synchronized, logged, and processed on the same TEA controller.

The following raw data were logged for subsequent turbulent flux calculations: horizontal and vertical wind velocity components, u, v, w; sonic temperature, T_s; CO_2 and H_2O molar densities; analyzer cell temperature and cell pressure; ambient air temperature, T; and air pressure, P. Further data on

the state of the TEA sampling system and the analysis were logged for attribution of the gas analyzer measurements to updraft and downdraft samples, for the selection of the bag sets, and for system monitoring and quality control.

The energy-efficient TEA system of the current study consumed 15 W of electrical power (excluding the gas analyzer), about 10 W of which was used by the three pumps. The pumping power required for the current TEA system was 2 orders of magnitude smaller than that of fast-flow closed-path eddy covariance systems using infrared gas analyzers or laser spectrometers of ca. 1 kW. The additional power consumption of typical current laser spectrometers would be on the order of 0.25 kW. The difference in pumping power between TEA and EC scales with the flow rate and sample cell vacuum of the EC application and is therefore even more important for most closed-path laser spectrometers than for infrared gas analyzers.

TEA flux computations

Turbulent fluxes of CO_2 were calculated from raw data of horizontal, u, v, and vertical, w, wind velocity components, sonic temperature, T_s (10 Hz), CO_2 dry mole fraction (converted from wet mole fraction) and H_2O dry mole fraction (converted from wet mole fraction) (1 Hz), ambient air temperature, T (10 min resolution), and pressure, P (10 min resolution).

Raw gas density measurements were processed prior to flux computations in order to filter the data for noise and aggregate individual readings to single representations of the gas density, one for the updraft and one for the downdraft reservoir, during any one 30 min period. Blocks of 150 s (see Fig. 2.6) of measurements at 1 Hz were filtered and aggregated to 30 min values (see Sect. 2.3, Fig. 2.11 for results). The following statistically robust procedure was used:

- Raw voltage signals of CO_2 and H_2O were converted to physical units of micromoles per mole ($\mu mol\,mol^{-1}$), and the band broadening effect of pressure on CO_2 observations was corrected for according to Licor (1996).
- The CO_2 wet mole fraction was converted to the dry mole fraction.
- Gas density data were checked for plausibility based on preset minimum and maximum values.
- The initial 30 s (dead-band filter) after switching channels was omitted to allow for purging of the shared gas handling components, i.e., valves, sample line, and gas analyzer sample cell.
- Raw data were de-spiked (spike filter) using the function “despike” from the R package “oce” (Kelley and Richards, 2017), replacing discarded values with the median of remaining values. The method identifies spikes with respect to a “reference” time series and replaces these spikes with the reference value, i.e., here the median.
- The time series were smoothed (smoothing filter) using the function “loess” (Cleveland et al., 1992) from the R package “stats” (R Core Team, 2017). The loess function fits a polynomial surface determined by one or more numerical predictors, using local fitting.
- Stable readings were selected (stationarity filter) by limiting maximum permissible gradients between individual samples for channel-specific data blocks of 150 s (120 s remaining after dead-band filter), with a maximum permissible change of 0.002 $\mu mol\,mol^{-1}\,s^{-1}$.

- Sufficient availability of data after filtering was checked for (availability filter): a data block was discarded if fewer than 30 (out of 120) values remained available after the stationarity filter.
- The remaining filtered data were aggregated per channel-specific data block of 150 s using the median function.
- The four replicates were aggregated per channel into a single value per 30 min as the weighted mean of the four samples, weighted by the number of accepted raw measurements in each of the four replicates, separately for updrafts and downdrafts.
- To quantify precision of the CO_2 molar fraction measurements using the LI-6262 infrared gas analyzer, the minimum and maximum molar fractions over the four replicated samples were estimated, separately for updrafts and downdrafts and propagated into minimum and maximum flux estimates, respectively.

Fluxes were then calculated through the following:

- plausibility check of wind data based on preset minimum and maximum values;
- de-spiking of raw wind data (Vickers and Mahrt, 1997);
- computation of the mole fraction difference between updraft and downdraft reservoirs per 30 min period;
- computation of uncorrected turbulent fluxes for 30 min intervals according to Eq. (2.8);
- computation of turbulent fluxes for 30 min intervals, corrected for volume mismatch between updraft and downdraft reservoirs, according to Eq. (2.13).

2.2.10 Eddy covariance (EC) reference flux measurements

EC instrumentation

A conventional EC system was set up for flux measurements of CO_2, sensible heat, and latent heat. The EC setup served as a reference for the TEA flux measurements. Instruments used were a three-dimensional sonic anemometer of type R3 (Gill Instruments Ltd, UK) and an infrared gas analyzer, type LI-7500 (Li-COR Env. Inc., USA). Wind and mole fraction data were recorded at a 20 Hz frequency at a height of 2.5 m a.g.l. The EC sensors were mounted side by side to a separate sonic anemometer and air inlet used for TEA. The two sonic anemometers were separated by a distance of 1 m. For quality assurance, in addition to the above primary eddy covariance setup, we used the sonic anemometer of the eddy covariance in combination with the open-path fast response gas analyzer (IRGA) for an alternative eddy covariance flux estimate. The horizontal separation between the EC sonic and the IRGA was 0.35 m, and the separation between the TEA sonic and the IRGA was 0.7 m.

EC flux computations

Eddy covariance raw data were post-processed to obtain fluxes at a resolution of 30 min using the EddyPro® software (LI-COR Env. Inc., USA), version 5.0.0. The flux processing comprised the following steps:

- statistical tests for raw data screening according to Vickers and Mahrt (1997), including spike count and removal, amplitude resolution, dropouts, absolute limits, skewness, and kurtosis;
- de-trending of raw time series by block averaging;
- compensation of time lag between sonic anemometer and gas analyzer measurements by covariance maximization;
- axis rotation for tilt correction using the planar fit method (Wilczak et al., 2001) with removal of the velocity bias (Van Dijk et al., 2004), in running window mode (1 d window, updated every 30 min) (TEA sonic) and fixed period (7 d) mode (EC sonic);
- flux quality check according to Foken et al. (2004), selecting classes 0 and 1 for further analysis on a scale of 0, 1, and 2.

2.3 Results and discussion

This section is organized as follows: (1) meteorological conditions during the experiment are presented, followed by (2) a characterization of mass flow control performance, a prerequisite for the (3) determination of concentration differences between accumulated updrafts and downdrafts, which, in combination with (4) vertical wind measurements, finally result in (5) trace gas fluxes. To inform the discussion on uncertainties of the eddy accumulation method, (6) coordinate rotation results, (7) uncertainties of vertical wind distributions, and (8) instrumental errors of the sonic anemometers and infrared gas analyzers used are presented.

2.3.1 Meteorological conditions

Meteorological conditions (Fig. 4.3) during the experimental period from 4 to 10 April 2015 were characterized by fair weather conditions with photosynthetically active radiation peaking at around 1500 µmol m^{-2} s^{-1} at noon (a). Air temperature was initially below 10 °C on the first day with frost during the night but then rapidly increased to more than 20 °C on the last day (b). Similarly, there was a positive soil temperature trend (d). No precipitation was observed during this period. Wind direction (f) was dominated by easterly winds except for 7 and 8 April with mostly westerly and stronger winds (e) and higher relative humidity (c). 7 April stands out as the day with highest wind speed (e), high friction velocity (h), low radiation (a), and low sensible heat flux (g). The sensible and latent heat fluxes (g) otherwise largely tracked radiation levels with the highest latent heat fluxes observed on 9 and 10 April and with a decreasing Bowen ratio.

2.3.2 Mass flow controller performance

Laboratory tests of the new digital mass flow controller used in this study showed that the accuracy and linearity of the digital mass flow controller for stationary flow were excellent: the maximum deviation of the new design from the conventional thermal mass flow controller used as reference was 0.3 % over the full operating range (Fig. 2.8). The minimum and maximum flow rates of the digital mass flow controller of 0.025 and 3 sml min^{-1} correspond to a dynamic range of 120, exceeding minimum performance requirements formulated by Hicks and McMillen (1984) for eddy accumulation, i.e., a dynamic range of 100 or higher. The tests also showed that the two controllers used for the updraft and

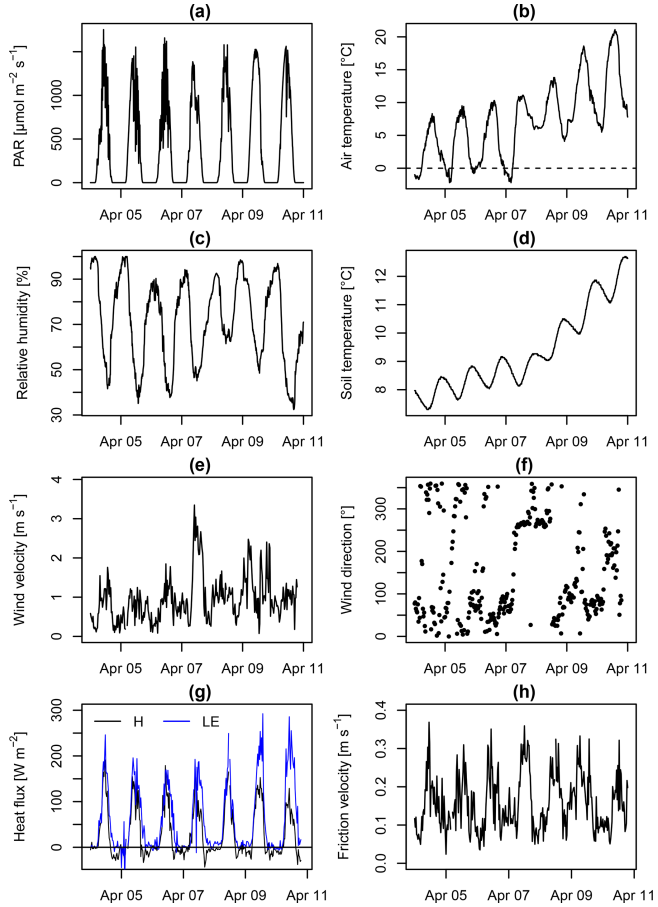

Figure 2.7: Meteorological conditions and turbulent energy fluxes during the experimental period from 4 to 10 April 2015: photosynthetically active radiation (PAR), air temperature, relative humidity, soil temperature, wind velocity, wind direction, sensible heat flux (H), latent heat flux (LE), and friction velocity. The wind and eddy covariance flux observations shown in panels **(e)**–**(h)** were obtained from the R3 sonic of the eddy accumulation system in combination with the LI-7500 gas analyzer.

downdraft channels of the TEA system, respectively, performed to the same level (red and blue line in Fig. 2.8).

We further compared the performance of the two mass flow controller designs under dynamic flow rate conditions (Fig. 2.9). The new digital mass flow controller was used to generate a highly dynamic reference signal for comparison with the conventional thermal mass flow controller. The uncertainty of the new digital mass flow controller (red uncertainty ranges in Fig. 2.9) was small relative to the dynamic signal itself. Conversely, the conventional thermal mass flow controller (blue line in Fig. 2.9) was unable to follow the dynamic reference signal, showing strong overshoot and overestimation of the reference flow rate.

Statistics of the mass flow controller comparison for the same data, as in the previous figure, are shown in the regression plots in Fig. 2.10. The new digital mass flow controller showed a perfect slope of 1.00, a high coefficient of determination of $R^2 = 0.999$, and a root mean square error (RMSE) of 8.8 sml min^{-1} (Fig. 2.10b), which is 50 times smaller than the RMSE of the conventional mass flow controller of 441.8 sml min^{-1} (Fig. 2.10a). The conventional mass flow controller further overestimated the reference

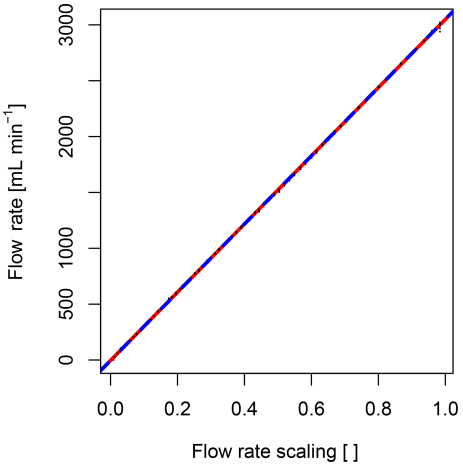

Figure 2.8: Linearity of two digital mass flow controllers verified by a conventional thermal mass flow controller for a series of 100 constant flow rate levels in the range of 0 to 3000 sml min^{-1}. The thermal mass flow controller reading is shown on the y axis versus the set point of the digital mass flow controllers on the x axis (black dots). The set point range on the x axis from 0 to 1.0 is linearly related to a flow rate range of 0 to 3000 sml min^{-1}. Observed linearity errors of the digital mass flow controllers shown here are below 0.3 % of the reading. Linear model fit of the digital mass flow controller of the "updraft channel" of the TEA system (dashed red line), and of the "downdraft channel" (dashed blue line), respectively.

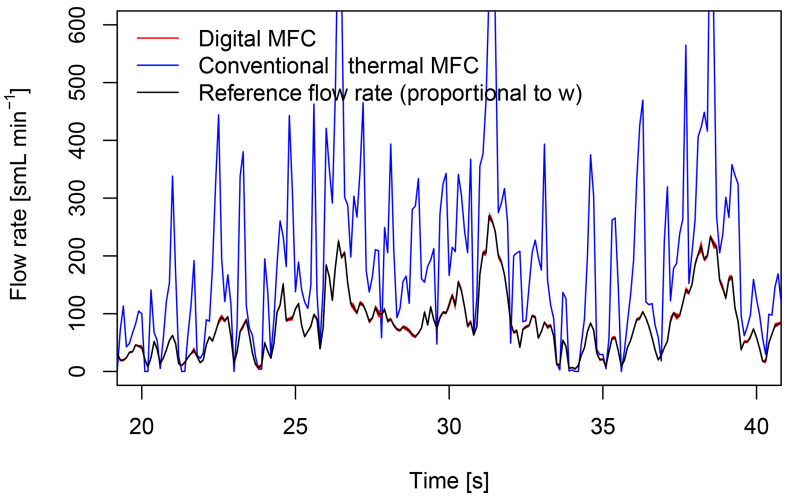

Figure 2.9: Mass flow rate readings of a conventional thermal mass flow controller (Vögtlin red-y smart series), in blue, measuring a dynamically changing reference flow (black). The magnitude of the reference flow rate, which is proportional to the magnitude of recorded vertical wind velocity data, varied at a frequency of 10 Hz. The reference flow (black) was generated using the new digital mass flow controller. The uncertainty range of the digital mass flow controller (red) is small. Conversely, the mass flow reading of the conventional thermal mass flow controller deviates significantly from the reference as the conventional mass flow controller is unable to follow the highly dynamic reference signal.

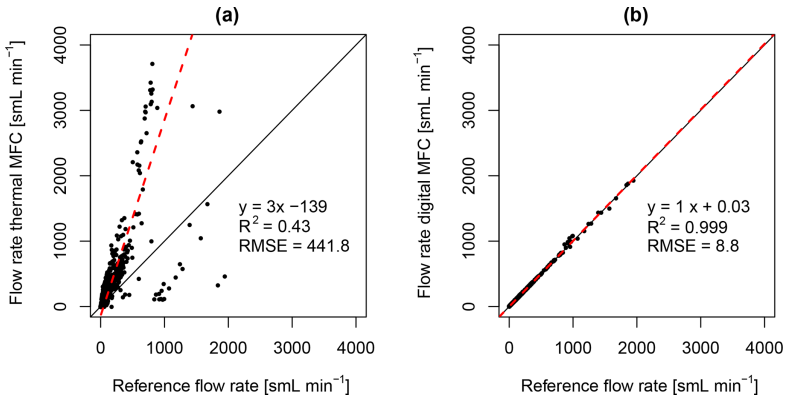

Figure 2.10: Regression of **(a)** the thermal mass flow controller flow rate versus the reference flow rate and **(b)** the digital mass flow controller flow rate with errors versus the reference flow rate. The reference flow rate was varied at a frequency of 10 Hz proportional to measured vertical wind velocity data. The black solid line denotes the 1 : 1 line, and the dashed red line denotes the linear model fit. Regression statistics: linear model equation; coefficient of determination, R^2; and root mean square error, RMSE.

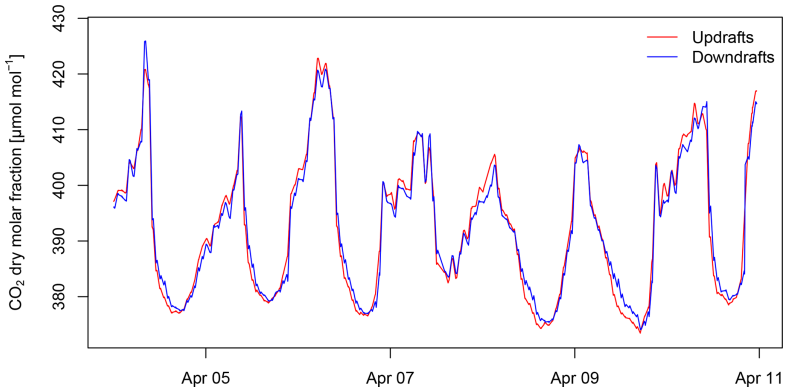

Figure 2.11: Dry molar fraction of CO_2 in the updraft and downdraft reservoirs of the true eddy accumulation device, in red and blue, respectively. The difference in molar fraction is a result of the vertical CO_2 flux.

by 300 % and matched less than half of the variance of the reference signal ($R^2 = 0.43$).

In conclusion, the dynamic response, precision, and accuracy of the digital mass flow controller are suitable for eddy accumulation sampling, while the conventional thermal mass flow controller is not.

2.3.3 CO_2 molar fraction and differences between accumulated updrafts and downdrafts

Time series of the CO_2 mole fraction obtained by the TEA system separately for the accumulated updrafts and downdrafts are shown in Fig. 2.11. Both the accumulated updrafts and downdrafts followed the common diurnal pattern of the CO_2 mole fraction with minimal CO_2 densities during the day when photosynthetic activity of the vegetation is at its maximum, a gradual buildup of CO_2 from the late afternoon through the night, and finally a rapid decrease of CO_2 in the morning when the daytime turbulence removes nightly accumulation of trace gases and photosynthesis then further draws down the ambient CO_2 mole fraction. As expected, despite the generally similar course of the CO_2 mole fraction of the updraft and downdraft reservoirs, there was a small but systematic difference

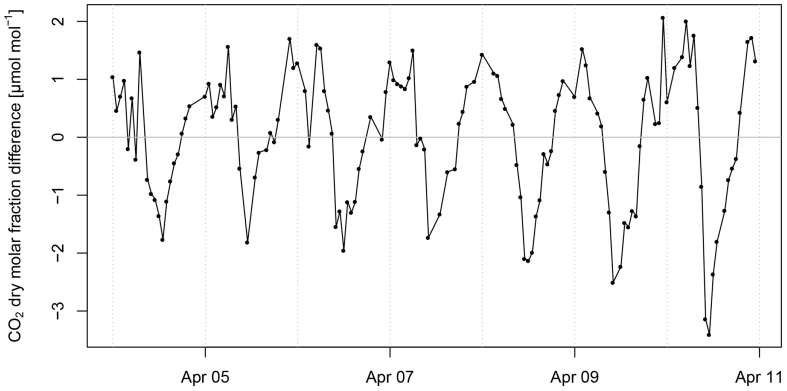

Figure 2.12: Difference in dry mole fractions of CO_2 between the updraft and downdraft reservoirs of the true eddy accumulation device. The 30 min raw time series shown is the result of subtracting the mole fraction in the downdraft reservoir from the mole fraction in the updraft reservoir (Fig. 2.11). A positive CO_2 mole fraction difference indicates a CO_2 flux away from the surface (respiration), and a negative CO_2 mole fraction difference indicates a CO_2 flux towards the surface (assimilation).

between the two, with the CO_2 mole fraction of the updrafts (red line in Fig. 2.11) being lower than the downdrafts (blue line in Fig. 2.11). This difference was caused by the relative CO_2 depletion of updraft air due to photosynthesis during the day. At night, the inverse pattern was observed whereby updraft air was systematically enriched in CO_2 through respiration from soil and vegetation.

The difference in the CO_2 mole fraction between updraft and downdraft reservoirs is shown in Fig. 2.12. This difference was positive during the night and negative during the day. Windy conditions during the day cause a smaller magnitude of CO_2 difference as seen on 7 April (see Fig. 4.3 for wind and Fig. 2.12 for CO_2). Likewise, calm conditions enhance the CO_2 difference between updraft and downdraft reservoirs (see 9 and 10 April 2015, Fig. 2.12).

2.3.4 Mean absolute vertical wind velocity

Vertical wind velocity measurements from the TEA system are shown in Fig. 2.13, separately for updrafts and downdrafts (red and blue lines, respectively). Both updrafts and downdrafts show similar magnitude, which is to be expected for a mean vertical wind velocity close to zero (black and cyan line in Fig. 2.13). On 9 and 10 April, absolute vertical wind velocity w during the day was lower than for other days (Fig. 2.13). Lower absolute w, indicating less vertical mixing, corresponded with more pronounced differences in the CO_2 molar fraction between updrafts and downdrafts, i.e., a more negative difference (Fig. 2.12) on the same 2 d. Under conditions of low winds and low turbulence, but intense radiation, the air close to the surface and the vegetation, which would be sensed as updrafts, was depleted in CO_2 through photosynthesis, relative to the air above.

Mean vertical wind velocity, $\overline{w}$, which ideally is zero over the 30 min flux integration intervals, rarely exceeded $\pm 4\,\mathrm{cm\,s^{-1}}$ (dashed black lines), a threshold which, according to a simulation by Hicks and McMillen (1984), should not be exceeded to avoid significant flux errors. On two occasions, $\overline{w}$ from the running window planar fit showed larger deviations from zero on 4 and 9 April 2015. Overall, the amplitude of $\overline{w}$ was smaller for the planar fit rotation using a single 7 d window compared to the running planar fit using 1 d windows.

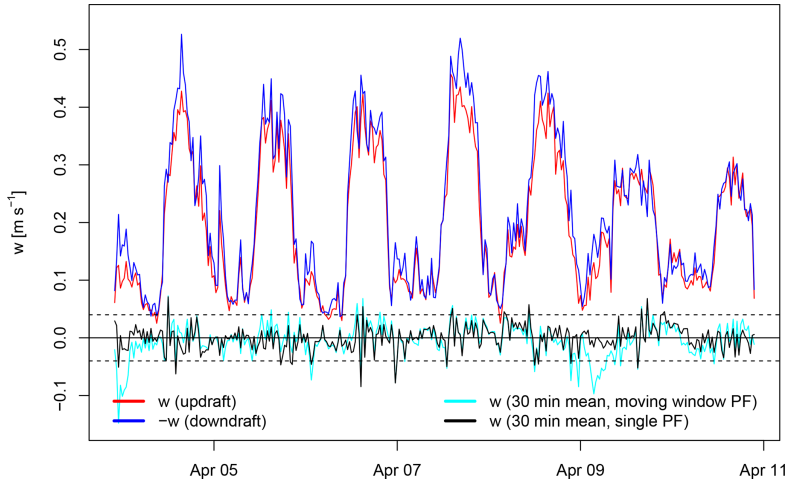

Figure 2.13: Vertical wind velocity of updrafts and downdrafts, in red and blue, respectively, averaged to 30 min resolution and shown as absolute values. Vertical velocity is subject to a 1 d running window real-time planar fit coordinate rotation as obtained from the TEA system. Mean vertical wind velocity at 30 min resolution after running window real-time planar fit coordinate rotation, in blue, and after a post-processing planar fit coordinate rotation with the fit period corresponding to the full period shown, in black. Note that updrafts (red) and downdrafts (blue) shown here are different from $\overline{|w|}$ used for flux calculation according to Eq. (2.7).

2.3.5 CO_2 fluxes

The turbulent exchange of CO_2 between the vegetation and the atmosphere as observed by TEA is displayed in Fig. 2.14. Fluxes clearly show CO_2 uptake during the day (photosynthesis, with values up to ca. $-20\,\mu mol\,m^{-2}\,s^{-1}$) and CO_2 release during the night (respiration, with values up to ca. $+5\,\mu mol\,m^{-2}\,s^{-1}$); see also the mean diurnal cycle in Fig. 2.15a. The temporal variability of CO_2 fluxes measured by TEA (Fig. 2.14) reflects variation in photosynthetically active radiation (PAR; Fig. 4.3): 8, 9, and 10 April 2015 with high levels of radiation and the least amount of cloud also show the highest fluxes. 6 April, which experienced more clouds during the day and therefore less abundant photosynthetically active radiation, also showed relatively small CO_2 fluxes during the day. Similarly, on 5 and 7 April, which were affected by clouds and reduced radiation in the early afternoon, the CO_2 fluxes during the afternoon were reduced compared to cloud-free days, e.g., 9 April.

Nighttime CO_2 fluxes measured by TEA showed a trend of increasing fluxes over the experimental period (Fig. 2.14). This trend corresponded to the observed trends of increasing air temperature and soil temperature (Fig. 4.3) over the same period. The observation of a positive correlation of positive CO_2 fluxes (respiration) with soil and air temperature is in line with the widely accepted mechanistic understanding that soil respiration is a function of soil temperature with a positive correlation over the temperature range presented. Overall, from an ecophysiological point of view, the observed CO_2 fluxes corresponded well with their meteorological drivers.

From a methodological point of view, a key step in assessing the TEA method's performance is the comparison of the TEA method with the established EC method. Fig. 2.14 shows CO_2 fluxes measured by both TEA (black line) and EC (red and blue points). The eddy covariance fluxes shown in Fig. 2.14 are quality-filtered, accepting flags ≤ 1 (Foken et al., 2004; on a scale of 0, 1, and 2). This filtering reduced the number of available 30 min eddy covariance flux estimates to 90 % and 93 %, and filtering for flag = 0 reduced the fraction of available data to 45 % and 46 % for the sonic anemometers of the TEA and

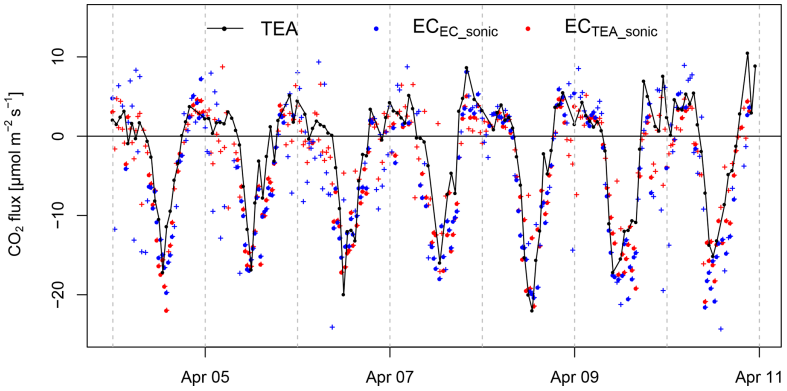

Figure 2.14: Comparison of CO_2 fluxes measured by true eddy accumulation (TEA) and eddy covariance (EC). Flux integration interval for both methods is 30 min. TEA fluxes were obtained every 60 min and EC fluxes every 30 min. The EC fluxes are quality-flag-filtered, accepting flags ≤ 1 on a scale of 0, 1, and 2 (Foken et al., 2004). The two alternative EC flux calculations shown, in blue and red, respectively, are from two separate Gill-R3 sonic anemometers using CO_2 density data from the same LI-7500 gas analyzer. The symbols indicate if EC flux estimates from the two sonic anemometers were within 50 % from each other (full circles) or not (crosses).

the EC system, respectively (both used for eddy covariance fluxes).

Generally, good agreement was observed between the TEA and EC methods. However, the intercomparison of the methods was complicated by the presence of high noise levels in the 30 min EC flux estimates. Analysis of R3 sonic anemometer raw data revealed that the EC sonic anemometer (blue line Fig. 2.14) was affected by correlated noise in the high-frequency wind and sonic temperature measurements, resulting in erroneously high sensible heat flux and momentum flux estimates. The erroneously high variance of the horizontal and vertical wind components was particularly pronounced during the night and decreased over the experimental period. Conversely, erroneously high sonic temperature variance increased over the experimental period. CO_2 fluxes were affected to a lesser degree because the noise in the R3 sonic anemometer data was not necessarily correlated with the LI-7500 infrared gas analyzer measurements.

The sonic anemometer of the TEA system seemed less affected by noise. Therefore we used it as an alternative input to the eddy covariance flux computations. However, the horizontal separation between the latter sonic anemometer and the open-path gas analyzer was large (0.7 m) relative to the low measurement height. Eddy covariance CO_2 fluxes from the TEA sonic anemometer were on average 18 % smaller compared to the EC sonic anemometer. However, after eliminating inconsistent fluxes whereby the fluxes from the two sonic anemometers disagreed by more than 50 % or alternatively 25 %, eddy covariance CO_2 fluxes from the TEA sonic anemometer were on average 6 % smaller and 2 % larger, respectively, compared to the EC sonic anemometer (Fig. 2.15).

A regression of CO_2 fluxes from the TEA method versus the EC method is shown in Fig. 2.15b, comparing TEA fluxes to the two alternative EC flux estimates after quality filtering eddy covariance fluxes with flags ≤ 1 (Foken et al., 2004). Before applying the above consistency filter, the coefficients of determination were R^2 = 76 % and 67 %, and the linear model slopes were 1.04 and 0.87 when quality filtering eddy covariance fluxes for flags ≤ 1 (Foken et al., 2004) and improved to R^2 = 71 % and 76 % and slopes of 0.99 and 0.92 for flags = 0, for (i) TEA fluxes versus EC fluxes (using the TEA sonic anemometer for EC) and (ii) TEA versus EC fluxes (using the EC sonic anemometer for EC), respectively. The correlation further improved when rejecting conflicting EC fluxes: limiting the difference of the two EC flux estimates

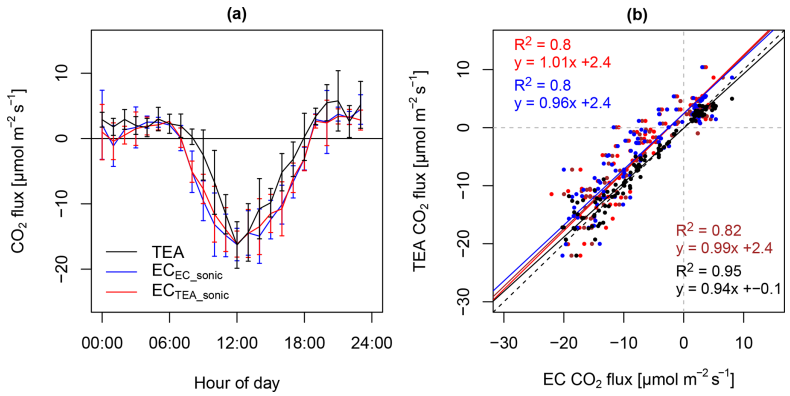

Figure 2.15: Mean diurnal cycle **(a)** and regression **(b)** of CO_2 fluxes measured by true eddy accumulation (TEA) and eddy covariance (EC) for the period 4–7 April 2015. Flux integration interval for both methods is 30 min. TEA fluxes were obtained every 60 min and EC fluxes every 30 min. The two alternative EC flux calculations shown, in blue and red, respectively, are from two separate Gill-R3 sonic anemometers using CO_2 density data from a single LI-7500 gas analyzer. The EC fluxes are quality-flag-filtered, accepting flags ≤ 1 on a scale of 0, 1, and 2 (Foken et al., 2004) and filtered for consistency of EC fluxes from the two anemometers, accepting EC fluxes with a maximum relative flux difference of 50 %. Error bars indicate ±1 standard deviation. **(b)** Scatterplot and linear model fit for TEA fluxes versus EC fluxes. The three EC flux versions shown are fluxes from the TEA sonic (in red), from the EC sonic (in blue), and the mean of the fluxes from the TEA and the EC sonic (in brown). Also shown are EC fluxes from EC sonic versus EC fluxes from TEA sonic (in black). Regression statistics shown are the coefficient of determination, R^2, and the linear model equation from a standard major axis regression (Legendre and Legendre, 1998; Sokal and Rohlf, 1995). The same color code (red, blue, brown, black) applies to all graphical elements, i.e., points, regression lines (solid lines), and regression coefficients. The dashed black line is the 1 : 1 line.

from the two independent sonic anemometers to 50 % of the mean of the two fluxes (flags ≤ 1), the coefficients of determination of TEA versus EC fluxes increased further to 80 %, 80 %, and 82 %, with linear model slopes of 1.01, 0.96, and 0.99, for (i) TEA fluxes versus EC fluxes (using the TEA sonic anemometers for EC), (ii) TEA versus EC fluxes (using the EC sonic anemometer for EC), and (iii) TEA versus EC fluxes (using the average of the TEA and EC sonic anemometers for EC), respectively (case shown in Fig. 2.15b).

While a certain fraction of the observed deviations between TEA and EC flux estimates can be attributed to the methodological differences, the two independent eddy covariance flux estimates also showed deficiencies in agreement, with coefficients of determination of the EC to EC regression of R^2 = 84 %, 86 %, and 85 % and slopes of 0.81, 0.82, 0.85, leaving 16 %, 14 %, and 15 % of the flux variance unexplained for quality flag filter thresholds of 2, 1, and 0. The percentage of additional unexplained variance in the TEA fluxes with R^2 = 74 % (regression of TEA fluxes versus mean EC fluxes from the two sonic anemometers, flag ≤ 1) relative to EC fluxes with R^2 = 86 % was 12 % only. There was a positive intercept for the above regression cases between TEA and EC fluxes which ranged from 1.8 to 2.4 µmol m^{-2} s^{-1}.

While the above-reported coefficients of determination for the EC versus EC flux regressions using various filter options were somewhat higher than for TEA versus EC fluxes, the differences between the TEA and EC methods were still of the same order of magnitude as the differences between the two EC flux estimates, which use the same infrared gas analyzer. It might seem from Fig. 2.15a and the above-reported statistics that the two EC flux estimates match more closely than TEA and EC fluxes. However, we note that the EC–EC agreement is to some degree artificial; i.e., only a part of this apparent

agreement relates to differences between TEA and EC methods, and another part is simply due to the "consistency filter" applied to the two EC flux estimates. This filter, which by definition discards EC flux values which are not similar, is not normally required but was introduced to deal with the above-mentioned deficiencies of the two EC setups.

We would expect from a side-by-side comparison of eddy covariance flux measurements, using identical models of research class sonic anemometers and sharing the same gas analyzer, that the R^2 would exceed 90 %. We interpret the compromised match of the two current EC estimates largely as a result of compromised wind and sonic temperature measurements by the two R3 anemometers. When excluding the first 4 d which were relatively more affected by erroneous w, filtering for quality flags ≤ 1 and again filtering EC fluxes to not exceed a relative difference between the two EC flux estimates of 50 %, then the match of TEA versus EC CO_2 fluxes improved further, yielding R^2 values of 84 %, 86 %, and 86 %, slopes of 1.04, 0.91, and 0.98, and intercepts of 2.0, 1.9, and 2.0 µmol m^{-2} s^{-1} for TEA fluxes versus EC fluxes using the TEA sonic anemometers, the EC sonic anemometers, and the mean of the TEA and EC sonic anemometers, respectively.

In relation to previous works on true eddy accumulation trace gas flux measurements, we note that, despite compromised data quality of one of the R3 sonic anemometers of the current study, the match of true eddy accumulation and eddy covariance CO_2 fluxes exceeded the match in any previously published true eddy accumulation experiments we are aware of. The closest results are those from Komori et al. (2004), who obtained a coefficient of determination for TEA versus EC CO_2 fluxes of $R^2 = 0.64$, a slope of 0.95, and a relatively high intercept of 8.6 µmol m^{-2} s^{-1} for 17 flux integration intervals.

2.3.6 Uncertainty of vertical wind measurements

Vertical wind measurements contribute to flux uncertainty in two ways: (i) instrumental errors of the sonic anemometer and (ii) nonideal wind field and nonzero mean vertical wind velocity over the flux integration period.

Sonic anemometer measurement errors

Systematic and random errors in sonic anemometer measurements contribute to scalar flux uncertainty both in the EC and TEA methods. For a detailed analysis of sonic anemometer measurement errors we refer to instrument comparisons and quantifications of measurement errors for common sonic anemometer types (Loescher et al., 2005; Mauder and Zeeman, 2018; Foken et al., 2019, and others). These studies suggest that measurement errors of sonic anemometers, including differences between different types of sonic anemometers and differences between different units of the same type of sonic anemometer, may account for anywhere from several percent up to about 25 % of the error in scalar flux measurements.

Regarding the R3-type sonic anemometer used in the current study, Loescher et al. (2005, Fig. 5) found in wind tunnel tests that the R3 sonic anemometer, like other post-mounted designs, suffered from flow distortion, systematically overestimating vertical wind velocity. The R3 overestimated vertical wind velocity for vertical velocities below 0.15 m s^{-1} by up to ca. 0.05 m s^{-1} for vertical velocities close to zero and underestimated vertical velocity by up to the same amount for vertical velocities up to 0.3 m s^{-1} (gain error). In addition, when the stanchions supporting the upper transducers were in the flow path, the vertical wind velocity response was nonlinear. Nonlinearity and gain errors can result

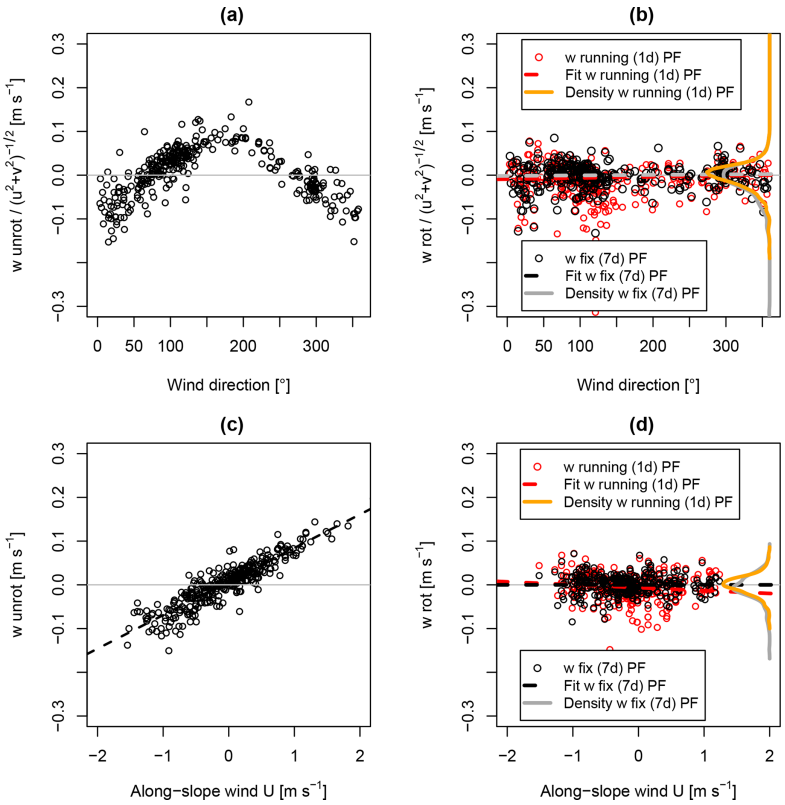

Figure 2.16: 30 min means of vertical wind velocity, w, before **(a, c)** and after **(b, d)** coordinate rotation as a function of wind direction **(a, b)** and as a function of along-slope wind, U **(c, d)**. The vertical wind velocity w in **(a)** and **(b)** is normalized by horizontal wind velocity. Panels **(b)** and **(d)** both differentiate between two approaches to the planar-fit coordinate rotation: the real-time planar fit applied in the TEA measurements, deploying a moving window of 1 d ("running PF", in red and orange), and a single planar fit, covering the full measurement period (7 d long) obtained in post-processing ("fix PF", in black and gray). The labels "rot" and "unrot" denote the rotated and unrotated vertical wind velocities, respectively.

in misalignment of the coordinate system with the mean streamlines (see Sect. 2.3.6) and apparent asymmetry of vertical wind distributions (see Sect. 2.3.6).

Coordinate rotation

The following analyses present nonzero mean vertical wind velocities, which cause scalar flux uncertainty. Figure 2.16 shows vertical wind before and after coordinate rotation. Vertical wind velocity scaled by horizontal wind velocity ideally follows a (co)sine function when anemometer coordinates are tilted relative to streamline coordinates (Fig. 2.16a). Planar fit rotation reduced the range of $\overline{w}$ from about $\pm 0.1\,\mathrm{m\,s^{-1}}$ to about $\pm 0.05\,\mathrm{m\,s^{-1}}$ (Fig. 2.16b). The range of $\overline{w}$ was slightly smaller for the 7 d rotation window compared to the running 1 d window. Figure 2.16c indicates that before coordinate rotation the sonic coordinate frame was tilted relative to the streamlines, which followed the terrain slope. The slope of the relation of $\overline{w}$ over along-slope wind U (c) vanished after planar fit rotation using the 7 d window (d). The running planar fit with a 1 d window did not fully remove the dependence of $\overline{w}$ from along-slope wind velocity, biasing $\overline{w}$ by up to $\pm 0.02\,\mathrm{m\,s^{-1}}$ over the range of along-slope velocities shown (d), corresponding to about 15 % of bias before tilt correction.

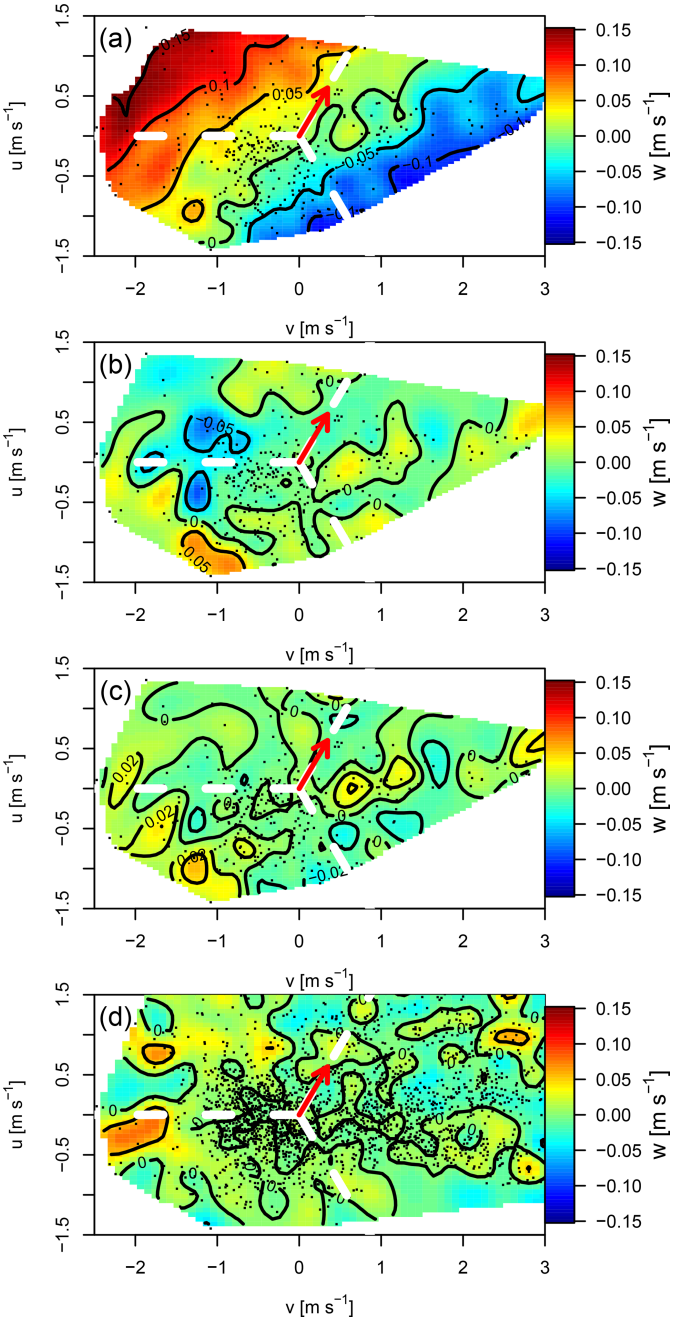

Figure 2.17: 30 min mean vertical wind velocity w as a function of horizontal wind velocities u and v before and after planar fit coordinate rotation for two different planar fit procedures and two periods. Wind velocities were obtained by the Gill-R3 sonic anemometer which was used for true eddy accumulation. **(a)** Unrotated vertical wind velocity. **(b)** Rotated vertical wind velocity from real-time 1 d moving window planar fit rotation performed by TEA system. **(c)** Rotated vertical wind velocity with single planar fit rotation period performed in post-processing. **(d)** Same as **(c)** but for a longer period, i.e., from 1 April to 31 May 2015. Panels **(a)** to **(c)** show data from the experimental period of the current study from 4 to 11 April 2015. Black dots indicate the location of individual 30 min mean vertical wind velocity readings in the u–v velocity space. Red arrows indicate the direction to north. Dashed lines, in white, indicate the azimuth of the vertical stanchions of the sonic head structure relative to the center of the sonic coordinate system.

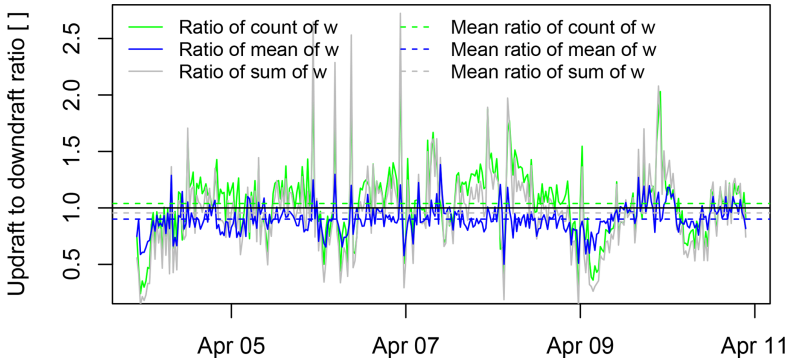

Figure 2.18: Ratio of statistical measures of vertical wind velocity of updrafts and downdrafts per 30 min flux integration interval. The statistical measures are the ratio of the count, the mean, and the sum of vertical wind velocity records during updrafts and downdrafts, respectively (solid lines). The dashed lines indicate the temporal mean of the above statistics over the period displayed.

Figure 2.17 presents residuals of mean vertical wind velocity $\overline{w}$ before and after coordinate rotation in u and v horizontal velocity space. This analysis relates $\overline{w}$ to wind direction, horizontal wind velocity, and obstacles causing flow distortion. $\overline{w}$ (in Fig. 2.17a) before tilt correction shows the effect of the terrain slope on wind measurements in sonic coordinates. The slope effect was fully removed through planar fit rotation (Fig. 2.17b). The 1 d running window planar fit led to a slight overcorrection of the tilt (Fig. 2.17b), as already noted regarding Fig. 2.16d, which was not the case for the planar fit rotation using a 7 d window. Residuals of $\overline{w}$ were small with the 1 d running planar fit, resulting in relatively larger $\overline{w}$ residuals up to about $\pm 0.05\,\mathrm{m\,s^{-1}}$ (Fig. 2.17b) compared to up to about $\pm 0.02\,\mathrm{m\,s^{-1}}$ for the 7 d planar fit (Fig. 2.17c).

Some dependence of $\overline{w}$ on horizontal wind velocity and direction was observed: for horizontal wind velocities of more than about $1\,\mathrm{m\,s^{-1}}$, residuals of $\overline{w}$ were mostly positive, particularly for southwesterly and northeasterly winds (Fig. 2.17b and c). This was confirmed by the planar fit rotation of a 2-month-long data set (Fig. 2.17d). Possible interpretations include flow distortion from trees and bushes in the southwest and northeast and velocity-dependent flow distortion of the sonic anemometer or nearby structures. No obvious influence of the stanchions of the anemometer on $\overline{w}$ was identified (Fig. 2.17a–d).

Updraft–downdraft asymmetries

The TEA method requires $\overline{w} = 0$, which would result from symmetry in updraft and downdraft statistics. However, we observed asymmetry in the mean, the count, and the sum of updraft and downdraft samples. Quantification of the flux uncertainty due to asymmetric distributions of w would require co-spectral information of w and CO_2 densities, which is generally absent for TEA measurements. Instead, we present a quantification of observed asymmetries of w, informing about the magnitude of the asymmetries and their variability over time.

Figure 2.18 shows that (i) on average, the count of updrafts was larger than the count of downdrafts; (ii) however, on average, the mean of updrafts was smaller than the mean of downdrafts; and (iii) on average, the sum of updrafts was slightly smaller than the sum of downdrafts. It is noteworthy that the mean of w can still be zero while the 7 d mean of the 30 min mean of updrafts and the 30 min mean of downdrafts are nonzero; or in other words, the ratio of the 30 min mean of the updrafts to the

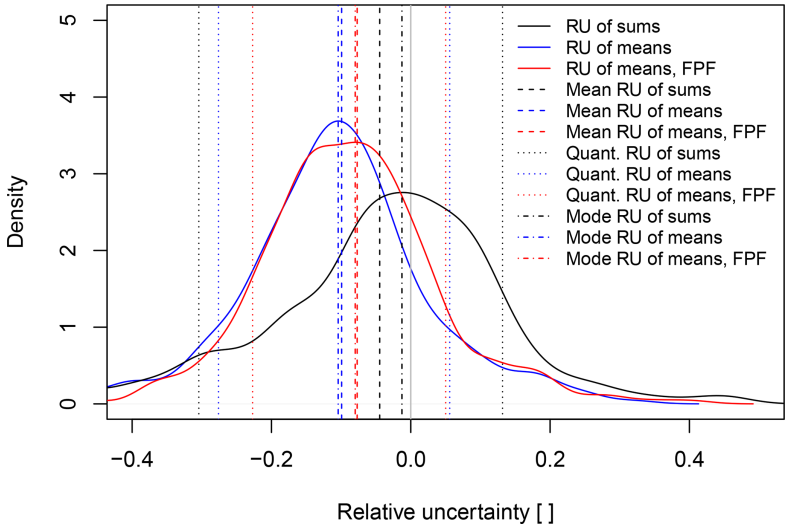

Figure 2.19: Probability density distributions of the relative uncertainty (RU) of the mean absolute vertical wind velocity, $\overline{|w|}$, due to nonzero mean vertical wind velocity over the 30 min flux integration periods (blue solid line). $\overline{|w|}$ is required for the determination of trace gas fluxes according to Eq. (2.2). The relative uncertainty of the mean vertical wind velocity was calculated as RU = $((\overline{w_{\mathrm{up}}} - \overline{|w_{\mathrm{down}}|})/2)/((\overline{w_{\mathrm{up}}} + \overline{|w_{\mathrm{down}}|})/2)$, where the overline denotes the temporal mean of vertical wind velocity over the 30 min flux integration interval, and subscripts "up" and "down" refer to updrafts and downdrafts, respectively. Results based on w from the real-time moving window planar fit coordinate rotation of the TEA system and from the fixed window post-processing planar fit rotation (FPF) are shown in blue and red, respectively. "Mean RU of means", "Mode RU of means", and "Quant. RU of means" indicate the mean, the mode, and the quantiles, respectively, for a probability of 10 % and 90 %. While mean vertical wind velocity $\overline{|w|}$ is needed for flux derivation, the sum of vertical wind velocity over the flux integration interval, $\sum|w|$, relates to the accumulated air sample volumes. The relative uncertainty of the sums, "RU of sums", corresponds to the contribution of vertical wind velocity to the volume mismatch correction defined in Sect. 5.3. Relative uncertainty of the sum of vertical wind velocity per 30 min flux integration interval was calculated as RU = $((\sum w_{\mathrm{up}} - \sum|w_{\mathrm{down}}|)/2)/((\sum w_{\mathrm{up}} + \sum|w_{\mathrm{down}}|)/2)$. "Mean RU of sums", "Mode RU of sums", and "Quant. RU of sums" indicate the mean, the mode, and the quantiles of the distribution, respectively, for 10 % and 90 % probability.

30 min mean of the downdrafts is different from unity as observed here. This can be understood by considering the different weights of updrafts and downdrafts in the mean which reflect the asymmetry in the counts of updrafts and downdrafts, respectively.

Figure 2.19 shows probability density distributions of the relative uncertainty of the mean absolute vertical wind as defined in the figure caption. The distribution of the sums of updrafts and downdrafts is centered around zero, with only a small negative bias of −0.01 for the mode of the distribution and a larger bias of −0.04 for the mean of the distribution. Conversely, the distribution of the relative uncertainty of the means peaked for both the mode and the mean of the distribution at a more negative bias of −0.11, as observed for the running window planar fit (Fig. 2.19, blue line). Similar results were obtained for the 7 d stationary planar fit although with a smaller negative bias of −0.08 (Fig. 2.19, red line). Less than 10 % percent of relative uncertainty values were more negative than −0.3, and less than 10 % of relative uncertainties were larger than +0.14. In summary, updraft–downdraft asymmetries were on the order of 10 % of the mean absolute vertical wind velocities used in flux calculations.

2.3.7 Uncertainty of trace gas concentration measurements

Trace gas flux errors are a function of accuracy and precision of the trace gas analysis. Regarding accuracy, bias between the two infrared gas analyzers used for the TEA and EC methods is more relevant than absolute accuracy for comparing the TEA method to the EC reference method. By comparing time-averaged time series of CO_2 concentrations of the LI-6262 and LI-7500 infrared gas analyzers, a time-variable bias was found, which accounted for up to 5 % of the scalar flux.

Regarding scalar flux errors from the TEA method, systematic errors leading to bias between measurements of updrafts and downdrafts and precision are important. Systematic errors biasing the concentration difference between updrafts and downdrafts are difficult to quantify. The following results quantify the precision of the gas analysis, based on the analysis of four replicated measurements of 120 s each of the accumulated updraft and downdraft concentrations, per 30 min flux integration interval. The results comprise precision of the gas analyzer at the measurement frequency of 1 Hz as well as precision of the TEA gas sampling storage and delivery system, feeding samples to the gas analyzer. The latter includes drift of the gas analyzer signal and of the trace gas concentration over the time required to determine a concentration difference between updrafts and downdrafts, i.e., 2 times 150 s.

Regarding the observed CO_2 concentration signal, 90 % of CO_2 dry molar fraction differences between updrafts and downdrafts at 30 min integration were between 0.14 and 2.08 µmol mol^{-1} (Fig. 2.20). Regarding the observed precision of the total gas analysis system under field conditions, for 90 % of flux integration intervals, the CO_2 dry molar fraction measurements over four replicated measurements of the updraft reservoir varied in the range of 0.033 to 0.48 µmol mol^{-1}. The precision of downdraft measurements was 50 % lower, with 90 % of the downdraft measurements showing a range of the four replicates of 0.05 and 0.73 µmol mol^{-1}.

For 85 % of the flux integration intervals, the signal, i.e., the dry molar fraction difference between updrafts and downdrafts, was larger than the nominal and extrapolated 120 s precision of the LI-6262 infrared gas analyzer used in this study, as well as the precision, i.e., Allan deviation, of two laser spectrometers we tested in the laboratory. The latter two instruments were not used in the current study, but characteristics are provided to put the instrument used in this study in the context of current state-of-the-art greenhouse gas monitors. Note that the indicated precision of the LI-6262 of 0.29 µmol mol^{-1} is an extrapolation of nominal precision and drift values to 120 s, for which nominal precision was given as peak-to-peak noise, rather than Allan deviation, which was used to characterize the laser spectrometers and is by definition smaller than or equal to the peak-to-peak noise.

Also note that the Allan deviation at 120 s integration of the G2301 (Picarro) instrument of 0.0125 µmol mol^{-1} appeared to be only 7.4 % of the Allan deviation of the FGGA (Los Gatos Research) laser spectrometer of 0.17 µmol mol^{-1}. However, in addition to differences in the design of the two spectrometers and any potential differences in test conditions, it appears from the analysis of Allan deviation that the G2301 (Picarro) instrument may be subject to some degree of internal smoothing of the gas concentration readings. We cannot say with certainty to which degree such potential smoothing might have affected the Allan deviation at 120 s integration time because the manufacturer of the instrument was unable to provide further information on the suspected filter beyond acknowledging its existence.

The observed signal-to-noise ratio (SNR) of the total trace gas analysis system under field conditions ranged between −9 and +21 (and one value at −66.7) and improved with the magnitude of the signal itself (Fig. 2.21a). The slope and intercept of an ordinary least-squares linear model fit to this relation were 3.2 µmol^{-1} mol and 0.48, respectively. The fact that this quasilinear relationship and the slope

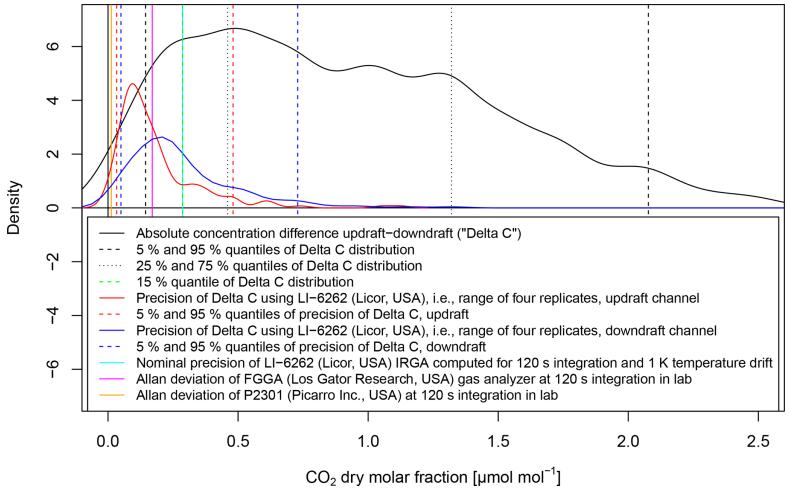

Figure 2.20: Density distributions and selected probabilities of the trace gas concentration difference signal and of the measurement uncertainties, and gas analyzer precision. The signal is the difference in molar fraction between accumulated updrafts and downdrafts (black line). The uncertainty of the measurements is expressed as the range of four replicated samples of the updraft and downdraft concentration, in red and blue, respectively. Vertical dashed lines indicate various probabilities of the above distributions. Vertical solid lines indicate the nominal precision of the LI-6262 (LI-COR, USA) infrared gas analyzer used in this study, calculated for an integration time of 120 s (cyan). Precision of two types of laser spectrometers are also shown for reference: Allan deviation of FGGA (Los Gatos Research, USA), in magenta, and G2301 (Picarro, USA), in orange, both determined in the laboratory.

significantly differed from zero means that larger fluxes have relatively smaller errors of the type considered, a feature reducing absolute uncertainty of trace gas flux budgets.

For 88 % of 30 min flux integration intervals, the signal-to-noise ratio was larger than 1 (Fig. 2.21b). Over the period of the experiment, the sum of the same noise data as above accounted for up to 25 % of the sum of the trace gas concentration signal, i.e., of the difference in CO_2 dry molar fraction between updraft and downdraft reservoirs. The percentage of 25 % is a maximum estimate for this type of noise, as it was determined from the range of the four replicates of concentration difference measurements, which is sensitive to extremes.

2.3.8 Uncertainty of trace gas flux measurements

The uncertainty of trace gas fluxes due to the uncertainty of the gas analysis is shown in Fig. 2.22. Over the period of the experiment, the sum of the noise range, i.e., the absolute value of the difference between the largest and smallest flux estimate, accounted for 37 % of the sum of the signal, i.e., the absolute value of the mean flux. As stated above for CO_2 concentrations, the percentage of 37 % is a maximum estimate of this type of noise because it was determined from the range of the four replicates of concentration difference measurements, which is sensitive to extremes, and because this estimate is additive. In practice, it is highly unlikely that this uncertainty range leads to additive errors; instead, some of the errors would cancel, leading to much smaller actual uncertainties.

Regarding the time series of trace gas flux noise, i.e., the range of maximum and minimum flux estimates (Fig. 2.22), calm conditions with low wind speeds and low friction velocities, e.g., on 10 April, result in relatively large concentration differences and relatively small vertical wind terms contributing to

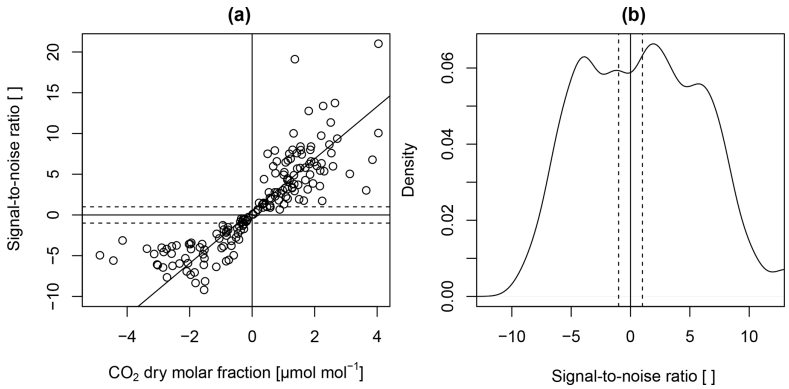

Figure 2.21: **(a)** Signal-to-noise ratio (SNR) of the trace gas dry molar fraction difference measurements as a function of the difference, the latter being proportional to the trace gas flux. The solid line is a linear model fit using ordinary least-squares regression. **(b)** Density distribution of the signal-to-noise ratio. Dashed lines in **(a)** and **(b)** indicate a signal-to-noise ratio of ±1, corresponding to probabilities of 37.7 % and 49.5 %, respectively. Consequently, in 88 % of the cases the signal-to-noise ratio is higher than 1, leaving 12 % of the cases unresolved. The display in **(a)** excludes one extreme value at SNR = −66.7.

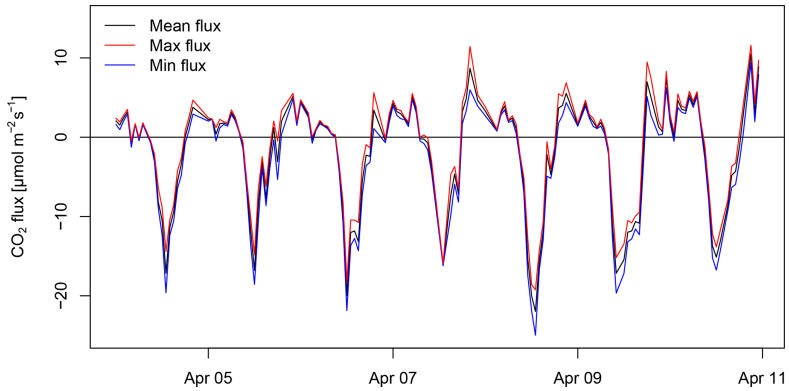

Figure 2.22: Range of CO_2 trace gas flux estimates observed by the true eddy accumulation method, accounting for the range of possible flux estimates from four replicated measurements of the dry molar fraction difference between accumulated updrafts and downdrafts per 30 min flux integration interval.

the trace gas flux calculations and therefore result in relatively low uncertainty of the flux due to the uncertainty of the gas analysis. The opposite can be observed for windy conditions with high friction velocity, e.g., on 7 April, which result in relatively small concentration differences and a relatively high contribution of the vertical wind term to the flux calculations and therefore a relatively high uncertainty of the flux due to the uncertainty of the gas analysis.

The total uncertainty of the trace gas flux needs to account for the uncertainty of the mass flow control, the uncertainty of the concentration differences, and the uncertainty of the vertical wind signal. Ideally, such analysis would incorporate the effect of different approaches of coordinate rotation not just on the residuals of $\overline{w}$ but also the effect on the fluxes themselves. This would require consideration of co-spectral information of wind and scalar using time-resolved high-frequency data and simulations of true eddy accumulation with different coordinate rotation approaches.

2.4 Conclusions

The following conclusions intend to summarize the performance of the true eddy accumulation method, put the results of the current experiment into context relative to existing published studies, summarize and quantify main sources of uncertainty, report on limitations and lessons learned during the current experiment, suggest future improvements regarding technical and methodological aspects, and finally identify applications in which true eddy accumulation can facilitate novel flux measurements in the future.

The current study has presented CO_2 fluxes measured by true eddy accumulation. The TEA system measured continuously and automatically fluxes at 30 min resolution over a duration of more than 7 d. The TEA measurements were able to capture fluxes representing the biological activity of the system. TEA flux measurements compared favorably with eddy covariance reference measurements, with R^2 values of up to 86 % and a regression slope of 0.98.

A novel implementation of dynamic mass flow control was key to the success. It was 50 times more accurate in terms of root mean square error than the conventional thermal mass flow controller reference during laboratory tests and proved to be robust and without failure during more than 3 years of operating time in the field. Further innovative features were the digital signal processing and the real-time sampling decisions, incorporating online coordinate rotation and correction of the mean vertical wind, and, finally, the elimination of dead volumes in the gas sampling system.

Compared to earlier studies published on true eddy accumulation flux measurements (Desjardins, 1977, on temperature fluxes; Speer et al., 1985, and Neumann et al., 1989, on water vapor fluxes; Rinne et al., 2000, on isoprene fluxes; and Komori et al., 2004, on CO_2 fluxes), the current study obtained the best fit of TEA fluxes to EC fluxes of any trace gas or scalar. The current study also presents the longest continuous CO_2 flux measurements by TEA.

A detailed analysis of uncertainties of the TEA method was presented in terms of the uncertainty of the mass flow controllers, the uncertainty of the trace gas handling and analysis system, and the uncertainty of the vertical wind velocity measurements and 30 min means. Uncertainties of the eddy covariance method and instruments were partially quantified through two replicated flux computations using two alternative sonic anemometers. Uncertainties of the EC fluxes explained a significant fraction of the mismatch between the TEA and EC methods. The signal-to-noise ratio of the TEA trace gas analysis system allowed the concentration difference signal to be detected in 88 % of 30 min flux intervals. Maximum uncertainty estimates of the TEA trace gas measurement precision accounted for up to 25 % of the concentration differences and up to 37 % of the fluxes. A comparison of the precision of three gas analyzers suggests that deployment of state-of-the-art laser spectrometers would significantly reduce TEA flux uncertainty due to uncertainties in the gas analysis, with preliminary analysis suggesting an improvement in precision by a factor of 10 or more for some instrument models. This would likely reduce the flux uncertainty due to the gas analysis to about 5 % or less. Residual mean vertical wind velocities were generally smaller than 0.05 m s^{-1}. Uncertainties of the mean of absolute vertical wind velocities, which are needed for flux calculations, in terms of undesired residuals of mean vertical wind velocities after coordinate rotation were frequently on the order of 5 %. The uncertainties of the mass flow control were relatively small compared to uncertainties of the gas analysis, uncertainties of residual mean vertical wind velocities, and uncertainties of the eddy covariance flux estimates.

The following two design limitations were discovered: firstly, the continuous and long-term operation with frequent charging and discharging of the air sampling bags with on the order of 1500 charge cycles

per month over time leads to increasing levels of fatigue of the material and in turn after a few weeks to a significant amount of leakage and therefore contamination of the samples with ambient air. The second observation relates to the intermittent nature of the gas flow, the variable accumulation volumes, and the intermittent gas analysis in the current bag-based accumulation design. Intermittent operation causes instationarity of the following parameters: air pressure in the gas handling system, temperatures of air and system components, and interactions of air constituents with the internal surfaces of the device such as adsorption and desorption of gas molecules on internal surfaces. Instationary conditions can lead to signal drift, variation of moisture content, and subsequently to less accurate flux measurements.

To address the above-mentioned limitations, we suggest exploring the idea of a new system design for TEA using rigid air containers of constant volume and with continuous-flow operation replacing flexible air bags. In such a new design the charging and discharging of the air reservoirs would happen continuously and at the same time. This new design principle would overcome the issue of material fatigue and compromised accuracy due to instationarities in the operation. A key methodological advantage of the new continuous-flow design is furthering the opportunity to merge the principles of true eddy accumulation sampling with eddy covariance sampling simultaneously with the very same measurement device, the same air samples, and the same gas analyzer.

Using a precise state-of-the-art laser spectrometer we have since implemented such a continuous-flow system suggested above and demonstrated its superior performance compared to conventional discrete cyclic charging of air bags. True eddy accumulation CO_2 fluxes observed with the new continuous-flow system were tightly correlated with eddy covariance fluxes, with R^2 values of up to 96 %. More details on the latter study will be reported separately.

The impact of coordinate rotation on true eddy accumulation fluxes has been discussed. We have suggested a new type of coordinate rotation, which we refer to as “surface fit”. Similar to the planar fit method, it aligns the coordinate system with the mean streamlines, accounting for a multidimensional parameter set including wind direction, flow distortion, and optionally other independent variables in an integrative, continuous way.

We would like to highlight the need for research on flux corrections for TEA in a comprehensive way similar to the body of work which exists on EC flux corrections. Future work needs to investigate and establish flux corrections specifically for the TEA method, including the equivalent to the correction of trace gas fluxes due to density fluctuations caused by simultaneous transfer of heat and water vapor (Webb et al., 1980). The derivation of this and other corrections specifically for the TEA method is nontrivial and will be addressed in separate work.

The current implementation of TEA suggests that this method has the potential to facilitate flux measurements of trace gases and other atmospheric constituents for which no fast gas analyzers are available. TEA is an alternative when the precision and accuracy of currently available analyzers are insufficient for high-frequency EC applications. The low power consumption of the current TEA systems with low sample flow rates will enable new applications, including off-grid use in solar- and battery-powered stationary and mobile applications. The long sample integration times give TEA a further advantage over EC, allowing for a simpler analyzer design compared to high-frequency analyzers at the same precision or alternatively providing ultimate precision through long integration times when using a high-quality analyzer.

It is evident that CO_2 fluxes in particular can be readily observed with alternative methods. However, the nonreactive and nonpolar trace gas CO_2 is an ideal candidate to assess the performance of the

TEA method. The current experiment is a successful proof of concept demonstrating that true eddy accumulation with dynamic and accurate air sampling proportional to vertical wind velocity can be achieved in practice today. The lessons learned during the present work provide concise avenues including the above-outlined machine design considerations and required flux corrections for further improving the true eddy accumulation method to enable accurate and reliable flux measurements of more trace gases and atmospheric constituents than ever before.

Data availability. The data supporting this publication can be found at doi:10.5281/zenodo.3338395 (Siebicke and Emad, 2019).

Author contributions. This study was conceptualized, designed, performed, analyzed, interpreted, managed, and written by LS with contributions to post-processing of gas analyzer data, to TEA flux calculations, and to discussions on the methods by AE. The mass flow control system used in this study was conceptualized, designed, built, and calibrated by LS.

Competing interests. The authors declare that they have no conflict of interest.

Disclaimer. Any statements about the performance of measurement devices presented in this study, including commercially available gas analyzers, sonic anemometers, or mass flow controllers, are based on observations from the actual units deployed in the current study and do not claim general validity for other types or different units of the same type or under different conditions.

Acknowledgements. We would like to thank the two anonymous referees and the editor for their constructive, useful comments, which have improved the manuscript. We gratefully acknowledge the support of the Bioclimatology group, Alexander Knohl, University of Göttingen, in particular technical assistance by Malte Puhan, Dietmar Fellert, Frank Tiedemann, and Heiner Kreilein during calibration, preparation, and setup of instruments in the field and for the provision of meteorological measurements. We further acknowledge Jelka Braden-Behrens and Christian Markwitz for fruitful discussions during preparation of the manuscript as well as Karly Conrads and Fernando Moyano for proofreading. Lukas Siebicke would like to thank Thomas Foken for exposure to the theory of eddy accumulation flux measurements as well as Benoit Burban, Jean-Yves Goret, James Morison, Mike Perks, and Dorothea Schreiber for their support and trust along the way.

Review statement. This paper was edited by Hartwig Harder and reviewed by two anonymous referees.

Bibliography

Ammann, C. and Meixner, F.: Stability dependence of the relaxed eddy accumulation coefficient for various scalar quantities, J. Geophys. Res.-Atmos., 107, ACL7-1–ACL7-9, 2002.

Aubinet, M., Heinesch, B., and Yernaux, M.: Horizontal and vertical CO_2 advection in a sloping forest, Bound.-Lay. Meteorol., 108, 397–417, 2003.

Baker, J.: Conditional sampling revisited, Agr. Forest Meteorol., 104, 59–65, doi:10.1016/S0168-1923(00)00147-7, 2000.

Baker, J., Norman, J., and Bland, W.: Field-scale application of flux measurement by conditional sampling, Agr. Forest Meteorol., 62, 31–52, doi:10.1016/0168-1923(92)90004-N, 1992.

Baldocchi, D.: Assessing the eddy covariance technique for evaluating carbon dioxide exchange rates of ecosystems: past, present and future, Glob. Change Biol., 9, 479–492, doi:10.1046/j.1365-2486.2003.00629.x, 2003.

Baldocchi, D.: Measuring fluxes of trace gases and energy between ecosystems and the atmosphere – the state and future of the eddy covariance method, Glob. Change Biol., 20, 3600–3609, doi:10.1111/gcb.12649, 2014.

Baldocchi, D. D., Hincks, B. B., and Meyers, T. P.: Measuring biosphere-atmosphere exchanges of biologically related gases with micrometeorological methods, Ecology, 69, 1331–1340, 1988.

Beier, N.: Measuring fluxes of chemical components by eddy accumulation, in: 7th Symposium on Meteorological Observations and Instrumentation, American Meteorological Society, Boston, MA, 1–5, 1991.

Bowling, D. R., Delany, A. C., Turnipseed, A. A., Baldocchi, D. D., and Monson, R. K.: Modification of the relaxed eddy accumulation technique to maximize measured scalar mixing ratio differences in updrafts and downdrafts, J. Geophys. Res.-Atmos., 104, 9121–9133, doi:10.1029/1999JD900013, 1999.

Buckley, D., Desjardins, R., Lalonde, J., and Brunke, R.: A linearized, fast response gas sampling apparatus for eddy accumulation studies, Comput. Electron. Agric., 2, 243–250, 1988.

Businger, J.: Evaluation of the accuracy with which dry deposition can be measured with current micrometeorological techniques, J. Clim. Appl. Meteorol., 25, 1100–1124, 1986.

Businger, J. A. and Oncley, S. P.: Flux Measurement with Conditional Sampling, J. Atmos. Ocean. Tech., 7, 349–352, 1990.

Cancelli, D. M., Chamecki, M., and Dias, N. L.: A Study of the Similarity between Scalars over a Heterogeneous Surface Using Large-Eddy Simulation, Am. J. Environ. Engineer., 5, 9–14, 2015.

Cleveland, W. S., Grosse, E., and Shyu, W. M.: Local regression models, in: Statistical Models in S, edited by: Chambers, J. and Hastie, T., chap. 8, Wadsworth & Brooks/Cole, 1992.

Desjardins, R.: Description and evaluation of a sensible heat flux detector, Bound.-Lay. Meteorol., 11, 147–154, doi:10.1007/BF02166801, 1977.

Desjardins, R. L.: A Study of Carbon Dioxide and Sensible Heat Fluxes Using the Eddy Correlation Technique, PhD thesis, Cornell University, 1972.

Finnigan, J. J.: A Re-Evaluation of Long-Term Flux Measurement Techniques Part II: Coordinate Systems, Bound.-Lay. Meteorol., 113, 1–41, 2004.

Finnigan, J. J., Clement, R., Malhi, Y., Leuning, R., and Cleugh, H.: A Re-Evaluation of Long-Term Flux Measurement Techniques Part I: Averaging and Coordinate Rotation, Bound.-Lay. Meteorol., 107, 1–48, 2003.

Foken, T. and Napo, C. J.: Micrometeorology, vol. 2, Springer, 362 pp., 2008.

Foken, T., Göckede, M., Mauder, M., Mahrt, L., Amiro, B. D., and Munger, J. W.: Post-field data quality control, in: Handbook of Micrometeorology: A Guide for Surface Flux Measurements, edited by: : Lee, X., Massman, W. J., and Law, B., 181–208, Kluwer, Dordrecht, 2004.

Foken, T., Babel, W., and Thomas, C.: Possible errors in flux measurements due to limited digitalization, Atmos. Meas. Tech., 12, 971–976, doi:10.5194/amt-12-971-2019, 2019.

Gao, W.: The vertical change of coefficient-b, used in the relaxed eddy accumulation method for flux measurement above and within a forest canopy, Atmos. Environ., 29, 2339–2347, doi:10.1016/1352-2310(95)00147-Q, 1995.

Gash, J. and Dolman, A.: Sonic anemometer (co)sine response and flux measurement. I. The potential for (co)sine error to affect sonic anemometer-based flux measurements, Agr. Forest Meteorol., 119, 195–207, 2003.

Griessbaum, F. and Schmidt, A.: Advanced tilt correction from flow distortion effects on turbulent CO_2 fluxes in complex environments using large eddy simulation, Q. J. Roy. Meteorol. Soc., 135, 1603–1613, doi:10.1002/qj.472, 2009.

Held, A., Patton, E., Rizzo, L., Smith, J., Turnipseed, A., and Guenther, A.: Relaxed Eddy Accumulation Simulations of Aerosol Number Fluxes and Potential Proxy Scalars, Bound.-Lay. Meteorol., 129, 451–468, doi:10.1007/s10546-008-9327-5, 2008.

Hicks, B. B. and McMillen, R. T.: A Simulation of the Eddy Accumulation Method for Measuring Pollutant Fluxes, J. Climate Appl. Meteorol., 23, 637–643, 1984.

Hicks, B. B., Hosker Jr., R. P., and Ma, G.-J.: A prototype concentration accumulation apparatus for determining time-averaged dry deposition of gaseous pollutants, in: Fifth Annual National Symposium on Recent advances in pollutant monitoring of ambient air and stationary sources, edited by: EPA, vol. /600/9-85/029, 16–22, 1986.

Högström, U. and Smedman, A. S.: Accuracy of sonic anemometers: Laminar wind-tunnel calibrations compared to atmospheric in situ calibrations against a reference instrument, Bound.-Lay. Meteorol., 111, 33–54, 2004.

Huq, S., De Roo, F., Foken, T., and Mauder, M.: Evaluation of probe-induced flow distortion of Campbell CSAT3 sonic anemometers by numerical simulation, Bound.-Lay. Meteorol., 164, 2–28, 2017.

Hyson, P., Garratt, J., and Francey, R.: Algebraic and electronic corrections of measured uw covariance in the lower atmosphere, J. Appl. Meteorol., 16, 43–47, 1977.

Kaimal, J. C. and Finnigan, J. J.: Atmospheric boundary layer flows: their structure and measurement, Oxford University Press, New York, 1994.

Katul, G., Finkelstein, P., Clarke, J., and Ellestad, T.: An investigation of the conditional sampling method used to estimate fluxes of active, reactive, and passive scalars, J. Appl. Meteorol., 35, 1835–1845, doi:10.1175/1520-0450(1996)035<1835:AIOTCS>2.0.CO;2, 1996.

Kelley, D. and Richards, C.: oce: Analysis of Oceanographic Data, available at: https://CRAN.R-project.org/package=oce (last access: 12 July 2019), r package version 0.9-22, 2017.

Komori, D., Aoki, M., Ishida, T., Suzuki, S., Satou, T., and Kim, W.: Development of an Air Sampling System for the True Eddy Accumulation Technique, J. Agric. Meteorol., 60, 263–272, doi:10.2480/agrmet.60.263, 2004.

Legendre, P. and Legendre, L.: Numerical ecology, Elsevier Science BV, Amsterdam, 2nd english Edn., 1998.

Lenschow, D., Mann, J., and Kristensen, L.: How long is long enough when measuring fluxes and other turbulence statistics?, J. Atmos. Ocean. Tech., 11, 661–673, 1994.

Li, M., Babel, W., Tanaka, K., and Foken, T.: Note on the application of planar-fit rotation for non-omnidirectional sonic anemometers, Atmos. Meas. Tech., 6, 221–229, doi:10.5194/amt-6-221-2013, 2013.

Licor: LI-6262 CO_2/H_2O Analyzer Operating and Service Manual, Licor, Inc., Lincoln, Nebraska, 3rd printing Edn., publication Number 9003-59, 1996.

Loescher, H. W., Ocheltree, T., Tanner, B., Swiatek, E., Dano, B., Wong, J., Zimmerman, G., Campbell, J., Stock, C., Jacobsen, L., Shiga, Y., Kollas, J., Liburdy, J., and Law, B. E.: Comparison of temperature and wind statistics in contrasting environments among different sonic anemometer–thermometers, Agr. Forest Meteorol., 133, 119–139, 2005.

Mauder, M. and Zeeman, M. J.: Field intercomparison of prevailing sonic anemometers, Atmos. Meas. Tech., 11, 249–263, doi:10.5194/amt-11-249-2018, 2018.

McMillen, R. T.: An eddy correlation technique with extended applicability to non-simple terrain, Bound.-Lay. Meteorol., 43, 231–245, 1988.

Milne, R., Beverland, I., Hargreaves, K., and Moncrieff, J.: Variation of the beta coefficient in the relaxed eddy accumulation method, Bound.-Lay. Meteorol., 93, 211–225, doi:10.1023/A:1002061514948, 1999.

Nakai, T. and Shimoyama, K.: Ultrasonic anemometer angle of attack errors under turbulent conditions, Agr. Forest Meteorol., 162, 14–26, 2012.

Nakai, T., Van der Molen, M., Gash, J., and Kodama, Y.: Correction of sonic anemometer angle of attack errors, Agr. Forest Meteorol., 136, 19–30, 2006.

Neumann, H., Den Hartog, G., and Guise-Bagley, L.: Evaluation of a digital-valve eddy accumulator using water vapour flux measurements and numerical simulations of its performance, Atmos. Environ., 23, 1305–1313, 1989.

Oldroyd, H. J., Pardyjak, E. R., Huwald, H., and Parlange, M. B.: Adapting Tilt Corrections and the Governing Flow Equations for Steep, Fully Three-Dimensional, Mountainous Terrain, Bound.-Lay. Meteorol., 159, 539–565, doi:10.1007/s10546-015-0066-0, 2016.

Oncley, S. P., Delany, A. C., Horst, T. W., and Tans, P. P.: Verification of flux measurement using relaxed eddy accumulation, Atmos. Environ. A-Gen., 27, 2417–2426, doi:10.1016/0960-1686(93)90409-R, 1993.

Pattey, E., Desjardins, R., and Rochette, P.: Accuracy of the relaxed eddy-accumulation technique, evaluated using CO_2 flux measurements, Bound.-Lay. Meteorol., 66, 341–355, doi:10.1007/BF00712728, 1993.

Paw U, K. T., Baldocchi, D. D., Meyers, T. P., and Wilson, K. B.: Correction Of Eddy-Covariance Measurements Incorporating Both Advective Effects And Density Fluxes, Bound.-Lay. Meteorol., 97, 487–511, doi:10.1023/A:1002786702909, 2000.

R Core Team: R: A Language and Environment for Statistical Computing, R Foundation for Statistical Computing, Vienna, Austria, available at: https://www.R-project.org/ (last access: 12 July 2019), 2017.

Rinne, H., Delany, A., Greenberg, J., and Guenther, A.: A true eddy accumulation system for trace gas fluxes using disjunct eddy sampling method, J. Geophys. Res.-Atmos., 105, 24791–24798, doi:10.1029/2000JD900315, 2000.

Ross, A. N. and Grant, E. R.: A new continuous planar fit method for calculating fluxes in complex, forested terrain, Atmos. Sci. Lett., 16, 445–452, doi:10.1002/asl.580, 2015.

Ruppert, J., Wichura, B., Delany, A., and Foken, T.: 2.8 Eddy sampling methods, A comparison using simulation results, in: Symposium on Boundary Layers and Turbulence, vol. 15, p. 27, American Meteorological Society, 2002.

Ruppert, J., Thomas, C., and Foken, T.: Scalar similarity for relaxed eddy accumulation methods, Bound.-Lay. Meteorol., 120, 39–63, doi:10.1007/s10546-005-9043-3, 2006.

Shaw, R. H.: On diffusive and dispersive fluxes in forest canopies, in: The Forest-Atmosphere Interaction, Springer, 407–419, 1985.

Siebicke, L., Hunner, M., and Foken, T.: Aspects of CO_2 advection measurements, Theor. Appl. Climatol., 109, 109–131, doi:10.1007/s00704-011-0552-3, 2012.

Siebicke, L. and Emad, A.: True Eddy Accumulation Trace Gas Flux Measurements: Proof of Concept, Atmospheric Measurement Techniques, 12, 4393–4420, doi:10.5194/amt-12-4393-2019, 2019.

Siebicke, L. and Emad, A.: Data set supporting Journal article: Siebicke, L., and Emad, A., "True eddy accumulation trace gas flux measurements: proof of concept", Atmos. Meas. Tech., 12, 1–28, 2019, [Data set], Atmospheric Measurement Techniques, Zenodo, doi:10.5281/zenodo.3338395, 2019.

Sokal, R. R. and Rohlf, F. J.: Biometry – The principles and practice of statistics in biological research, W. H. Freeman, New York, 3rd Edn., 1995.

Speer, R., Peterson, K., Ellestad, T., and Durham, J.: Test of a prototype eddy accumulator for measuring atmospheric vertical fluxes of water vapor and particulate sulfate, J. Geophys. Res.-Atmos., 90, 2119–2122, doi:10.1029/JD090iD01p02119, 1985.

Speer, R. E., Ellestad, T. G., and Durham, J. L.: An eddy accumulator for dry deposition measurements, in: Fifth Annual National Symposium on Recent advances in pollutant monitoring of ambient air and stationary sources, edited by: EPA, vol. /600/9-85/029, 7–15, 1986.

Sun, J., Burns, S. P., Delany, A. C., Oncley, S. P., Turnipseed, A. A., Stephens, B. B., Lenschow, D. H., LeMone, M. A., Monson, R. K., and Anderson, D. E.: CO_2 transport over complex terrain, Agr. Forest Meteorol., 145, 1–21, 2007.

Tanner, C. B. and Thurtell, G. W.: Anemoclinometer measurements of Reynolds stress and heat transport in the atmospheric surface layer, Tech. rep., Wisconsin Univ.-Madison Dept. of Soil Science, 1969.

Turnipseed, A. A., Pressley, S. N., Karl, T., Lamb, B., Nemitz, E., Allwine, E., Cooper, W. A., Shertz, S., and Guenther, A. B.: The use of disjunct eddy sampling methods for the determination of ecosystem level fluxes of trace gases, Atmos. Chem. Phys., 9, 981–994, doi:10.5194/acp-9-981-2009, 2009.

van der Molen, M., Gash, J., and Elbers, J.: Sonic anemometer (co)sine response and flux measurement. II. The effect of introducing an angle of attack dependent calibration, Agr. Forest Meteorol., 122, 95–109, 2004.

Van Dijk, A., Moene, A., and De Bruin, H.: The principles of surface flux physics: theory, practice and description of the ECPACK library, Meteorology and Air Quality Group, Wageningen University, Wageningen, the Netherlands, 99, 525, 2004.

Vickers, D. and Mahrt, L.: Quality control and flux sampling problems for tower and aircraft data, J. Atmos. Ocean. Tech., 14, 512–526, 1997.

Webb, E. K., Pearman, G. I., and Leuning, R.: Correction of flux measurements for density effects due to heat and water vapour transfer, Q. J. Roy. Meteor. Soc., 106, 85–100, 1980.

Wichura, B., Buchmann, N., and Foken, T.: Fluxes of the stable carbon isotope 13C above a spruce forest measured by hyperbolic relaxed eddy accumulation method, in: 14th Symposium on Boundary Layer and Turbulence, 559–562, Am. Meteorol. Soc., Boston, Aspen, CO, 2000.

Wilczak, J. M., Oncley, S. P., and Stage, S. A.: Sonic anemometer tilt correction algorithms, Bound.-Lay. Meteorol., 99, 127–150, 2001.

Wyngaard, J.: The effects of probe-induced flow distortion on atmospheric turbulence measurements, J. Appl. Meteorol., 20, 784–794, 1981.

Wyngaard, J. and Moeng, C.: Parameterizing turbulent-diffusion through the joint probability density, Bound.-Lay. Meteorol., 60, 1–13, doi:10.1007/BF00122059, 1992.

Yuan, R., Kang, M., Park, S.-B., Hong, J., Lee, D., and Kim, J.: Expansion of the planar-fit method to estimate flux over complex terrain, Meteorol. Atmos. Phys., 110, 123–133, doi:10.1007/s00703-010-0113-9, 2011.

3 True eddy accumulation – Part 1: Solutions to the problem of non-vanishing mean vertical wind velocity

Paper published in *Atmospheric measurement techniques* and selected as highlight paper (Emad and Siebicke, 2023).

Emad, A. and Siebicke, L.: True eddy accumulation – Part 1: Solutions to the problem of non-vanishing mean vertical wind velocity, Atmos. Meas. Tech., 16, 29–40, doi:10.5194/amt-16-29-2023, 2023.

Abstract

The true eddy accumulation (TEA) method provides direct measurements of ecosystem-level turbulent fluxes for a wide range of atmospheric constituents. TEA utilizes conditional sampling to overcome the requirement for a fast sensor response demanded by the state-of-the-art eddy covariance (EC) method.

The TEA method is formulated under the assumption of ideal conditions with a zero mean vertical wind velocity during the averaging interval. However, this idealization is rarely met under field conditions. Additionally, unlike in EC, this assumption cannot be imposed in post-processing due to the real-time nature of sampling and the absence of high-frequency measurements of the scalar. Consequently, fluxes measured with the TEA method are biased with a non-turbulent advective term that scales with the scalar mean concentration.

Here, we explore the magnitude of this biased advective term and potential ways to minimize or remove it. We propose a new formulation to calculate TEA fluxes that minimizes the bias term. The new formulation shows that the magnitude of the error is constrained to $\overline{w}/\overline{|w|}$ when the stationarity criterion is fulfilled. Here, w is the vertical wind velocity, and the overbar denotes time averaging. The error is shown to be dependent on the asymmetry of atmospheric transport, represented by the coefficient α_c. Two methods of estimating the coefficient α_c are proposed: a probabilistic treatment of turbulent transport and a method utilizing the assumption of scalar similarity. We show how other formulas for calculating the TEA flux are linked to the new formulation and explore the different corrections in a numerical simulation.

The new formulation avoids the direct dependence of the bias term on the scalar background concentration. This result increases confidence in applying the TEA method to measuring fluxes of atmospheric constituents. This is particularly relevant to scalars with a large background concentration and a small flux. This paper is Part 1 of a two-part series on true eddy accumulation.

3.1 Introduction

Micrometeorological methods provide noninvasive, in situ, integrated, and continuous point measurements for ecosystem fluxes on a scale ideal for ecosystem study (Baldocchi et al., 1988; Baldocchi, 2014). Among micrometeorological methods, eddy covariance (EC) has become the de facto method for measuring ecosystem fluxes for the past 40 years. The EC method is the most direct micrometeorological method. It is also relatively easy to set up and operate. These features have led to the wide use and adoption of the EC method at hundreds of sites worldwide, including several regional and global flux measurement networks such as ICOS and FLUXNET (Hicks and Baldocchi, 2020).

The EC method depends on the fast measurement of vertical wind velocity and the scalar concentration (such as an atmospheric constituent). The requirement for fast measurement frequency (10 to 20 Hz) limits the application of the method to a handful of atmospheric constituents for which fast gas analyzers are available. Alternative methods that work for slow gas analyzers include (i) signal downsampling methods (Lenschow et al., 1994), such as disjunct eddy accumulation (H. J. I. Rinne et al., 2000; Turnipseed et al., 2009) and disjunct eddy covariance (Rinne and Ammann, 2012), and (ii) indirect methods such as flux gradient methods (e.g., J. Rinne et al., 2000) which depend on the Monin–Obukhov similarity theory (Monin and Obukhov, 1954) and relaxed eddy accumulation (REA) which assumes flux-variance similarity (Businger and Oncley, 1990). The true eddy accumulation (TEA) method (Desjardins, 1977) is the most direct and mathematically equivalent alternative to eddy covariance among accumulation methods. Unlike EC, the TEA method requires the concentration

measurements to be carried out once every averaging interval (30 min) (Businger and Oncley, 1990). The TEA method is formulated under ideal conditions assuming a zero mean vertical wind velocity during the averaging interval. This assumption is almost never met under field conditions, and it is not possible to enforce in post-processing due to lacking high-frequency information on the scalar concentration. As a result, the non-vanishing vertical mean velocity will contribute to a systematic error in the flux. Nonzero mean vertical wind velocity is a source of error for all eddy accumulation methods, including TEA (Hicks and McMillen, 1984), relaxed eddy accumulation (REA) (Pattey et al., 1993; Businger and Oncley, 1990; Bowling et al., 1998), and disjunct eddy accumulation (DEA) (Turnipseed et al., 2009). The reported bias in the flux due to nonzero $\overline{w}$ varies with different studies and accumulation methods. For TEA, Hicks and McMillen (1984) recommended that $\overline{w}$ should not exceed $0.0005\,\sigma_w$ if accumulated mass is measured and $0.02\,\sigma_w$ when concentrations are measured directly. Turnipseed et al. (2009) reported that a mean vertical wind bias of $\pm\,0.25\,\sigma_w$ leads to a $\pm\,15\,\%$ mean systematic bias in the flux using the disjunct eddy accumulation method. Values reported for the REA method show a systematic bias of approximately 5 % of the flux due to a $\overline{w}$ of $0.20\,\sigma_w$ (Pattey et al., 1993), which agrees with the recommendations of Businger and Oncley (1990). The magnitude of the residual mean vertical velocity depends on the meteorological and topographic features of the measurement site and is larger at complex sites (Rannik et al., 2020).

In this paper, we revise the theory of the true eddy accumulation method and obtain a generalized equation that isolates the error due to nonzero vertical wind velocity. The new equation shows that the error in the flux is a function of the atmospheric transport represented by the transport asymmetry coefficient, α_c. We study the value and the interpretation of this coefficient in the framework of quadrant analysis and define its boundary conditions. Next, we show analytical and empirical ways to obtain the transport asymmetry coefficient and explore the implications of these estimates for the flux in a numerical simulation. Finally, we show how existing formulations for calculating the TEA flux are special cases of the new equation.

3.2 Theory

3.2.1 Eddy covariance

The net ecosystem exchange (NEE) $\overline{\mathrm{N}_c}$ of a scalar c (such as an atmospheric constituent) is the total vertical flux $\overline{wc}$ across the measurement plane at a height h and the change in storage below that height (Gu et al., 2012):

$$\overline{\mathrm{N}_c} = \overline{wc}\big|_h + \int_0^h \frac{\partial c}{\partial t}\mathrm{d}z, \tag{3.1}$$

where w is the vertical wind velocity ($\mathrm{m\,s^{-1}}$), and c is the molar density ($\mathrm{mol\,m^{-3}}$) of the scalar of interest (such as CO_2). The previous equation can be reached either from a holistic mass balance approach or by averaging the continuity equation for the scalar c and integrating from the surface to measurement height h. In both cases, horizontal advection is ignored as a virtue of the assumption of horizontal homogeneity, and molecular diffusion is ignored due to its small magnitude (Gu et al., 2012). For a full discussion on the equations of surface flux, see, for example Finnigan et al. (2003) and Foken et al. (2012a).

The storage term measurements and value are beyond the scope of this study, and therefore we ignore them. Consequently, the total vertical flux is represented by the first term on the right-hand side of

Eq. (3.1), which can be further decomposed into turbulent and mean advective parts.

$$\overline{wc} = \overline{w'c'} + \overline{w}\,\overline{c} \tag{3.2}$$

The overlines denote ensemble averages that obey Reynolds averaging rules. Primes represent departures from the mean. The ensemble averages are estimated experimentally by time averages. Thus, for a stationary time series drawn from an ensemble, the turbulent flux for the averaging period, Δt, can be written as

$$F_{\Delta t} = \frac{1}{\Delta t}\int_0^{\Delta t} w'(t)c'(t)\,\mathrm{d}t = \overline{w'c'}, \tag{3.3}$$

where $w(t)$ and $c(t)$ are realizations of the vertical wind velocity and the scalar quantity such as CO_2 concentration, respectively.

3.2.2 True eddy accumulation

The true eddy accumulation method circumvents the need to record the fluctuations of scalar concentration at a frequency sufficient to represent the individual flux transport eddies. Instead, it is sufficient to measure the mean product $\overline{wc}$ for updraft and downdraft once for each averaging interval, Δt (e.g., 30 min).

The product of w and c is realized by physically collecting air samples with a flow rate proportional to the vertical wind velocity, w. The method is formulated assuming ideal conditions in which the mean vertical wind velocity during the averaging period is assumed to be zero. When $\overline{w} = 0$, the second term on the right-hand side of Eq. (3.2) will be zero and the turbulent flux $\overline{w'c'}$ will equal the total ecosystem flux $\overline{wc}$. By separating $\overline{wc}$ depending on the direction of the vertical wind velocity we can write

$$\overline{wc} = \frac{1}{\Delta t}\int_0^{\Delta t} (\delta^+ cw + \delta^- cw)\,\mathrm{d}t, \tag{3.4}$$

$$\text{where } \begin{cases} w > 0 & \delta+ = 1;\ \delta- = 0 \\ w < 0 & \delta+ = 0;\ \delta- = 1. \end{cases} \tag{3.5}$$

Hence, by sampling air with a flow rate proportional to the magnitude of vertical wind velocity and accumulating it according to its direction in updraft and downdraft reservoirs, one can measure the quantity $\overline{wc}$ and consequently the flux without having to measure the high-frequency fluctuations of the scalar, c (Desjardins, 1977; Hicks and McMillen, 1984).

Sampling air proportional to the magnitude of vertical wind velocity requires a scaling parameter, A, that ensures the proportionality of the flow rate to the magnitude of vertical wind velocity. The scaling parameter is the product of the pump calibration coefficients and other coefficients used to adjust the system's dynamic range. For a short interval of time $\mathrm{d}t$, a sample of the volume $V_{\text{sample}} = A|w|\,\mathrm{d}t$ will be collected in the system. The accumulated sample volume in each of the two reservoirs during a long enough averaging period Δt (30 to 60 min) will be

$$V_{\text{total}} = \frac{1}{\Delta t}\int_0^{\Delta t} A|w|\,\mathrm{d}t. \tag{3.6}$$

By the end of the averaging period, Δt, the flux will be equal to the difference in the scalar accumulated

mass between updraft and downdraft reservoirs.

If it is desired to formulate the flux in terms of the accumulated scalar concentration (mol m^{-3}) instead of the accumulated mass, the average scalar density of accumulated samples in each of the reservoirs will equal the accumulated mass of the scalar divided by the accumulated volume:

$$C_{\mathrm{acc}}^{\uparrow\downarrow} = \frac{m}{V} = \frac{\overline{c\,|w^{\uparrow\downarrow}|}}{\overline{|w^{\uparrow\downarrow}|}}, \tag{3.7}$$

where C_{acc} is the accumulated scalar density and the arrows indicate the reservoir. The measured concentration in Eq. (3.7) is the weighted mean of the scalar concentration and the magnitude of the vertical wind velocity.

When $\overline{w}$ is assumed to be zero, $\overline{|w^{\uparrow}|} = \overline{|w^{\downarrow}|} = \overline{|w|}/2$, and we can write the flux in terms of concentrations of accumulated samples, similar to Hicks and McMillen (1984):

$$F_{\mathrm{TEA}} = \frac{\overline{|w|}}{2}(C_{\mathrm{acc}}^{\uparrow} - C_{\mathrm{acc}}^{\downarrow}), \tag{3.8}$$

where $\overline{|w|}$ is the mean of the magnitude of the vertical wind velocity.

3.2.3 The problem of nonzero mean vertical wind

Although the total ecosystem flux is defined to be $\overline{wc}$ in Eq. (3.2), it is not possible to directly use the measured w and c to calculate the total flux. The reason is the difficulty of obtaining an accurate measurement of w. Any non-turbulent offset (bias) in the mean vertical velocity will lead to a flux biased with $\overline{wc}$. Several factors contribute to a biased mean vertical wind velocity including topography at particular in complex sites, non-alignment of the anemometer with local topography, biases in anemometers, flow perturbations, and meteorological factors induced by local circulation or topographical drainage (Lee et al., 2005; Paw U et al., 2000; Heinesch et al., 2007). Therefore, the measured biased advective term needs to be discarded and the true physical term, known as the "Webb term" or Webb–Pearman–Leuning (WPL) term, needs to be estimated by other means (Webb et al., 1980; Fuehrer and Friehe, 2002). The original formulation of the TEA method assumes a zero mean vertical wind velocity during the flux averaging interval and thus assumes the total ecosystem flux to be equal to the turbulent flux, $\overline{w'c'}$. However, this assumption is rarely valid under field conditions for the reasons outlined earlier, and the measured TEA flux will be a biased total vertical flux, $\overline{wc}$. If the turbulent flux is to be measured using the TEA method, the biased term $\overline{wc}$ needs to be removed.

Previous efforts have been focused on minimizing $\overline{w}$ to reduce the bias in the TEA flux. However, since the wind information cannot be changed after sampling, any treatments for the wind velocity measurements are final when the air samples have been collected. Thus, there is no way to guarantee a zero mean vertical velocity. A common approach to nullifying mean vertical wind velocity in EC measurements is to rotate the wind coordinates in post-processing to force $\overline{w}$ to zero for each averaging interval. This method – commonly referred to as double rotation – is not feasible in eddy accumulation methods. The planar fit method (Wilczak et al., 2001) and its variants, such as the sector-wise planar fit (Foken et al., 2004), are better suited for online application in the TEA method (Siebicke and Emad, 2019).

The planar fit method aligns the sonic coordinates with the long-term streamline coordinates by aligning the wind vector with the plane that minimizes the sum of squares of the vertical wind velocity means for a long period of time (weeks to months). This approach, while minimizing the vertical wind velocity means of the individual averaging intervals, does not force them to be zero. Considerable spread of $\overline{w}$ values around zero can still be observed after applying the planar fit method (Sun, 2007; Rannik et al., 2020).

3.2.4 TEA equation under nonzero $\overline{w}$ conditions

The goal here is to enable measuring the turbulent flux $\overline{w'c'}$ from TEA measurements when $\overline{w} \neq 0$. The key to extending the TEA equation to conditions of nonzero $\overline{w}$ is to obtain an estimate of the scalar mean $\overline{c}$ from TEA measurements and consequently remove the biased advective term $\overline{w}\,\overline{c}$. We achieve this by using the weighted mean of c and $|w|$ as an estimate for c after correcting for the correlation between them.

The weighted mean of the scalar, c, and the vertical wind velocity magnitude, $|w|$, can be obtained from TEA measurements according to Eq. (3.7). By decomposing $\overline{c|w|}$ into mean and fluctuating parts,

$$\overline{c|w|} = \overline{c'|w|'} + \overline{c}\,\overline{|w|}. \tag{3.9}$$

The value of $\overline{c}$ can be found to be

$$\overline{c} = \frac{\overline{c|w|}}{\overline{|w|}} - \frac{\overline{c'|w|'}}{\overline{|w|}}. \tag{3.10}$$

Substituting $\overline{c}$ in Eq. (3.2), we can write the flux as

$$\overline{w'c'} = \overline{wc} - \frac{\overline{w}}{\overline{|w|}}\,\overline{|w|c} + \frac{\overline{w}}{\overline{|w|}}\,\overline{|w|'c'}. \tag{3.11}$$

We can obtain all the terms in Eq. (3.11) from our measurements except for the covariance term $\overline{|w|'c'}$. We define the "transport asymmetry coefficient" for the scalar c (α_c) as the ratio of the covariance between the wind magnitude and the scalar to the covariance between the wind and the scalar.

$$\alpha_c \equiv \frac{\overline{c'|w|'}}{\overline{c'w'}} \tag{3.12}$$

We notice that α_c is conveniently independent of the scalar standard deviation. It can be written as

$$\alpha_c = \frac{\rho_{c|w|}\sigma_{|w|}}{\rho_{cw}\sigma_w}, \tag{3.13}$$

where $\rho_{c|w|}$ and ρ_{cw} are the correlation coefficients between c and $|w|$ and between c and w, respectively. $\sigma_{|w|}$ and σ_w are the standard deviations of $|w|$ and w, respectively. After substitution, we write the turbulent flux as

$$\overline{w'c'} = \overline{wc} - \frac{\overline{w}}{\overline{|w|}}\,\overline{|w|c} + \frac{\overline{w}}{\overline{|w|}}\,\alpha_c\,\overline{w'c'}. \tag{3.14}$$

Finally, we rearrange Eq. (3.14) and obtain the generalized TEA flux equation that gives a turbulent TEA

flux when the mean vertical wind velocity is nonzero:

$$\overline{w'c'} = \frac{\overline{wc}\,\overline{|w|} - \overline{|w|c}\,\overline{w}}{\overline{|w|} - \alpha_c \overline{w}}. \tag{3.15}$$

Calculating the corrected TEA flux

The new general equation for TEA (Eq. 3.15) extends the validity of the method to conditions in which the mean vertical wind velocity is nonzero. We show here how the turbulent TEA flux can be calculated from the measured physical quantities.

The weighted mean over an averaging period Δt can be written as

$$\frac{\overline{c|w|}}{\overline{|w|}} = \overline{c|w\uparrow|}\,\frac{\overline{|w\uparrow|}\Delta t^{\uparrow}}{\overline{|w|}\Delta t} + \overline{c|w\downarrow|}\,\frac{\overline{|w\downarrow|}\Delta t^{\downarrow}}{\overline{|w|}\Delta t}, \tag{3.16}$$

which in terms of the quantities we are measuring, translates to

$$\overline{c|w|} = \overline{|w|}\left(\frac{C^{\uparrow}_{\mathrm{acc}} V^{\uparrow} + C^{\downarrow}_{\mathrm{acc}} V^{\downarrow}}{V_{\mathrm{total}}}\right). \tag{3.17}$$

Similarly,

$$\overline{cw} = \overline{|w|}\left(\frac{C^{\uparrow}_{\mathrm{acc}} V^{\uparrow} - C^{\downarrow}_{\mathrm{acc}} V^{\downarrow}}{V_{\mathrm{total}}}\right). \tag{3.18}$$

After substitution and simplification, we obtain the TEA flux in terms of the measured quantities:

$$\begin{aligned} F_{\mathrm{TEA}} = {} & \frac{C^{\uparrow}_{\mathrm{acc}}\, V^{\uparrow}\left(\overline{|w|} - \overline{w}\right) - C^{\downarrow}_{\mathrm{acc}}\, V^{\downarrow}\left(\overline{|w|} + \overline{w}\right)}{\overline{|w|} - \alpha_c \overline{w}} \\ & \times \frac{\overline{|w|}}{V_{\mathrm{total}}}, \end{aligned} \tag{3.19}$$

where F_{TEA} is the kinematic flux density ($\mathrm{mol\,m\,s^{-1}}$). $C^{\uparrow}_{\mathrm{acc}}$ and $C^{\downarrow}_{\mathrm{acc}}$ are the mean concentrations ($\mathrm{mol\,m^{-3}}$) of the scalar c in updraft and downdraft reservoirs at the end of the averaging period, Δt. $V^{\uparrow}$ and $V^{\downarrow}$ are the accumulated sample volumes ($\mathrm{m^3}$) in updraft and downdraft reservoirs during the averaging period. $\overline{|w|}$ is the mean of the absolute vertical wind velocity ($\mathrm{m\,s^{-1}}$) during the averaging period.

3.2.5 Values of the transport asymmetry coefficient α_c

Quadrant analysis of α_c

The value of α_c can be analyzed using the framework of quadrant analysis. Quadrant analysis is commonly used to inspect the contributions from different quadrants in the (w', c') plane by sorting the instantaneous values into four categories (S_1 .. S_4) according to the sign of the two fluctuating components (e.g., Katul et al., 1997; Raupach, 1981; Katsouvas et al., 2007). Here, S_i is the fraction of the flux transported by contributions in quadrant i. Following the definition of Thomas and Foken

(2007), the pairs S_2 and S_4 are ejections and sweeps for downward-directed net flux (negative ρ_{wc}) and S_1 and S_3 for upward-directed net flux (positive ρ_{wc}).

The total flux is the sum of the contributions from the four quadrants. We similarly find that the covariance term $\overline{|w'|c'}$ can be written as

$$\overline{|w'|c'} = S_1 + S_4 - S_2 - S_3. \tag{3.20}$$

It follows that α can be written in terms of quadrants as

$$\alpha = \frac{S_1 + S_4 - (S_2 + S_3)}{S_1 + S_2 + S_3 + S_4}. \tag{3.21}$$

It should be noted that when $\overline{w} \neq 0$, $\overline{|w'|c'}$ is an approximation for $\overline{|w|'c'}$, the latter can be found to be

$$\overline{|w|'c'} = \overline{|w' + \overline{w}|'c'}. \tag{3.22}$$

The contributions of $\overline{|w|'c'}$ can be accommodated in this analysis by partitioning the contributions into six categories: the four quadrants and two additional bands for the contributions when w' falls between 0 and $\overline{w}$. However, the contribution from the additional bands is small and has little impact on the interpretation of this analysis.

Consider that the quadrants $S1$ and $S4$ represent the contribution of updrafts to the flux. Similarly, $S2$ and $S3$ represent the contribution of downdrafts to the flux. We define

$$\text{flux}^{\uparrow} = S1 + S4, \tag{3.23}$$

$$\text{flux}^{\downarrow} = S2 + S3. \tag{3.24}$$

Here, the arrows indicate the direction of the wind and not the sign of the flux; e.g., $\text{flux}^{\uparrow}$ is the portion of the flux transported with updrafts which can be either positive or negative flux. If follows that α_c can be written as

$$\alpha_c = \frac{\text{flux}^{\uparrow} - \text{flux}^{\downarrow}}{\text{flux}^{\uparrow} + \text{flux}^{\downarrow}}. \tag{3.25}$$

The previous equation indicates that if the flux transported with updrafts, $\text{flux}^{\uparrow}$, has the same sign as the flux transported with downdrafts, $\text{flux}^{\downarrow}$, then the value of $|\alpha_c|$ will be smaller than 1. If $|\alpha_c| > 1$ then $\text{flux}^{\uparrow}$ and $\text{flux}^{\downarrow}$ have opposing signs, which indicates that the wind and the scalar are correlated for updrafts and anticorrelated for downdrafts or vice versa, indicating nonstationary conditions.

Analytical value of α_c

An analytical expression for the value of α can be obtained from knowledge of the joint probability distribution of the vertical wind velocity and the scalar. If the wind and the scalar are assumed to follow a Gaussian joint probability density function, we find the analytical value of α_c in terms of the

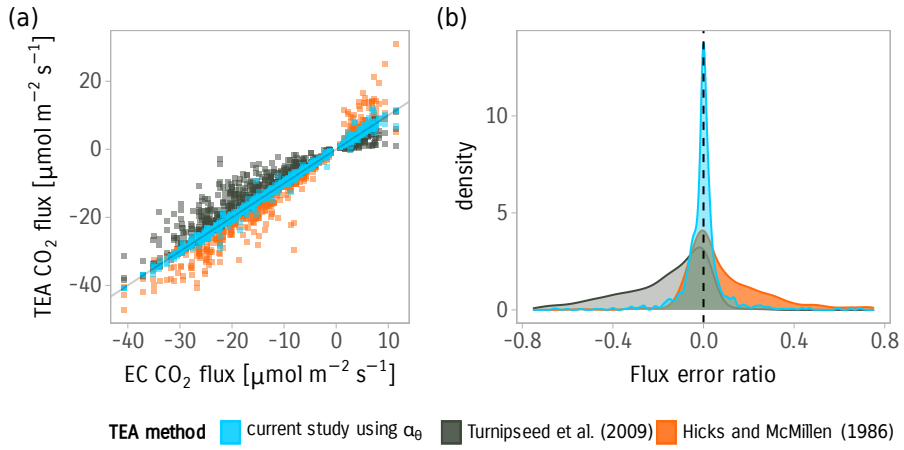

Figure 3.1: (a) Comparison of different equations of TEA flux calculation against a reference EC flux. Data were obtained from high-frequency measurements over 12 d from 15 June 2020 to 26 June 2020 and included an added random $\overline{w}$ offset in the range −0.25 to 0.25 m s^{-1}. Colors represent different formulas. **(b)** Kernel density estimates of the flux error ratio using the three different formulas.

moments of the joint probability density function to be

$$\alpha_c = \mathrm{erf}\left(\frac{\overline{w}}{\sqrt{2}\sigma_w}\right), \tag{3.26}$$

where erf is the error function, and σ_w is the wind standard deviation.

We can use the analytical value of α_c and further substitute the expected value of $|w|$ with the mean of the folded normal distribution (Leone et al., 1961) to obtain an analytical expression for the expectation of the flux error due to a nonzero vertical wind velocity using $\overline{w}$ and σ_w. The analytical expression of the relative error in the flux is found to be

$$F_{\mathrm{err}} = \overline{w}\sqrt{\pi}\left(\sqrt{2}\sigma_w \mathrm{e}^{-\frac{(\overline{w})^2}{2\sigma_w{}^2}} + \mathrm{erf}\left(\frac{\overline{w}}{\sqrt{2}\sigma_w}\right)\overline{w}\sqrt{\pi}\right)^{-1}\alpha_c. \tag{3.27}$$

Here, F_{err} is the error in the TEA flux when failing to account for the correlation between the scalar and the magnitude of vertical wind velocity.

Scalar similarity to estimate α_c

The assumption of scalar similarity provides a potential empirical way to estimate the value of α_c, i.e., by calculating the value of α_c from another scalar for which high-frequency measurements are available, e.g., sonic temperature. The assumption of scalar similarity is supported by experimental evidence that has shown that different scalars behave similarly due to a similar transfer mechanism (Ohtaki, 1985; Wesely, 1988). However, the assumption of scalar similarity cannot be always guaranteed and should be used with caution. Nonetheless, we believe it is a useful assumption to approximate the value of α_c given that the value of α_c is determined by the distribution of turbulent transport in different quadrants, which is expected to have the same effect on different scalars under good mixing conditions.

3.3 Methods

3.3.1 Numerical simulations

We set up a numerical simulation to test the magnitude of the error due to nonzero $\overline{w}$ on the flux and investigate the values of the coefficient α_c. For this simulation, we used 10 Hz measurements obtained from a field experiment measuring vertical wind velocity and scalar concentration using an infrared gas analyzer (IRGA) and a sonic anemometer. We used data from a period of 12 d from 15 June 2020 to 26 June 2020. The data were collected at an ideal flat agricultural site in Braunschweig, Germany. A full description of the site and the instrumentation is provided in the accompanying paper (Emad and Siebicke, 2023). We added a random $\overline{w}$ offset in the range -0.25 to $0.25\,\mathrm{m\,s^{-1}}$ to each averaging interval but limited $\overline{w}$ to smaller than $2\sigma_w$. We obtained three repetitions and calculated the flux according to different formulas. In total, there were about 1400 30 min averaging intervals. The methods compared were (i) the flux calculated using the concentrations formula of Hicks and McMillen (1984) shown in Eq. (3.8), (ii) the equation for DEA including the non-equal volume correction of Turnipseed et al. (2009), and (iii) the new generalized equation proposed in the current study (Eq. 3.14) utilizing α_θ values calculated from sonic temperature and the analytical value of α_c.

We applied minimal quality checks to the resulting fluxes before the comparison. Tests for stationarity following Foken et al. (2005) removed 22 % of the averaging intervals. We limited the values of $|\alpha_\theta|$ to less than 1, which removed an additional 4 % of the averaging intervals. Furthermore, when the sonic temperature was used for calculating α_θ, periods with low turbulence intensity ($|\rho_{w\theta}| < 0.2$) were excluded. The excluded averaging intervals occurred almost exclusively during nighttime conditions.

3.4 Results and discussion

We first discuss the newly proposed TEA equation, then compare it to different TEA formulations. Then, we discuss the interpretation of the transport asymmetry coefficient α and different ways of estimating it.

3.4.1 Nonzero mean vertical wind velocity

The newly proposed TEA equation (Eq. 3.14) successfully constrained the biased advective term $\overline{wc}$. The new equation employs information about the scalar transport to allow the estimation of $\overline{c}$ from available TEA measurements and consequently get an estimate of the biased advective term. Besides the correction of the nonzero $\overline{w}$ bias, the estimation of the scalar mean, $\overline{c}$, is essential for the WPL correction and the calculation of storage fluxes.

The terms of Eq. (3.14) account for different contributions to the flux. The first term on the right-hand side is equivalent to calculating the flux as the difference in accumulated mass between updraft and downdraft. When $\overline{w} = 0$, the equation is reduced to this term only. The second term accounts for the bias introduced by the biased advective term $\overline{w}\,\overline{c}$ by using the weighted mean of the scalar and the magnitude of wind as an estimate for $\overline{c}$. We show that when $\overline{w} \neq 0$, the first two terms are equivalent to using the concentration formula of Hicks and McMillen (1984) shown in Eq. (3.8), with the unequal volume correction of Turnipseed et al. (2009) that accounts for the small difference between the weighted mean $\overline{c}_\mathrm{W}$ and average of concentrations $(C^{\uparrow}_{\mathrm{acc}} + C^{\downarrow}_{\mathrm{acc}})/2$. Refer to Appendix 3.5 for details about this equality. The new third term $\overline{c'|w|'}/\overline{|w|}$ corrects for the correlation between the scalar and

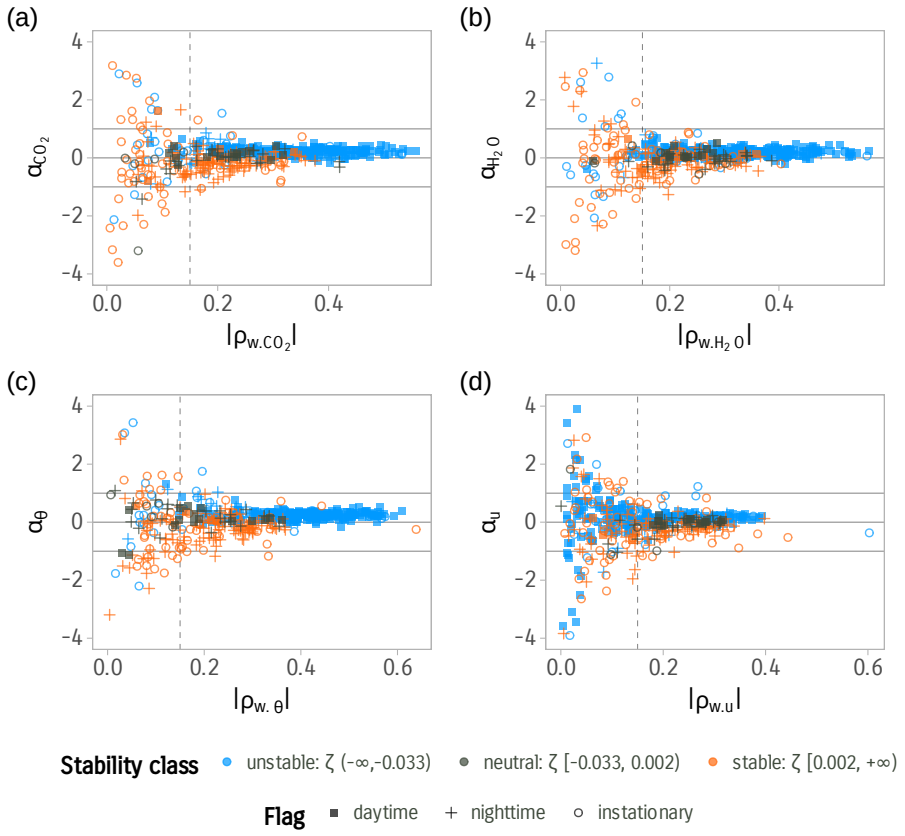

Figure 3.2: Observed values of the transport asymmetry coefficient α vs. the correlation coefficient for four variables calculated from high-frequency measurements. **(a)** CO_2, **(b)** H_2O, **(c)** sonic temperature, θ, and **(d)** wind velocity component, u. Colors distinguish different stability classes. The point shape differentiates daytime, nighttime, and instationary conditions following Foken and Wichura (1996). The vertical dashed line is set to $x = 0.15$, and the horizontal lines are set to $y = -1$ and $y = 1$.

the magnitude of the wind. Ignoring the third term will result in a flux biased with the ratio $\overline{w}/\overline{|w|}\alpha_c$.

The new TEA equation reveals an important insight. When using the new equation to calculate the flux, the error in the flux when $\overline{w} \neq 0$ is independent of the scalar concentration and is governed by the characteristics of the turbulent transport. This strengthens confidence in using the TEA method for measuring atmospheric constituents with a high background concentration and small flux (low deposition velocity).

Using the new TEA formula with an estimated value for α_c was effective in reducing the uncertainty and the systematic error in the calculated fluxes (Fig. 3.1). To quantify the magnitude of the systematic bias and uncertainty resulting from nonzero $\overline{w}$ on the fluxes, we used the simulation results to obtain the slope and the coefficient of determination, R^2, from a linear fit of the calculated fluxes against the reference EC flux. The simulation results show an increased bias and uncertainty in the fluxes when $\overline{w} \neq 0$ and a significant improvement when using an estimate of α for correction (Fig. 3.1).

We found that using the accumulated mass difference to calculate the TEA flux (first term in Eq. 3.14) produced the largest errors. Values of $\overline{w}$ as small as $0.01\,\sigma_w$ were sufficient to produce more than a 10 % mean bias in the flux magnitude for CO_2 in our dataset.

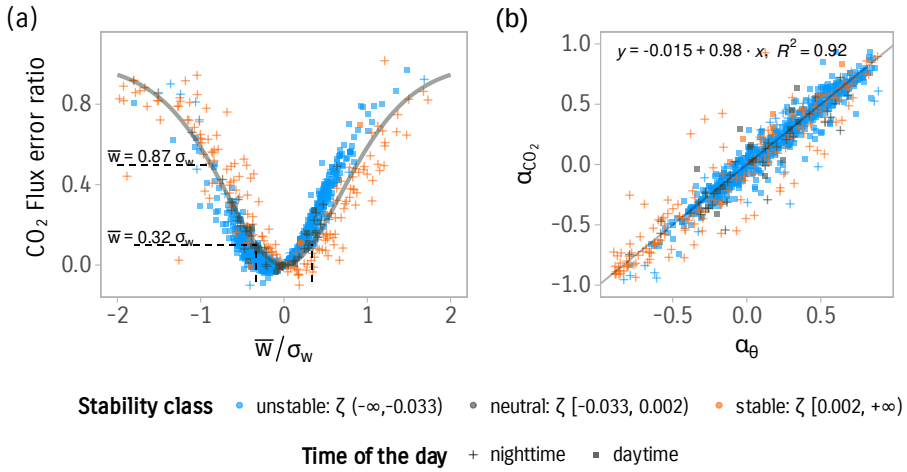

Figure 3.3: (a) The error ratio in the CO_2 flux calculated using the TEA method due to nonzero mean vertical wind. The solid gray line represents the analytical values of the error in the flux (if a joint Gaussian probability distribution is assumed). The points are the observed error calculated from high-frequency measurements colored according to stability classes. The point shape distinguishes daytime and nighttime data. **(b)** Relation of α_{CO_2} calculated for CO_2 and α_θ calculated from sonic temperature along with a 1-to-1 line for reference.

The use of the concentration TEA equation of Hicks and McMillen (1984) was a considerable improvement over using the mass difference but still overestimated the TEA flux. The slope of the linear fit was 1.12 ($R^2 = 0.94$). Using the DEA equation of Turnipseed et al. (2009), which includes an additional term to correct for the effect of unequal volume on the flux, led to underestimating the TEA flux, yielding a slope of 0.84 ($R^2 = 0.93$). The correction of nonzero $\overline{w}$ using α_θ utilizing the assumption of scalar similarity significantly reduced the bias and the uncertainty and gave a slope of 1.005 ($R^2 = 0.995$). The use of the analytical value of α_c using Eq. (3.26) similarly reduced the bias but with a smaller reduction in uncertainty, yielding a slope of 0.991 ($R^2 = 0.97$). The higher uncertainty when using the analytical value of α_c is likely due to the deviation from the assumed Gaussian probability distribution.

These results indicate that the proposed corrections using an estimate of α_c are very effective in minimizing or removing the bias from TEA flux when $\overline{w} \neq 0$ even when using the analytical value of α_c.

3.4.2 Value and interpretation of the transport asymmetry coefficient α

The value of α_c defined in Eq. (3.12) indicates the disparity of the flux transport between updrafts and downdrafts. Values of α_c larger than 1 indicate that updraft flux ($S_1 + S_4$) and downdraft flux ($S_2 + S_3$) have opposing signs. This pattern indicates that the wind and the scalar are correlated for updraft flux and anticorrelated for the downdraft flux (or the other way around). This pattern violates the stationarity conditions.

Therefore, we conclude that for stationary flows the systematic error in the TEA flux is smaller than $\pm\overline{w}/|\overline{w}|$. Observed values of α for H_2O, CO_2, θ, and the wind component, u, are shown in Fig. 3.2. The data confirm that values of $|\alpha|$ are consistently below 1 for the four scalars when the stationarity criterion is met. However, when the correlation between w and the scalar is low during conditions associated with low developed turbulence, spurious correlations might lead to values of $|\alpha|$ larger than 1.

We found that the value of α for CO_2 moderately correlates with the skewness of the measured scalar ($r = 0.61$, data not shown). The observed mean of α for CO_2 and sonic temperature calculated from high-frequency measurements for periods with negligible $\overline{w}$ was approximately 0.2 for unstable and good turbulent mixing conditions ($|\rho_{wc}| > 0.25$) with a standard error of SE = 0.01. For stable stratification ($\zeta > 0$), the mean of α was approximately equal to -0.18 but with a higher spread around the mean: SE = 0.09. These values indicate that updrafts have a larger contribution to the flux under unstable stratification and smaller contribution during stable stratification. The results generally agree with values found from studies using conditional sampling (Greenhut and Khalsa, 1982) and large eddy simulations (LESs) (Wyngaard and Moeng, 1992), which found that updraft contribution to the flux is 2 to 3 times larger than downdraft contribution under unstable conditions due to the contribution of convective thermals.

The sign of α indicates whether updrafts or downdrafts have a larger contribution to the flux. Inspecting Eq. (3.25), we find that a positive α indicates that the magnitude of updraft contribution to the flux is larger than the magnitude of the downdraft contribution ($|\text{flux}^{\uparrow}| > |\text{flux}^{\downarrow}|$), while the opposite is true for a negative α.

The analytical value of α from Eq. (3.26) was effective in minimizing the systematic bias as confirmed by the simulation results. However, the assumption of a Gaussian distribution, although used in the literature, e.g., Wyngaard and Moeng (1992), is not adequate. While the wind might be normally distributed for most stability classes (Chu et al., 1996), the scalar can significantly depart from normality (Berg and Stull, 2004). Other distributions might be more suited for approximating the joint probability distribution (Frenkiel and Klebanoff, 1973). For example, Katsouvas et al. (2007), using experimental data, showed that a third-order Gram–Charlier distribution was necessary and sufficient in most cases for describing the quadrant time and flux contributions. It is worth considering this distribution to find a better analytical formula to calculate the expectation of α.

The hypothesis of scalar similarity was proposed as another source for estimating the values of α. The similarity was empirically confirmed by investigating the values of α_θ and α_c from high-frequency measurements (Fig. 3.3). A linear fit with a slope of 0.98 and R^2 of 0.92 was obtained during steady-state and well-developed turbulence conditions. During such conditions, α_θ can substitute α_c to calculate the flux correction ratio. However, the correction becomes large and unreliable in periods when σ_w and ρ_{cw} are small, associated with small fluxes during nighttime and stable conditions. Additionally, temperature is considered a poor proxy during nearly neutral conditions due to its contribution to buoyancy (McBean, 1973; Hicks et al., 1980). We noticed that the variance in α values is higher under weakly developed turbulence and experimentally determined the threshold for the optimum use of α_θ for the correction as $|\rho_{cw}| = 0.2$. Below this threshold, values of α_θ larger than 1 are observed, making the correction unreliable. This threshold can be seen as an indicator for the violation of assumptions of homogeneity and stationarity or other problematic conditions. Similar uses for the correlation coefficient are common in the literature, e.g., Foken and Wichura (1996).

Another use of the formulation using α is to find a $\overline{w}$ threshold above which the TEA flux measurement becomes unreliable. For example, if we define the bias in the flux as not exceeding 10 % of the flux, we can experimentally find that the error in the flux due to nonzero $\overline{w}$ becomes larger than 10 % when $\overline{w}$ exceeds $0.21\sigma_w$ for periods with good turbulent mixing conditions ($|\rho_{w,CO_2}| > 0.2$). This threshold is close to the analytical value of $0.323\,\sigma_w$ obtained from the Gaussian joint probability distribution. To push this threshold further, α_θ calculated from sonic temperature can be used during good turbulent mixing conditions ($|\rho_{w,CO_2}| > 0.2$). Simulations indicate that the average relative confidence interval for the predicted value of α_θ from α_{CO_2} is 0.17 % of the fit value. In summary for this example, to keep

the error in the flux below 10 %, α_θ can be safely used to correct for biased $\overline{w}$ as long as $\overline{w} < 0.7\,\sigma_w$. This limit is considered forgiving and easy to achieve with online coordinate rotation and further rather simple online treatments. The only time when this limit is expected to be reached is when σ_w is very small (e.g., during nighttime conditions) where other problems such as low turbulent mixing and violations of the assumptions of the EC and TEA methods are expected to occur. These periods largely overlap with periods considered to be of low quality and are usually excluded from the analysis (Foken et al., 2012b).

To summarize, we find that the error in the TEA flux is constrained to $\overline{w}/\overline{|w|}$ for $|a| < 1$, which was shown here to be true for stationary conditions, which are at the focus of turbulent flux measurements. If a correction is desired to minimize this error, two options were presented to estimate α_c: first, an analytical solution, and second, an estimate employing scalar similarity. Finally, with the use of α_c, the typically observed systematic flux bias due to nonzero mean vertical wind velocity could be effectively characterized and minimized.

3.5 Conclusions

In this paper, we revised the theory of the true eddy accumulation method and extended its applicability to measure turbulent fluxes under nonideal conditions in which the mean vertical wind velocity during the averaging interval is not zero. The new generalized equation allows estimating the scalar mean during the flux averaging interval and defining conditions in which the error in the flux is significant.

The new formulation allowed constraining the relative systematic error in the TEA flux to the ratio $\overline{w}/\overline{|w|}$ under stationarity conditions. This systematic error was reduced to be a function of the disparity of atmospheric transport instead of having it scale with the scalar background concentration. This development significantly reduces the systematic bias in TEA fluxes under nonideal conditions, allowing the TEA method to be used indifferently with various atmospheric constituents.

The coefficient α_c, defined to quantify the atmospheric transport asymmetry, has proved to be very useful in estimating and removing the error in measured TEA fluxes. We showed two methods for estimating α_c to reduce the flux systematic bias: (i) an estimate of α_c based on the assumption of flux variance similarity and (ii) an analytical expression based on the assumption of a Gaussian joint probability distribution of the scalar concentration and vertical wind velocity. Both of these estimation methods were shown to be effective in minimizing the systematic error in the flux when compared to conventional TEA formulas.

In conclusion, the results presented in this paper showed that it is possible to achieve minimum bias in the TEA flux under most atmospheric conditions as well as identify those conditions which are less favorable. We believe that these results increase confidence in using the TEA method for different atmospheric constituents and under a variety of atmospheric conditions.

Appendix

Hicks and McMillen formulation

We show here how the TEA flux formula of Hicks and McMillen (1984), originally formulated under the assumption of $\overline{w} = 0$, is equivalent to using $(C^{\uparrow}_{\mathrm{acc}} + C^{\downarrow}_{\mathrm{acc}})/2$ as an estimate for $\overline{c}$ in the second term on

the right-hand side of Eq. (3.2).

We write the conditional expectation of $\overline{w}$ as

$$\overline{w} = \overline{\left(\overline{w|\mathrm{sign}(w)}\right)} = \overline{|w^{\uparrow}|}\,\mathrm{P}(w^{\uparrow}) - \overline{|w^{\downarrow}|}\,\mathrm{P}(w^{\downarrow}), \tag{3.28}$$

where sign(w) is the sign of vertical wind velocity. P($w^{\uparrow}$) and P($w^{\downarrow}$) are the observed probabilities of the sign of w, which equals the ratio of the time the wind is positive or negative to the total integration interval time:

$$\overline{w} = \overline{|w^{\uparrow}|}\frac{\Delta t^{\uparrow}}{\Delta t} - \overline{|w^{\downarrow}|}\frac{\Delta t^{\downarrow}}{\Delta t} \tag{3.29}$$

and similarly

$$\overline{|w|} = \overline{|w^{\uparrow}|}\frac{\Delta t^{\uparrow}}{\Delta t} + \overline{|w^{\downarrow}|}\frac{\Delta t^{\downarrow}}{\Delta t}. \tag{3.30}$$

By substituting $\overline{|w|}/2$ with

$$\frac{\overline{|w|}}{2} = \overline{|w^{\uparrow}|}\frac{\Delta t^{\uparrow}}{\Delta t} - \frac{\overline{w}}{2} = \overline{|w^{\downarrow}|}\frac{\Delta t^{\downarrow}}{\Delta t} + \frac{\overline{w}}{2}, \tag{3.31}$$

we obtain

$$C^{\uparrow}_{\mathrm{acc}}(\overline{w^{\uparrow}}\,\frac{\Delta t^{\uparrow}}{\Delta t} - \frac{\overline{w}}{2}) - C^{\downarrow}_{\mathrm{acc}}(\overline{|w^{\downarrow}|}\,\frac{\Delta t^{\downarrow}}{\Delta t} + \frac{\overline{w}}{2}). \tag{3.32}$$

After rearrangement and simplification we get to

$$F_{\mathrm{EA}} = \overline{cw} - \overline{w}\left(\frac{C^{+}_{\mathrm{acc}} + C^{-}_{\mathrm{acc}}}{2}\right). \tag{3.33}$$

When Eq. (3.33) is compared with Eq. (3.2), it is clear that the term $\frac{C^{+}_{\mathrm{acc}}+C^{-}_{\mathrm{acc}}}{2}$ is used as an estimate for $\overline{c}$.

Symbols and subscripts with units

Symbols		
c	mol m^{-3}	Molar density of a scalar
w	m s^{-1}	Vertical wind velocity
Δt	s	Flux averaging interval
A	–	TEA sampling scaling factor
V	m^3	Volume
C	mol m^{-3}	Mean concentration of accumulated samples
α_c	–	Transport asymmetry coefficient for scalar c
ρ	–	Correlation coefficient
S_i	–	Flux contribution from quadrant i
Subscripts		
acc		Accumulated samples
$\uparrow$		Updraft buffer volume
$\downarrow$		Downdraft buffer volume
c		Atmospheric constituent

Code and data availability. Data and scripts needed for producing the results and the figures presented in this paper are provided in Emad and Siebicke (2022).

Author contributions. AE developed the generalized TEA equation, implemented needed software, analyzed the data, and wrote the paper. LS provided supervision and feedback on the results, analysis, and paper.

Competing interests. The contact author has declared that none of the authors has any competing interests.

Disclaimer. Publisher's note: Copernicus Publications remains neutral with regard to jurisdictional claims in published maps and institutional affiliations.

Acknowledgements. We would like to thank the two referees (Christoph Thomas and an anonymous reviewer) and the editor for their constructive, useful, and detailed comments, which have significantly improved the paper. We gratefully acknowledge the support of the Bioclimatology group, led by Alexander Knohl at the University of Göttingen, in particular technical assistance by Justus Presse, Frank Tiedemann, Marek Peksa, Dietmar Fellert, and Edgar Tunsch. We thank Christian Brümmer, Jean-Pierre Delorme from the Thünen Institute for Agricultural Climate Protection, and Mathias Herbst from the Center for Agrometeorological Research of the German Meteorological Service (DWD) for facilitating the fieldwork in Braunschweig. We further acknowledge Christian Markwitz for the fruitful discussions during the preparation of the paper and for reading and commenting on the paper. We thank Alexander Knohl, Nicolò Camarretta, Justus van Ramshorst, and Yannik Wardius for reading the paper and providing useful comments.

Financial support. This research has been supported by the Niedersächsische Ministerium für Wissenschaft und Kultur (Wissenschaft.Niedersachsen.Weltoffen grant), the H2020 European Research Council (grant no. 682512), and the Deutsche Forschungsgemeinschaft (grant no. INST 186/1118-1 FUGG).

This open-access publication was funded by the University of Göttingen.

Review statement. This paper was edited by Hartwig Harder and reviewed by Christoph Thomas and one anonymous referee.

Bibliography

Baldocchi, D.: Measuring Fluxes of Trace Gases and Energy between Ecosystems and the Atmosphere – the State and Future of the Eddy Covariance Method, Global Change Biol., 20, 3600–3609, doi:10.1111/gcb.12649, 2014.

Baldocchi, D. D., Hicks, B. B., and Meyers, T. P.: Measuring Biosphere-Atmosphere Exchanges of Biologically Related Gases with Micrometeorological Methods, Ecology, 69, 1331–1340, doi:10.2307/1941631, 1988.

Berg, L. K. and Stull, R. B.: Parameterization of Joint Frequency Distributions of Potential Temperature and Water Vapor Mixing Ratio in the Daytime Convective Boundary Layer, J. Atmos. Sci., 61, 813–828, doi:10.1175/1520-0469(2004)061<0813:POJFDO>2.0.CO;2, 2004.

Bowling, D. R., Turnipseed, A. A., Delany, A. C., Baldocchi, D. D., Greenberg, J. P., and Monson, R. K.: The Use of Relaxed Eddy Accumulation to Measure Biosphere-Atmosphere Exchange of Isoprene and Other Biological Trace Gases, Oecologia, 116, 306–315, doi:10.1007/s004420050592, 1998.

Businger, J. A. and Oncley, S. P.: Flux Measurement with Conditional Sampling, J. Atmos. Ocean. Technol., 7, 349–352, doi:10.1175/1520-0426(1990)007<0349:FMWCS>2.0.CO;2, 1990.

Chu, C. R., Parlange, M. B., Katul, G. G., and Albertson, J. D.: Probability Density Functions of Turbulent Velocity and Temperature in the Atmospheric Surface Layer, Water Resour. Res., 32, 1681–1688, doi:10.1029/96WR00287, 1996.

Desjardins, R. L.: Energy Budget by an Eddy Correlation Method, J. Appl. Meteorol., 16, 248–250, doi:10.1175/1520-0450(1977)016<0248:EBBAEC>2.0.CO;2, 1977.

Emad, A. and Siebicke, L.: Reproduction Data and Code for the Paper: True Eddy Accumulation – Part 1: Solutions to the Problem of Non-Vanishing Mean Vertical Wind Velocity, Zenodo [data set, code], doi:10.5281/zenodo.7047610, 2022.

Emad, A. and Siebicke, L.: True eddy accumulation – Part 1: Solutions to the problem of non-vanishing mean vertical wind velocity, Atmos. Meas. Tech., 16, 29–40, doi:10.5194/amt-16-29-2023, 2023.

Emad, A. and Siebicke, L.: True eddy accumulation – Part 2: Theory and experiment of the short-time eddy accumulation method, Atmos. Meas. Tech., 16, 41–55, doi:10.5194/amt-16-41-2023, 2023.

Finnigan, J. J., Clement, R., Malhi, Y., Leuning, R., and Cleugh, H.: A Re-Evaluation of Long-Term Flux Measurement Techniques Part I: Averaging and Coordinate Rotation, Bound. Lay. Meteorol., 107, 1–48, doi:10.1023/A:1021554900225, 2003.

Foken, T. and Wichura, B.: Tools for Quality Assessment of Surface-Based Flux Measurements, Agr. Forest Meteorol., 78, 83–105, doi:10.1016/0168-1923(95)02248-1, 1996.

Foken, T., Gockede, M., Mauder, M., Mahrt, L., Amiro, B., and Munger, W.: Post-Field Data Quality Control, Handbook of Micrometeorology, 29, 181–208, doi:10.1007/1-4020-2265-4_9, 2004.

Foken, T., Göockede, M., Mauder, M., Mahrt, L., Amiro, B., and Munger, W.: Post-Field Data Quality Control, in: Handbook of Micrometeorology: A Guide for Surface Flux Measurement and Analysis, edited by: Lee, X., Massman, W., and Law, B., Atmospheric and Oceanographic Sciences Library, 181–208, Springer Netherlands, Dordrecht, doi:10.1007/1-4020-2265-4_9, 2005.

Foken, T., Aubinet, M., and Leuning, R.: The Eddy Covariance Method, in: Eddy Covariance: A Practical Guide to Measurement and Data Analysis, edited by: Aubinet, M., Vesala, T., and Papale, D., Springer Atmospheric Sciences, 1–19, Springer Netherlands, Dordrecht, doi:10.1007/978-94-007-2351-1_1, 2012a.

Foken, T., Leuning, R., Oncley, S. R., Mauder, M., and Aubinet, M.: Corrections and Data Quality Control, in: Eddy Covariance: A Practical Guide to Measurement and Data Analysis, edited by: Aubinet, M., Vesala, T., and Papale, D., Springer Atmospheric Sciences, 85–131, Springer Netherlands, Dordrecht, doi:10.1007/978-94-007-2351-1_4, 2012b.

Frenkiel, F. N. and Klebanoff, P. S.: Probability Distributions and Correlations in a Turbulent Boundary Layer, The Phys. Fluids, 16, 725–737, doi:10.1063/1.1694421, 1973.

Fuehrer, P. L. and Friehe, C. A.: Flux Corrections Revisited, Bound. Lay. Meteorol., 102, 415–458, doi:10.1023/A:1013826900579, 2002.

Greenhut, G. K. and Khalsa, S. J. S.: Updraft and Downdraft Events in the Atmospheric Boundary Layer Over the Equatorial Pacific Ocean, J. Atmos. Sci., 39, 1803–1818, doi:10.1175/1520-0469(1982)039<1803:UADEIT>2.0.CO;2, 1982.

Gu, L., Massman, W. J., Leuning, R., Pallardy, S. G., Meyers, T., Hanson, P. J., Riggs, J. S., Hosman, K. P., and Yang, B.: The Fundamental Equation of Eddy Covariance and Its Application in Flux Measurements, Agr. Forest Meteorol., 152, 135–148, doi:10.1016/j.agrformet.2011.09.014, 2012.

Heinesch, B., Yernaux, M., and Aubinet, M.: Some Methodological Questions Concerning Advection Measurements: A Case Study, Bound. Lay. Meteorol., 122, 457–478, doi:10.1007/s10546-006-9102-4, 2007.

Hicks, B. B. and Baldocchi, D. D.: Measurement of Fluxes Over Land: Capabilities, Origins, and Remaining Challenges, Bound. Lay. Meteorol., 177, 365–394, doi:10.1007/s10546-020-00531-y, 2020.

Hicks, B. B. and McMillen, R. T.: A Simulation of the Eddy Accumulation Method for Measuring Pollutant Fluxes, J. Climate Appl. Meteorol., 23, 637–643, doi:10.1175/1520-0450(1984)023<0637:ASOTEA>2.0.CO;2, 1984.

Hicks, B. B., Wesely, M. L., and Durham, J. L.: Critique of Methods to Measure Dry Deposition Workshop Summary, Tech. Rep. PB-81126443; EPA-600/9-80-050, Argonne National Lab., IL (USA), Environmental Protection Agency, Research Triangle Park, NC (USA), 1980.

Katsouvas, G. D., Helmis, C. G., and Wang, Q.: Quadrant Analysis of the Scalar and Momentum Fluxes in the Stable Marine Atmospheric Surface Layer, Bound. Lay. Meteorol., 124, 335–360, doi:10.1007/s10546-007-9169-6, 2007.

Katul, G., Kuhn, G., Schieldge, J., and Hsieh, C.-I.: The Ejection-Sweep Character of Scalar Fluxes in the Unstable Surface Layer, Bound. Lay. Meteorol., 83, 1–26, doi:10.1023/A:1000293516830, 1997.

Lee, X., Finnigan, J., and Paw U, K. T.: Coordinate Systems and Flux Bias Error, in: Handbook of Micrometeorology: A Guide for Surface Flux Measurement and Analysis, edited by: Lee, X., Massman, W., and Law, B., Atmospheric and Oceanographic Sciences Library, 33–66, Springer Netherlands, Dordrecht, doi:10.1007/1-4020-2265-4_3, 2005.

Lenschow, D. H., Mann, J., and Kristensen, L.: How Long Is Long Enough When Measuring Fluxes and Other Turbulence Statistics?, J. Atmos. Ocean. Technol., 11, 661–673, doi:10.1175/1520-0426(1994)011<0661:HLILEW>2.0.CO;2, 1994.

Leone, F. C., Nelson, L. S., and Nottingham, R. B.: The Folded Normal Distribution, Technometrics, 3, 543–550, doi:10.1080/00401706.1961.10489974, 1961.

McBean, G. A.: Comparison of the Turbulent Transfer Processes near the Surface, Bound. Lay. Meteorol., 4, 265–274, doi:10.1007/BF02265237, 1973.

Monin, A. S. and Obukhov, A. M.: Basic Laws of Turbulent Mixing in the Ground Layer of the Atmosphere, Translated for Geophysics Research Directorate, AF Cambridge Research Center... by the American meteorological Society, Tr. Akad. Nauk SSSR Geophiz. Inst., Boston, MA, 24, 163–187, 1954.

Ohtaki, E.: On the Similarity in Atmospheric Fluctuations of Carbon Dioxide, Water Vapor and Temperature over Vegetated Fields, Bound. Lay. Meteorol., 32, 25–37, doi:10.1007/BF00120712, 1985.

Pattey, E., Desjardins, R. L., and Rochette, P.: Accuracy of the Relaxed Eddy-Accumulation Technique, Evaluated Using CO2 Flux Measurements, Bound. Lay. Meteorol., 66, 341–355, doi:10.1007/BF00712728, 1993.

Paw U, K. T., Baldocchi, D. D., Meyers, T. P., and Wilson, K. B.: Correction Of Eddy-Covariance Measurements Incorporating Both Advective Effects And Density Fluxes, Bound. Lay. Meteorol., 97, 487–511, doi:10.1023/A:1002786702909, 2000.

Rannik, Ü., Vesala, T., Peltola, O., Novick, K. A., Aurela, M., Järvi, L., Montagnani, L., Mölder, M., Peichl, M., Pilegaard, K., and Mammarella, I.: Impact of Coordinate Rotation on Eddy Covariance Fluxes at Complex Sites, Agr. Forest Meteorol., 287, 107940, doi:10.1016/j.agrformet.2020.107940, 2020.

Raupach, M. R.: Conditional Statistics of Reynolds Stress in Rough-Wall and Smooth-Wall Turbulent Boundary Layers, J. Fluid Mechan., 108, 363–382, doi:10.1017/S0022112081002164, 1981.

Rinne, J. and Ammann, C.: Disjunct Eddy Covariance Method, in: Eddy Covariance: A Practical Guide to Measurement and Data Analysis, edited by: Aubinet, M., Vesala, T., and Papale, D., Springer Atmospheric Sciences, 291–307, Springer Netherlands, Dordrecht, doi:10.1007/978-94-007-2351-1_10, 2012.

Rinne, H. J. I., Delany, A. C., Greenberg, J. P., and Guenther, A. B.: A True Eddy Accumulation System for Trace Gas Fluxes Using Disjunct Eddy Sampling Method, J. Geophys. Res.-Atmos., 105, 24791–24798, doi:10.1029/2000JD900315, 2000.

Rinne, J., Tuovinen, J.-P., Laurila, T., Hakola, H., Aurela, M., and Hypén, H.: Measurements of Hydrocarbon Fluxes by a Gradient Method above a Northern Boreal Forest, Agr. Forest Meteorol., 102, 25–37, doi:10.1016/S0168-1923(00)00088-5, 2000.

Siebicke, L. and Emad, A.: True eddy accumulation trace gas flux measurements: proof of concept, Atmos. Meas. Tech., 12, 4393–4420, doi:10.5194/amt-12-4393-2019, 2019.

Sun, J.: Tilt Corrections over Complex Terrain and Their Implication for CO_2 Transport, Bound. Lay. Meteorol., 124, 143–159, doi:10.1007/s10546-007-9186-5, 2007.

Thomas, C. and Foken, T.: Flux Contribution of Coherent Structures and Its Implications for the Exchange of Energy and Matter in a Tall Spruce Canopy, Bound. Lay. Meteorol., 123, 317–337, doi:10.1007/s10546-006-9144-7, 2007.

Turnipseed, A. A., Pressley, S. N., Karl, T., Lamb, B., Nemitz, E., Allwine, E., Cooper, W. A., Shertz, S., and Guenther, A. B.: The use of disjunct eddy sampling methods for the determination of ecosystem level fluxes of trace gases, Atmos. Chem. Phys., 9, 981–994, doi:10.5194/acp-9-981-2009, 2009.

Webb, E. K., Pearman, G. I., and Leuning, R.: Correction of Flux Measurements for Density Effects Due to Heat and Water Vapour Transfer, Q. J. Roy. Meteorol. Soc., 106, 85–100, doi:10.1002/qj.49710644707, 1980.

Wesely, M. L.: Use of Variance Techniques to Measure Dry Air-Surface Exchange Rates, Bound. Lay. Meteorol., 44, 13–31, doi:10.1007/BF00117291, 1988.

Wilczak, J. M., Oncley, S. P., and Stage, S. A.: Sonic Anemometer Tilt Correction Algorithms, Bound. Lay. Meteorol., 99, 127–150, doi:10.1023/A:1018966204465, 2001.

Wyngaard, J. C. and Moeng, C.-H.: Parameterizing Turbulent Diffusion through the Joint Probability Density, Bound. Lay. Meteorol., 60, 1–13, doi:10.1007/BF00122059, 1992.

4 True eddy accumulation – Part 2: Theory and experiment of the short-time eddy accumulation method

Paper published in *Atmospheric measurement techniques* (Emad and Siebicke, 2023).

Emad, A. and Siebicke, L.: True eddy accumulation – Part 2: Theory and experiment of the short-time eddy accumulation method, Atmos. Meas. Tech., 16, 41–55, doi:10.5194/amt-16-41-2023, 2023.

Abstract

A new variant of the eddy accumulation method for measuring atmospheric exchange is derived, and a prototype sampler is evaluated. The new method, termed short-time eddy accumulation (STEA), overcomes the requirement of fixed accumulation intervals in the true eddy accumulation method (TEA) and enables the sampling system to run in a continuous flow-through mode. STEA enables adaptive time-varying accumulation intervals, which improves the system's dynamic range and brings many advantages to flux measurement and calculation.

The STEA method was successfully implemented and deployed to measure CO_2 fluxes over an agricultural field in Braunschweig, Germany. The measured fluxes matched very well against a conventional eddy covariance system (slope of 1.04, R^2 of 0.86). We provide a detailed description of the setup and operation of the STEA system in the continuous flow-through mode, devise an empirical correction for the effect of buffer volumes, and describe the important considerations for the successful operation of the STEA method.

The STEA method reduces the bias and uncertainty in the measured fluxes compared to conventional TEA and creates new ways to design eddy accumulation systems with finer control over sampling and accumulation. The results encourage the application of STEA for measuring fluxes of more challenging atmospheric constituents such as reactive species. This paper is Part 2 of a two-part series on true eddy accumulation.

4.1 Introduction

Monitoring the exchange of trace gases and energy between the Earth's surface and the atmosphere is a key problem in ecology and climate science. The eddy covariance method (EC) has become the standard method for estimating the flux density on the scale of plant canopies (Baldocchi, 2014; Hicks and Baldocchi, 2020). The flux in the EC method is calculated as the covariance between the vertical wind velocity and the scalar concentration. For this, EC requires the availability of high-frequency measurements of the vertical wind velocity and the concentration of the atmospheric constituent (≥ 10 Hz). This requirement limits the EC method to a few trace gases for which fast-response gas analyzers are available. For constituents for which only slow-response gas analyzers are available, several methods for measuring the fluxes exist (Rinne et al., 2021). Among these methods, true eddy accumulation (TEA) (Desjardins, 1977) is the most direct and the closest to EC. TEA is formulated using similar principles and assumptions as the EC method. However, unlike EC, the TEA method requires the scalar concentration measurements to be carried out once every averaging interval (30 min). For a long time, the development of the TEA method was hindered by the difficulty of fast airflow rate control and strict operational requirements (Businger and Oncley, 1990; Hicks and McMillen, 1984). A recent improvement to the TEA method used a new type of mass flow controller, online coordinate rotation, and several online treatments of the signal to overcome important limitations of the method's applicability (Siebicke and Emad, 2019). The new system showed a good match with a reference eddy covariance system, with coefficients of determination of up to 86 % and a slope of 0.98. While this study demonstrated a successful proof of concept of TEA using modern sampling, it also showed that further research was required for continuous accumulation and long-term field operation, which we address with the current study.

The absence of high-frequency measurements of the scalar concentration creates unique challenges for the TEA method. The sampling decisions in TEA need to be made in real time without complete

knowledge of the wind statistics of the averaging interval. The problem of nonzero mean vertical wind velocity, a direct consequence of this limitation, is discussed in the companion paper (Emad and Siebicke, 2023).

Furthermore, the lack of high-frequency scalar measurements implies that sample accumulation needs to happen on a timescale similar to the flux averaging interval (30 to 60 min). Therefore, a minimum limit is imposed on the sampling accumulation interval before the scalar concentration measurement can be conducted. This time limit imposes restrictive design considerations related to the size and function of sample accumulation reservoirs. It also dictates that the sampling apparatus needs to accommodate a large dynamic range (up to 5 σ_w) to cover the range of wind velocities during flux averaging intervals (Hicks and McMillen, 1984). The minimum time limit is also problematic if the sampled scalar changes in concentration over time, e.g., reactive species. Additionally, the accumulation for long time intervals and the discontinuous nature of sample collection are particularly sensitive to nonstationary conditions in the accumulation apparatus (Siebicke and Emad, 2019). Furthermore, the use of expandable bags in discrete sampling for the accumulation reservoirs was found to be unreliable and prone to mechanical fatigue (Siebicke and Emad, 2019). Therefore, a more flexible approach is needed whereby the accumulation interval can be adapted to the requirements of the sampling system and to the trace gas being measured.

In this paper, we address the limitations of fixed accumulation intervals in TEA by developing a novel method for eddy accumulation and providing a prototype implementation of such a system. First, we derive a new eddy accumulation method, which we call short-time eddy accumulation (STEA). The STEA method enables the sample accumulation to be carried out at variable shorter intervals, which brings many improvements to the TEA method including the ability to accumulate samples in a continuous flow-through mode and an increased dynamic range. Next, we discuss the effect of using buffer volumes on the concentration measurements and develop an empirical correction for the use of buffer volumes. Finally, we show a prototype and experimental measurements for CO_2 fluxes using the newly developed STEA method in the flow-through mode and compare the measured fluxes to reference EC measurements. We discuss the advantages and steps required to carry out flux measurements using the STEA method, different constraints, and operational requirements.

4.2 Theory

A detailed description of the TEA method derivation and assumptions is provided in the companion paper (Emad and Siebicke, 2023). Here we provide a brief overview of the TEA method and the assumptions that are required for the derivation of the short-time eddy accumulation method.

Under the assumptions of flow homogeneity and stationarity, the vertical exchange of the atmospheric scalar c is the flux across the measurement plane at height h. The flux F_c is expressed as (Finnigan et al., 2003; Gu et al., 2012)

$$F_c = \overline{cw}. \tag{4.1}$$

Here, w is the vertical wind velocity ($\mathrm{m\,s^{-1}}$), c is the scalar density ($\mathrm{mol\,m^{-3}}$), and the overbar denotes time averages that follow Reynolds averaging rules.

The true eddy accumulation method is formulated by partitioning the average $\overline{wc}$ using the direction of the vertical wind velocity. Therefore, we write the flux as the expected value of the random variable

wc conditional on the sign of the vertical wind velocity, sign(w),

$$\overline{wc} = \overline{w^{\uparrow} c^{\uparrow}}\, \mathrm{P}(w^{\uparrow}) + \overline{w^{\downarrow} c^{\downarrow}}\, \mathrm{P}(w^{\downarrow}), \tag{4.2}$$

where the arrows denote the direction of the vertical wind velocity, with ↑ for updrafts and ↓ for downdrafts. $\mathrm{P}(w^{\uparrow\downarrow})$ is the probability that the observed wind velocity is in the respective direction. The TEA method makes use of this simple partitioning by physically realizing the terms $\overline{w^{\uparrow} c^{\uparrow}}$ and $\overline{w^{\downarrow} c^{\downarrow}}$ using sample accumulation instead of measuring individual realizations of w and c. For the practical implementation of a TEA system, a parameter A is necessary to relate the sampling flow rate to the measured w.

4.2.1 Short-time eddy accumulation

The original formulation of the true eddy accumulation method requires the samples to be accumulated for the entire averaging interval Δt before the concentration measurement is ready for flux calculation. This formulation poses a challenge for the practical implementation of the TEA method. First, the longer averaging times require the sampling apparatus to cover a larger range of wind speeds (high dynamic range). And, second, the fixed averaging times limit the flexibility of the sampling system to adapt to changing conditions, therefore making it more prone to flow nonstationarities.

To achieve a higher dynamic range for the sampling system and realize a more robust flow-through eddy accumulation system, we propose a modification to the TEA method whereby samples can be accumulated for a sequence of shorter intervals τ_i that add up to the averaging period Δt. Therefore, the flux $\overline{wc}$, and consequently the sample accumulation, is partitioned based on two conditions: the sign of the vertical wind velocity and the variable I that divides the averaging interval into a sequence of shorter intervals τ_i.

This formulation can be achieved by applying the law of total expectation to the random variable cw with respect to a partitioning variable I that divides the averaging period Δt into multiple non-overlapping partitions with the length τ_i. This partitioning scheme is applied independently to updrafts and downdrafts, i.e., after partitioning with the direction of vertical wind velocity, therefore allowing the short intervals for updrafts and downdrafts to be different. We write the expectation of $\overline{c^{\uparrow} w^{\uparrow}}$ as

$$\overline{c^{\uparrow} w^{\uparrow}} = \overline{\left(\overline{(c^{\uparrow} w^{\uparrow})|I}\right)} = \sum_i \overline{(c^{\uparrow} w^{\uparrow})|I_i}\, \mathrm{P}(I_i). \tag{4.3}$$

The previous equation is similarly valid for the downdraft flux $\overline{c^{\downarrow} w^{\downarrow}}$. The measured concentration during a short averaging interval i is given by

$$C_i = \frac{\overline{cw|I_i}}{\overline{|w|}}. \tag{4.4}$$

The probability of the short averaging interval can be obtained easily as $\mathrm{P}(I_i) = \tau_i / \Delta t$.

V_i is the volume accumulated during the short interval i, defined as

$$V_i = A_i \int_t^{t+\tau_i} |w|\, \mathrm{d}t. \tag{4.5}$$

The concentration in either updraft or downdraft reservoirs for the averaging interval Δt is the weighted mean of the short interval concentration measurements, C_i:

$$C_{\mathrm{acc}}^{\uparrow\downarrow} = \frac{1}{\overline{|w|}\Delta t} \sum_{i=1}^{i=j} C_i^{\uparrow\downarrow} \overline{|w_i|}\tau_i. \tag{4.6}$$

We notice here that $\overline{|w_i|}\tau_i = V_i / A_i$ and $\overline{w}\,\Delta t = \sum_{i=1}^{i=j} V_i / A_i$.

The obtained $C_{\mathrm{acc}}^{\uparrow}$ and $C_{\mathrm{acc}}^{\downarrow}$ can be used to calculate the STEA flux (Emad and Siebicke, 2023) as

$$F_{\mathrm{STEA}} = \frac{C_{\mathrm{acc}}^{\uparrow}\, V^{\uparrow}\left(\overline{|w|} - \overline{w}\right) - C_{\mathrm{acc}}^{\downarrow}\, V^{\downarrow}\left(\overline{|w|} + \bar{w}\right)}{\overline{|w|} - \alpha_c \overline{w}} \times \frac{\overline{|w|}}{V_{\mathrm{total}}}, \tag{4.7}$$

where F_{STEA} is the kinematic flux density (mol m s^{-1}). $C_{\mathrm{acc}}^{\uparrow}$ and $C_{\mathrm{acc}}^{\downarrow}$ are the mean molar densities (mol m^{-3}) of the scalar c in updraft and downdraft reservoirs for the whole accumulation period Δt as calculated from Eq. (4.6). $V^{\uparrow}$ and $V^{\downarrow}$ are the accumulated sample volumes (m^3) in updraft and downdraft reservoirs during the averaging period. It is important here to use $V^{\uparrow}$ and $V^{\downarrow}$ as $\overline{|w|}\,\Delta t^{\uparrow}$ since the parameter A was not constant for different short intervals. $\overline{|w|}$ is the mean of the absolute vertical wind velocity (m s^{-1}) during the averaging period. $\overline{w}$ is the mean of the vertical wind velocity. α_c is the transport asymmetry coefficient for the scalar c (dimensionless) and is defined as the ratio of the covariance $\overline{c'|w'|}$ to the flux $\overline{c'w'}$. Methods for estimating α_c and the derivation of the TEA flux equation are discussed in the companion paper (Emad and Siebicke, 2023).

4.2.2 Effect of buffer volumes

The short-time eddy accumulation method can be achieved in at least two ways, either using expandable buffer volumes (e.g., bags), which are emptied after each short interval measurement C_i, or using a flow-through system with rigid buffer volumes. The flow-through system has practical operational benefits but requires additional correction to reverse the effect of buffer volumes on the scalar concentration signal. Buffer volumes act as low-pass filters (Cescatti et al., 2016). They attenuate the magnitude of the high-frequency part and shift the phase of the signal. The buffer concentration at time step n is dependent on the new input sample concentration and the buffer concentration from the previous step $y[n-1]$. Thus, the buffer volume concentration y_n response to an input C_i can be described with the following linear difference equation:

$$y_{[n]} = C_{i[n]}\, \dot{q}_i + (1 - \dot{q}_i)\, y_{[n-1]}, \tag{4.8}$$

where $\dot{q}$ is a dimensionless flow rate that is defined as the ratio between the sample mass to the total mass of air in the buffer volume at each time step n. Therefore, the dimensionless flow rate is the fraction of the air mass in the buffer volume that is replaced by the new sample mass.

$$\dot{q}_n = \frac{V_i\, \rho_i}{V_{\mathrm{b}}\, \rho_{\mathrm{b}}} \tag{4.9}$$

Here V_i and ρ_i are the volume and density of the accumulated sample during the interval i, respectively. V_{b} and ρ_{b} are the volume and the air density of the air in the buffer volume, respectively. Equation (4.8) characterizes a first-order linear filter.

The mixing in the buffer volume is assumed to be instantaneous and perfect. Additionally, the ac-

cumulated short samples in the STEA method are considered individually separable homogeneous parcels of air as they are forwarded to the gas analyzer. This discrete behavior is best modeled with a discrete-time system as shown in Eq. (4.8). The system response is characterized by the dimensionless flow rate or the time constant τ. The time constant of the system is defined as the required time for the system to reach $1/e$ from a step increase and relates to $\dot{q}$ by

$$\tau = -\frac{\Delta s}{\ln\left(1-\dot{q}\right)}, \tag{4.10}$$

(Taylor et al., 2013) where Δs is the length of the sampling interval.

Figure 4.1 shows the filter's magnitude and phase responses. The magnitude response $|H|$ plot shows how the magnitudes of different frequencies are attenuated. The smaller the dimensionless flow rate, the larger the time constant and the stronger the attenuation.

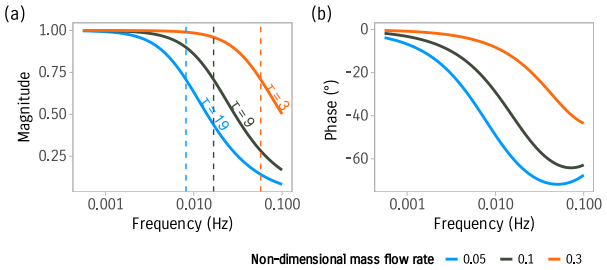

Figure 4.1: Frequency response for the first-order linear filter used to model the buffer volumes for three different time constants. **(a)** Magnitude response of the filter. Vertical dashed lines represent the cutoff frequencies for the respective time constants. **(b)** Phase response of the filter.

4.3 Methods

4.3.1 Experimental site

Flux measurements were performed over a flat agricultural field of the Thünen Institute, located at 52.297° N, 10.449° E in Braunschweig, Germany. The site has an altitude of 76 m above sea level. During the measurement period, the fields south and north of the tower were planted with oats and corn, respectively. Both crops had a similar height of approximately 50 cm above the ground at the start of the comparison period.

4.3.2 Experiment period

Fluxes were measured throughout the year 2020. We selected 6 weeks of good quality in summer based on instrument performance and weather conditions, spanning from 18 June 2020 to 31 July 2020, to compare the different methods. Meteorological conditions (Fig. 4.3) during the experimental period from 18 June to 31 July 2020 were characterized by warm weather conditions with net radiation peaking around 600 $\mathrm{W\,m^{-2}}$ at noon. Air temperature was predominantly above 10° and averaged 18°. Several precipitation events were observed during the experiment period. Precipitation totaled 66 mm, with several high precipitation events, in particular starting from the second and third weeks of the experiment. Precipitation data were obtained from the German weather service (DWD) station

i Braunschweig (number: 00662), which is located 600 m from the measurement tower. Soil water content tracked precipitation events except for one distinct occasion on 27 June when precipitation is not registered at the DWD station. Wind direction was dominated by southerly and easterly winds.

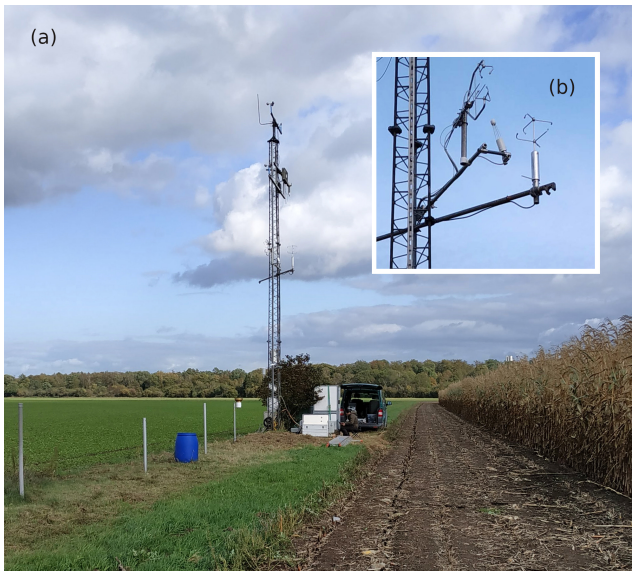

Figure 4.2: Photograph of the experimental field site showing the measurement tower **(a)** and a close-up of the flux instruments mounted on the tower **(b)**. The status of the vegetation seen in the picture is not representative of the measurement period.

4.3.3 Instruments

EC and STEA measurement complexes were mounted at 5 m height above the ground (Fig. 4.2). The instruments used in the experiment for flux measurements and data analysis are listed in Table 4.1. Meteorological variables were logged using a Sutron 9210 XLite logger (Sterling, USA). All the raw data needed for flux processing were synchronized on the STEA computer and remote servers for real-time processing.

The EC system comprised a dedicated sonic anemometer (uSonic-3 Omni H) and an open-path infrared gas analyzer (IRGA). Wind and scalar density data were acquired at 20 Hz frequency. Relative to the Class-A sonic anemometer used for STEA, the northward, eastward, and vertical separation of the IRGA was −17, 26, and −15 cm, respectively. The Class-A sonic anemometer had a north offset azimuth of 90°. Relative to the Omni sonic anemometer used for EC, the northward, eastward, and vertical separation of the IRGA was 20, −15.3, and −20 cm. The north offset of the Omni sonic anemometer was 169°.

4.3.4 STEA system description

The STEA system used in the experiment is based on an earlier system of Siebicke and Emad (2019). The new system used the same mass flow controllers and shared most of the operating software. It has, however, several differences and improvements. One major difference is the use of fixed stainless-steel buffer volumes instead of expandable bags. The system was initially developed as a hybrid TEA–EC method to run the TEA method in a continuous flow-through mode (Siebicke, 2016). The system was set up to operate in the STEA continuous flow-through mode. A constant duration for the short

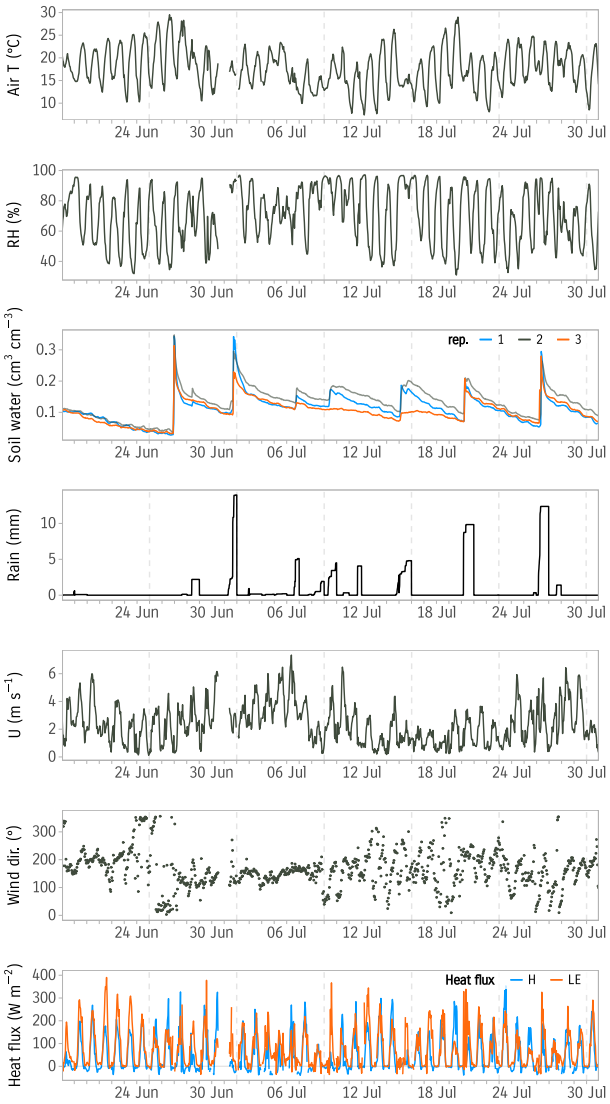

Figure 4.3: Meteorological conditions and turbulent energy fluxes during the experiment period from 18 June to 31 July 2020: air temperature, relative humidity, soil water content, cumulative daily precipitation, wind velocity, wind direction, sensible heat flux (H), and latent heat flux (LE). Precipitation data were obtained from the German weather service (DWD) station in Braunschweig (number: 00662), which is located 600 m from the measurement tower.

intervals (τ_i) equal to 1 min was used. The STEA system is comprised of two identical sampling lines, one for updrafts and one for downdrafts. Each of the sampling lines has two rigid buffer volumes in a sequence connected using 6 mm Teflon tube (Fig. 4.4).

The STEA sampling inlets were installed near the sonic anemometer's center of the measurement volume. The horizontal separation was 22 cm, while the vertical separation between the two inlets was 2 cm. Upon sampling, the collected samples were carried using 6 mm Teflon tubes to the first set of buffers. The sampling can be summarized in the following steps (see a detailed description of the system operation and sampling in Siebicke and Emad, 2019).

Table 4.1: Variables and instruments. Manufacturer key: METEK GmbH (Elmshorn, Germany), LI-COR Environmental Inc. (Lincoln, Nebraska, USA), LGR, (Los Gatos Research Inc., USA), Bosch (Bosch Sensortec GmbH, Germany), Vaisala (Helsinki, Finland), Kipp & Zonen (Delft, the Netherlands), Delta-T Devices Ltd (UK), Stevens Water Monitoring Systems, Inc (Oregon, USA), Texas Electronics (Dallas, USA).

Variable	Sensor	Manuf.	Method	Freq.
Wind u, v, w	uSonic-3 Omni H	METEK	EC	20 Hz
Sonic temp. T_s	uSonic-3 Omni H	METEK	EC	20 Hz
Wind u, v, w	uSonic-3 Class A	METEK	TEA	10 Hz
Sonic temp. T_s	uSonic-3 Class A	METEK	TEA	10 Hz
CO_2 density	LI-7500A	LI-COR	EC	10 Hz
H_2O density	LI-7500A	LI-COR	EC	10 Hz
CO_2 ppm	FGGA-24r-EP	LGR	TEA	1 Hz
H_2O ppm	FGGA-24r-EP	LGR	TEA	1 Hz
CH_4 ppm	FGGA-24r-EP	LGR	TEA	1 Hz
Air pressure P	BME280	Bosch	TEA	50 Hz
Air temperature	BME280	Bosch	TEA	50 Hz
Air humidity	HMP155	Vaisala	Meteo	10 min
Air temperature	HMP155	Vaisala	Meteo	10 min
Net radiation	CNR4	KIPP	Meteo	10 min
Global radiation	BF5	DELTA-T	Meteo	10 min
Soil heat flux	HFP01	LI-COR	Meteo	10 min
Soil moisture	SDI-12	Stevens	Meteo	10 min
Precipitation	TR-525M	Texas Elec.	Meteo	10 min

1. 3D wind measurements are acquired from the sonic anemometer (uSonic-3 Class A) with a 10 Hz sampling frequency.

2. Wind coordinates are rotated into the streamline coordinates using the planar fit method without an intercept (Dijk et al., 2004). The fit is performed online as a running window operation with a window width of 2 d and an update frequency of once every 30 min.

3. The mean vertical wind from the previous 30 min interval is removed to minimize $\overline{w}$. This is equivalent to applying a high-pass filter to the vertical wind velocity measurements.

4. The active sampling line is determined (updraft or downdraft) based on the direction of the rotated vertical wind velocity component.

5. The sampling scaling factor A_i is calculated based on wind conditions in the near past and the calibration coefficients of the mass flow controllers. The scaling factor should be constant during the short accumulation intervals.

6. Air samples are collected, and the controllers are adjusted to collect an air sample with a volume equal to $A_i\,|w|$.

7. When enough sample volume is accumulated in the respective buffer volume, samples are forwarded to the gas analyzer for analysis. The amount of sample volume needed is determined based on the required flow rate for the gas analyzer and the time needed to flush the tubes and the measurement cell as well as to perform enough repeated measurements.

8. Mean concentrations of accumulated samples are measured. The slow gas analyzer (LGR FGGA-24r-EP) alternates measuring the concentrations C_i of the accumulated samples for updraft

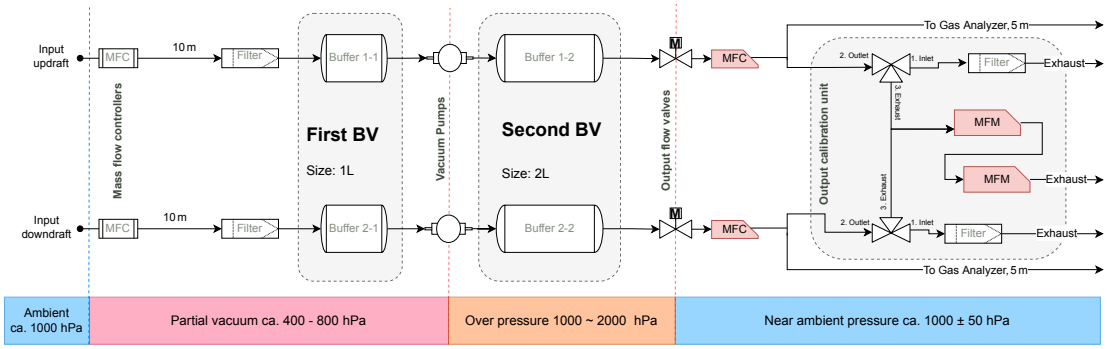

Figure 4.4: Functional and pneumatic schematic of the implemented flow-through STEA system showing components, layout, properties, and operation conditions. Air samples are collected at the input and travel in distinct sampling lines for updrafts and downdrafts. Samples travel through tubes (lengths are shown) and through filters and are then collected into two sets of buffer volumes shown here as "first BV" and "second BV" separated by two vacuum pumps. The "output flow valves" followed by mass flow controllers (MFCs) control the output flow rate from the second set of buffers to the gas analyzers. Finally, samples can optionally be forwarded to a set of mass flowmeters (MFMs) used for calibration purposes. The colored bottom bar below shows the range of pressure values at each stage.

and downdraft. The accumulation time for the short intervals was set to a fixed interval of 1 min instead of an adaptive interval duration. During each short interval, the gas analyzer performs repeated measurements for the gas concentration. The observed variability for repeated measurements in the short averaging intervals was SD = 0.501 ppm, which was similar to the measured repeatability of the gas analyzer for a similar time interval.

4.3.5 STEA flux computations

This section describes the steps followed to obtain the final and corrected STEA flux. Firstly, we discuss the effect of water vapor on the measured concentrations of other scalars and how we corrected the remaining water cross-sensitivity. Then, we present the procedure of data quality screening. Next, we detail the steps of calculating the final STEA flux. Finally, we present the buffer volume empirical correction we applied.

Water vapor correction

The gas analyzer used for the STEA measurements (LGR FGGA-24r-EP) reports the molar fraction of CO_2 and CH_4 of moist air in parts per million (ppm). The measurements of CO_2 cannot be used directly, as they are affected by the presence of water vapor. The presence of varying water vapor concentrations in the sample affects the measurements of CO_2 and CH_4 in cavity ring-down spectroscopy instruments in at least two ways: (i) the dilution effect and (ii) spectroscopic line broadening (Rella, 2010). Rella (2010) proposed a quadratic equation to correct for the combined effect of line broadening and water vapor dilution. The correction involves estimating the parameters (a) and (b) in the equation

$$r_c = \frac{\chi_c}{1 + a\,\chi_w + b\,\chi_w^2}, \tag{4.11}$$

where r_c is the dry mole fraction of the species c, χ_c is the wet mole fraction measured by the instrument, and χ_w is the water mole fraction measured by the instrument. For CO_2 measured by the LGR gas

analyzer in parts per million, Hiller et al. (2012) experimentally estimated these coefficients as $a = -1.219 \times 10^{-6}$ and $b = 1.229 \times 10^{-12}$. We found that using the same parameters could not control for all the effects of water vapor on measured CO_2 signals. A linear slope different from zero was still found when supplying the gas analyzer with air of varying water concentration and of constant CO_2. This suggested a remaining cross-sensitivity of CO_2 to the presence of water vapor. To control for this small remaining cross-sensitivity, we conducted a field experiment in which we measured the CO_2 concentration in air of varying water concentration and then used the results in a linear fit to obtain a correction slope. We were not able to source the necessary equipment and gas cylinders to supply the gas analyzer with air of known CO_2 concentration and varying water vapor in the field. Instead, we used the system's buffer volumes to collect and pressurize ambient air from the atmosphere, closed the inlets, and supplied the gas analyzer with enough sample flow rate for measurement. This procedure utilizes the effect of air drying due to decompression to deliver a varying water vapor content. The experiment involved collecting ambient humid air near saturation (RH ≈ 90 %, $T = 21$ °C) in the system's buffer volumes to a pressure of 2.6 bar. As a result of the high pressure, the water partial pressure in the pressurized buffer volumes will become higher than the saturation vapor pressure and water will precipitate, leading to dryer air. Air is then decompressed and forwarded to the analyzer. As the buffer pressure is decreasing, water vapor content will increase to reach the same level of atmospheric humidity. Using this method we were able to modulate the water vapor content in the air from 6000 to 14 000 ppm. The accumulated sample was enough to supply the gas analyzer for ca. 10 min. We repeated the measurements several times and used the obtained dataset to correct the remaining cross-sensitivity using a linear fit.

Raw data quality screening

Raw measurements of the wind velocity and scalar concentration were screened for outliers due to measurement errors and instrument malfunction. This included the following steps.

- Statistical screening: despiking, dropout removal (Vickers and Mahrt, 1997), and plausibility limits of the raw gas analyzer and wind measurements (Sabbatini et al., 2018).

- Flushing time removal: measurement of the short interval events involves regularly switching the sampling line coming to the gas analyzer between updraft and downdraft reservoirs. This caused subsequent samples to get contaminated. We experimentally chose a 25 s threshold at the start of each short interval event to account for the flushing time. The measurements falling before the threshold were discarded. Figure 4.5 shows an example of discarded flushing times at the start of each averaging interval.

- Detection of sample contamination: periods during which the flow rate to the gas analyzer is smaller than 400 mL min^{-1} are flagged. Under these conditions, ambient air might enter the system and contaminate the collected samples. When the number of flagged data points exceeded 10 % of the total points in the sampling interval, data in the sampling interval were discarded.

STEA flux calculation

After measurements are quality-checked and erroneous data points are excluded, the final STEA flux is calculated as follows.

- Short interval statistics: for each short interval sample, the gas analyzer will have several repeated measurements for the concentrations C_i. However, only one value is needed for the flux calculation. We use the median to obtain the representative value in order to minimize uncertainty and exclude outliers. Figure 4.5 shows an example of data quality checking and choice.
- Calculate air molar volume: the molar volume of air is needed to express the flux in units of $\mathrm{mol\,m^{-2}\,s^{-1}}$. The molar volume is calculated using sonic temperature, pressure, and humidity measurements.
- Calculate short interval weights: following Eq. (4.6), the measured short interval concentration should be weighted by the ratio of the accumulated volume during that interval to the total buffer volume.
- Calculate values of α_θ: values of the transport asymmetry coefficient α_θ are calculated using vertical wind velocity and sonic temperature measurements. Values of α_θ larger than 1 are discarded as they indicate a problem with the measurement as discussed in the companion paper (Emad and Siebicke, 2023).
- Calculate updraft and downdraft mean concentrations: $C^{\uparrow}_{\mathrm{acc}}$ and $C^{\uparrow}_{\mathrm{acc}}$ are calculated for the averaging period Δt.
- Calculate the flux: the STEA flux equation shown in Eq. (4.7) is used to obtain the final flux.

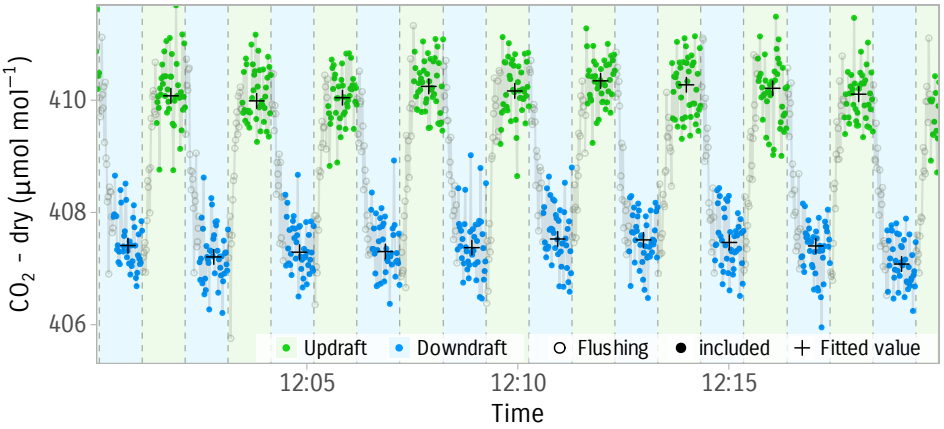

Figure 4.5: Data choice and fitting procedure for the STEA method. Points represent consecutive concentration measurements from the gas analyzer. Updraft and downdraft samples are highlighted in blue and green, respectively. Gray hollow points are excluded from the data fitting (flushing time). Crosses show the chosen representative concentrations for each short interval (the median). Further quality checks for raw data are outlined in Sect. 4.3.5. Data are from 21 June 2020 at midday.

Buffer volume empirical correction

Buffer volumes act on the signal as a low-pass filter and introduce systematic bias to the fluxes. We used Eq. (4.10) to estimate the time constant of the buffer volumes used in our experiment. For each of the buffer volumes, a measurement point is acquired every 2 min. The mean dimensionless mass flow rate to the gas analyzer was estimated from the pressure, the volume, and the estimated volumetric flow rate to the gas analyzer. We simulated the effect of buffer volumes on the high-frequency sonic

temperature signal and parameterized the flux loss by artificially degrading the sonic temperature in a procedure similar to Goulden et al. (1996) and Berger et al. (2001).

4.3.6 EC reference flux measurements and computations

The raw data from the two sonic anemometers and the high-frequency gas density measurements from the IRGA were used to compute eddy covariance fluxes for water vapor and CO_2 in the period from 1 April 2020 to 1 November 2020 using EddyPro® software (LI-COR Env. Inc. USA) version 7.0.4. The flux processing steps were chosen to be as similar as possible to the STEA processing scheme. The calculation of EC fluxes involved statistical screening for the data quality issues following Vickers and Mahrt (1997), mean removal by block averaging, compensation for the time lag between the wind and the scalar time series using covariance maximization, tilt correction using the planar fit method without an intercept (Dijk et al., 2004) similar to STEA, and analytical high- and low-frequency corrections to correct for the spectral attenuation of the IRGA (Moncrieff et al., 2005, 1997).

Density fluctuation correction

Due to using a closed-path gas analyzer, the TEA and STEA methods do not require the WPL (Webb, Pearman, and Leuning) correction (Webb et al., 1980). WPL accounts for the effect of density fluctuations due to changes in temperature, humidity, and pressure. In TEA and STEA, after samples are collected and mixed in buffer volumes, the mean mixing ratio is measured. Therefore, no correction for density effects is needed as long as accurate mass flow sampling of air is maintained. The measured TEA and STEA flux is equivalent to the flux measured with mixing ratios $\overline{r_c' w'}$.

4.3.7 Data selection for method comparison

To compare the fluxes calculated from both methods, we selected averaging intervals according to the following criteria.

- Spike removal: this is done following Vickers and Mahrt (1997) using a window width of 6 h and a threshold of 2 standard deviations. This was mainly to account for unreliably elevated CO_2 concentrations recorded by the open-path gas analyzer due to water condensation.
- Rainy period exclusion: data records during rainy weather conditions were excluded.
- Flux quality flags: periods when the flux quality flag is 1 or 2 according to Foken et al. (2005) were excluded.
- STEA low flow rate: averaging intervals flagged with the low flow rate flag described earlier were discarded.

After applying the above criteria, 992 averaging intervals remained. They accounted for 54.4 % of the whole comparison period. Nighttime data were the majority of excluded values with only 33 % of averaging intervals valid during nighttime compared to 70 % during daytime. The open-path gas analyzer used for EC produced unreliable measurements during high humidity conditions at night due to water condensation. Table 4.2 shows a summary of data quality-check results.

Table 4.2: Summary of data quality checks for STEA and EC fluxes used in the EC–STEA flux intercomparison showing the number of averaging intervals that were excluded and the ratio of the excluded averaging intervals to the total for each criterion. Details on the criteria and the thresholds used are provided in Sect. 4.4.3.

Criteria	Averaging intervals	Ratio (%)
Spikes	3	0.2
EC missing value	16	0.9
Technical failure	38	2.1
Rain	91	5.0
STEA low flow rate	107	5.9
Flux quality flag 2	195	10.7
Flux quality flag 1	382	20.9
OK data	992	54.4

To compare the overall difference between the two methods, we used the coefficient of determination R^2 and the slope of the orthogonal distance regression (ODR) (also known as major-axis regression and model II regression). ODR considers the errors in x and y as opposed to ordinary least squares (OLS) regression, which assumes that the error in x is negligible (Wehr and Saleska, 2017).

4.4 Results and discussion

We first discuss the newly proposed short-time eddy accumulation method. Then, we discuss some results and aspects of the STEA flux calculations. Afterward, we present the flux intercomparison between STEA and EC. Finally, we discuss the effect of using fixed buffer volumes on the fluxes and the proposed empirical correction.

4.4.1 Short-time eddy accumulation

Using the STEA method reduced the dynamic range requirement for eddy accumulation sampling. For a short averaging interval of 1 min, the range was on average 60 % of the range required for the conventional eddy accumulation. As a result, the upper bound of the required dynamic range for w reported by Hicks and McMillen (1984) as $5\sigma_w$ is lowered to $3\sigma_w$. The reduction of the required dynamic range improves the accuracy and performance of the STEA system. The accumulation on shorter timescales brings many advantages. First, it allows adapting to the local range of vertical wind velocity values, which improves the resolution and dynamic range of the system. This can be achieved by exploiting the autocorrelation of the wind velocity signal to predict a scaling parameter, A_i, better adapted to the local velocity field for each interval. For a short interval, the range that the sampling apparatus needs to cover will be smaller on average than the range of the whole averaging interval.

Additionally, the accumulation on varying intervals means the measurement frequency can be adjusted to match that of the gas analyzer or the precision requirements. This can be useful for reactive species and other trace gases, for which relatively fast gas analyzers are available but not fast enough for EC.

Figure 4.6 demonstrates how the STEA method works. In this example, the high-frequency samples are collected at 5 Hz frequency for a 30 min averaging interval. The averaging interval is divided

into 30 short intervals with a duration varying from 70 to 190 s. The flux in this example equals $-14.24\,\mu\text{mol}\,\text{m}^{-2}\,\text{s}^{-1}$.

Finally, the STEA method facilitates using the STEA system in a continuous flow-through mode using rigid reservoirs. The operation in flow-through mode requires two sets of buffer volumes in a series as shown in Fig. 4.4, with two buffer volumes for each sampling line. The ideal operation of such a system can be achieved as follows.

1. Wind velocity is measured and rotated, and the value of the scaling parameter A_i is updated based on wind statistics and the flow calibration parameters.
2. For each sampling line, air samples are collected into the respective set of buffer volumes continuously according to the sign of the vertical wind velocity and proportional to its magnitude and the value of A_i until a predefined accumulated volume is reached.
3. When the predefined accumulated volume is reached, the second buffer volume in the sampling line is disconnected from the first. Sample accumulation time, τ_i, and accumulated mass are recorded. Then, samples are forwarded to the gas analyzer.
4. The slow gas analyzer alternates measuring scalar concentration for each interval C_i from the second set of buffer volumes for updraft and downdraft.

The successful use of this scheme requires keeping the mass flow rate of air from the second set of buffer volumes to the gas analyzer constant for consecutive short intervals since the model used to represent the buffer volumes in Eq. (4.8) assumes the flow rate to be constant with respect to time.

4.4.2 STEA fluxes computations

In this section, we discuss some aspects related to the calculation of the STEA fluxes. We first discuss the effects of water vapor on CO_2 concentration measurements. Then, we discuss the effect of coordinate rotation on the fluxes.

Water vapor correction

Treatment of the residual cross-sensitivity of CO_2 to water vapor content using a linear fit produced a small slope of -1.17×10^{-4} shown in Fig. (4.7). Thus, a difference in water concentration of 4000 ppm between updraft and downdraft reservoirs, typically observed in extreme conditions, will lead to a difference on the order of 0.5 ppm for CO_2. Applying the water vapor correction using the quadratic fit and the slope correction reduced the magnitude of STEA fluxes in comparison to the direct calculation of mixing ratios. However, it improved the fit between the STEA and the reference EC flux (slope decreased from 1.18 to 1.04, and R^2 increased from 0.80 to 0.86).

Coordinate rotation

The online coordinate rotation produced rotation angles with low variability over the experiment period. The eddy covariance fluxes calculated using the Class-A sonic anemometer with a 2-month-long dataset (1 June 2020 to 1 August 2020) produced the following rotation angles: $x-\text{pitch} = 0.6^\circ$; $y-\text{roll} = -4.3^\circ$ (using the YXZ Euler convention), whereas for the TEA moving-window online rotation,

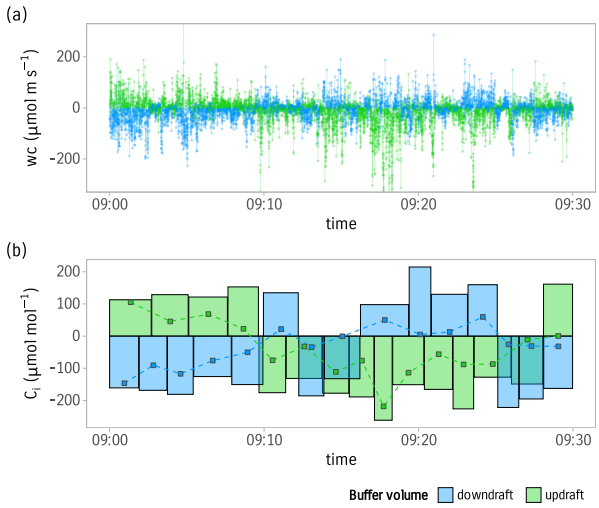

Figure 4.6: Sample accumulation using the STEA method. An example of 30 min of measurements: **(a)** samples wc are collected based on wind direction and proportional to its magnitude. **(b)** Short intervals are accumulated. The variable short interval duration guarantees equal accumulated volume for consecutive short intervals. Points are the concentrations C_i measured by the gas analyzer. The area of each rectangle represents the accumulated sample volume in arbitrary units and is equal to the relative weight for each concentration measurement. The sum of all measurements C_i weighted by the relative sample volume will equal the covariance. Data are from 20 June 2020.

larger pitch angles were observed with a mean of 3.6° and values slowly climbing from 1.2 to 6° during the 6-week comparison period. The roll angle ranged from −0.9 to −0.24° with an average of −0.4°.

The use of online rotation with a moving window of 2 d minimized the residual mean vertical wind in comparison to using the whole period of the experiment. This is likely due to a better adaptation to the local wind field. Furthermore, the distribution of normalized mean vertical wind velocity of the short moving window had less spread and thinner tails, and it showed more symmetry around the mean compared to the whole-dataset rotation. The residual mean magnitude of rotated w for the short moving window was $0.04\,\sigma_w$. The first and third quartiles were −0.03 and 0.03 σ_w, whereas for the whole-dataset rotation, the mean magnitude was $0.17\,\sigma_w$ and the first and third quartiles were −0.07 and 0.22 σ_w, respectively.

To estimate the effect of the online rotation method on the fluxes, we calculated EC fluxes using the two different rotation approaches while keeping other treatments constant. The comparison revealed that the online rotation with a moving window had a minimal effect on the fluxes: a slope of approximately 1 and an R^2 of 0.98 were obtained when using a linear fit. Nevertheless, this comparison only included data of good quality from an ideal site. These results might differ for nonideal conditions at a more complex site.

4.4.3 STEA–EC flux intercomparison

The measured CO_2 fluxes using the STEA method in flow-through mode showed a good match with the reference EC fluxes (Fig. 4.8).

The time series of measured CO_2 fluxes in Fig. (4.8a) shows that the STEA method was able to reproduce

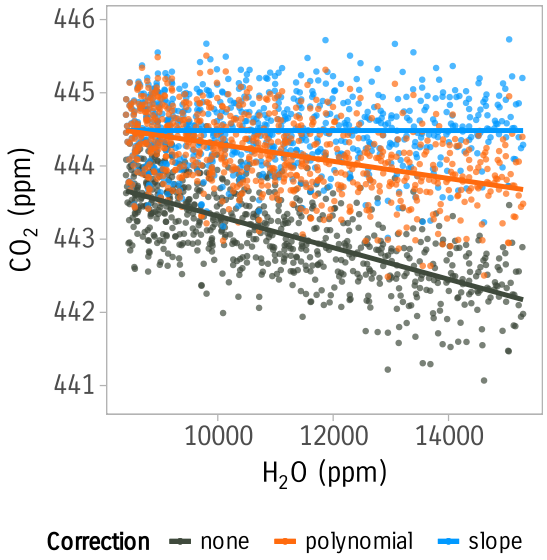

Figure 4.7: Effect of water correction on the measured CO_2 concentration using the LGR FGGA-24r-EP instrument. Points represent measured CO_2 by the gas analyzer when air with constant CO_2 concentration and varying H_2O concentration was supplied. Lines represent linear regression fits. Red-colored points and the red line represent CO_2 measurements after applying the polynomial correction (Hiller et al., 2012; Rella, 2010). In blue are the CO_2 measurements after applying our slope adjustment correction to remove additional cross-sensitivity to water.

the daily dynamics of CO_2 flux very well. The estimated fluxes using the STEA method appear to have fewer spikes and are smoother in general; this is likely due to the smoothing effect of buffer volumes and the lower sensitivity of the closed-path gas analyzer to rain and high humidity, in particular during nighttime. The correction for nonzero mean vertical wind velocity using α_θ was on average less than 1.5 % of the flux magnitude. This is due to the ideal topography of the site and the online rotation of the coordinates. The correction at less ideal sites with more complex topography may differ.

The mean diurnal cycle estimates from the two methods match very well (Fig. 4.8b). However, a small time shift can be observed in the mean diurnal cycle as a result of the phase shift introduced by the low-pass-filtering effect of the buffer volumes.

The linear regression in Fig. 4.8c shows that the measured CO_2 fluxes using the STEA method in flow-through mode have very good agreement with the reference EC fluxes. The magnitude of STEA fluxes was comparable to EC fluxes (ODR slope = 1.04). This indicates that the STEA method does not introduce systematic error to the fluxes.

Cumulative fluxes for the entire 6-week experiment period show generally good agreement between STEA and EC (Fig. 4.9). The cumulative CO_2 flux was estimated to be -168.3 ± 1.42 gr C m^{-2} using EC and 179.3 ± 1.42 gr C m^{-2} using STEA. The difference between the two methods is -10.9 gr C m^{-2}, which is about 6 % of the cumulative flux. While this difference falls slightly outside the uncertainty of the two methods, we note that the uncertainty estimates are based on the sampling error only and do not include other sources of uncertainty such as the different gas analyzers, the different data treatments, and the additional uncertainty contributions of sampling and buffers volumes in STEA. Furthermore, the difference between the two methods seems to increase in the last 3 weeks of the experiment, which coincides with intermittent rainfall and more variance in wind direction. Therefore, we believe this

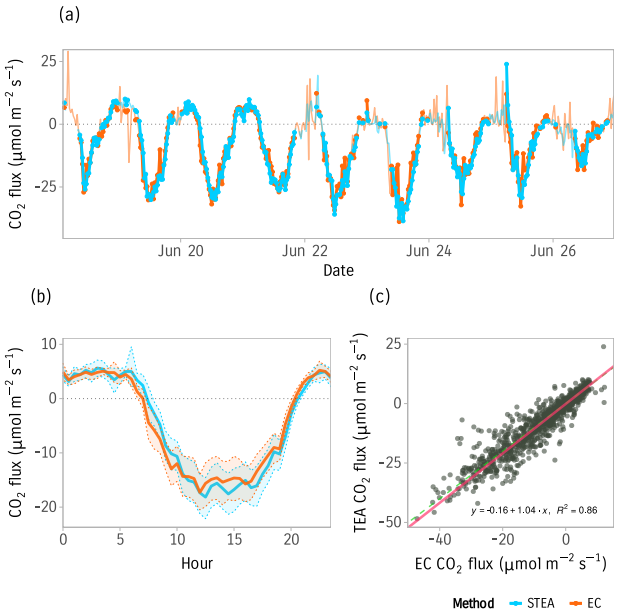

Figure 4.8: STEA and EC flux intercomparison. **(a)** Time series of EC and STEA CO_2 fluxes for a subset period of 9 d. Points and thick lines indicate the averaging intervals used for comparison after filtering for quality. **(b)** Mean diurnal cycle of CO_2 fluxes of STEA and EC. Bands are 95 % confidence intervals of the mean calculated using nonparametric bootstrapping. **(c)** Scatter plot of STEA CO_2 fluxes against reference EC fluxes. The red line is the linear fit using orthogonal distance regression (ODR). The dashed green line is a 1-to-1 line for reference. Data used for panels **(b)** and **(c)** are from 18 June to 31 July 2020, while for panel **(a)** a 9 d subset from 18 to 27 June 2020 was used.

difference does not indicate a systematic error in the flux estimates.

The coefficient of determination of the measured fluxes during the whole experiment period R^2 was 0.86. The remaining 13 % of unexplained variance is the joint contribution of the uncertainties of the two flux estimates from the EC and STEA methods. The observed uncertainty from the two methods calculated as the standard deviation of the difference was 4.36 µmol m^{-2} s^{-1}. We suggest three different mechanisms contributing to the observed uncertainty leading to the unexplained variance between the two estimates. First, the random sampling error arising from the stochasticity of turbulence (Hollinger and Richardson, 2005). The mean random sampling error of EC fluxes calculated following Finkelstein and Sims (2001) was 1.58 µmol m^{-2} s^{-1}. The standard deviation of the difference between the two methods can be estimated to be 2.34 µmol m^{-2} s^{-1} if STEA fluxes are assumed to have a similar random sampling error. Therefore, the random sampling error of the two methods accounts for more than half of the observed variance. The difference between the two methods also shows heteroscedasticity, with the error increasing along with the absolute magnitude of the flux; a similar behavior of the random sampling error was observed by Hollinger and Richardson (2005) when comparing two tower estimates. The second source of uncertainty is the use of different gas analyzers for STEA and EC. Polonik et al. (2019) compared five different analyzers for measuring CO_2 fluxes. They showed that the root mean square error (RMSE) was in the range of 1 to 3.35 µmol m^{-2} s^{-1} depending on the analyzer type and the spectral correction method applied, with larger discrepancies observed when comparing open-path to closed-path sensors. Our results have an RMSE value of 4.39 µ mol m^{-2} s^{-1}. While our result is slightly higher, it should be noted that RMSE is not an ideal metric for cross-study comparison. A relative metric, such as R^2, would be more comparable but was unavailable. The third source of uncertainty is

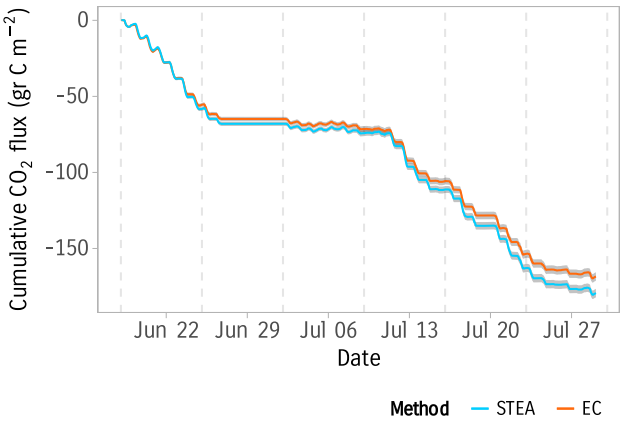

Figure 4.9: Cumulative fluxes of STEA and EC during the experimental period from 18 June to 31 July 2020. Bands represent the flux random error (2σ) estimated from the random sampling error of the EC fluxes. Only data with good quality were used, and no gap filling was applied.

the use of buffer volumes in the STEA method. Figure 4.10a demonstrates the increase in scatter in the measured fluxes due to the use of buffer volumes. Finally, the different processing steps between the two methods can contribute to the uncertainty, in particular the effects of time-lag compensation, spectral corrections, and statistical screening. We determined the combined effect of these processing treatments by calculating the EC flux with and without the treatments and found that the systematic errors in the flux were negligible.

4.4.4 Effect of buffer volumes

Using fixed buffer volumes attenuates the signal. To understand the effect of buffer volume use on the measured scalar concentration, we carried out a simulation on a surrogate signal generated from sonic temperature. The simulation showed that buffer volumes caused a decline that can reach up to 10 % of the fluxes under operation ranges similar to those of our experiment (for $\tau = 11$ min) (Fig. 4.10). The empirical correction was consistently able to mitigate most of the attenuation when the filter properties are assumed to be constant (i.e., the flow rate needs to be constant for consecutive short intervals). This assumption was difficult to maintain using the 1 min switching regime. The simulation showed that the empirical correction for the buffer volumes worked best when the correction factor was obtained using a linear fit, as opposed to taking a ratio of the attenuated flux to the true flux for each averaging interval. The correction factor, in this case, is the reciprocal of the slope of the linear regression between the attenuated flux and the true flux. The correction factor calculated using Eq. (4.10) shows good agreement between sensible heat flux and CO_2. However, the uncertainty of the correction factor increased with increasing buffer volume time constant. For our experiment, the average time constant for the first-order linear filter used to model the buffer volume was estimated to be $\tau = 700$ s. This value was used to simulate the loss on the fluxes using the sensible heat flux calculated from the sonic anemometer. The correction factor was obtained from the slope of the attenuated flux and was equal to 1.18.

The empirical correction scheme achieved here by simulating the loss on sensible heat flux lacks a proper treatment of the phase shift introduced by the first-order filter. Additionally, the similarity of transport between sensible heat flux and CO_2 is an approximation that is expected to be valid only on

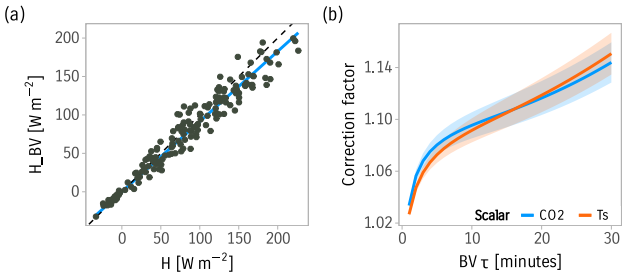

Figure 4.10: Empirical buffer volume correction. **(a)** Effect of buffer volume attenuation on sensible heat flux with a time constant $\tau = 11$ min. The blue solid line is the linear fit between the two. **(b)** Empirical correction factor for the effect of buffer volumes calculated as the reciprocal of the slope of attenuated flux for CO_2 and sensible heat flux. Bands are the estimated slope ± 1 standard error of the slope.

average as evidenced by the large scatter around the regression line in Fig. 4.10. Therefore, a direct correction that can estimate the original signal before attenuation is needed. Such a correction has since been developed and is the topic of a future publication (Emad, 2022).

4.5 Conclusions

In this paper, we proposed a new variety of the eddy accumulation method as an alternative to eddy covariance for the measurement of ecosystem-level fluxes. The new method, referred to here as short-time eddy accumulation (STEA), allows the sample accumulation to be carried out on shorter intervals of varying length. The STEA method offers more flexibility than the conventional TEA method and has many potential benefits. Most importantly, STEA provides a higher dynamic range and better accuracy than the TEA method and enables operating sample accumulation under a flow-through scheme using fixed buffer volumes. The flexibility introduced by the STEA method offers new ways to design eddy accumulation systems that are particularly suited for specific atmospheric constituent gas analyzers. For example, the accumulation time can be tailored to measure reactive species with lifetimes shorter than a conventional flux integration interval or to distribute the gas analyzer time to measure fluxes at different heights.

Furthermore, we presented a prototype evaluation of the STEA method under the flow-through regime. We described the details of the system design and operation. We compared flux measurements from our new system against a reference EC system over a flat agricultural field. The fluxes from the two methods were in very good agreement. We highlighted the importance of different processing and design aspects between the two methods and their potential effects on the fluxes.

Finally, we analyzed the effect of buffer volumes in the flow-through operational mode on the fluxes and proposed an empirical correction to correct for the underestimation resulting from the low-pass-filtering behavior of the buffer volumes.

In summary, the new STEA method provides a direct flux measurement method that complements the state-of-the-art EC method. It extends the coverage of micrometeorological methods to new trace gases and atmospheric constituents beyond the scope of the EC method.

Appendix

subsectionSymbols and subscripts with units

Symbols		
c	$\mathrm{mol\,m^{-3}}$	Molar density of a scalar
w	$\mathrm{m\,s^{-1}}$	Vertical wind velocity
Δt	s	Flux averaging interval
A	–	TEA sampling scaling factor
V	$\mathrm{m^3}$	Volume
C	$\mathrm{mol\,m^{-3}}$	Mean concentration of accumulated samples
α_c	–	Transport asymmetry coefficient for scalar c
ρ	–	Correlation coefficient
$\dot{q}$	–	Dimensionless mass flow rate
τ	s	Time constant of the buffer volume
r_c	ppm	Mixing ratio in dry air for a scalar, c
Subscripts		
acc		Accumulated samples
$\uparrow$		Updraft buffer volume
$\downarrow$		Downdraft buffer volume
c		Atmospheric constituent

Code and data availability. The data and code required to produce the figures in this paper are provided at doi:10.5281/zenodo.7451511 (Emad and Siebicke, 2022).

Author contributions. AE developed the theory of the STEA method and the empirical correction for the effect of buffer volumes, implemented needed software, performed the experiment, analyzed the data, interpreted the results, and wrote the paper. LS conceptualized the idea of a flow-through eddy accumulation system, built the TEA system used in the experiment, planned and supervised the experiment, and provided feedback on the results, the analysis, and the paper.

Competing interests. The contact author has declared that none of the authors has any competing interests.

Disclaimer. Publisher's note: Copernicus Publications remains neutral with regard to jurisdictional claims in published maps and institutional affiliations.

Acknowledgements. We gratefully acknowledge the support of the Bioclimatology group, led by Alexander Knohl at the University of Göttingen, in particular technical assistance by Justus Presse, Frank Tiedemann, Marek Peksa, Dietmar Fellert, and Edgar Tunsch. We thank Christian Brümmer and Jean-Pierre Delorme from the Thünen Institute for Agricultural Climate Protection and Mathias Herbst from the Center for Agrometeorological Research of the German Meteorological

Service (DWD) for facilitating the fieldwork in Braunschweig. We further acknowledge Christian Markwitz for the fruitful discussions during the preparation of the paper and for reading and commenting on the paper. We thank Alexander Knohl, Nicolò Camarretta, Justus van Ramshorst, and Yannik Wardius for reading the paper and providing useful comments.

Financial support. This research has been supported by the Niedersächsische Ministerium für Wissenschaft und Kultur (Wissenschaft.Niedersachsen.Weltoffen grant), the H2020 European Research Council (grant no. 682512 – OXYFLUX), and the Deutsche Forschungsgemeinschaft (grant no. INST 186/1118-1 FUGG).

This open-access publication was funded by the University of Göttingen.

Review statement. This paper was edited by Hartwig Harder and reviewed by Christoph Thomas and one anonymous referee.

Bibliography

Baldocchi, D.: Measuring Fluxes of Trace Gases and Energy between Ecosystems and the Atmosphere – the State and Future of the Eddy Covariance Method, Global Change Biol., 20, 3600–3609, doi:10.1111/gcb.12649, 2014.

Berger, B. W., Davis, K. J., Yi, C., Bakwin, P. S., and Zhao, C. L.: Long-Term Carbon Dioxide Fluxes from a Very Tall Tower in a Northern Forest: Flux Measurement Methodology, J. Atmos. Ocean. Technol., 18, 529–542, doi:10.1175/1520-0426(2001)018<0529:LTCDFF>2.0.CO;2, 2001.

Businger, J. A. and Oncley, S. P.: Flux Measurement with Conditional Sampling, J. Atmos. Ocean. Technol., 7, 349–352, doi:10.1175/1520-0426(1990)007<0349:FMWCS>2.0.CO;2, 1990.

Cescatti, A., Marcolla, B., Goded, I., and Gruening, C.: Optimal use of buffer volumes for the measurement of atmospheric gas concentration in multi-point systems, Atmos. Meas. Tech., 9, 4665–4672, doi:10.5194/amt-9-4665-2016, 2016.

Desjardins, R. L.: Energy Budget by an Eddy Correlation Method, J. Appl. Meteorol., 16, 248–250, doi:10.1175/1520-0450(1977)016<0248:EBBAEC>2.0.CO;2, 1977.

Dijk, A., Moene, A., and de Bruin, H.: The Principles of Surface Flux Physics: Theory, Practice and Description of the ECPACK Library, The Principles of Surface Flux Physics: Theory, Practice and Description of the ECPACK Library, 2004/1, 525–2004, Meteorology and Air Quality Group, Wageningen University, Wageningen, the Netherlands, 2004.

Emad, A.: Optimal Frequency-Response Corrections for Eddy Covariance Flux Measurements Using the Wiener Deconvolution Method, PREPRINT – available at Research Square, doi:10.21203/rs.3.rs-2075158/v1, 2022.

Emad, A. and Siebicke, L.:Reproduction Data and Code for the Paper: True Eddy Accumulation – Part 2: Theory and Experiment of the Short-Time Eddy Accumulation Method, Zenodo [data set], doi:10.5281/zenodo.7451511, 2022.

Emad, A. and Siebicke, L.: True eddy accumulation – Part 1: Solutions to the problem of non-vanishing mean vertical wind velocity, Atmos. Meas. Tech., 16, 29–40, doi:10.5194/amt-16-29-2023, 2023.

Emad, A. and Siebicke, L.: True eddy accumulation – Part 2: Theory and experiment of the short-time eddy accumulation method, Atmos. Meas. Tech., 16, 41–55, doi:10.5194/amt-16-41-2023, 2023.

Finkelstein, P. L. and Sims, P. F.: Sampling Error in Eddy Correlation Flux Measurements, J. Geophys. Res.-Atmos., 106, 3503–3509, doi:10.1029/2000JD900731, 2001.

Finnigan, J. J., Clement, R., Malhi, Y., Leuning, R., and Cleugh, H.: A Re-Evaluation of Long-Term Flux Measurement Techniques Part I: Averaging and Coordinate Rotation, Bound.-Lay. Meteorol., 107, 1–48, doi:10.1023/A:1021554900225, 2003.

Foken, T., Göockede, M., Mauder, M., Mahrt, L., Amiro, B., and Munger, W.: Post-Field Data Quality Control, in: Handbook of Micrometeorology: A Guide for Surface Flux Measurement and Analysis, edited by: Lee, X., Massman, W., and Law, B., Atmospheric and Oceanographic Sciences Library, 181–208, Springer Netherlands, Dordrecht, doi:10.1007/1-4020-2265-4_9, 2005.

Goulden, M. L., Munger, J. W., Fan, S.-M., Daube, B. C., and Wofsy, S. C.: Measurements of Carbon Sequestration by Long-Term Eddy Covariance: Methods and a Critical Evaluation of Accuracy, Global Change Biol., 2, 169–182, doi:10.1111/j.1365-2486.1996.tb00070.x, 1996.

Gu, L., Massman, W. J., Leuning, R., Pallardy, S. G., Meyers, T., Hanson, P. J., Riggs, J. S., Hosman, K. P., and Yang, B.: The Fundamental Equation of Eddy Covariance and Its Application in Flux Measurements, Agr. Forest Meteorol., 152, 135–148, doi:10.1016/j.agrformet.2011.09.014, 2012.

Hicks, B. B. and Baldocchi, D. D.: Measurement of Fluxes Over Land: Capabilities, Origins, and Remaining Challenges, Bound.-Lay. Meteorol., 177, 365–394, doi:10.1007/s10546-020-00531-y, 2020.

Hicks, B. B. and McMillen, R. T.: A Simulation of the Eddy Accumulation Method for Measuring Pollutant Fluxes, J. Clim. Appl. Meteorol., 23, 637–643, doi:10.1175/1520-0450(1984)023<0637:ASOTEA>2.0.CO;2, 1984.

Hiller, R. V., Zellweger, C., Knohl, A., and Eugster, W.: Flux correction for closed-path laser spectrometers without internal water vapor measurements, Atmos. Meas. Tech. Discuss., 5, 351–384, doi:10.5194/amtd-5-351-2012, 2012.

Hollinger, D. Y. and Richardson, A. D.: Uncertainty in Eddy Covariance Measurements and Its Application to Physiological Models, Tree Physiol., 25, 873–885, doi:10.1093/treephys/25.7.873, 2005.

Moncrieff, J., Clement, R., Finnigan, J., and Meyers, T.: Averaging, Detrending, and Filtering of Eddy Covariance Time Series, in: Handbook of Micrometeorology: A Guide for Surface Flux Measurement and Analysis, edited by: Lee, X., Massman, W., and Law, B., Atmospheric and Oceanographic Sciences Library, 7–31, Springer Netherlands, Dordrecht, doi:10.1007/1-4020-2265-4_2, 2005.

Moncrieff, J. B., Massheder, J. M., de Bruin, H., Elbers, J., Friborg, T., Heusinkveld, B., Kabat, P., Scott, S., Soegaard, H., and Verhoef, A.: A System to Measure Surface Fluxes of Momentum, Sensible Heat, Water Vapour and Carbon Dioxide, J. Hydrol., 188–189, 589–611, doi:10.1016/S0022-1694(96)03194-0, 1997.

Polonik, P., Chan, W. S., Billesbach, D. P., Burba, G., Li, J., Nottrott, A., Bogoev, I., Conrad, B., and Biraud, S. C.: Comparison of Gas Analyzers for Eddy Covariance: Effects of Analyzer Type and Spectral Corrections on Fluxes, Agr. Forest Meteorol., 272–273, 128–142, doi:10.1016/j.agrformet.2019.02.010, 2019.

Rella, C.: Accurate Greenhouse Gas Measurements in Humid Gas Streams Using the Picarro G1301 Carbon Dioxide/Methane / Water Vapor Gas Analyzer, White paper, Picarro Inc, Sunnyvale, CA, USA, 18 p., 2010.

Rinne, J., Ammann, C., Pattey, E., Paw U, K. T., and Desjardins, R. L.: Alternative Turbulent Trace Gas Flux Measurement Methods, in: Springer Handbook of Atmospheric Measurements, edited by: Foken, T., Springer Handbooks, 1505–1530, Springer International Publishing, Cham, doi:10.1007/978-3-030-52171-4_56, 2021.

Sabbatini, S., Mammarella, I., Arriga, N., Fratini, G., Graf, A., Hörtnagl, L., Ibrom, A., Longdoz, B., Mauder, M., Merbold, L., Metzger, S., Montagnani, L., Pitacco, A., Rebmann, C., Sedlák, P., Šigut, L., Vitale, D., and Papale, D.: Eddy Covariance Raw Data Processing for CO_2 and Energy Fluxes Calculation at ICOS Ecosystem Stations, Int. Agrophys., 32, 495–515, doi:10.1515/intag-2017-0043, 2018.

Siebicke, L.: A True Eddy Accumulation – Eddy Covariance Hybrid for Measurements of Turbulent Trace Gas Fluxes, Geophys. Res. Abstracts EGU General Assembly, 18, 2016–16124, 2016.

Siebicke, L. and Emad, A.: True eddy accumulation trace gas flux measurements: proof of concept, Atmos. Meas. Tech., 12, 4393–4420, doi:10.5194/amt-12-4393-2019, 2019.

Taylor, C. J., Young, P. C., and Chotai, A.: True Digital Control: Statistical Modelling and Non-Minimal State Space Design, Wiley, 1st Edn., ISBN 978-1-118-53552-3, 2013.

Vickers, D. and Mahrt, L.: Quality Control and Flux Sampling Problems for Tower and Aircraft Data, J. Atmos. Ocean. Technol., 14, 512–526, doi:10.1175/1520-0426(1997)014<0512:QCAFSP>2.0.CO;2, 1997.

Webb, E. K., Pearman, G. I., and Leuning, R.: Correction of Flux Measurements for Density Effects Due to Heat and Water Vapour Transfer, Q. J. Roy. Meteorol. Soc., 106, 85–100, doi:10.1002/qj.49710644707, 1980.

Wehr, R. and Saleska, S. R.: The long-solved problem of the best-fit straight line: application to isotopic mixing lines, Biogeosciences, 14, 17–29, doi:10.5194/bg-14-17-2017, 2017.

5 Optimal frequency-response corrections for eddy covariance flux measurements using the Wiener deconvolution method

Paper published in *Boundary layer meteorology* (Emad, 2023).

Emad, Anas: Optimal Frequency-Response Corrections for Eddy Covariance Flux Measurements Using the Wiener Deconvolution Method, Boundary-Layer Meteorology, 188, 29–53, doi:10.1007/s10546-023-00799-w, 2023.

Abstract

We describe a new direct correction approach to accurately restore frequency attenuated eddy covariance (EC) measurements. The new approach utilizes the Wiener deconvolution method to optimally estimate the original signal from noisy atmospheric measurements. Key features over conventional EC spectral correction methods include i) the use of physics-based response functions, ii) the ability to account for the non-linear phase contributions, and iii) the direct restoration of the original signal rather than simulating the effect on an ideal reference spectrum. The new correction approach is compared to conventional spectral correction methods in a numerical simulation where the magnitude of the key limitations of conventional methods is explored under conditions relevant to common EC set-ups. The simulation results showed that the spectral correction methods commonly used for calculating EC fluxes introduced systematic error up to 10% to the restored fluxes and substantially increased their random uncertainty. The errors are attributed to the effect of using inappropriate response functions, failing to account for the contribution of the non-linear phase, and due to the assumption of spectral similarity on the scale of averaging intervals. The Wiener deconvolution method is versatile, can be applied under non-ideal conditions, and provides an opportunity to unify analytical and “in-situ" spectral correction methods by applying existing transfer functions to directly restore attenuated spectra. Furthermore, the Wiener deconvolution approach is adaptable for use with various micrometeorological measurement techniques such as eddy accumulation and flux profile measurements.

5.1 Introduction

The eddy covariance (EC) method has become the de facto method for measuring the atmospheric exchange of energy, momentum, and atmospheric trace constituents. EC enables direct and continuous measurements of a range of atmospheric fluxes, such as CO_2, H_2O, sensible and latent heat fluxes, on a scale suitable for ecosystem studies (Baldocchi, 2014; Hicks and Baldocchi, 2020). The turbulent flux of a scalar in EC is calculated as the covariance between the scalar concentration c and the coincident vertical wind velocity w. In ecological applications, the covariance between w and c is commonly calculated for a long-enough averaging interval (30 to 60 minutes) using the high-frequency measurements of the scalar concentration and the wind. Typically, measurement frequencies of 10 Hz or more are required to resolve relevant scales of flux-carrying turbulent eddies (Aubinet et al., 1999).

Fluxes measured using the EC method suffer from unavoidable biases caused by the frequency response limitations of the EC system and data processing methods. Measured signals required for flux calculation are often attenuated due to interactions with the measurement apparatus. This attenuation can result from limitations of the instrument design, data processing methods, or due to physical processes such as water adsorption and desorption on the walls of tubes. Signal attenuation is notably more significant in closed-path EC systems and when sorbing scalars like water vapor are involved, with the underestimation of measured fluxes under these configurations reaching up to 40(Shaw et al., 1998; Ibrom et al., 2007).

Attenuated signals can be more comfortably identified and treated in the frequency domain by inspecting their spectra and cospectra. Therefore, depending on the part of the spectrum affected, the attenuation can be classified into high-frequency losses equivalent to the effect of a low-pass filter and low-frequency losses equivalent to the effect of a high-pass filter (Massman and Clement, 2005; Foken et al., 2012).

Methods for correcting spectral attenuation can be broadly put into two classes based on their assumptions and how they are applied. The analytical method, also called the transfer function method or the theoretical method (Moore, 1986), and the empirical (or in-situ) method (Goulden et al., 1996a). The analytical method aims to derive transfer functions that describe the response of the measurement system to individual causes of attenuation, which is then multiplied by a model cospectrum to estimate the required correction. Early examples of analytical methods dealt with distortions introduced by line averaging of sonic anemometers (Kaimal et al., 1968; Silverman, 1968). The net frequency response of the EC system in the analytical method is considered as the product of the several independent response functions that account individually for different causes of spectral attenuation. The resulting net frequency response function is multiplied by a model of the unattenuated cospectra of the scalar and vertical wind velocity to obtain a correction factor (Moore, 1986). Several phenomenological models of turbulence spectra and cospectra have been utilized in the analytical method, most notably the models of Kaimal et al. (1972, 1976). Empirical methods have different assumptions about the net transfer function and the ideal unattenuated spectrum. A different scalar undergoing little to no attenuation is assumed to be a reference. The spectrum of the reference scalar is considered to be the ideal spectrum by utilizing the hypothesis of spectral similarity (Ohtaki, 1985). Most commonly, the spectrum of the sonic temperature measured using a sonic anemometer is considered the unattenuated ideal spectrum. The net system response is typically assumed to be a first-order low pass filter (RC filter) with one parameter to estimate, the time constant τ (Goulden et al., 1996b). The filter's time constant is estimated from the ratio of the attenuated scalar spectrum to the ideal spectrum (Ibrom et al., 2007). But also the use of the cospectra is common (Mammarella et al., 2009). Less commonly, τ can be experimentally estimated by adding CO_2 to the analyzer (Goulden et al., 1996b) or by utilizing the observed phase shift (Shaw et al., 1998). The estimated filter is used to simulate the attenuation on the reference scalar (sonic temperature) and obtain a correction factor that can be used directly to correct the attenuated fluxes or parameterized using wind speed and atmospheric stability classes (Goulden et al., 1997; Berger et al., 2001; Ibrom et al., 2007; Fratini et al., 2012). Other methods that do not fit exactly in this classification scheme are the ogive method, which involves comparing the cumulative frequency curves (ogives) of sensible heat flux and the scalar to determine the flux loss (Ammann et al., 2006) and the wavelet approach, in which the variance of the attenuated scalars is adjusted to match the theoretical power law in the inertial sub-range in the wavelet domain (Nordbo and Katul, 2013). Both of these methods make similar assumptions regarding the ideal shape of the spectra or the cospectra.

The analytical and the empirical methods both have known limitations. Firstly, the use of ideal reference spectra and cospectral to estimate the attenuation is not well-justified, regardless of whether these ideal spectra and cospectra are obtained from turbulence spectral models or based on the assumption of spectral similarity. Experimental data point at a large degree of variability and significant deviations from the ideal spectra and cospectra (Mamadou et al., 2016). This variability often results in varying correction estimates, depending on the chosen correction method (Reitz et al., 2022; Zhu et al., 2015). Furthermore, although the spectral similarity might hold for a large ensemble of averaged spectra under favorable conditions, there is no reason why the spectra should be similar in each averaging interval, as implied by empirical methods. In addition to the measurement height and meteorological conditions, variations in spectra can be caused by the differences in spatial and vertical distribution of sources and sinks of different scalars and by the contribution of sonic temperature to buoyancy (McBean, 1973). Secondly, conventional methods lack a proper treatment for the contribution of the phase spectrum to the attenuated covariance. The contribution of the phase spectrum, also known as the contribution of quadrature spectrum and the out-of-phase contribution to the covariance (Kaimal and Finnigan, 1994) is caused by the changes of the phase angle between w and c due to the phase

shifting effect of the attenuating filter. This contribution has been acknowledged before (Hicks, 1972; Kristensen and Lenschow, 1988; Eugster and Senn, 1995; Horst, 2000). However, it was either ignored (Moore, 1986), replaced by an approximation based on simplifying assumptions (Eugster and Senn, 1995; Peltola et al., 2021), assumed negligible (Massman, 2000; Horst, 2000; Mammarella et al., 2009), or, assumed that digitally shifting the time series would compensate for the contribution of phase spectra (Ibrom et al., 2007; Fratini et al., 2012). Finally, the consequences of some assumptions and treatments of empirical methods are subject to ongoing discussion such as model assumptions, noise effect on the spectra, interactions with the time lag correction, and how the spectral transfer functions are applied (Peltola et al., 2021; Aslan et al., 2021).

A direct spectral correction approach for EC measurements remains a desired goal. Few studies have attempted to directly restore the original signal or the (co)spectra. Massman (2000) mentioned that a direct correction is possible but too computationally expensive. Wilczak and Bedard (2004) used simple inverse filtering to correct pressure measurements but eliminated frequencies below a critical limit to avoid noise amplification. (Nordbo and Katul, 2013) proposed an empirical wavelet-based approach to restore the original signals by compensating for the estimated variance loss in the wavelet space. More recently, Polonik et al. (2019) have evaluated directly correcting the attenuated cospectra with empirically estimated transfer function. Despite these efforts, a general direct spectral correction approach that optimally restores the attenuated signals in the presence of noise is currently unavailable. The goal here is to develop such an approach.

This paper aims to revise the theoretical basis of the problem of signal attenuation in EC flux measurements and show that the Wiener deconvolution is an optimal solution to estimate the original signal. In order to estimate the size of the problems addressed here, a numerical simulation is utilized to examine the extent of the key limitations of common spectral correction methods that can be resolved by the Wiener deconvolution method. Future work will present an extended evaluation of the Wiener deconvolution method using field measurements from multiple sensors.

We start in Section 5.2 by examining the theoretical basis of the spectral attenuation of EC measurements in the framework of linear system theory. We derive an accurate cospectral transfer function which forms the basis for subsequent analysis of the role of phase spectrum and measurement noise in signal restoration. Based on this analysis, the Wiener deconvolution method is proposed as an optimal solution for restoring attenuated noisy atmospheric measurements in Section 5.2.2. Subsequently, we discuss the theoretical aspects of modeling the system response and estimating its parameters within this framework. We then proceed to explore the key limitations of conventional methods in a numerical simulation. The simulation set-up and evaluation are presented in Section 5.3 where the effects of three interrelated issues are investigated: i) the inappropriate assumptions of the attenuation model, ii) the contribution of the non-linear phase to the attenuation, and iii) the consequences of the spectral similarity assumption. We present and discuss the simulation results in Section 5.4. Finally, we discuss the requirements and practical limitations of applying the Wiener deconvolution method to restore attenuated atmospheric scalars.

5.2 Theory

We begin by providing a short overview of signal attenuation in EC measurements, followed by the construction of a simple accurate cospectral transfer function. Next, we present the Wiener deconvolution as an optimal solution to the problem of signal attenuation. We then discuss the models of attenuation and the problem of model parameter estimation.

It is worth noting that different concepts in the EC literature are interchangeably referred to as “transfer function". This study uses terminology consistent with linear system theory and signal processing (e.g. Smith (2007)). An overview of the notation used is provided in Table 5.1.

5.2.1 Spectra and cospectra of atmospheric signals

For an infinite stationary time series $c(t)$ of a scalar, c, (such as an atmospheric constituent) observed over a region of finite-time T, the power spectrum of the scalar c, S_{cc} is defined as (Miller and Childers, 2012)

$$S_{cc}(\omega) = \lim_{(T\to\infty)} \frac{1}{T} \left| C(\omega)^2 \right| \tag{5.1}$$

where $\omega = 2\pi f$ is the angular frequency, and $C(\omega)$ denotes the Fourier transform of $c(t)$. It is customary in EC literature to define the power spectrum in terms of the autocorrelation function of the scalar c over a distance r_1 in the x direction, $R(r_1)$. Such a definition can be shown to be equal to the previous definition since $R(r_1)$ and the spectrum $S(\omega)$ form a Fourier transform pair. Time and space in $R(r_1)$ can be interchanged in the previous definition by making use of Taylor’s frozen turbulence hypothesis (Kaimal and Finnigan, 1994).

The phase spectrum of C is defined as $\angle C(\omega) \equiv \arg(C(\omega))$ where arg is the argument of C. The area under the spectrum equals the biased variance of the signal, σ_c^2 (Parseval’s theorem).

$$\int_{-\infty}^{+\infty} S_{cc}(\omega)\mathrm{d}\omega = \sigma_c^2 \tag{5.2}$$

For two variables such as the scalar $c(t)$ and the vertical wind speed $w(t)$, the cross-spectrum Cr_{cw} is similarly defined as

$$\int_{-\infty}^{+\infty} Cr_{wc}(\omega)\,\mathrm{d}\omega = \int_{-\infty}^{+\infty} W(\omega)[C(\omega)]^*\,\mathrm{d}\omega \tag{5.3}$$

where $[C(\omega)]^*$ is the complex conjugate of $C(\omega)$. The cross-spectrum has a real part and an imaginary part. The real part of the cross-spectrum is the cospectrum C_{wc} and the imaginary part is the quadrature spectrum Q_{wc}. It can be shown that the quadrature spectrum is the Fourier transform of the odd part of the cross-covariance function $R_{wc}(r_1)$ and that it makes no contribution to the cross-covariance at $(r_1 = 0)$, $R_{wc}(0)$ (Kaimal and Finnigan, 1994).

Similar to the spectrum, integrating the cospectrum of w and c, C_{wc} gives the covariance $\overline{wc}$

$$\int_{-\infty}^{+\infty} C_{wc}(\omega)\,\mathrm{d}\omega = \int_{-\infty}^{+\infty} \Re(Cr_{wc}(\omega))\,\mathrm{d}\omega = \overline{wc} \tag{5.4}$$

The spectra and cospectra for atmospheric measurements are usually binned, normalized, averaged, or weighted by the frequency to emphasize certain features (Stull, 1988). They are also often defined as one-sided (0 to $+\infty$) since the signals we deal with are real-valued. Several methods exist to estimate the true spectral density from a limited number of samples of a random process (Percival and Walden, 1993). In EC measurements, a variant of the periodogram method is used to calculate the spectra for half-hourly intervals (Bartlett, 1948).

Signal attenuation

For a system measuring a scalar quantity, the observed signal at time step t, $c_m(t)$ can be described as the convolution of the true signal $c(t)$ and the impulse response function of the measurement system $h(t)$

$$c_m(t) = c(t) * h(t) \tag{5.5}$$

where $*$ denotes convolution. The response of the system is assumed to be Linear and Time-Invariant (LTI). Consequently, the impulse response function $h(t)$ completely characterizes the behavior of the system. The impulse response function $h(t)$ represents the output of the dynamic system in response to a sudden change (impulse) in the time domain. The assumption of linearity implies that the system satisfies the superposition principle, which means that a linear change in the system's input will induce a linear change in the output. Time invariance implies that the system output does not depend on the time of the measurement. The LTI system can also be characterized by its representation in the frequency domain $H(\omega)$. The (complex) frequency response function of the system $H(\omega)$ is defined as the Laplace transform of the impulse response function $h(t)$. The convolution from Eq. 5.5 is equivalent to multiplication in the frequency domain (the convolution theorem), therefore

$$C_m(\omega) = C(\omega) \cdot H(\omega) \tag{5.6}$$

where $C_m(\omega)$ and $C(\omega)$ are the Fourier transforms of the attenuated signal $c_m(t)$ and the true signal $c(t)$, respectively, $H(\omega)$ is the frequency response of the system, and $\cdot$ denotes point-wise multiplication.

In the case of EC measurements and assuming the attenuation is only affecting the scalar c, the attenuated (measured) covariance, $\overline{wc}_{attn}$ is the integral of the real part of the cross-spectrum

$$\overline{wc}_{attn} = \int_{-\infty}^{+\infty} \Re\left(W(\omega) \cdot [C(\omega) \cdot H(\omega)]^*\right) \mathrm{d}\omega \tag{5.7}$$

Here, $\overline{wc}$ is considered in the general case, but $\overline{w'c'}$ can be easily obtained by removing the zero-frequency component (mean of the time series). For notational simplicity, we drop the frequency from the notation (e.g., $H \cdot W$ instead of $H(\omega) \cdot W(\omega)$).

We can write Eq. 5.7 using the amplitude and the phase shift as

$$\overline{wc}_{attn} = \int_{-\infty}^{+\infty} |Cr_{cw}| \cdot |H| \cdot \cos(\angle Cr_{cw} + \angle H) \mathrm{d}\omega \tag{5.8}$$

where the phase cross-spectrum, $\angle Cr_{cw}$, is the phase shift between c and w at each frequency, $\angle H$ is the phase spectrum of the filter, $|Cr_{cw}|$ is the amplitude cross-spectrum, and $|H|$ is the magnitude response of the filter. The previous equation can be further decomposed to relate the attenuation to the spectra of c, and w as

$$\overline{wc}_{attn} = \int_{-\infty}^{+\infty} |C| \cdot |W| \cdot |H| \cdot \cos(\angle C - \angle W + \angle H) \mathrm{d}\omega \tag{5.9}$$

where $\angle C$ and $\angle W$ are the phase spectra of $c(t)$ and $w(t)$, respectively.

A cospectral transfer function is often defined in the EC literature as the transfer function that will produce the attenuated cospectra when multiplied by the true cospectra. The earliest use of such a function is the formulation of Moore (1986) where he used the magnitude response of the filter, $|H|$ (in

his notation $\sqrt{H}$) to express the attenuation on the cospectra. Eugster and Senn (1995) approximated the phase induced attenuation for an RC filter as $|H|$, thereby using $|H|^2$ as a cospectral transfer function which was further supported by Horst (1997, 2000). To evaluate these formulations, we construct an accurate cospectral transfer function. We rearrange Eq. 5.8 to isolate the cospectra

$$\overline{wc}_{attn} = \int_{-\infty}^{+\infty} Co_{cw} \cdot |H| \, \frac{\cos(\angle Cr_{cw} + \angle H)}{\cos(\angle Cr_{cw})} \, \mathrm{d}\omega \tag{5.10}$$

Therefore, the function $\Lambda(\omega)$ defined when $\angle Cr_{cw} \neq \left(\frac{\pi}{2} + n\pi\right)$ as

$$\Lambda(\omega) = |H| \, \frac{\cos(\angle Cr_{cw} + \angle H)}{\cos(\angle Cr_{cw})} \tag{5.11}$$

can be considered an accurate cospectral transfer function that will produce the desired attenuation when multiplied by the cospectrum.

The function $\Lambda(\omega)$ highlights the importance of considering the phase shift introduced to individual frequency components if it is to be used for correcting attenuated cospectra. This raises the question of whether simply shifting the time series in time would correct for the phase shift. To answer this question, it is important to consider the concept of group delay. Group delay represents the time delay each frequency component undergoes due to phase shift and is defined as the derivative of the phase spectra with respect to frequency (Mandal and Asif, 2007). If the phase shift is a linear function of the frequency, all frequency components would be shifted equally and the net effect on the time series would be similar to shifting the time series by a constant time lag. Therefore, the time lag correction procedure, which is commonly applied in EC data processing and involves shifting the scalar time series to maximize its correlation with the vertical wind velocity, can only correct for linear phase shifts at best. Any remaining effects on the cospectra due to the nonlinearity of the phase will continue to bias the fluxes. We refer to these remaining effects on the flux as “nonlinear phase contribution" to the flux attenuation.

5.2.2 Signal reconstruction using the Wiener deconvolution method

Using the properties of convolution, recovering the original signal seems conceptually simple. The original signal can be restored by dividing the Fourier transform of the attenuated signal by the frequency response function of the filter and then taking the inverse Fourier transform. Rearranging Eq. 5.6, we can write

$$C = C_m \cdot \frac{1}{H} \tag{5.12}$$

and the original signal will be

$$c(t) = \mathscr{F}^{-1}(C) \tag{5.13}$$

However, the problem with this approach, commonly called “naive deconvolution", is that the noise in the signal will be amplified, particularly in regions of the spectrum where the attenuation is high and the signal is low. This results in a recovered signal dominated by noise and is often unrecognizable. In most real-world applications, the measured signal is contaminated by noise. Therefore, the observed signal $c_m(t)$ can be more accurately described as a sum of the attenuated signal and an additive noise term $\varepsilon(t)$ independent of $c(t)$

$$c_m(t) = h(t) * c(t) + \varepsilon(t) \tag{5.14}$$

In the presence of noise, we wish to get the best estimate of the original signal $c(t)$ denoted as $\hat{c}(t)$. The goal is then to find the optimal filter G that, when applied to the measured signal, results in the best estimate of the original signal such as

$$\hat{C} = G \cdot C_m \tag{5.15}$$

This objective can be expressed as minimizing the mean squared error between the original signal and the estimated signal. The error that needs to be minimized can be written as

$$\epsilon(\omega) = \mathbb{E}\left|C - \hat{C}\right|^2 \tag{5.16}$$

where $\mathbb{E}$ denotes mathematical expectation. We substitute the estimated signal $\hat{C}$ with its expression from Eq. 5.15 and the frequency domain representation of Eq. 5.14. We can then write the error as

$$\begin{aligned} \epsilon(\omega) &= \mathbb{E}\,|C - G \cdot (C \cdot H + \mathscr{E})|^2 \\ &= \mathbb{E}\,|[1 - G \cdot H] \cdot C - G \cdot \mathscr{E}|^2 \end{aligned} \tag{5.17}$$

where $\mathscr{E}$ is the Fourier transform of the noise $\varepsilon(t)$. Expanding the previous equation, we find

$$\begin{aligned} \epsilon(\omega) = &\left[1 - G \cdot H\right]\left[1 - G \cdot H\right]^* \mathbb{E}|C|^2 \\ &- \left[1 - G \cdot H\right] \cdot G^* \,\mathbb{E}\left\{C \cdot \mathscr{E}^*\right\} \\ &- G\left[1 - G \cdot H\right]^* \mathbb{E}\left\{C^* \cdot \mathscr{E}\right\} \\ &+ G \cdot G^* \,\mathbb{E}|\mathscr{E}|^2 \end{aligned} \tag{5.18}$$

Considering that the noise is assumed independent of the signal, we have $\mathbb{E}\left\{C \cdot \mathscr{E}^*\right\} = \mathbb{E}\left\{C^* \cdot \mathscr{E}\right\} = 0$. Substituting $\mathbb{E}|C|^2$ and $\mathbb{E}|\mathscr{E}|^2$ with their corresponding mean power spectral densities, $\bar{S}(\omega)$ and $\bar{S}_N(\omega)$, we obtain

$$\epsilon(\omega) = \left[1 - G \cdot H\right]\left[1 - G \cdot H\right]^* \bar{S} + G \cdot G^* \bar{S}_N \tag{5.19}$$

This optimization problem was solved by Wiener (1964). Further details of the different aspects of the solution are also provided by Meditch (1969) and Kay (2006). The minimum value of the error in Eq. 5.19 is found by taking the Wirtinger derivative with respect to G and setting it equal to 0. The solution that minimizes the error is found to be

$$G^* \bar{S}_N - H \cdot [1 - G \cdot H]^* \bar{S} = 0 \tag{5.20}$$

Rearranging the previous equation, we find the formulation to the optimal deconvolution filter as

$$G(\omega) = \frac{1}{H} \cdot \left(\frac{1}{1 + 1/\left(|H|^2 \cdot \mathrm{SNR}\right)} \right) \tag{5.21}$$

where SNR is the mean signal-to-noise ratio spectrum defined as:

$$\mathrm{SNR}(\omega) = \frac{\bar{S}(\omega)}{\bar{S}_N(\omega)} \tag{5.22}$$

The Wiener deconvolution method combines knowledge about the noise spectra and the system response to produce the best estimate for the original signal $c(t)$. The estimated signal $\hat{c}$ minimizes the least-squares error between the observed signal $c_m(t)$ and the original signal $c(t)$.

After constructing the deconvolution filter $G(\omega)$, the estimated signal $\hat{c}$ is obtained by multiplying the deconvolution filter by the Fourier transform of the measured signal and taking the inverse Fourier transform of the product

$$\hat{c}(t) = \mathscr{F}^{-1}(C_m \cdot G) \tag{5.23}$$

5.2.3 Modeling the system response

The knowledge of the response function of the linear time-invariance (LTI) system is essential for the application of the Wiener deconvolution method and conventional spectral correction methods. The response function can be derived from the mathematical description of the system, usually by finding the differential equations that govern the system and applying the Laplace transform to them. However, a description of the physical dynamics of the system is not always possible. In such a case, the system can be assumed to follow a certain simplified response approximating the true system behavior. Therefore, we distinguish between models developed from the underlying physical dynamics of the system and empirical models approximating the behavior of the system.

Empirical models

Empirical models for the system response function are assumed based on the observation of the magnitude response $|H|$ of the system. The simplest form of these models is the first order low-pass filter, also known as the RC filter and the infinite impulse response filter. The first order system (such as an RC circuit) is described using the following differential equation

$$\tau \frac{\partial y(t)}{\partial t} + y(t) = x(t) \tag{5.24}$$

where τ is the characteristic time constant of the system. The frequency response function of this system in the Laplace domain is given by

$$H(s) = \frac{1}{1 + \tau s} \tag{5.25}$$

where s is a complex variable known as the Laplace variable. The magnitude squared response of the RC filter is given by

$$|H(\omega)|^2 = \frac{1}{1 + (\omega\tau)^2} \tag{5.26}$$

The inverse Laplace transform of Eq. 5.25 gives the impulse response function of the RC filter in the continuous time domain

$$h(t) = \frac{\mathrm{e}^{-t/\tau}}{\tau} \tag{5.27}$$

The low-pass RC filter is well-suited to model certain sensors with simple responses such as the gain of a resistor-capacitor circuit. However, the overall system response of an EC system is typically more complex and involves multiple sources of attenuation which makes it difficult to be adequately described by such a simple response function. Despite this, the magnitude response of the RC filter has been extensively used to model the attenuation caused by EC systems in numerous studies (Moore, 1986; Eugster and Senn, 1995; Goulden et al., 1996b; Horst, 1997; Berger et al., 2001; Ibrom et al., 2007; Mammarella et al., 2009; Fratini et al., 2012; Peltola et al., 2021). However, the RC filter was found to be a poor approximation for the observed attenuation on many EC systems (de Ligne et al., 2010) which motivated the use of modified functions to model the observed spectral attenuation ratio such as the Gaussian function (Aubinet et al., 2001), or the Gaussian function with an adjustable exponent (de Ligne et al., 2010). These functions, while effective for modeling the spectral shape, do not qualify as valid filters for application as convolution as they do not include information about the phase shift.

Process-based models

In process-based models, the system's response function is developed by describing the physical mechanism causing the attenuation. A good example relevant to this study is the process-based physical model for the behavior of water vapor in tubes. This model describes the attenuation of scalars experiencing absorption and desorption as a diffusion process in addition to Taylor dispersion (Kekäläinen et al., 2011; Nordbo et al., 2013) The model describes the mechanism in which water drops adsorb and condense on tube walls in periods of high humidity until an equilibrium is reached. Then, condensed liquid water evaporates in less humid conditions enhancing the content of air with water vapor. This mechanism is formulated as an advection-diffusion equation and its solution under appropriate boundary conditions for the breakthrough curve gives the frequency response function of the system. The sorption model was tested in laboratory and field conditions and was shown to be a good representation of the attenuation of water signals in EC systems (Nordbo et al., 2013, 2014). The frequency response function of the sorption model is given by the solution in the Laplace domain

$$H(s) = \exp\left(\frac{1-\sqrt{1+4\mu^2(s+\lambda\sqrt{s}\tanh(\kappa\sqrt{s}))}}{2\mu^2}\right) \tag{5.28}$$

where μ, λ, and κ are dimensionless variables that characterize the response function. The parameter μ is related to molecular diffusion in air and Taylor dispersion and can be estimated from the system dimensions using Taylor theory (Taylor, 1954). The parameter λ is related to the relative area available for condensation and evaporation. The parameter κ is related to the length scale attached to the diffusive evaporation process. The model parameters λ and κ are not easy to know a priori and need to be estimated from the data. They were found to correlate with the material, the age, and the dirtiness of tubes and particle filters (Nordbo et al., 2014). The inverse Laplace transform for Eq. 5.28 gives the impulse response to the system $h(\tau)$

$$h(\tau) = \frac{\exp\left(\frac{1}{2\mu^2}\right)}{\mu\sqrt{\pi}} \times \int_0^\tau \frac{\exp\left[-\frac{1}{4\mu^2}\left(\frac{z}{1}+\frac{1}{z}\right)\right]F(z,\tau-z)}{z^{3/2}}\,\mathrm{d}z \tag{5.29}$$

The function F and a detailed account of this solution are provided in (Kekäläinen et al. (2011), Eq. 65)

5.2.4 System response parameter estimation

As discussed earlier, the parameters for the system frequency response are often unavailable and need to be estimated from the data. The magnitude squared of the response function can be found from Eq. 5.6 to be the ratio of the attenuated spectrum to the true spectrum

$$|H|^2 = \frac{|C_m|^2}{|C|^2} \tag{5.30}$$

In practice, the true spectrum is not known and is substituted with that of another scalar, based on the assumption of spectral similarity. The spectra typically used for parameter estimation are long-term averaged spectra chosen during favorable atmospheric conditions. Therefore, this use is rather valid and different from using the spectral similarity hypothesis for estimating the loss on the short scale of averaging intervals.

Once $|H|^2$ is known, the filter parameters can be estimated using non-linear regression (Ibrom et al., 2007; Fratini et al., 2012; Nordbo et al., 2014). The use of the cospectra to estimate $|H|$ or $|H|^2$ e.g. (Aubinet et al., 1999, 2001; Mammarella et al., 2009) will create biased estimates due to the effect of the phase shift as can be seen from Eq. 5.10.

In the presence of noise, the measured spectra contain the spectra of the noise. The measured spectrum of noisy signal $|C_m|^2$ can be written as

$$|C_m|^2 = |C + \mathscr{E}|^2 = |C|^2 + |\mathscr{E}|^2 + 2\Re[C\mathscr{E}^*] \tag{5.31}$$

Here, the measured spectrum $|C_m|^2$ is the sum of the true spectrum $|C_m|^2$, the noise spectrum $|\mathscr{E}|^2$, and a correlation term between the noise and the signal $2\Re[C\mathscr{E}^*]$. The correlation term will converge to its expected value of zero given an additive uncorrelated noise. Therefore, the noise spectra can be subtracted from the measured spectra prior to fitting. A discussion of the effect of noise on model parameter estimation is provided in (Aslan et al., 2021).

5.3 Methods

5.3.1 Numerical simulation

The simulation aims to estimate the extent of the problems that can be potentially addressed with the Wiener deconvolution method. This goal is realized by analyzing the sensitivity of the corrected flux to the individual and the combined effects of three related issues that are intrinsic to conventional methods i) inappropriate system response, ii) the contribution of the non-linear phase to the attenuated flux, and iii) the consequences of the spectral similarity assumption. The simulation is limited to the common practices that are believed to contribute most to biases and uncertainties in the corrected fluxes. It does not aim to provide a comprehensive evaluation of all variations of EC spectral correction methods.

Starting from a high-frequency dataset of EC measurements, two models for attenuation were considered: i) a first-order low pass filter similar to Eq. 5.25 commonly used in EC literature (hereafter referred to as RC), and ii) a physical process-based model for sorbing scalars shown in Eq. 5.28. Both filters were discretized using the bilinear transform and applied to each averaging interval in the frequency

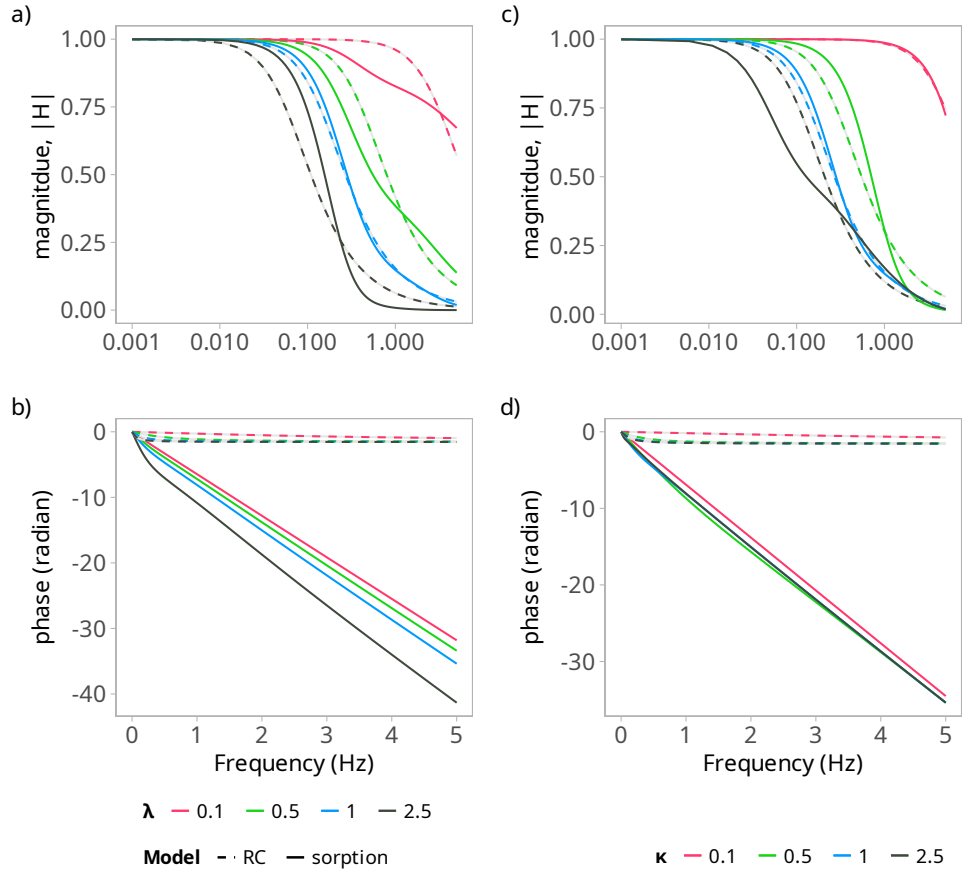

Figure 5.1: Bode plot showing the magnitude and phase response functions of the sorption model in Eq. 5.28 (solid line) and a matching RC filter (dashed line) that approximates its magnitude response for a range of parameters. The phase is unwrapped, and the x-axis is log-transformed. The parameter μ was used as a fixed parameter for both plots ($\mu = 10^{-3}$). a) and b) fixed values of κ, $\kappa = 1$ and 4 values of λ shown in colors. c) and d) fixed values of λ: $\lambda = 1$ and 4 values of κ shown in colors

domain, similar to Eq. 5.7. The process was repeated by varying the filter parameters to cover a range of values that are similar to field conditions relevant to eddy covariance setups. For each combination of the sorption model parameters, a matching RC filter that approximates its magnitude response was considered. The time constant τ of the RC filter was estimated using non-linear least squares, such that it minimizes the mean square error between the magnitude response of the RC filter and the sorption model.Both of these models are shown in Fig. 5.1 for a few selected parameters.

In addition to direct convolution, the attenuation was also applied by multiplying the cospectra by the magnitude response of the filter without considering the phase contribution similar to the approach used in (Moore, 1986; Fratini et al., 2012; Nordbo et al., 2014). The attenuated flux in this approach is calculated as

$$\overline{w'c'}_{no.\phi} = \int_{\omega_0}^{\omega_n} Co_{wc} \cdot |H| \mathrm{d}\omega \tag{5.32}$$

The results of the two different attenuation methods were evaluated by computing correction factors for all the scalars using three strategies that are analogous to the ways conventional methods are applied: i) F_{comp}, which is the ratio of the true flux to the attenuated flux, ii) F_{tl}, which is the correction factor obtained after removing the introduced time lag in the attenuated flux by covariance maximization, and iii) $F_{no.\phi}$, which is the correction factor of fluxes that were attenuated without the phase response using Eq. 5.32. The investigation of the three issues proceeded as follows

1. Inappropriate response function: The use of the RC filter to model the response of the attenuation process is prevalent in the EC literature. The consequences of this simplifying assumption were investigated for the range of parameters of the sorption model. Scalars were attenuated using both the sorption model and the RC filter. The ratios of the attenuated fluxes were compared with and without the correction for time lag, using F_{comp} and F_{tl}, respectively.

2. Contribution of the non-linear phase: As discussed in the theory section, time lag correction can only account for the contribution of the linear phase to the attenuation. Here, the contribution of the non-linear phase is investigated for both the RC and the sorption filters by comparing the attenuated flux with no phase $F_{no.\phi}$ to the time lag corrected attenuated flux F_{tl}. The difference between the two is considered the non-linear phase contribution.

3. Consequences of spectral similarity assumption: The assumption of spectral similarity is used in all empirical methods. The systematic bias and uncertainty due to this assumption were investigated by comparing the attenuated fluxes of sonic temperature and the scalar under examination using both the RC and the sorption filters.

The interactions between these three issues were explored using three restoration strategies closely imitating conventional empirical methods.

- $R_{no.\phi}$ restoration strategy: This strategy involves removing the time lag of the attenuated scalar through covariance maximization, followed by correcting the flux using the correction factor obtained from simulating the attenuation on sensible heat flux while ignoring the phase $F_{no.\phi}$. This strategy assumes that the effect of phase shift is eliminated by time lag correction, and therefore simulates the attenuation using Eq. 5.32. A similar approach can be found in (Fratini et al., 2012; Nordbo et al., 2014). The strategy $R_{no.\phi}$ is prone to biases arising from spectral similarity assumption and the non-linear phase contributions on the restored fluxes.

- R_{comp}: In this strategy, the correction factor F_{comp} of sensible heat flux is used to correct the attenuated flux without correcting for phase shift. The R_{comp} strategy is prone to biases from the combination of spectral similarity, linear phase, and non-linear phase to scalar attenuation. This strategy is not commonly used and is included only to facilitate the comparison of the combined attenuation effect.

- R_{tl}: In this strategy, time lag removal by covariance maximization is applied to both the attenuated scalar and the simulated attenuation on sensible heat flux. Then, the correction factor F_{tl} of sensible heat flux is used to correct the time-lag corrected attenuated flux. This approach is similar to the one employed by (Goulden et al., 1997)

These correction strategies cover most of the varieties of empirical spectral correction methods. However, certain variants were not included, such as the evaluation with $|H|^2$, as well as methods that depend entirely on parametrization (e.g. (Ibrom et al., 2007)). This is because these variants could introduce additional uncertainty to the evaluation.

High-frequency dataset

A high-frequency EC dataset was used as an input for the simulation. Measurements were taken over an ideal flat agricultural field of the Thünen Institute, located at 52.297 N, 10.449 E in Braunschweig, Germany. A complete description of the site and instrumentation is available elsewhere (Emad and Siebicke, 2023). Data used for the simulation spanned 10 days from 15 June 2020 until 26 June 2020 and comprised 512 30-minute averaging intervals. The variables used in the simulation were the three-dimensional wind velocity components measured using a sonic anemometer (uSonic-3 Class A, Metek GmbH, Germany) and gas concentration measurements of CO_2 and H_2O obtained from an open-path infra-red gas analyzer (LI-7500A, LI-COR Biosciences GmbH, Germany).

The raw data were prepared for the simulation by applying common statistical screening for data quality issues (Vickers and Mahrt, 1997). The initial time lag between the wind and the scalar time series was compensated using covariance maximization. The wind coordinates were rotated using the planar fit method (Wilczak et al., 2001), and any remaining residual $\bar{w}$ was removed.

Simulation parameters

The parameters adopted for the sorption model were based on empirically determined parameters from experimental data and are considered typical for closed-path eddy covariance setups (Nordbo et al., 2014). The parameter μ was set at a fixed value, $\mu = 0.001$ since its value was found to have a minor effect on the shape of the spectrum within its reasonable range compared to λ and κ. The range of values considered for λ and κ was from 10^{-5} to 2.5 for both parameters. The tube length considered was fixed at $L = 1$ m, and the flow velocity was set to $v = 1$ m s^{-1}. The simulation covered a total of 5000 treatments.

Simulation results quality control

Fluxes were calculated for 30-min averaging intervals. Then, quality checks were applied to computed fluxes and simulation results. Averaging intervals with low developed turbulence, low u^*, and low fluxes of CO_2, sensible and latent heat were excluded from the analysis similar to typical quality checks

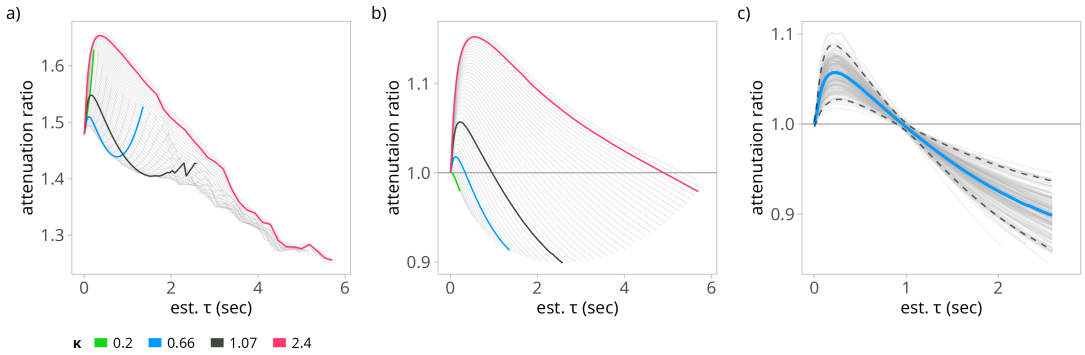

Figure 5.2: Ratio of CO_2 fluxes attenuated using a process-based sorption model to the same fluxes attenuated using its matching RC filter averaged across the whole dataset. Colors highlight chosen representative values of the parameter κ, gray lines in a) and b) are the different values of κ and in c) the individual averaging intervals. a) Attenuation ratios without any treatment to the phase shift, large attenuation ratios are seen due to the stronger phase shift of the sorption model. b) Attenuation ratios after correcting the linear phase shift by covariance maximization. c) Attenuation ratios for a fixed value of κ, $\kappa = 1.07$, showing the variability of response of individual averaging intervals to the attenuation by the two models and the mean attenuation ratio (blue line), dashed lines represent the mean ± 2SD

of EC fluxes and spectra (Sabbatini et al., 2018). After quality checks, 34% of high-quality averaging intervals remained for the final evaluation. Additionally, for simulation treatments that required time lag optimization, unrealistic estimated time lags that produced spurious correlations were eliminated.

5.4 Simulation results

The simulation results are limited to fairly ideal conditions and high-quality fluxes. The input data were taken from a flat site where the variability of spectra is not expected to be very high. Furthermore, moderate simulation parameters were chosen for the sorption model. In particular, the ratio of the tube length to flow velocity was set to 1. Finally, the quality checks employed left only very well-behaved periods to be considered in the evaluation. Therefore, we note that the estimates obtained from the simulation strictly relate to the current conditions and are expected to vary for other scalars and sites, with more complex sites likely giving more variable results.

5.4.1 Inappropriate response function

Using an RC filter to model the response of the sorption process introduces systematic bias to the fluxes. If the filter-induced time lag is not corrected, the sorption filter will always attenuate the signal more than its approximated RC counterpart (Fig. 5.2a). This is not surprising as the time lag caused by the strong phase shift of the sorption filter will lead to the degradation of the covariance. On average the attenuation caused by the sorption model was 1.3 to 1.7 times higher compared to the RC low pass filter.

Correcting the linear phase shift by time lag optimization reduces the attenuation ratio considerably (Fig. 5.2b). However, the remaining effects of the non-linear phase shift and the differences in the filter's magnitude response lead to a systematic bias reaching up to 15% of the recovered fluxes in either direction (underestimation or overestimation). The magnitude and direction of the bias are mainly

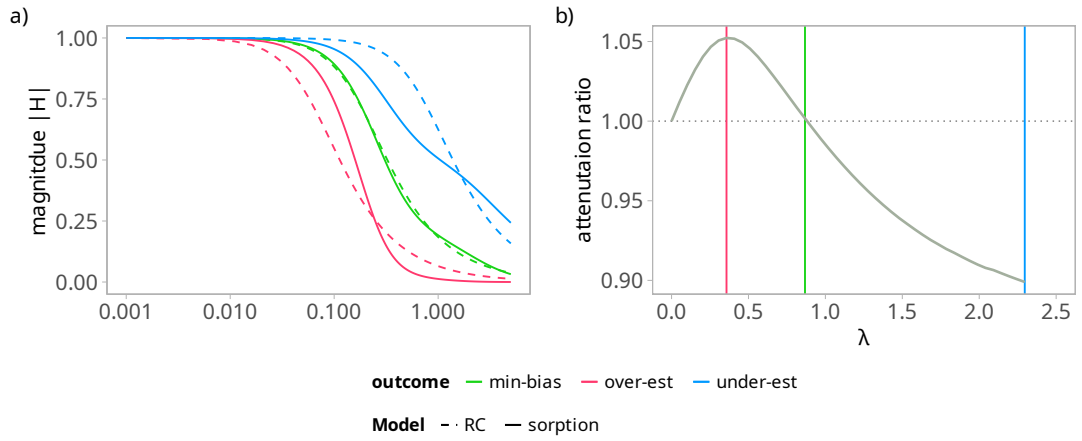

Figure 5.3: The effect of the filter magnitude response on the attenuation ratio outcome after correcting the effect of linear phase shift. a) Magnitude responses of the sorption model (solid lines) and the RC filter approximating its response (dashed) for three values of λ and a fixed value of κ, $\kappa = 1.02$ that represent three possible outcomes: **over-est**: the RC filter is causing stronger attenuation to the flux ($\lambda = 0.36$). **under-est**: the sorption filter is causing stronger attenuation to the flux ($\lambda = 2.3$). **min-bias**: minimum bias between the sorption and the RC filter ($\lambda = 0.86$). b) Ratio of attenuated CO_2 fluxes using a process-based sorption model to fluxes attenuated using a matching RC filter

controlled by the shape of the filter's magnitude response. The inability of the RC filter to accurately approximate the shape of the sorption filter leads to uneven attenuation at different frequencies. The mismatch between the two filters is manifested by two features (Fig. 5.3). The first feature is the different steepness of the two filters (roll-off) as seen from the "over-est" scenario, here the RC filter is causing stronger attenuation due to having a slower roll-off (less steep). The importance of the filter's roll-off in the attenuation is due to the unequal distribution of energy in the spectra of turbulence. The second feature is the dip in the magnitude response of the sorption filter observed around the 0.1 Hz frequency in the treatment "under-est". The dip is not possible to emulate using the simple RC filter and its position is controlled by the model parameters κ and λ (Nordbo et al., 2014).

The observed spread for individual averaging intervals around the mean is shown for one set of parameters in (Fig. 5.2c). The spread translates to increased random uncertainty in the restored fluxes and is mainly driven by the variability in the distribution of spectral energy within different averaging intervals. The spread shows dependence on the discrepancy between the RC and the sorption filter, therefore the largest bias is accompanied by the largest variability.

5.4.2 Phase non-linearity

The contribution of the non-linear phase to the attenuation of the fluxes can reach up to 5% of the flux for both the RC filter and sorption filters (Fig. 5.4). The average non-linear phase contribution shows an increase with increased attenuation. This non-linear contribution was considered as the difference between the attenuated fluxes using cospectra adjustment without a phase to the attenuated flux after removing time lag using covariance maximization. This procedure assumes that the time lag correction will remove the effects of the linear phase. The mechanism by which the non-linear phase shift contributes to the attenuation is by causing different phase shifts to different frequency components of the signal. The net effect on the time series of the scalar is a nonuniform distortion

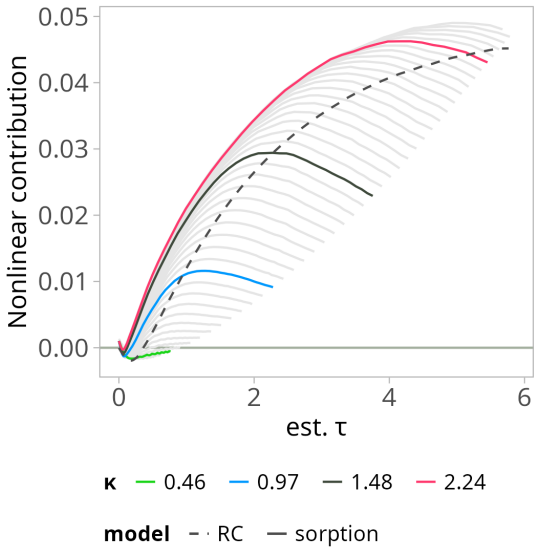

Figure 5.4: Contribution of the non-linear phase to the attenuated fluxes over a range of model parameters averaged over the whole dataset. Lines represent different values of the parameter κ with a focus on four chosen values distinguished in colors. Line shape represents the filter type. Solid lines are the sorption filter and the dashed line is the matching RC filter for each parameter combination.

that is more likely to reduce the correlation between w and c. The correlation loss can not be corrected by digitally shifting the time series. Conversely, it will likely reduce the effectiveness of the time lag correction procedure.

5.4.3 Limitations of spectral similarity

The assumption of spectral similarity introduced a small averaged systematic bias of up to 3% of the corrected fluxes if other aspects of the correction were treated optimally. However, a larger increase was observed in the uncertainty of the corrected fluxes. The standard deviation of restored fluxes increased up to 10% of the flux value (Fig. 5.5). The observed systematic bias is likely caused by the slight differences between the averaged spectra shapes as well as the differences in individual averaging intervals spectra (Fig. 5.6). The variability in the spectra from one averaging interval to another is not uniform across frequencies and different scalars (Fig. 5.6b). The observed variability in the outcome of the applied filter to different scalars showed a very weak dependence on wind speed and stability classes. While the wind speed and stability explain part of the variability of the spectra, large variability remained after controlling for wind speed and stability (not shown). This variability is potentially due to the distributions of sources and sinks in addition to buoyancy in the case of sonic temperature.

5.4.4 Combined effects on the corrected fluxes

All three conventional methods for restoring the fluxes introduced varying degrees of systematic bias and increased uncertainty to the recovered fluxes (Fig. 5.7 and 5.8). With regard to systematic bias, the strategy $R_{no.\phi}$ was by far the worst performer when using either the RC or the sorption filter, followed by R_{comp}, then R_{tl}. The same dynamics are observed when using an RC filter to model the sorption process but with much larger biases.

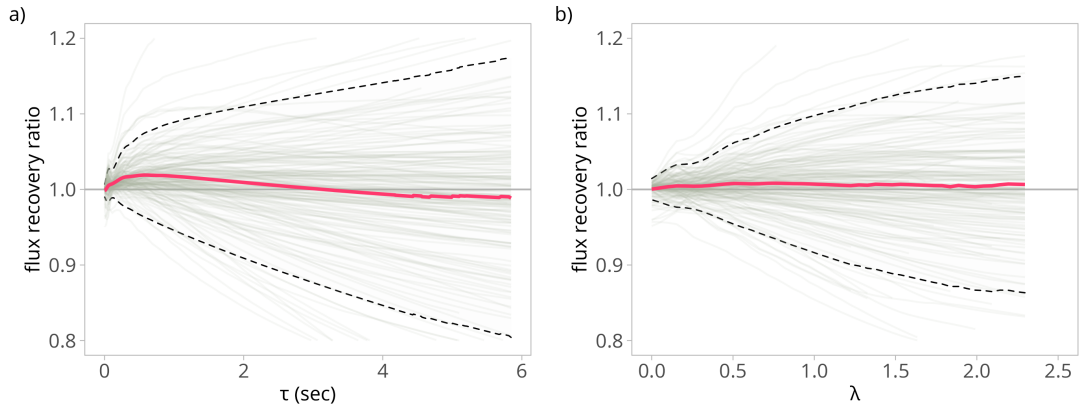

Figure 5.5: Effects of the assumption of spectral similarity on restored fluxes in conventional method. Ratio of recovered to attenuated flux when a correction factor obtained by simulating the attenuation effect on sonic temperature is used to correct CO_2 fluxes attenuated with the same filter a) if an RC filter is used. b) if the sorption filter is used ($\kappa = 1.83$). Gray lines show the recovery ratio for individual averaging periods, red line is the mean for the whole dataset, and the dashed lines represent the mean ± 2 SD

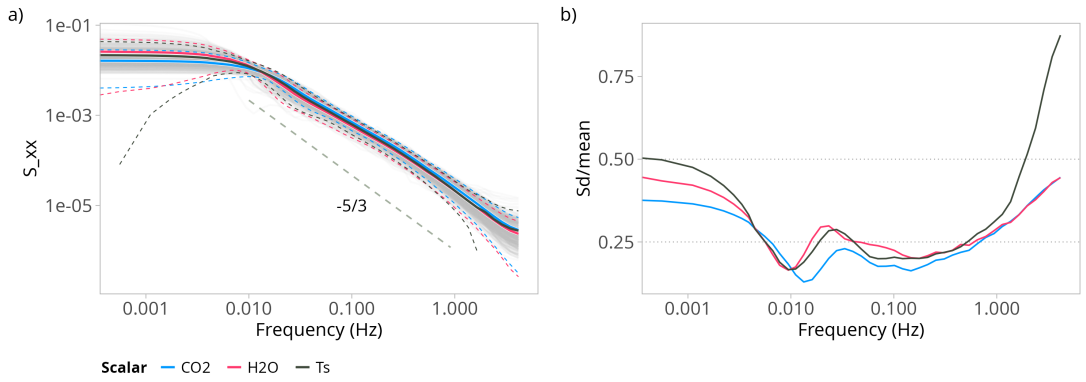

Figure 5.6: a) Spectra of three scalars: CO_2, H_2O, and Ts demonstrating spectral similarity of averaged spectra. Gray lines show spectra from individual averaging periods, dashed lines represent the mean ± 2 SD. b) Variability of the spectra across frequencies, calculated as the ratio of the standard deviation to the mean for binned frequencies ($n = 176$).

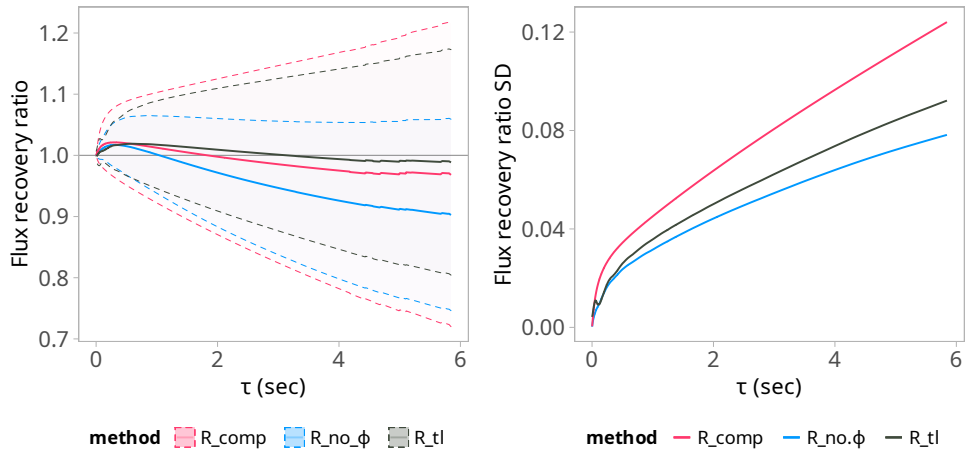

Figure 5.7: Combined effects of phase contributions and the similarity assumption on the recovered fluxes when using an RC model for attenuation and recovery. Three conventional correction strategies are shown where the attenuated scalar is corrected by simulating the attenuation on sensible heat flux. R_{comp} the attenuation is simulated as convolution (magnitude and phase). $R_{no.\phi}$ assumes the phase shift is corrected by time lag correction and simulates the attenuation on the cospectra without a phase shift. R_{tl} attenuation is simulated as convolution but linear phase shift is corrected separately by covariance maximization. a) Solid lines represent the mean systematic bias averaged for the whole dataset. Dashed lines show the variability in restored fluxes represented as the mean ± 2 SD. b) Variability in restored fluxes for individual averaging intervals shown as the standard deviation of the recovery ratios.

These results can be understood by considering the three attenuation sources: the damping of the spectra due to the filter's magnitude, the attenuation due to the linear phase shift, and the attenuation due to the non-linear phase shift. The different responses to these attenuation sources between the sonic temperature and the scalar as well as whether a correction method accounts for one or more attenuation sources are what drive the observed biases and uncertainties. $R_{no.phi}$ is applied to the time lag corrected fluxes and only corrects the attenuation attributed to the magnitude of the cospectra while ignoring the contribution of the non-linear phase. Thus, correcting the attenuated flux (that still has the additional attenuation of the non-linear phase) using $R_{no.phi}$ will introduce the largest bias. This is still valid, even though no phase similarity between Ts, and CO_2 was observed, potentially because accounting for the non-linear phase reduces the systematic bias by randomizing the systematic error leading to increased variability in the result, as seen in Fig.5.7.

However, including the linear phase in the correction factor does not improve the recovery as evident by the better performance of the R_{tl} strategy. Accounting for both linear and non-linear components of the phase with R_{comp} has inferior performance compared to accounting for the non-linear phase and removing the effect of the linear phase using time lag correction in the R_{tl} strategy. The reason is likely the difference in the contribution of the linear phase between sonic temperature and the scalar, thus it is better to remove them separately rather than including them in the correction.

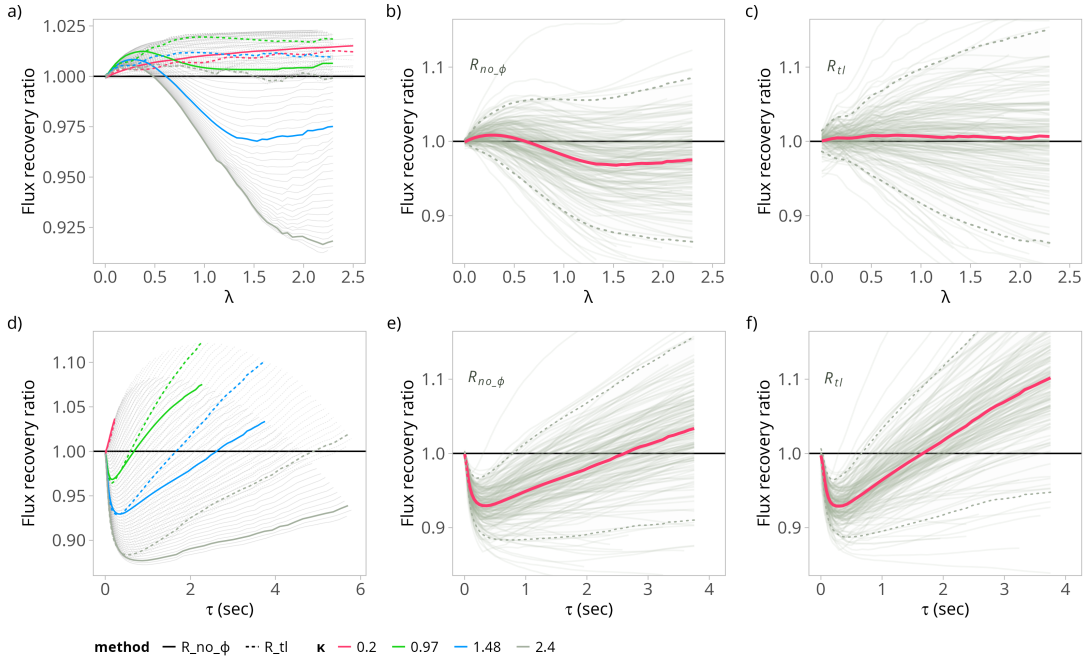

Figure 5.8: Combined effects of phase contributions, spectral similarity assumption, and the use of a simplifying model on the recovery of fluxes attenuated with a sorption model. Two conventional correction strategies are shown where the attenuated scalar is corrected by simulating the attenuation on sensible heat flux. Each of the two methods is evaluated in the case of using the correct sorption model for simulating the loss (first row) and when a simplifying RC filter is used (second row). $R_{no.\phi}$ assumes the phase shift is corrected by time lag correction and simulates the attenuation on the cospectra without a phase shift. R_{tl} attenuation is simulated as convolution but linear phase shift is corrected separately by covariance maximization. a) Using a sorption filter for correction. b) Using a simplifying RC filter for correction. Lines represent the mean systematic bias averaged for the whole dataset. Line shapes represent the method used, solid lines for $R_{no.\phi}$ and dashed for R_{tl}. b) and c) Variability in restored fluxes for individual averaging intervals for $R_{no.\phi}$ and R_{tl} respectively. e) and f) Variability in restored fluxes for individual averaging intervals for $R_{no.\phi}$ and R_{tl} respectively

5.5 Discussion

5.5.1 Limitations of conventional spectral correction methods

The analysis presented in this paper demonstrates that both analytical and empirical conventional spectral correction methods have inherent shortcomings due to the inadequate representation of the true cospectra, the inappropriate simplified models, and ignoring the nonlinear phase effects. Consequently, these methods are likely to produce unreliable approximations for flux corrections.

To examine the limits of conventional analytical correction methods, we formulated in Eq. 5.11 an accurate cospectral transfer function that does not assume a specific shape of the attenuation filter. The equation shows that the use of a cospectral transfer function for estimating the attenuation requires the knowledge of the phase shift between c and w represented by the phase spectrum, $\angle Cr_{cw}$ and the phase shift introduced by the attenuation filter. The phase spectra have no available models, unlike the spectra, and are not expected to be similar among different scalars. The equation suggests that the commonly used $|H|$ is only correct if the filter has no phase shift, an unachievable condition for causal physical processes (Smith, 2007). Alternatively, $|H|$ can be used if time lag correction eliminates the impact of the phase shift. However, as explained in the theory section, shifting the time series can only effectively correct constant group delay that is caused by a linear phase shift. In nearly all practical scenarios, the phase is non-linear, and the remaining non-linear phase distortion will lead to biased corrected flux. This occurs because a non-linear phase will shift the individual frequency components of the cospectrum at varying rates and thus will change the signal in a way that cannot be predicted solely from the spectrum. This generally supports the recommendation of using $|H|$ after time lag correction (Peltola et al., 2021). However, this approach is a first-order approximation and is not exact. For similar reasoning, estimating $|H|$ as the ratio of attenuated to ideal cospectra is considered an approximation.

In addition to the incomplete representation the phase distortion, the use of modeled spectra and cospectra in the analytical method is likely to increase the uncertainty and systematic biases in corrected fluxes. This is because these models are generally simplistic and fail to capture the variability of the cospectral shapes across time and site-specific conditions.

Empirical methods face similar challenges related to the accuracy of the ideal spectrum and the models of the attenuation filter. However, a key difference is that instead of simulating the attenuation on a model spectrum, empirical methods assume that the ideal spectrum originates from another scalar, based on the assumption of spectral similarity.

The extent of these issues on empirical methods was investigated in a numerical simulation. The results revealed that the largest systematic biases arose from the use of simplified response functions, followed by ignoring the non-linear contribution of the phase shift, and finally, from assuming spectral similarity on the scale of averaging intervals. When combined, these effects can lead to more than 10% systematic bias in the corrected fluxes even for small filter time constants, as demonstrated by the correction strategy $R_{no.\phi}$ (Fig. 5.8, d). Many EC flux correction methods, including the widely used in-situ methods (Ibrom et al., 2007; Fratini et al., 2014), adopt a similar approach and are expected to produce similar systematic biases when applied to correct water vapor fluxes in closed-path EC systems. The use of spectral similarity assumption has been found to increase the uncertainty in restored fluxes, in general this increase depended on the magnitude of the attenuation and reached values of more than 10% (1 SD).

In summary, the limitations of conventional methods result from the incomplete representation of the transfer function, the use of inappropriate response functions, and the reliance on indirect simulation of the attenuation on a proxy scalar or model cospectra rather than directly correcting the signal.

5.5.2 Signal restoration using the Wiener deconvolution method

The current study demonstrated that the Wiener deconvolution method is an optimal solution to restore attenuated signals of atmospheric scalars. The Wiener deconvolution method offers the best estimate of the original signal from noisy measurements by minimizing the mean squared error between the true and the measured signals. As a direct method, the Wiener deconvolution avoids many of the shortcomings in conventional methods that arise from the assumption of an ideal cospectrum or spectral similarity and brings many advantages for flux calculation. Unlike conventional methods that are often limited by atmospheric conditions that influence the ideal cospectrum, the performance of the Wiener deconvolution method is not dependent on the properties of the input signal once the attenuation model parameters have been estimated. Additionally, the direct restoration of the scalar signal in Wiener deconvolution allows for obtaining corrected statistics of the original scalar, such as variance and the integral time scale. Furthermore, the Wiener deconvolution completely corrects the phase distortions, making it independent from time lag correction procedures that may still be applied after signal estimation to correct for time lag introduced by sources other than the system response.

The successful application of Wiener deconvolution requires meeting three criteria: (i) knowledge of the system frequency response function, (ii) the response function must be linear and time-invariant, and (ii) the knowledge of the mean signal-to-noise ratio spectrum. The knowledge of the system's frequency response function requires modeling the physical process leading to the attenuation. While models for certain processes are available, such as the sorption model shown earlier, other causes of attenuation might not have readily available models. The analytical models developed for conventional methods, such as line averaging and sensor separation, are good candidates for use with the Wiener deconvolution method. In this regard, the Wiener deconvolution method offers a chance to unify analytical and in-situ methods where physics-based models are applied to the observed spectrum instead of the modeled one.

Once the frequency response function is known, it needs to satisfy the conditions of linearity and time invariance. These assumptions are not specific to the Wiener deconvolution method, although they are not stated explicitly for conventional methods, they are implied by expressing the spectral attenuation as convolution e.g. (Moore, 1986; Massman and Clement, 2005). Linearity implies that for a linear combination of inputs, the system produces a linear combination of outputs. This idealization is rarely met by physical systems. However, in most cases, the response function can be assumed to be linear or approximated as such without significant error. The assumption of time invariance means that the system's output does not depend on the time the filter is applied. Time invariance is not always guaranteed, as demonstrated by the sorption model shown earlier, where the model parameters λ and κ are dependent on relative humidity, which can vary during the averaging interval when the correction is applied. The violation of time invariance will lead to biases in the restored signal. This issue can be mitigated by applying the correction over shorter intervals where the model parameters are assumed to be constant. However, there is a limit on how fine the time resolution can be as the signal can not be sharply defined in both time and frequency domains (Gabor limit) (Downey, 2016). The application of the Wiener deconvolution method also requires finding the signal-to-noise (SNR) spectrum, which requires the knowledge of the power spectral density of the signal before attenuation. This information is usually unavailable. However, knowledge of the approximate power spectral density of the true signal

is usually sufficient. For atmospheric scalars, the ensemble average of the sonic temperature spectra or the modeled spectra of Kaimal et al. (1976) should be sufficient for most cases. The SNR spectrum is used to suppress the noise in the restored signal by balancing the trade-off between amplifying the signal and suppressing the noise. An imperfect SNR spectrum may result in noisier estimates, but is unlikely to introduce systematic errors to the restored fluxes. The noise behavior of the sensor can be statistically estimated from instrument measurements if not known beforehand. For instance, experiments can be performed to measure the variance of a measured signal of known concentration in the case of gas analyzers. In cases where experimentation is not feasible and the noise is assumed to be white, the noise spectrum can be estimated by extrapolating the slope in the inertial subrange to zero and attributing the remaining measured power at the higher range of the spectrum to the noise.

5.5.3 Limits of signal recovery

The recovery of attenuated frequencies is only possible if attenuated frequencies do not fall below the detection limit of the measurement apparatus. If any frequency components are attenuated to zero or below the noise level, the information is lost and can not be recovered. In such a case, the contribution of the lost frequencies to flux must be estimated using a different source of information, which will likely increase the flux uncertainty. Therefore, the conditions that result in the elimination of frequencies should be avoided by adjusting the system design and operation. For example, in the case of water vapor in tubes, the response function can be solved for the lowest magnitude resolvable by the measuring device to determine safe thresholds for controllable parameters such as tube length and flow rate.

5.6 Conclusions

Reliable estimates of the atmospheric exchange require an optimal recovery of attenuated fluxes due to signal frequency losses. The analysis in this paper showed that conventional spectral correction methods introduce systematic biases and increased random uncertainty to the corrected fluxes. These biases and increased uncertainty are due to using simplified response functions, ignoring the contribution of non-linear phase shift, and the assumptions of spectral similarity and model spectra. A new approach based on Wiener deconvolution was shown to be an optimal solution to directly restore attenuated signals without relying on the assumptions of spectral similarity for individual averaging intervals. The Wiener deconvolution approach has wide applications for micrometeorological methods where an ideal spectrum can not be assumed or when the spectrum is distorted due to aliasing, such as in the case of eddy accumulation methods (Emad and Siebicke, 2023), flux profile measurements (Kaimal, 1986), and disjunct eddy covariance method (Rinne and Ammann, 2012; Hill et al., 2017).

More research is currently underway to evaluate the impact of using the Wiener deconvolution method for a larger dataset covering multiple sites on yearly flux estimates and energy balance budget, and to compare it against conventional spectral correction methods.

Table 5.1: Symbols and definitions

Symbols	
S_{cc}	Spectrum of the scalar c
$C(\omega)$	Fourier transform of the scalar c
ω	Angular frequency in rad $s^{-}1$
σ_c^2	Variance of the scalar c
Cr_{wc}	Cross-spectrum of the two variables, w and c
Co_{wc}	Cospectrum of the two variables, w and c
$\angle C(\omega)$	Phase spectrum of C
Q_{wc}	Quadrature spectrum of the two variables, w and c
$R_{wc}(r_1)$	Auto covariance function of w and c
$\Re(C)$	Real component of the complex variable C
$[C]^*$	Complex conjugate of C
$h(t)$	Impulse response function in the time domain
$H(\omega)$	Complex frequency response function
$\lvert H(\omega)\rvert$	Magnitude response function
$\lvert H(\omega)\rvert^2$	Magnitude response squared
c	Molar density of a scalar mol m^{-3}
w	Vertical wind velocity m s^{-1}
τ	Time constant in seconds
λ	A dimensionless parameter related to the area of the tube wall available for condensation in the sorption model
κ	A dimensionless parameter related to the length scale of the diffusive evaporation process in the sorption model
μ	A dimensionless parameter related to molecular diffusion and Taylor dispersion in tube flow in the sorption model

Appendix 1: List of symbols

Acknowledgements. The author would like to thank Lukas Siebicke and Alexander Knohl for their encouragement, advice, and helpful discussions during the preparation of this manuscript, and for reading and commenting on the manuscript. Thanks also to Justus van Ramshorst for reading and commenting on the manuscript.

Financial support. This study received partial financial support from the Ministry of Lower-Saxony for Science and Culture (MWK), by the European Research Council under the European Union's Horizon 2020 research and innovation programme (grant agreement no. 682512 - OXYFLUX), and by the Deutsche Forschungsgemeinschaft (INST 186/1118-1 FUGG).

Bibliography

Ammann, C., Brunner, A., Spirig, C., and Neftel, A.: Technical Note: Water Vapour Concentration and Flux Measurements with PTR-MS, Atmospheric Chemistry and Physics, 6, 4643–4651, doi:10.5194/acp-6-4643-2006, 2006.

Aslan, T., Peltola, O., Ibrom, A., Nemitz, E., Rannik, Ü., and Mammarella, I.: The High-Frequency Response Correction of Eddy Covariance Fluxes – Part 2: An Experimental Approach for Analysing Noisy Measurements of Small Fluxes, Atmospheric Measurement Techniques, 14, 5089–5106, doi:10.5194/amt-14-5089-2021, 2021.

Aubinet, M., Grelle, A., Ibrom, A., Rannik, Ü., Moncrieff, J., Foken, T., Kowalski, A. S., Martin, P. H., Berbigier, P., Bernhofer, Ch., Clement, R., Elbers, J., Granier, A., Grünwald, T., Morgenstern, K., Pilegaard, K., Rebmann, C., Snijders, W., Valentini, R., and Vesala, T.: Estimates of the Annual Net Carbon and Water Exchange of Forests: The EUROFLUX Methodology, in: Advances in Ecological Research, edited by Fitter, A. H. and Raffaelli, D. G., vol. 30, pp. 113–175, Academic Press, doi:10.1016/S0065-2504(08)60018-5, 1999.

Aubinet, M., Chermanne, B., Vandenhaute, M., Longdoz, B., Yernaux, M., and Laitat, E.: Long Term Carbon Dioxide Exchange above a Mixed Forest in the Belgian Ardennes, Agricultural and Forest Meteorology, 108, 293–315, doi:10.1016/S0168-1923(01)00244-1, 2001.

Baldocchi, D.: Measuring Fluxes of Trace Gases and Energy between Ecosystems and the Atmosphere - the State and Future of the Eddy Covariance Method, Global Change Biology, 20, 3600–3609, doi:10.1111/gcb.12649, 2014.

Bartlett, M. S.: Smoothing Periodograms from Time-Series with Continuous Spectra, Nature, 161, 686–687, doi:10.1038/161686a0, 1948.

Berger, B. W., Davis, K. J., Yi, C., Bakwin, P. S., and Zhao, C. L.: Long-Term Carbon Dioxide Fluxes from a Very Tall Tower in a Northern Forest: Flux Measurement Methodology, Journal of Atmospheric and Oceanic Technology, 18, 529–542, doi:10.1175/1520-0426(2001)018<0529:LTCDFF>2.0.CO;2, 2001.

de Ligne, A., Heinesch, B., and Aubinet, M.: New Transfer Functions for Correcting Turbulent Water Vapour Fluxes, Boundary-Layer Meteorology, 137, 205–221, doi:10.1007/s10546-010-9525-9, 2010.

Downey, A.: Think DSP: Digital Signal Processing in Python, "O'Reilly Media, Inc.", 2016.

Emad, A.: Optimal Frequency-Response Corrections for Eddy Covariance Flux Measurements Using the Wiener Deconvolution Method, Boundary-Layer Meteorology, 188, 29–53, doi:10.1007/s10546-023-00799-w, 2023.

Emad, A. and Siebicke, L.: True Eddy Accumulation – Part 2: Theory and Experiment of the Short-Time Eddy Accumulation Method, Atmospheric Measurement Techniques, 16, 41–55, doi:10.5194/amt-16-41-2023, 2023.

Eugster, W. and Senn, W.: A Cospectral Correction Model for Measurement of Turbulent NO2 Flux, Boundary-Layer Meteorology, 74, 321–340, doi:10.1007/BF00712375, 1995.

Foken, T., Aubinet, M., and Leuning, R.: The Eddy Covariance Method, in: Eddy Covariance: A Practical Guide to Measurement and Data Analysis, edited by Aubinet, M., Vesala, T., and Papale, D., Springer Atmospheric Sciences, pp. 1–19, Springer Netherlands, Dordrecht, doi:10.1007/978-94-007-2351-1_1, 2012.

Fratini, G., Ibrom, A., Arriga, N., Burba, G., and Papale, D.: Relative Humidity Effects on Water Vapour Fluxes Measured with Closed-Path Eddy-Covariance Systems with Short Sampling Lines, Agricultural and Forest Meteorology, 165, 53–63, doi:10.1016/j.agrformet.2012.05.018, 2012.

Fratini, G., McDermitt, D. K., and Papale, D.: Eddy-Covariance Flux Errors Due to Biases in Gas Concentration Measurements: Origins, Quantification and Correction, Biogeosciences, 11, 1037–1051, doi:10.5194/bg-11-1037-2014, 2014.

Goulden, M., Munger, J., Fan, S., Daube, B. C., and Wofsy, S. C.: Exchange of Carbon Dioxide by a Deciduous Forest: Response to Interannual Climate Variability, Science, doi:10.1126/science.271.5255.1576, 1996a.

Goulden, M. L., Munger, J. W., Fan, S.-M., Daube, B. C., and Wofsy, S. C.: Measurements of Carbon Sequestration by Long-Term Eddy Covariance: Methods and a Critical Evaluation of Accuracy, Global Change Biology, 2, 169–182, doi:10.1111/j.1365-2486.1996.tb00070.x, 1996b.

Goulden, M. L., Daube, B. C., Fan, S.-M., Sutton, D. J., Bazzaz, A., Munger, J. W., and Wofsy, S. C.: Physiological Responses of a Black Spruce Forest to Weather, Journal of Geophysical Research: Atmospheres, 102, 28 987–28 996, doi:10.1029/97JD01111, 1997.

Hicks, B. B.: Propeller Anemometers as Sensors of Atmospheric Turbulence, Boundary-Layer Meteorology, 3, 214–228, doi:10.1007/BF02033920, 1972.

Hicks, B. B. and Baldocchi, D. D.: Measurement of Fluxes Over Land: Capabilities, Origins, and Remaining Challenges, Boundary-Layer Meteorology, 177, 365–394, doi:10.1007/s10546-020-00531-y, 2020.

Hill, T., Chocholek, M., and Clement, R.: The Case for Increasing the Statistical Power of Eddy Covariance Ecosystem Studies: Why, Where and How?, Global Change Biology, 23, 2154–2165, doi:10.1111/gcb.13547, 2017.

Horst, T. W.: A Simple Formula for Attenuation of Eddy Fluxes Measured with First-Order-Response Scalar Sensors, Boundary-Layer Meteorology, 82, 219–233, doi:10.1023/A:1000229130034, 1997.

Horst, T. W.: On Frequency Response Corrections for Eddy Covariance Flux Measurements, Boundary-Layer Meteorology, 94, 517–520, doi:10.1023/A:1002427517744, 2000.

Ibrom, A., Dellwik, E., Flyvbjerg, H., Jensen, N. O., and Pilegaard, K.: Strong Low-Pass Filtering Effects on Water Vapour Flux Measurements with Closed-Path Eddy Correlation Systems, Agricultural and Forest Meteorology, 147, 140–156, doi:10.1016/j.agrformet.2007.07.007, 2007.

Kaimal, J. C.: Flux and Profile Measurements from Towers in the Boundary Layer, in: Probing the Atmospheric Boundary Layer, edited by Lenschow, D. H., pp. 19–28, American Meteorological Society, Boston, MA, doi:10.1007/978-1-944970-14-7_3, 1986.

Kaimal, J. C. and Finnigan, J. J.: Atmospheric Boundary Layer Flows: Their Structure and Measurement, Oxford University Press, 1994.

Kaimal, J. C., Wyngaard, J. C., and Haugen, D. A.: Deriving Power Spectra from a Three-Component Sonic Anemometer, Journal of Applied Meteorology, 7, 827–837, doi:10.1175/1520-0450(1968)007<0827:DPSFAT>2.0.CO;2, 1968.

Kaimal, J. C., Wyngaard, J. C., Izumi, Y., and Coté, O. R.: Spectral Characteristics of Surface-Layer Turbulence, Quarterly Journal of the Royal Meteorological Society, 98, 563–589, doi:10.1002/qj.49709841707, 1972.

Kaimal, J. C., Wyngaard, J. C., Haugen, D. A., Coté, O. R., Izumi, Y., Caughey, S. J., and Readings, C. J.: Turbulence Structure in the Convective Boundary Layer, Journal of the Atmospheric Sciences, 33, 2152–2169, doi:10.1175/1520-0469(1976)033<2152:TSITCB>2.0.CO;2, 1976.

Kay, S.: Intuitive Probability and Random Processes Using MATLAB®, Springer US, doi:10.1007/b104645, 2006.

Kekäläinen, P., Voutilainen, M., Poteri, A., Hölttä, P., Hautojärvi, A., and Timonen, J.: Solutions to and Validation of Matrix-Diffusion Models, Transport in Porous Media, 87, 125–149, doi:10.1007/s11242-010-9672-y, 2011.

Kristensen, L. and Lenschow, D. H.: The Effect of Nonlinear Dynamic Sensor Response on Measured Means, Journal of Atmospheric and Oceanic Technology, 5, 34–43, doi:10.1175/1520-0426(1988)005<0034:TEONDS>2.0.CO;2, 1988.

Mamadou, O., Gourlez de la Motte, L., De Ligne, A., Heinesch, B., and Aubinet, M.: Sensitivity of the Annual Net Ecosystem Exchange to the Cospectral Model Used for High Frequency Loss Corrections at a Grazed Grassland Site, Agricultural and Forest Meteorology, 228–229, 360–369, doi:10.1016/j.agrformet.2016.06.008, 2016.

Mammarella, I., Launiainen, S., Gronholm, T., Keronen, P., Pumpanen, J., Rannik, Ü., and Vesala, T.: Relative Humidity Effect on the High-Frequency Attenuation of Water Vapor Flux Measured by a Closed-Path Eddy Covariance System, Journal of Atmospheric and Oceanic Technology, 26, 1856–1866, doi:10.1175/2009JTECHA1179.1, 2009.

Mandal, M. and Asif, A.: Continuous and Discrete Time Signals and Systems with CD-ROM, Cambridge University Press, 2007.

Massman, W. and Clement, R.: Uncertainty in Eddy Covariance Flux Estimates Resulting from Spectral Attenuation, in: Handbook of Micrometeorology: A Guide for Surface Flux Measurement and Analysis, edited by Lee, X., Massman, W., and Law, B., Atmospheric and Oceanographic Sciences Library, pp. 67–99, Springer Netherlands, Dordrecht, doi:10.1007/1-4020-2265-4_4, 2005.

Massman, W. J.: A Simple Method for Estimating Frequency Response Corrections for Eddy Covariance Systems, Agricultural and Forest Meteorology, 104, 185–198, doi:10.1016/S0168-1923(00)00164-7, 2000.

McBean, G. A.: Comparison of the Turbulent Transfer Processes near the Surface, Boundary-Layer Meteorology, 4, 265–274, doi:10.1007/BF02265237, 1973.

Meditch, J. S.: Stochastic Optimal Linear Estimation and Control, McGraw-Hill, 1969.

Miller, S. L. and Childers, D.: CHAPTER 10 - Power Spectral Density, in: Probability and Random Processes (Second Edition), edited by Miller, S. L. and Childers, D., pp. 429–471, Academic Press, Boston, doi:10.1016/B978-0-12-386981-4.50013-8, 2012.

Moore, C. J.: Frequency Response Corrections for Eddy Correlation Systems, Boundary-Layer Meteorology, 37, 17–35, doi:10.1007/BF00122754, 1986.

Nordbo, A. and Katul, G.: A Wavelet-Based Correction Method for Eddy-Covariance High-Frequency Losses in Scalar Concentration Measurements, Boundary-Layer Meteorology, 146, 81–102, doi:10.1007/s10546-012-9759-9, 2013.

Nordbo, A., Kekäläinen, P., Siivola, E., Lehto, R., Vesala, T., and Timonen, J.: Tube Transport of Water Vapor with Condensation and Desorption, Applied Physics Letters, 102, 194 101, doi:10.1063/1.4804639, 2013.

Nordbo, A., Kekäläinen, P., Siivola, E., Mammarella, I., Timonen, J., and Vesala, T.: Sorption-Caused Attenuation and Delay of Water Vapor Signals in Eddy-Covariance Sampling Tubes and Filters, Journal of Atmospheric and Oceanic Technology, 31, 2629–2649, doi:10.1175/JTECH-D-14-00056.1, 2014.

Ohtaki, E.: On the Similarity in Atmospheric Fluctuations of Carbon Dioxide, Water Vapor and Temperature over Vegetated Fields, Boundary-Layer Meteorology, 32, 25–37, doi:10.1007/BF00120712, 1985.

Peltola, O., Aslan, T., Ibrom, A., Nemitz, E., Rannik, Ü., and Mammarella, I.: The High-Frequency Response Correction of Eddy Covariance Fluxes – Part 1: An Experimental Approach and Its Interdependence with the Time-Lag Estimation, Atmospheric Measurement Techniques, 14, 5071–5088, doi:10.5194/amt-14-5071-2021, 2021.

Percival, D. B. and Walden, A. T.: Spectral Analysis for Physical Applications, Cambridge University Press, Cambridge, doi:10.1017/CBO9780511622762, 1993.

Polonik, P., Chan, W. S., Billesbach, D. P., Burba, G., Li, J., Nottrott, A., Bogoev, I., Conrad, B., and Biraud, S. C.: Comparison of Gas Analyzers for Eddy Covariance: Effects of Analyzer Type and Spectral Corrections on Fluxes, Agricultural and Forest Meteorology, 272–273, 128–142, doi:10.1016/j.agrformet.2019.02.010, 2019.

Reitz, O., Graf, A., Schmidt, M., Ketzler, G., and Leuchner, M.: Effects of Measurement Height and Low-Pass-Filtering Corrections on Eddy-Covariance Flux Measurements Over a Forest Clearing with Complex Vegetation, Boundary-Layer Meteorology, doi:10.1007/s10546-022-00700-1, 2022.

Rinne, J. and Ammann, C.: Disjunct Eddy Covariance Method, in: Eddy Covariance: A Practical Guide to Measurement and Data Analysis, edited by Aubinet, M., Vesala, T., and Papale, D., Springer Atmospheric Sciences, pp. 291–307, Springer Netherlands, Dordrecht, doi:10.1007/978-94-007-2351-1_10, 2012.

Sabbatini, S., Mammarella, I., Arriga, N., Fratini, G., Graf, A., Hörtnagl, L., Ibrom, A., Longdoz, B., Mauder, M., Merbold, L., Metzger, S., Montagnani, L., Pitacco, A., Rebmann, C., Sedlák, P., Šigut, L., Vitale, D., and Papale, D.: Eddy Covariance Raw Data Processing for CO2 and Energy Fluxes Calculation at ICOS Ecosystem Stations, International Agrophysics, 32, 495–515, doi:10.1515/intag-2017-0043, 2018.

Shaw, W. J., Spicer, C. W., and Kenny, D. V.: Eddy Correlation Fluxes of Trace Gases Using a Tandem Mass Spectrometer, Atmospheric Environment, 32, 2887–2898, doi:10.1016/S1352-2310(98)00036-3, 1998.

Silverman, B. A.: The Effect of Spatial Averaging on Spectrum Estimation, Journal of Applied Meteorology and Climatology, 7, 168–172, doi:10.1175/1520-0450(1968)007<0168:TEOSAO>2.0.CO;2, 1968.

Smith, J.: Introduction to Digital Filters with Audio Applications, W3K Publishing, 2007.

Stull, R. B.: An Introduction to Boundary Layer Meteorology, Atmospheric and Oceanographic Sciences Library, Springer Netherlands, doi:10.1007/978-94-009-3027-8, 1988.

Taylor, G. I.: The Dispersion of Matter in Turbulent Flow through a Pipe, Proceedings of the Royal Society of London. Series A. Mathematical and Physical Sciences, 223, 446–468, doi:10.1098/rspa.1954.0130, 1954.

Vickers, D. and Mahrt, L.: Quality Control and Flux Sampling Problems for Tower and Aircraft Data, Journal of Atmospheric and Oceanic Technology, 14, 512–526, doi:10.1175/1520-0426(1997)014<0512:QCAFSP>2.0.CO;2, 1997.

Wiener, N.: Extrapolation, Interpolation, and Smoothing of Stationary Time Series: With Engineering Applications, The MIT Press, Cambridge/Mass, 1964.

Wilczak, J. and Bedard, A.: A New Turbulence Microbarometer and Its Evaluation Using the Budget of Horizontal Heat Flux, Journal of Atmospheric and Oceanic Technology - J ATMOS OCEAN TECHNOL, 21, doi:10.1175/1520-0426(2004)021<1170:ANTMAI>2.0.CO;2, 2004.

Wilczak, J. M., Oncley, S. P., and Stage, S. A.: Sonic Anemometer Tilt Correction Algorithms, Boundary-Layer Meteorology, 99, 127–150, doi:10.1023/A:1018966204465, 2001.

Zhu, Z., Zhao, F., Voss, L., Xu, L., Sun, X., Yu, G., and Meixner, F. X.: The Effects of Different Calibration and Frequency Response Correction Methods on Eddy Covariance Ozone Flux Measured with a Dry Chemiluminescence Analyzer, Agricultural and Forest Meteorology, 213, 114–125, doi:10.1016/j.agrformet.2015.06.016, 2015.

6 Technical note: An integrated platform for near real-time flux data management and analysis

Abstract

Management and analysis of atmospheric flux data present a significant challenge. Besides the common challenges associated with big data such as volume, variety, and velocity, flux measurements require a sequence of specialized processing pipelines that involve complex and lengthy calculations and several quality tests to reach defensible flux estimates.

Here we describe an integrated platform that was developed within this thesis to manage, curate, process, and provide near real-time access to flux data and intermediate products. The platform combines open-source software and custom-built tools into a single integrated workflow. An open-source R package was developed to provide the core functionality of data management and processing.

The solution presented here was used to manage the flux data of the experiments conducted in this thesis. It enabled timely access to final calculated fluxes and all intermediate processing levels of the data which accelerated the development of the measurement systems and the analysis procedures.

6.1 Introduction

Recent decades have seen a rapid increase in the number of flux measurement sites. This was accompanied by an increase in the amount of data collected at these sites, the number of measured variables, and the complexity of the data processing pipelines (Hicks and Baldocchi, 2020). The management, analysis, representation, and communication of flux data have become a challenging task (Papale et al., 2012). Measurements of atmospheric quantities used to calculate and interpret fluxes share many of the challenges facing Big data. Atmospheric measurements are heterogeneous, usually have large volumes, and have varying degrees of uncertainty (veracity challenge). Furthermore, flux data are often used in multidisciplinary research projects that require the integration of data from multiple sources such as model outputs and satellite earth observation data. Therefore, maximizing the timely access to processed fluxes will increase the value and the effectivity of the data to the respective research communities.

As the number of flux data users is increasing, data interoperability and sharing have become more relevant questions. A standardized way of sharing, easy access and integration with other sources of

geospatial data is essential (Papale, 2020).

The goal here was to build a platform for flux data acquisition, analysis, quality control, archival, and presentation. Special focus is given to near real-time processing of the fluxes for early detection of problems and maximum usability. We first describe the design principles of such as system. Then, we describe the system architecture and the technical implementation. The platform makes the final calculated flux available within minutes and provides full access to the calculation history. The described system improves the accessibility of flux data and facilitates sharing and collaboration.

6.2 Design principles

The design of the analysis and data management platform was grounded in four principles that inspired the choice of technology and the system architecture: data traceability, quality control, interoperability, and maximizing accessibility. The chosen design principles are closely related to the principles of open science and data reusability (Wilkinson et al., 2016).

6.2.1 Data traceability

Traceability refers to the ability to trace the origin of the data and all the transformations the data went through. This ensures keeping relevant information accessible, such as the type and configuration of instruments, measurement sites, and the choice of processing steps.

Traceability can be extended beyond keeping records of metadata to a form of sensitivity analysis where the effect of every decision on flux processing can be traced. Final calculated fluxes are usually a result of a long and complex processing procedure that requires many steps. The choice of processing algorithms and their parameters at each step has an impact on the final result. Many of the calculation steps have a non-linear, sometimes unpredictable, outcome on the final fluxes under certain circumstances. Therefore, it is important to be able to trace the impact of each processing step to be able to differentiate whether certain features of the data are true physical signals or artifacts of certain processing steps.

Data traceability requires that the data and metadata are assigned a globally unique and persistent identifier. Metadata should be well described using a defined vocabulary, should be indexed and should be easily searchable.

6.2.2 Quality control

The quality of flux data is a key factor in the trustworthiness of the data and the final flux estimates. Data quality has multiple facets and is relevant to all stages of the flux data life cycle. Certain aspects of data quality can be guaranteed by the database design. For example by using integrity constraints to prevent redundancy and ensure data integrity.

Quality tests serve different purposes at each level of the data life cycle. At the collection and transport phase, quality checks ensure integrity, accuracy, and completeness of raw measurements. During analysis and interpretation, quality checks are used to identify and remove periods where the data is not suitable for analysis. For example, periods where the assumptions of the eddy covariance methods are violated or periods where the data is corrupted by instrument failures.

An automated rule-based system to flag data using a predefined set of quality flags is a convenient way to maintain high-quality data throughout collection and analysis. The rules should be defined in a human-readable format and should be easily modified and extended.

6.2.3 Interoperability

Interoperability means that the system can integrate data from multiple sources and provide access to the data in a variety of formats. Interoperability guarantees the communication and exchange of data between different components of the system or with different systems.

The choice of data formats and communication protocols are key elements to enable system-wide interoperability. Interoperability additionally can be extended to mean the ability of different systems to automatically interpret the information exchanged to produce a useful result.

To ensure interoperability, the system needs to have a well-defined vocabulary and use open standards.

6.2.4 Maximizing accessibility

Maximizing accessibility refers to simplifying and improving access to data throughout the different stages of the data life cycle. This includes making the data easily accessible to different components of the system and providing several ways to access and acquire data.

Visualization of the data using interactive dashboards is a quick way to access and explore final fluxes and raw measurements. It also provides a way to monitor the status of the measurement station in near real time.

Near real-time processing of the fluxes is an important aspect of maximizing data accessibility. By minimizing the time between data collection and access to the final flux, problems can be detected early and the data can be used for timely interpretation.

6.3 System architecture and implementation

The system architecture was chosen to be modular and flexible to allow for easy integration of new components and to enable the system to be easily extended to new use cases.

The system was deployed on a cloud computing platform (GWDG Cloud server) using open-source solutions for the different components of the system. Docker (www.docker.com) was used to containerize the system components and to enable easy deployment and scaling.

The system architecture is shown in Figure 6.1. The system is composed of four main components that match the life cycle of flux data: collection and transport, cataloging and archival, analysis, and communication.

6.3.1 Collection and transport

The collection of data in the field is the first stage of the flux data life cycle. Atmospheric measurements come from a variety of sensors and instruments with different communication protocols and mea-

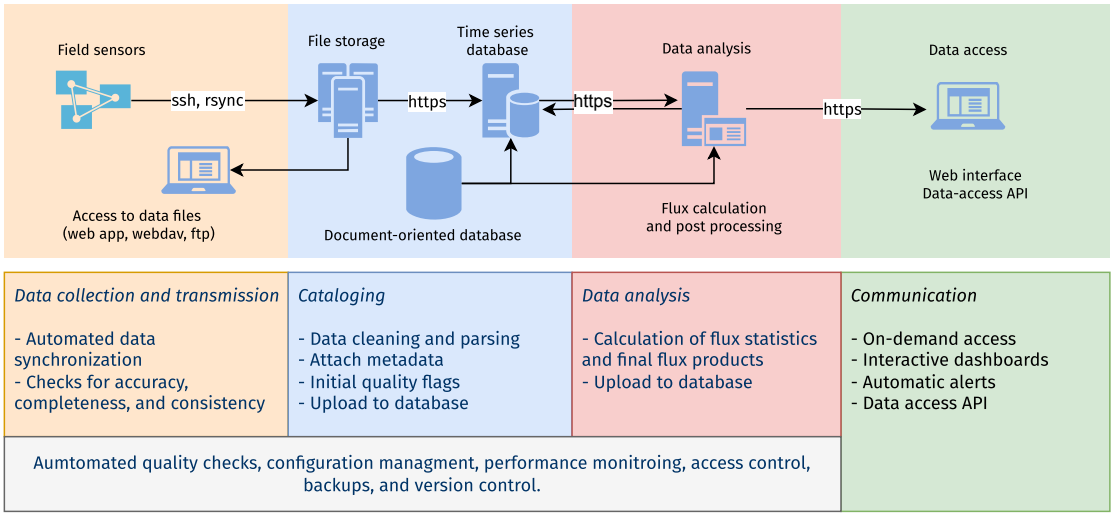

Figure 6.1: System architecture of the flux data management platform. The figure shows the four main components that match the life cycle of flux data and highlights the data flow between the components and the main tasks and considerations for each component.

surement frequencies. Traditionally, scientific loggers are used to collect data from sensors and store them locally. We used single-board computers (RaspberryPi) to collect data from different sensors and transmit them to a central server. The use of single-board computers allows for a low-cost and energy-efficient solution for data collection. Data synchronization between different measurement systems in the field was achieved using a combination of the protocols FTP, SSH, and MQTT. The communication to field stations was maintained using reverse ssh tunneling which proved to be a reliable and robust solution.

The transmission of data was designed to be robust and efficient. Data were transferred incrementally. Therefore, only changed data were transmitted to the server to avoid the need to transmit the entire data set each time which allowed the transmission of data from the field to the server in a near real-time fashion.

6.3.2 Cataloging and storage

Upon transmission, data were kept on the storage server as files using different formats. The raw files copy was considered the master copy of the data and kept in a read-only state. Automated data cataloging was set up to start as new files are detected. A new R package (influxr) [1] was developed to handle the cataloging of flux data.

The influxr package provides a convenient way to read and parse raw measurement files and store them in a time series database. InfluxDB (https://www.influxdata.com) is a time series database that is optimized for storing and querying large amounts of time series data. It offers a different approach to storing data compared to relational databases, which can limit some of the benefits of relational databases such as integrity constraints. However, the performance and flexibility of time series oriented InfluxDB were required in light of the data rates and volumes and therefore justified the design tradeoff.

[1] Published on GitHub: https://github.com/influxr/influxr

The description of data sources is specified using a human-readable configuration file (YAML). The configuration files specify the location of the raw data files, the format of the files, and the metadata associated with the data.

During the cataloging process, unique identifiers are added to the data. Configuration files are tracked using version control (git). Non-tabular data are stored in an associated document database (MongoDB).

Initial quality checks are performed during cataloging to ensure the integrity and correctness of the data. Data files that have corrupted records are cleaned. Automated alerts are sent to the users to notify of any issues.

Regular backups were performed with versioning, deduplication, and encryption to minimize the risk of data loss or corruption due to instrument or software failures. Backups were stored on separate servers and were regularly tested to ensure the integrity of the data.

6.3.3 Flux analysis

Jobs for flux data analysis were scheduled using a simple workflow manager based on cron. Fluxes were calculated continuously in a near real-time fashion (every 10 minutes).

Configurations and parameters for the flux analysis were specified using a human-readable configuration file (YAML) and tracked using a version control system (git). The configuration format was designed to be hierarchical such that a range of parameters can be specified at different levels of the configuration file.

Flux analysis starts by reading raw measurements from the time series database and the relevant configuration files. This approach was proven to be superior to reading the raw data files directly as it separates the raw data parsing from the analysis.

A new R package (eddyr) was developed to handle the flux analysis. The package provides complete processing pipelines for true eddy accumulation and eddy covariance fluxes including quality checks. The package eddyr was designed to allow for efficient continuous calculation of the fluxes by applying certain processing steps on a rolling basis such as the calculation of the wind rotation matrix and the ensemble spectra which usually require the entire experiment dataset. Once fluxes are calculated and quality flags are assigned, calculated fluxes are uploaded to the time series database using the package influxr.

Individual flux periods are assigned unique identifiers and the intermediate stages of flux analysis are kept in the database therefore guaranteeing full traceability of the flux analysis.

6.3.4 Data access and communication

The final calculated fluxes as well as the raw measurements are made available to data users through a web interface. The web interface is based on the open-source software Grafana (https://grafana.com) Fig. (6.2). Grafana provides a flexible way to visualize data and create interactive dashboards. Automated notifications are sent to users when predefined conditions are met. For example, when certain anomalies are detected in measured fluxes.

Figure 6.2: Screenshot of the interactive dashboard (Grafana). The dashboard provides easy and near real-time access to measured fluxes and ancillary data through a variety of customizable visualizations.

Additionally, a data access API to enable programmatic access to the data was provided by the package influxr. The API provides an easy way to query the data and download the results in a variety of formats.

6.4 Conclusions and future work

Management of flux data has become an increasingly important challenge in the flux community. Increased accessibility of flux data and the ability to process and analyze them in real-time enables new and innovative uses of flux data.

We presented a processing and management platform for flux data that enables the collection, storage, and analysis of flux data on a near real-time basis. The presented platform enables the traceability of flux data. It increases the usefulness of flux data by facilitating collaboration and data sharing and allows for early detection of problems in the data. Moreover, we believe that specifically for the development of the true eddy accumulation method, not only were advances in theory and in sampling apparatus and hardware needed but providing accessible solutions to working with the large amounts of complex data were key for us to advancing the TEA method to the next level presented in this work. We further believe similar approaches will be essential for a wider application of the TEA method in general and at the same time provide the next level for the eddy covariance and related methods alike by their nature.

Future work will focus on streamlining the data processing and management platform to serve more use cases and on the integration with existing public data repositories potentially enabling a distributed network of flux data processing and management platforms.

Bibliography

Hicks, B. B. and Baldocchi, D. D.: Measurement of Fluxes Over Land: Capabilities, Origins, and Remaining Challenges, Boundary-Layer Meteorology, 177, 365–394, doi:10.1007/s10546-020-00531-y, 2020.

Papale, D.: Ideas and Perspectives: Enhancing the Impact of the FLUXNET Network of Eddy Covariance Sites, Biogeosciences, 17, 5587–5598, doi:10.5194/bg-17-5587-2020, 2020.

Papale, D., Agarwal, D. A., Baldocchi, D., Cook, R. B., Fisher, J. B., and van Ingen, C.: Database Maintenance, Data Sharing Policy, Collaboration, in: Eddy Covariance: A Practical Guide to Measurement and Data Analysis, edited by Aubinet, M., Vesala, T., and Papale, D., Springer Atmospheric Sciences, pp. 399–424, Springer Netherlands, Dordrecht, doi:10.1007/978-94-007-2351-1_17, 2012.

Wilkinson, M. D., Dumontier, M., Aalbersberg, I. J., Appleton, G., Axton, M., Baak, A., Blomberg, N., Boiten, J.-W., da Silva Santos, L. B., Bourne, P. E., Bouwman, J., Brookes, A. J., Clark, T., Crosas, M., Dillo, I., Dumon, O., Edmunds, S., Evelo, C. T., Finkers, R., Gonzalez-Beltran, A., Gray, A. J. G., Groth, P., Goble, C., Grethe, J. S., Heringa, J., 't Hoen, P. A. C., Hooft, R., Kuhn, T., Kok, R., Kok, J., Lusher, S. J., Martone, M. E., Mons, A., Packer, A. L., Persson, B., Rocca-Serra, P., Roos, M., van Schaik, R., Sansone, S.-A., Schultes, E., Sengstag, T., Slater, T., Strawn, G., Swertz, M. A., Thompson, M., van der Lei, J., van Mulligen, E., Velterop, J., Waagmeester, A., Wittenburg, P., Wolstencroft, K., Zhao, J., and Mons, B.: The FAIR Guiding Principles for Scientific Data Management and Stewardship, Scientific Data, 3, 160 018, doi:10.1038/sdata.2016.18, 2016.

7 Synopsis

The TEA method offers great potential to expand direct micrometeorological measurements beyond what is currently possible with the EC method. However, unlike the EC method which is well-established and has relatively standardized protocols for setup and flux processing, TEA has fewer published studies and no available commercial instrumentation or software. Furthermore, the implications of the theoretical basis of the TEA method such as the assumption of a zero mean vertical wind velocity are not fully understood. Therefore, the thesis aimed at addressing the core challenges of the TEA method in theory and implementation to reach a defensible estimate of the flux.

The first goal of this work was to evaluate the implementation of the prototype TEA system presented in Ch. 2 and to develop the processing pipeline for TEA fluxes. A working prototype was critical to examine the practical limitations of the TEA sampler under field conditions and to refine the implementation and processing software.

From a theoretical perspective, TEA has similar foundations and limitations as EC. However, it has additional constraints due to the lack of high frequency measurements of the scalars concentration. The most important consequence of this additional constraint is the inability to enforce the assumption of a zero mean vertical wind velocity during the flux averaging intervals. The violation of this assumption leads to systematically biased fluxes. Therefore, the second goal of this thesis was to characterize and correct this systematic bias.

The conventional implementation with a fixed accumulation time was sensitive to non-stationarities and required the sampling apparatus to cover a high dynamic range of vertical wind velocity. The implementation of a conventional prototype eddy accumulation system made it clear that a more robust and flexible flow-through TEA system is needed. The third goal of this thesis was to develop the flow-through TEA system in which the flux averaging time and the sample accumulation time are decoupled.

Finally, a common challenge to fluxes measured with TEA and EC methods is signal attenuation due to frequency losses. Conventional spectral correction methods used with EC measurements do not work with TEA because the assumptions about the ideal spectra and cospectra are difficult to justify for TEA due to the unavailability of high-frequency measurements of the scalar concentration. Besides, conventional spectral correction methods are indirect since the attenuation is estimated by simulating the attenuation on ideal spectra that are assumed to approximate the true spectra. Therefore, the fourth goal of this thesis was to develop a direct spectral correction method that can restore the attenuated signals directly.

With the following findings, we give an account of how we addressed the above four objectives. We show which specific solution we realized for each of the above challenges and we then identify open questions and suggest avenues on how to address them in future work.

7.1 Overview of the key results

7.1.1 TEA system prototype implementation and verification

A conventional TEA system prototype was presented in (Ch. 2). The system was built around a new dynamic mass flow controller than can resolve turbulence at a frequency of 10 Hz and higher. The new dynamic mass flow controller showed a good ability of accurate high-frequency air acquisition which allowed controlling the air mass flow rate proportional to the magnitude of the instantaneous vertical wind velocity. The TEA system was designed to minimize time lags, jitter, and dead volumes in the gas sampling system.

The proof-of-concept TEA system was deployed in the field adjacent to a conventional EC measurement setup to evaluate the operation and performance of the system. The experiment took place over a grassland experimental field site of the University of Göttingen, Germany. The measured fluxes matched well between the two systems with an R^2 of 86% and a slope of 0.98.

The successful implementation of the TEA system prototype required developing a new measurement protocol to perform automated gas handling and online wind processing. The online treatment to align the wind coordinates to the streamline coordinate system was a crucial step toward the field operation of the TEA system. A new running window planar fit correction was shown to be well suited for the use with TEA and produced results comparable to the conventional application of the planar fit method. In addition to online tilt correction, further treatments of the vertical wind velocity component were applied to reduce the residual mean vertical wind velocity and to choose a better sampling proportionality factor A. The improved choice of this factor helped reduce the required dynamic range of the sampling apparatus.

The work conducted in this thesis contributed to the verification of the field performance and the calibration of the new mass flow controllers, the characterization of density effects on air sampling, the optimization of system timing and jitter, the development of flux processing software, and the calculation of the final fluxes from raw data. Several field experiments were conducted as part of this thesis to verify the performance of the different system components that were initially only tested in the lab.

The field evaluation of the TEA prototype presented in this study helped to identify the next challenges that needed to be addressed for more robust and accurate flux measurements using the TEA method. The online treatments for the vertical wind velocity were not enough to set the residual mean vertical velocity to zero. Therefore, it was important to investigate the consequences of this discrepancy. Additionally, bag-based accumulation has shown to be impractical and prone to nonstationarities.

7.1.2 Extending the TEA method to non-ideal conditions

Solutions to constrain the error when using the TEA method under non-ideal conditions were presented in Ch. 3.

The TEA equation is formulated assuming a zero mean vertical wind velocity during the flux averaging interval. However, under field conditions, this assumption is not valid and cannot be enforced through post-processing. Therefore, it is important to constrain and correct the systematic error in the flux due to nonzero mean vertical wind velocity.

This issue was addressed by putting forward a new formulation for the TEA equation that isolates the error term due to nonzero mean vertical wind velocity. Using the new formulation, the error in the flux was shown to be equal to $\bar{w}/\overline{|w|}\alpha_c$. Here, $\bar{w}$ is the mean vertical wind velocity and $\overline{|w|}$ is the mean of the absolute value of the vertical wind velocity, and α_c is the coefficient of transport asymmetry. A clear advantage of the new expression is that it isolates error to be only dependent on the symmetry of the atmospheric transport instead of having it scale with the scalar background concentration.

The coefficient α_c emerges naturally as the ratio of the covariance $\overline{c'|w|'}$ to the flux covariance $\overline{c'w'}$. α_c was shown to be useful to estimate and remove the error in the TEA flux. The value of α_c was analyzed using quadrant analysis and was shown to remain below one under stationary conditions. Effectively constraining the relative error in the flux to below $\bar{w}/\overline{|w|}$ when the stationarity criterion is met. This value was confirmed empirically for several atmospheric scalars. Values of α_c are shown to have an approximate average of 0.2 under unstable conditions and -0.2 under non-stationarity conditions.

We showed two methods for estimating α_c to further reduce the error. i) an estimate of α_c based on the assumption of flux variance similarity, and ii) an analytical expression based on the assumption of a Gaussian joint probability distribution of the scalar concentration and vertical wind velocity. Both of these methods were shown to be effective in minimizing systematic error in the flux when compared to conventional TEA formulas.

Furthermore, the new formulation was shown to be a general expression that unifies the existing formulas for calculating the TEA flux. The performance of the new correction was explored in a numerical simulation based on field-measured data. The simulation results showed that using α_c was effective in removing the systematic bias under conditions of nonzero mean vertical velocity.

7.1.3 A new continuous flow-through eddy accumulation method

A new eddy accumulation method called short-time eddy accumulation (STEA) was developed and evaluated in Ch. 4. The new method represents a formulation to accumulate samples continuously which is necessary to run the TEA system in a flow-through manner.

The field evaluation of the prototype TEA system described in Ch. 2 was found to be prone to nonstationarities. In particular, The sample accumulation in bags was sensitive to flow nonstationarities and required the sampling apparatus to cover a larger dynamic range of vertical wind velocity.

The STEA method was formulated by partitioning the concentration measurements conditionally on a time partitioning variable. This partitioning scheme allows the sample accumulation to be carried out on variable time intervals shorter than the flux averaging interval.

This rather simple modification brings multiple advantages to the eddy accumulation method. It enables the STEA method to be operated in a hybrid way between eddy accumulation and eddy covariance which brings multiple advantages:

- i) it increases the dynamic range of the TEA sampling apparatus by requiring the system to cover

a smaller range of wind velocities. This in turn increases the accuracy and reduces the random uncertainty of sampling. Testing on field measured data showed that accumulating using 1 minute instead of 30 minutes almost doubles the dynamic range of the sampling apparatus.

- ii) STEA can be operated in a flow-through accumulation scheme. The details of such a setup using a series of two buffer volumes was detailed and implemented in the field. Such a setup has been shown to improve the overall system performance by avoiding the effect of local nonstationary flows on the sampling system.

- iv) STEA enables the match of the sampling frequency and the ideal measurement frequency of the analyzer. This can be beneficial if the atmospheric constituents change with time such as with reactive species. Under such a case, the ideal measurement interval can be long enough to match the analytical capabilities of the instrument, while being as short as possible to minimize the reactive constituent's decay.

A prototype implementation of the STEA system in flow-through mode was evaluated in a flat agricultural field in Braunschweig, Germany. The setup included an adjacent reference conventional EC system. Measured CO_2 fluxes matched very well between the two methods yielding a slope of 1.04 and R^2 of 86%. While these results are comparable to the traditional TEA system presented in Ch. 2, the variability reported here, demonstrated by R^2 values, is due to the less-than-ideal operation of the STEA system in this particular experiment. The choice of the switching interval in this experiment (1 minute) was shown later to be suboptimal. Therefore, it is expected to achieve a better fit with adaptive averaging-interval lengths.

The use of buffer volumes in the continuous STEA method was investigated. The effect of buffer volumes was modeled as a first-order linear filter and an empirical correction was proposed to account for the flux loss due to the smoothing effect of buffer volumes.

7.1.4 A novel direct spectral correction method for eddy covariance and TEA fluxes

A novel spectral correction approach was addressed in Ch. 5.

Motivated by the need for a direct spectral correction approach that can be used with eddy accumulation methods, the problem of spectral attenuation of measured atmospheric signals was analyzed in the framework of linear system theory.

Conventional methods of spectral correction estimate the flux loss by simulating the attenuation on an ideal spectrum. The assumption of an ideal spectrum is a major source of uncertainty and systematic bias in the corrected fluxes. Furthermore, the most common way of applying this simulation by using a copsectral transfer function lacks a proper treatment of the phase shift induced by the process causing the attenuation.

The analysis in this work started by deriving an exact cospectral transfer function. The function shown in Eq. (5.11) highlights the importance of phase shift in restoring attenuated signals.

Based on this analysis, A novel correction approach based on Wiener deconvolution is proposed to directly restore measured attenuated signals. The new approach does not require the assumption of an ideal spectrum and offers an ideal treatment for the noise.

The limitations of the conventional approaches were further explored in a numerical simulation.

The simulation results showed that the common way conventional methods are applied can lead to systematic biases that can be as large as 15% of the flux even at rather small values of the time constant.

7.1.5 A new platform for flux data management and near real-time processing

A new platform that provides near real-time processing and data management was developed in Ch. 6. The platform enables fast and efficient archival, curation, processing, and representation of flux data. It brings several features that increase the usefulness of flux data: it provides easy and timely access to the raw data and the final fluxes, it enables the traceability of flux data to raw measurements, and it maximizes the accessibility to flux data and metadata and the ability to assess the data quality. An implementation of the platform using open-source software was developed and deployed on a cloud computing platform.

7.2 The broader context: new opportunities for micrometeorological measurements

The improvements in the TEA method, the new STEA method, and the direct spectral correction method presented in this thesis have the potential to improve the current estimates of atmospheric exchange and provide new opportunities to directly measure new atmospheric constituents that will ultimately lead to a better understanding of the biosphere-atmosphere interactions and ecosystem processes.

TEA and STEA methods enable the expansion of micrometeorological measurements in four promising areas

- **Measuring fluxes of new atmospheric constituents using non-conventional analytical methods.** The ability to use slow analyzers with the TEA method allows studying the atmospheric exchange of new constituents using new types of analytical methods.

  For example, as suggested in Ch. 2, fluxes of bacteria and DNA are a promising application of the TEA method and have multiple applications in ecology and atmospheric chemistry. Bacteria exist in the atmosphere in concentrations exceeding 10^4 cells m^{-3}. The measurement of their exchange enables investigating their role of atmospheric chemistry, microbial biogeography, and ecosystem health (Burrows et al., 2009b,a; Pöschl, 2005). Several techniques exist for the automated quantification and identification of bacteria such as the quantitative polymerase chain reaction (Q-PCR) (Brodie et al., 2007).

  Fluxes of environmental DNA allow to monitor the population and to asses the diversity of terrestrial ecology by identifying species and their ecological interactions (Clare et al., 2022). For this purpose, analytical techniques such as DNA metabarcoding are promising candidates. DNA metabarcoding enables the identification of taxa from mixed samples using DNA sequencing (van Klink et al., 2022).

  The TEA method can also be used to monitor the spatiotemporal development of atmospheric constituents relevant to public health, such as allergenic pollen in ambient air (Polling et al., 2022), and road dust and mutagens in urban air (Khan and Strand, 2018). The fluxes of such constituents will be a great asset to understanding the transport and deposition of these compounds and ultimately reduce their harmful effects on the human body.

- **TEA as an alternative to indirect micrometeorological methods**. The fluxes of several important atmospheric constituents are routinely measured using indirect micrometeorological methods. For example, fluxes of volatile organic compounds (VOCs) play a major role in the composition of atmospheric chemistry and the quality of the air. Currently, VOCs are mostly measured using disjunct-eddy covariance (Rinne and Ammann, 2012; Rantala et al., 2016). Gradient methods (Rinne et al., 2000), or relaxed eddy accumulation (REA) (Bowling et al., 1998). TEA and STEA have the potential to offer more accurate direct flux measurements for VOCs. More generally, atmospheric scalars currently measured with indirect methods such as REA are perfect candidates for TEA and STEA. For example, nitrous acid (Ren et al., 2011), mercury (Skov et al., 2006), ammonia (Nelson et al., 2017), dry deposition (Matsuda et al., 2015), herbicides, and pesticides (Pattey et al., 1995). As a direct method, TEA is expected to provide higher accuracy measurements than indirect methods which will provide a better understanding of the dynamics, the sources and the sinks of these compounds.

- **Low-cost alternative to EC measurements**. The new STEA method offers a more flexible and robust approach to sample accumulation than traditional TEA. This approach is promising to use with cheaper slow-response gas analyzers to measure CO_2 and H_2O fluxes as a low-cost alternative to EC. Recently, there has been an increased interest in low-cost eddy covariance systems to increase the statistical confidence of the annual flux estimates by increasing the spatial replication (Hill et al., 2017; Markwitz and Siebicke, 2019). Currently, the low-cost EC method depends on sampling at a lower frequency than what is commonly used with EC method which increases the uncertainty of flux estimates. STEA and TEA methods approaches have the potential to improve the low-cost EC measurements without increasing the flux uncertainty.

  However, the overhead of adding an accumulation sampler will increase the complexity and cost of such a system. Therefore, this use remains a trade-off between the cost of a TEA sampler and a fast-response gas analyzer. Nevertheless, the flexibility of an eddy accumulation system might justify such use.

- **Measuring fluxes with sample return**. TEA allows the decoupling of the analyzer from wind measurements, which enables innovative uses for flux measurements, for example, using the TEA method, it is feasible to collect samples for later analysis in a laboratory for constituents where the analytical methods are not field-ready. Unmanned aerial systems (UAS) have seen increasing use in atmospheric measurements recently (e.g. (Allen et al., 2019; Bretschneider et al., 2022; Alekseychik et al., 2021)), TEA enables the use of UAS for flux measurements by providing a means to collect and return samples to the laboratory where measurements of several constituents can be conducted at once. The flexibility of UAS means increased spatial coverage for flux measurements enabling more insights into the horizontal distribution of surface fluxes. This is very costly and often unfeasible to conduct with tower-based approaches. However, the use of TEA samplers with UAS would necessarily require the minimization of the system's components to meet the weight and power constraints.

The new spectral correction method using Wiener deconvolution offers a rigorous solution to restoring attenuated signals while taking into account the phase shift and the noise in the measured original signal. We see the biggest opportunity of this new approach is to unite the analytical and the in-situ methods in eddy flux measurements. The new method was demonstrated to reduce uncertainty and bias compared to using conventional methods. The uncertainty reduction and the ability to accurately restore attenuated fluxes have a large potential to help investigate two of the big challenges the EC method is facing: the nighttime fluxes and the energy closure problem (Sun et al., 2021; Leuning et al.,

2012).

7.3 Outlook and future work

Based on the research presented in this thesis, several important research questions were identified that could direct future research

- The effect of density fluctuations on TEA sampling is currently accounted for using the measurements of sonic temperature. However, an improvement of this treatment is possible by incorporating additional measurements of water vapor content. A correction can likely be developed to be applied in post-processing using the measurements of sensible and latent heat fluxes.
- α_c has emerged as a useful metric for the direction and magnitude of transport symmetry, it was shown that α_c is a good indicator of stationarity conditions. The use of α_c as a flag for the quality of atmospheric transport can be investigated further, e.g., by using LES simulations. A better definition of the values of α_c would facilitate the use of alpha as a metric for the quality of measured fluxes. Furthermore, the analytical value of α_c presented in this thesis was found using an assumption of a Gaussian distribution. The use of other distributions which are better suited for representing atmospheric transport should be investigated.
- The correction proposed for the attenuation of buffer volumes used with STEA method was shown to introduce random uncertainty to the corrected fluxes. A direct correction scheme based on the Wiener deconvolution method presented in Ch.5 is feasible and should be investigated.
- The proposed Wiener deconvolution method for spectral correction needs to be tested on a larger dataset to characterize the limitations and the performance of the method. Preferably using experimental data from co-located open-path and closed-path EC systems.
- Empirical models used to describe spectral attenuation in EC and TEA measurements were shown to be inadequate. Improvements are possible by repurposing existing analytical transfer functions for use with the Wiener deconvolution method. Alternatively, the use of approximating functions can be further investigated.
- Conventional spectral correction methods were shown to introduce a systematic bias to the corrected flux. The implications of the identified systematic bias on the global NEE and energy budget estimates need to be investigated.
- More generally, the developments presented in this work have shown that the TEA method has become mature enough as an alternative to EC. Further application of the TEA method with new atmospheric constituents would be a natural next step. Potential new applications might require the adaptation of the sampling apparatus to the specific requirements of the measured constituents.

7.4 General conclusions

In conclusion, the developments presented in this thesis fulfill the objective to address the core challenges facing the TEA method. A graphical summary of the main conclusions is shown in Fig 7.1.

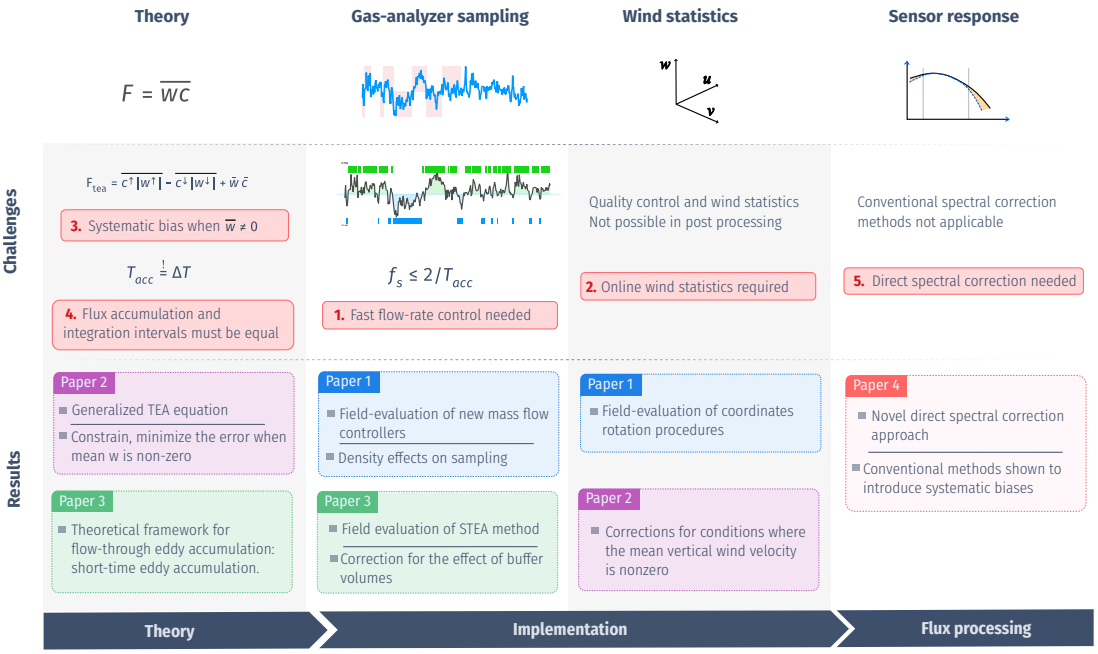

Figure 7.1: Conceptual figure summarizing the challenges and the main results addressed in this thesis. The first row shows the challenges of the EC method and the TEA method. The second row shows the main results of this thesis.

This thesis presented two implementations of the TEA method. It showed that by using a new type of mass flow controller and real-time processing of wind statistics it is possible to conduct accurate measurements of ecosystem-level fluxes. A new formulation for the TEA equation demonstrated that it is possible to characterize and remove the systematic error under non-ideal conditions where the mean vertical wind velocity is nonzero using the properties of atmospheric transport. A new flow-through TEA system was developed and implemented to remove the requirement for constant accumulation time. A new direct spectral correction approach based on the Wiener deconvolution method was proposed as a viable alternative to correct attenuated measured atmospheric signals.

We believe that the new developments presented in this thesis bring the TEA method to a field-ready status with comparable performance to EC method.

Bibliography

Alekseychik, P., Katul, G., Korpela, I., and Launiainen, S.: Eddies in Motion: Visualizing Boundary-Layer Turbulence above an Open Boreal Peatland Using UAS Thermal Videos, Atmospheric Measurement Techniques, 14, 3501–3521, doi:10.5194/amt-14-3501-2021, 2021.

Allen, G., Hollingsworth, P., Kabbabe, K., Pitt, J. R., Mead, M. I., Illingworth, S., Roberts, G., Bourn, M., Shallcross, D. E., and Percival, C. J.: The Development and Trial of an Unmanned Aerial System for the Measurement of Methane Flux from Landfill and Greenhouse Gas Emission Hotspots, Waste Management, 87, 883–892, doi:10.1016/j.wasman.2017.12.024, 2019.

Bowling, D. R., Turnipseed, A. A., Delany, A. C., Baldocchi, D. D., Greenberg, J. P., and Monson, R. K.: The Use of Relaxed Eddy Accumulation to Measure Biosphere-Atmosphere Exchange of Isoprene and Other Biological Trace Gases, Oecologia, 116, 306–315, doi:10.1007/s004420050592, 1998.

Bretschneider, L., Schlerf, A., Baum, A., Bohlius, H., Buchholz, M., Düsing, S., Ebert, V., Erraji, H., Frost, P., Käthner, R., Krüger, T., Lange, A. C., Langner, M., Nowak, A., Pätzold, F., Rüdiger, J., Saturno, J., Scholz, H., Schuldt, T., Seldschopf, R., Sobotta, A., Tillmann, R., Wehner, B., Wesolek, C., Wolf, K., and Lampert, A.: MesSBAR—Multicopter and Instrumentation for Air Quality Research, Atmosphere, 13, 629, doi:10.3390/atmos13040629, 2022.

Brodie, E. L., DeSantis, T. Z., Parker, J. P. M., Zubietta, I. X., Piceno, Y. M., and Andersen, G. L.: Urban Aerosols Harbor Diverse and Dynamic Bacterial Populations, Proceedings of the National Academy of Sciences, 104, 299–304, doi:10.1073/pnas.0608255104, 2007.

Burrows, S. M., Butler, T., Jöckel, P., Tost, H., Kerkweg, A., Pöschl, U., and Lawrence, M. G.: Bacteria in the Global Atmosphere – Part 2: Modeling of Emissions and Transport between Different Ecosystems, Atmospheric Chemistry and Physics, 9, 9281–9297, doi:10.5194/acp-9-9281-2009, 2009a.

Burrows, S. M., Elbert, W., Lawrence, M. G., and Pöschl, U.: Bacteria in the Global Atmosphere – Part 1: Review and Synthesis of Literature Data for Different Ecosystems, Atmospheric Chemistry and Physics, 9, 9263–9280, doi:10.5194/acp-9-9263-2009, 2009b.

Clare, E. L., Economou, C. K., Bennett, F. J., Dyer, C. E., Adams, K., McRobie, B., Drinkwater, R., and Littlefair, J. E.: Measuring Biodiversity from DNA in the Air, Current Biology, 32, 693–700.e5, doi:10.1016/j.cub.2021.11.064, 2022.

Hill, T., Chocholek, M., and Clement, R.: The Case for Increasing the Statistical Power of Eddy Covariance Ecosystem Studies: Why, Where and How?, Global Change Biology, 23, 2154–2165, doi:10.1111/gcb.13547, 2017.

Khan, R. K. and Strand, M. A.: Road Dust and Its Effect on Human Health: A Literature Review, Epidemiology and Health, 40, e2018 013, doi:10.4178/epih.e2018013, 2018.

Leuning, R., van Gorsel, E., Massman, W. J., and Isaac, P. R.: Reflections on the Surface Energy Imbalance Problem, Agricultural and Forest Meteorology, 156, 65–74, doi:10.1016/j.agrformet.2011.12.002, 2012.

Markwitz, C. and Siebicke, L.: Low-Cost Eddy Covariance: A Case Study of Evapotranspiration over Agroforestry in Germany, Atmospheric Measurement Techniques, 12, 4677–4696, doi:10.5194/amt-12-4677-2019, 2019.

Matsuda, K., Watanabe, I., Mizukami, K., Ban, S., and Takahashi, A.: Dry Deposition of PM2.5 Sulfate above a Hilly Forest Using Relaxed Eddy Accumulation, Atmospheric Environment, 107, 255–261, doi:10.1016/j.atmosenv.2015.02.050, 2015.

Nelson, A. J., Koloutsou-Vakakis, S., Rood, M. J., Myles, L., Lehmann, C., Bernacchi, C., Balasubramanian, S., Joo, E., Heuer, M., Vieira-Filho, M., and Lin, J.: Season-Long Ammonia Flux Measurements above Fertilized Corn in Central Illinois, USA, Using Relaxed Eddy Accumulation, Agricultural and Forest Meteorology, 239, 202–212, doi:10.1016/j.agrformet.2017.03.010, 2017.

Pattey, E., Cessna, A. J., Desjardins, R. L., Ken, L. A., Rochette, P., St-Amour, G., Zhu, T., and Headrick, K.: Herbicides Volatilization Measured by the Relaxed Eddy-Accumulation Technique Using Two Trapping Media, Agricultural and Forest Meteorology, 76, 201–220, doi:10.1016/0168-1923(95)02225-M, 1995.

Polling, M., Sin, M., de Weger, L. A., Speksnijder, A. G. C. L., Koenders, M. J. F., de Boer, H., and Gravendeel, B.: DNA Metabarcoding Using nrITS2 Provides Highly Qualitative and Quantitative Results for Airborne Pollen Monitoring, Science of The Total Environment, 806, 150 468, doi:10.1016/j.scitotenv.2021.150468, 2022.

Pöschl, U.: Atmospheric Aerosols: Composition, Transformation, Climate and Health Effects, Angewandte Chemie International Edition, 44, 7520–7540, doi:10.1002/anie.200501122, 2005.

Rantala, P., Järvi, L., Taipale, R., Laurila, T. K., Patokoski, J., Kajos, M. K., Kurppa, M., Haapanala, S., Siivola, E., Petäjä, T., Ruuskanen, T. M., and Rinne, J.: Anthropogenic and Biogenic Influence on VOC Fluxes at an Urban Background Site in Helsinki, Finland, Atmospheric Chemistry and Physics, 16, 7981–8007, doi:10.5194/acp-16-7981-2016, 2016.

Ren, X., Sanders, J. E., Rajendran, A., Weber, R. J., Goldstein, A. H., Pusede, S. E., Browne, E. C., Min, K.-E., and Cohen, R. C.: A Relaxed Eddy Accumulation System for Measuring Vertical Fluxes of Nitrous Acid, Atmos. Meas. Tech, 4, 2093–2103, doi:10.5194/amt-4-2093-2011, 2011.

Rinne, J. and Ammann, C.: Disjunct Eddy Covariance Method, in: Eddy Covariance: A Practical Guide to Measurement and Data Analysis, edited by Aubinet, M., Vesala, T., and Papale, D., Springer Atmospheric Sciences, pp. 291–307, Springer Netherlands, Dordrecht, doi:10.1007/978-94-007-2351-1_10, 2012.

Rinne, J., Tuovinen, J.-P., Laurila, T., Hakola, H., Aurela, M., and Hypén, H.: Measurements of Hydrocarbon Fluxes by a Gradient Method above a Northern Boreal Forest, Agricultural and Forest Meteorology, 102, 25–37, doi:10.1016/S0168-1923(00)00088-5, 2000.

Skov, H., Brooks, S. B., Goodsite, M. E., Lindberg, S. E., Meyers, T. P., Landis, M. S., Larsen, M. R. B., Jensen, B., McConville, G., and Christensen, J.: Fluxes of Reactive Gaseous Mercury Measured with a Newly Developed Method Using Relaxed Eddy Accumulation, Atmospheric Environment, 40, 5452–5463, doi:10.1016/j.atmosenv.2006.04.061, 2006.

Sun, J., Massman, W. J., Banta, R. M., and Burns, S. P.: Revisiting the Surface Energy Imbalance, Journal of Geophysical Research: Atmospheres, 126, e2020JD034 219, doi:10.1029/2020JD034219, 2021.

van Klink, R., August, T., Bas, Y., Bodesheim, P., Bonn, A., Fossøy, F., Høye, T. T., Jongejans, E., Menz, M. H. M., Miraldo, A., Roslin, T., Roy, H. E., Ruczyński, I., Schigel, D., Schäffler, L., Sheard, J. K., Svenningsen, C., Tschan, G. F., Wäldchen, J., Zizka, V. M. A., Åström, J., and Bowler, D. E.: Emerging Technologies Revolutionise Insect Ecology and Monitoring, Trends in Ecology & Evolution, doi:10.1016/j.tree.2022.06.001, 2022.

Acknowledgements

I am deeply grateful to all of the friends, colleagues, and mentors who have supported me throughout my PhD journey.

I am especially indebted to Dr. Lukas Siebicke and Prof. Alexander Knohl who supervised and supported this work. Without their support and guidance, this work would not have been possible. I would also like to thank the members of my thesis committee, Prof. Edzo Veldkamp and Prof. Janne Rinne for their support and constructive feedback which have been instrumental in shaping this work. Additionally, I want to express my gratitude towards Prof. Christoph Thomas for reviewing this work and being part of the examination board.

I am grateful for the financial support that made this research possible. This research received partial financial support by the Ministry of Lower-Saxony for Science and Culture (MWK) under the fellowship Wissenschaft.Niedersachsen.Weltoffen, by the European Research Council under the European Union's Horizon 2020 research and innovation programme (grant agreement no. 682512 - OXYFLUX), by the Deutsche Forschungsgemeinschaft (INST 186/1118-1 FUGG), and by the Bioclimatology group of the Faculty of Forest Sciences and Forest Ecology of the University of Göttingen.

The present study was carried out at the Bioclimatology group of Faculty of Forest Sciences and Forest Ecology of the University of Göttingen. I would like to thank all my colleagues in the Bioclimatology group for being very welcoming and kind and for their support and assistance throughout the different stages of this work. I would like to especially thank Jelka Braden-Behrens and Christian Markwitz for their help in translating the abstract, Daphne Paulmann and Justus Presse for their support in the field work in Finland and Germany, and Justus van Ramshorst for the constant encouragement and support.

I am grateful to all my friends who have been a constant source of encouragement and inspiration throughout my academic journey, and finally, I am deeply grateful to my family who have provided unlimited love and support - my parents, brother Malik, sister Lobna, and my wife Hiba and son Julian.

Göttingen, June 21, 2023 Anas Emad